Genomics-Driven Investigation of Three Classes of Bioactive Secondary Metabolites from *Burkholderia* Species

Genom-getriebene Erforschung von Drei Bioaktiven Naturstoff-Klassen aus *Burkholderia* Bakterien

Dissertation

Der Mathematisch-Naturwissenschaftlichen Fakultät

der Eberhard Karls Universität Tübingen

zur Erlangung des Grades eines

Doktors der Naturwissenschaften

(Dr. rer. nat.)

Vorgelegt von

Junjing Jiao

aus Henan, V.R. China

Tübingen

2021

Gedruckt mit Genehmigung der Mathematisch-Naturwissenschaftlichen Fakultät der Eberhard Karls Universität Tübingen.

Tag der mündlichen Qualifikation:	21.05.2021
Dekan:	Prof. Dr. Thilo Stehle
1. Berichterstatter:	Prof. Dr. Harald Groß
2. Berichterstatter:	PD Dr. Bertolt Gust

Statement on the Originality of This Thesis

I hereby declare that I alone wrote the doctoral work submitted here under the title 'Genomics-driven Investigation of Three Classes of Bioactive Secondary Metabolites from *Burkholderia* Species', that I only used the sources and materials cited in the work, and that all citations, whether word for word or paraphrased are given as such. I declare that I adhered to the guidelines set forth by the University of Tübingen to guarantee proper academic scholarship (Senate Resolution 25.05.2000). I declare that these statements are true and that I am concealing nothing. I understand that any false statements can be punished with a jail term of up to three years or a financial penalty.

Parts of this work have been published in

J Jiao, J Du, A Frediansyah, G Jahanshah and H Gross* (2020) Structure elucidation and biosynthetic locus of trinickiabactin from the plant pathogenic bacterium *Trinickia caryophylli*. J. Antibiot., 73, 28-34.

…… ……

Place, Date Signature

„Learning without thought is labour lost

thought without learning is perilous"

Confucius

"学而不思则罔，思而不学则殆"

－孔子

Contribution of Other Scientists to This Work

Trinickia caryophylli DSM 50341

The antibacterial activity assays of trinickiabactin were performed by my colleague Dr. Andri Frediansyah.

Burkholderia oklahomensis DSM 21774

In this project, the determination of the stereocenter of the side chain of all hybridobactins was conducted by Ryan Karongo from the Prof. Lämmerhofer group (University of Tübingen). The proteasome inhibition and cell proliferation assays were perfomed by my colleague Dr Nicole Staudt. The isolated glidobactins were kindly provied by Dr. Thomas Böttcher (Department of Chemistry, University of Konstanz).

High Resolution Mass Spectrometry (HRMS)

HRMS measurements were obtained by Dr. Dorothee Wistuba (Department of Mass Spectrometry, Universität Tübingen).

Contents

Publications and Poster

Publications

J Jiao, J Paterson, T Busche, C Rückert, J Kalinowski, D Harwani and H Gross* (2018) Draft Genome Sequence of *Streptomyces* sp. Strain DH-12, a Soilborne Isolate from the Thar Desert with Broad-Spectrum Antibacterial Activity. *Genome Announc.*, 6(9), e00108-18.

J Jiao, J Du, A Frediansyah, G Jahanshah and H Gross* (2020) Structure elucidation and biosynthetic locus of trinickiabactin from the plant pathogenic bacterium *Trinickia caryophylli*. *J. Antibiot*., 73, 28-34. (Selected as Bullet Point on the cover page: Trinickiabactin, an antibacterial lipopeptide siderophore with diazeniumdiolate moieties)

R Karongo, J Jiao, H Gross and M Lämmerhofer* (2021) Direct enantioselective gradient reversed-phase ultra-high performance liquid chromatography-tandem mass spectrometry method for 3-hydroxy alkanoic acids in lipopeptides on immobilized 1.6 μm amylose-based chiral stationary phase. *J. Sep. Sci.*, accepted.

Poster

J. Jiao, N. Aryal, G. Jahanshah and H. Gross. Chemical Exploration of Secondary Metabolites from the Rhizosphere Bacterium *Micromonospora* sp. MW13, presented at International VAAM Workshop 2019: Biology of Bacteria Producing Natural Products. Hans-Knöll-Institut. 15^{th}-17^{th} September 2019, Jena, Germany; Abstract P28.

Abbreviations

°C	degrees Celsius
1D	one dimensional
2D	two dimensional
$[\alpha]_D^T$	specific optical rotation (T = temperature; D = sodium D line (589 nm))
Δ	difference
δ	NMR chemical shift (ppm)
ε	(UV spectroscopy) molar attenuation coefficient
λ	wavelength
μ	micro (10^{-6})
A(domain)	adenylation domain
ACP	Acyl Carrier Protein
AMP	adenosine monophosphate
AT	acetyltransferase
Bcc	*Burkholderia cepacia* complex
BGC	Biosynthetic Gene Cluster
C (domain)	condensation domain
d	(NMR) doublet
dd	(NMR) doublet of doublets
Da	Dalton
DAD	Diode Array Detector
DCl	Deuterium chloride
DEPT	Distortionless Enhancement by Polarisation Transfer
DMSO	dimethyl sulphoxide
E (domain)	epimerization domain
ESI	electrospray ionisation
Fe(II)	ferrous iron
Fe(III)	ferric iron
G	gram
Ga	gallium
HCl	hydrochloric acid
HHA	hydroxyl-hexanoic acid
HMBC	Heteronuclear Multiple Bond Correlation
HOA	hydroxyl-octanoic acid
HR	(MS) high resolution
HSQC	Heteronuclear Single Quantum Coherence
Hz	Hertz
IR	Infrared
J	Spin-spin coupling constant [Hz]
KR	ketoreductase
KS	ketosynthase
L	liter

LC	Liquid Chromatography
LR	(MS) low resolution
Lys	lysine
m/z	mass to charge ratio
mL	milliliter
mM	millimolar
m	(NMR) multiplet
mg	milligram
min	minutes
MeOH	methanol
MIC	Minimum Inhibition Concentration
MHz	Megahertz
MRSA	Methicillin-resistant *Staphylococcus aureus*
MS	Mass Spectroscopy
MS/MS	Tandem Mass Spectrometry
NMR	Nuclear Magnetic Resonance
NOESY	Nuclear Overhauser Effect Spectroscopy
NRPS	Non-Ribosomal Peptide Synthetase
Orn	ornithine
OSMAC	One Strain Many Compounds
ppm	parts per million
pH	potential of hydrogen
PCP	Peptidyl Carrier Protein
PKS	Polyketide Synthase
Ppant	phosphopantetheine
RP	Reversed Phase
s	(NMR) singlet
SAM	S-adenosyl methionine
t	(NMR) triplet
t_R	retention time
T (domain)	thiolation domain
TE (domain)	thioesterase domain
Te (domain)	thioesterase domain
Thr	threonine
TOCSY	Total Correlation Spectroscopy
UV	ultraviolet (spectroscopy)
VIS	visible (spectroscopy)
XU	The concept of exchange units
XUC	The concept of exchange unit condensation

List of Figures

List of Tables

Summary

During the last decade, strains of the *Burkholderia* sensu lato group have turned out to be a promising source of natural products, which exhibit a high structural diversity and exquisite biological activities. The biological and chemical characterization of the secondary metabolites contributed either to the understanding of the ecological context and virulence-mechanisms or to find pharmaceutically active lead structures. Recent genome analyses confirmed, that these strains belong to the group of talented producers and that still numerous compounds await their discovery. Driven by this potential, the focus of this work was put on the screening, isolation and characterization of new and bioactive secondary metabolites from strains of the *Burkholderia* sensu lato group.

The first project stemmed from the plant pathogenic strain *Trinickia caryophylli* DSM 50341, that secreted a novel siderophore. Following upscaled cultivation and chromatographic purification of this siderophore led to the discovery of trinickiabactin. Whole genome sequencing allowed the identification of its biosynthetic gene cluster. The structure of trinickiabactin bears a rare diazeniumdiolate ligand system and was elucidated by a combination of NMR- and MS-spectroscopy and bioinformatics. Furthermore, trinickiabactin was found to be antibacterial towards several Gram-negative bacteria (MIC values ranged from 0.004 to 0.04 mM).

The second project constitutes an investigation of a set of proteosome inhibitors which are produced by *Burkholderia oklahomensis* DSM 21774. The OSMAC-based chemical screening allowed the identification of a new class of compounds that could not be dereplicated. The integration of bioinformatics hinted readily that this class of compounds belongs to the syrbactin class. This led to the successful isolation and structural characterization of four novel syrbactins, which were dubbed hybridobactins A-D, since they represent a recombination of fragments of known syrbactins to give a novel compound. Subsequently, combining Marfey's analysis, chiral LC/MS analysis and bioinformatics, their absolute configuration could be elucidated as well. In proteosome inhibition assays, they exhibited potent activities, especially hybridobactin D, which could compete with the established standard epoxomicin.

The last project was focused on the isolation of a new acybolin congener, which belongs to the cytotoxic bactobolin compound family. Upon upscaling of the fermentation process, the new congener acybolin J was obtained, together with several known bactobolin-related compounds. The structure of acybolin J was enabled by spectroscopic analysis using extensive 1D- and 2D

NMR experiments. Its finding enriched the diversity of acybolins and the comparative analysis of the corresponding gene cluster raised several biosynthetic questions for the future.

Zusammenfassung

Burkholderia sensu lato Stämme haben sich in der letzten Dekade als eine vielversprechende Quelle für Naturstoffe erwiesen. Diese weisen eine hohe strukturelle Diversität und hervorragende biologische Aktivitäten auf. Die chemisch-biologische Charakterisierung von Sekundärmetaboliten trug entweder zum besseren Verständnis der ökologischen Zusammenhänge und Virulenz-Mechanismen bei oder führte zur Entdeckung von pharmazeutisch-verwertbaren Leitstrukturen. Die jüngsten Genomanalysen kommen zu dem gleichen Schluss und bestätigen, dass diese Stämme zur Gruppe der talentierten Produzenten gehört und dass es immer noch zahlreiche chemische Verbindungen zu entdecken gibt. Angesichts dieses hohen Potentials, wurde in der vorliegenden Arbeit der Schwerpunkt auf das Screening nach bzw. die Isolation und Charakterisierung von neuen und biologisch aktiven Naturstoffen von *Burkholderia* sensu lato Stämmen gelegt.

Das erste Projekt hatte den pflanzenpathogenen Stamm *Trinickia caryophylli* DSM 50341 zum Gegenstand, der einen neuartigen Siderophor sekretierte. Nach erfolgter hochskalierter Fermentation und chromatographischer Aufreinigung wurde der Siderophor Trinickiabactin entdeckt. Die Analyse des Gesamt-Genoms erlaubte zudem die Identifikation des biosynthetischen Genclusters. Das Grundgerüst enthält ein seltenes Diazeniumdiolat-Liganden System und wurde mittels einer Kombination von NMR und MS-Spektroskopie sowie bioinformatischen Methoden aufgeklärt. Des Weiteren fiel in Bioassays auf, dass Trinickiabactin eine antibakterielle Wirkung gegenüber Gram-negativen Bakterien besitzt (MHKs variierten je nach Organismus zwischen 0.004 und 0.04 mM).

Das zweite Projekt drehte sich um die Untersuchung von Proteasom-Inhibitoren, die von dem Bakterium *Burkholderia oklahomensis* DSM 21774 generiert wurden. Ein OSMAC-basierter Screening-Ansatz führte hierbei zur Identifikation einer neuen Substanzklasse, die nicht derepliziert werden konnte. Eine weitere bioinformatische Analyse ergab Hinweise, dass die gesuchten Verbindungen der Syrbactin-Gruppe zuzuordnen sind. Dies führte zur erfolgreichen Isolation und Strukturaufklärung von vier neuartigen Syrbactinen, die Hybridobactine A-D genannt wurden, da die Verbindungen Rekombinationen von Strukturfragmenten von bekannten Syrbactinen darstellen. Die absolute Konfiguration der Verbindungen wurde durch die kombinierte Anwendung von Bioinformatik, chiraler LC/MS und der Marfey-Methode erarbeitet. In Proteasom-Inhibitions-Assays zeigten die Substanzen eine potente Wirkung,

insbesondere Hybridobactin D, welches nahezu die gleiche Wirkstärke wie die etablierten Standard-Substanz Epoxomicin aufwies.

Da letzte Projekt hatte die Isolation eines neuen Acybolin-Derivates zum Ziel, die der Gruppe der zytotoxischen Bactoboline zuzuordnen sind. Die Hochskalierung des Fermentations-prozesses ermöglichte dann die Isolation und Aufreinigung des neuen Derivats Acybolin J, zusammen mit zahlreichen bekannten Bactobolinen. Die Strukturaufklärung gelang durch die Anwendung von umfangreichen 1D- und 2D Experimenten. Das Ergebnis bereichert die Diversität der Substanzgruppe und die vergleichende Analyse des zugehörigen Genclusters wirft zahlreiche weiterführende biosynthetische Fragestellungen auf.

1 Introduction

1.1 *Burkholderia* - A Rich Source of Bacterial Natural Products

1.1.1 The Role of Bacterial Natural Products

Natural products have been utilized as an significant source of drugs since ancient times for the treatment of many diseases and illnesses[1]. Especially in the last four decades of the previous century, almost half of the newly approved small molecules were derived from natural products[2]. As one of the most important branches of natural products, the microbe's world received increasing attention, particularly after the discovery-of-the-century wonder drug – penicillin[3], which greatly contributed to the fight against infectious diseases. From then on, a series of excellent bioactive scaffolds from microbes, especially from the bacterial world, were discovered and developed as drugs for the clinical treatment of cancer and infectious diseases[4,5].

So far, among the chemical entity producers of the bacterial community, the gram-positive *Actinobacteria* have been proven as highly talented producers because they offered most of the clinically used drugs in the field of antibiotics, immunosuppressants and anticancer treatment[6]. Nonetheless, recently, gram-negative bacteria have been newly evaluated as an underexplored source of novel biology and chemistry[7]. Some gram-negative bacteria, for example, *Pseudomonas*-, myxobacterial and cyanobacterial species, are deemed to be the most frequent producers, in total producing more than 1,800 bioactive metabolites based on statistical data[8]. For instance, mupirocin isolated from *Pseudomonas fluorescens* already stands in the queue of clinical treatments for superficial methicillin-resistant *Staphylococcus aureus* (MRSA) infections[9]. Based on these facts, a reappraised value of gram-negative bacteria is presented to the natural product scientific community. Within this family, the *Burkholderia* species were found to be the most fascianting, offering quite compelling chemical scaffolds with therapeutic bioactivities as shown in Figure 1-1[10-22].

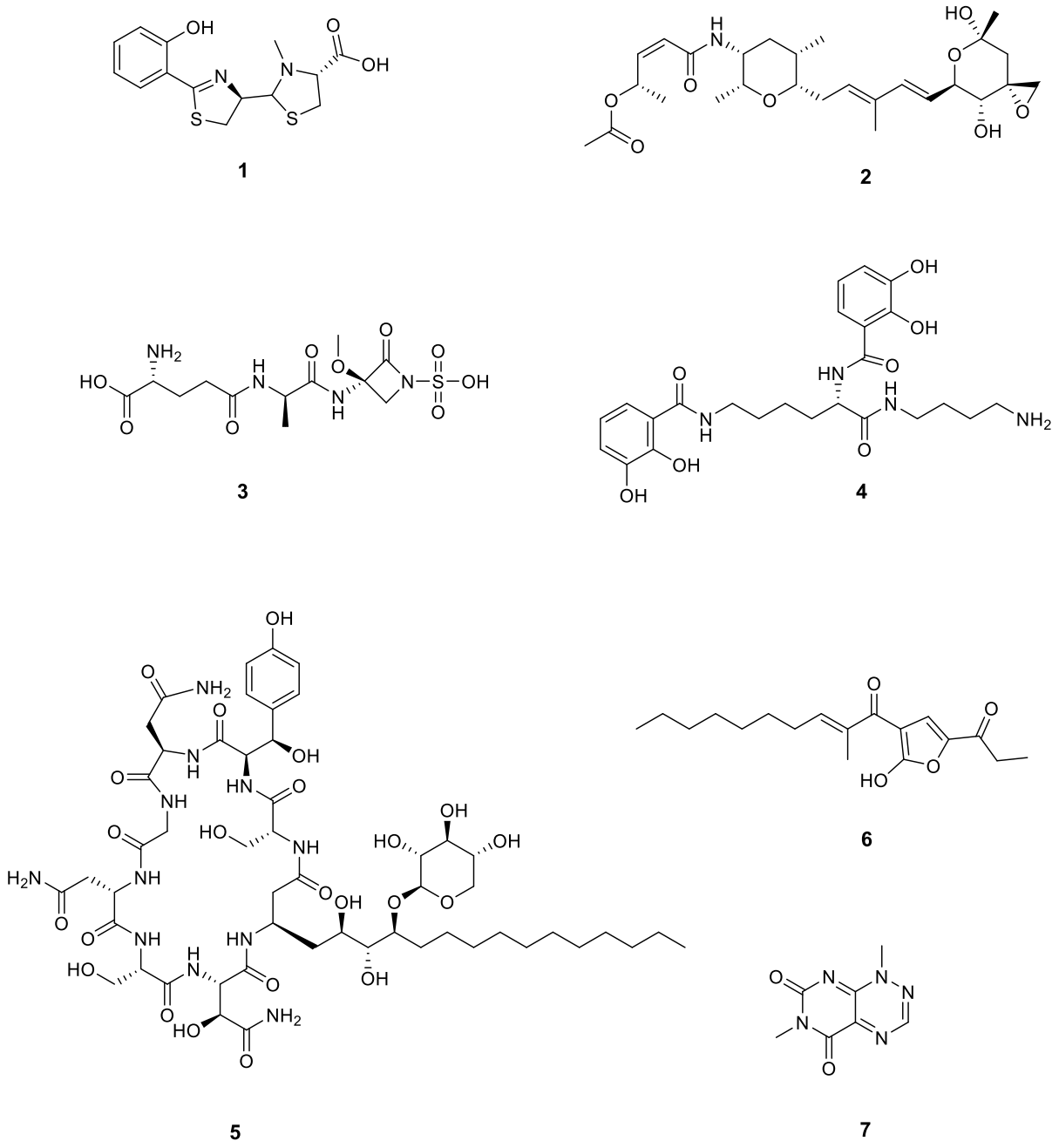

Figure 1-1 Natural products isolated from *Burkholderia* species. Pyochelin (**1**), FR901464 (**2**), sulfazecin (**3**), cepaciachelin (**4**), burkholdine 1213 (**5**), malleilactone (**6**) and toxoflavin (**7**).

Regarding genomic aspects, the unlocking of the bioactive potential of *Burkholderia* has already been initiated. A recent phylogenomic analysis of biosynthetic gene clusters (BGCs) from microbes gave more insight into gram-negative bacterial biosynthetic capabilities, indicating that the genus *Burkholderia* has taken the front position in terms of biosynthetic diversity as shown in Figure 1-2[23]. Intriguingly, the BGC count in the *Burkholderia* genome is only second to that of actinobacteria, higher than those of bacilli, cyanobacteria, myxobacteria,

and fungi. All these relevant research data suggested that gram-negative bacteria, including the genus *Burkholderia*, would be valuable to engage with in terms of natural product discovery.

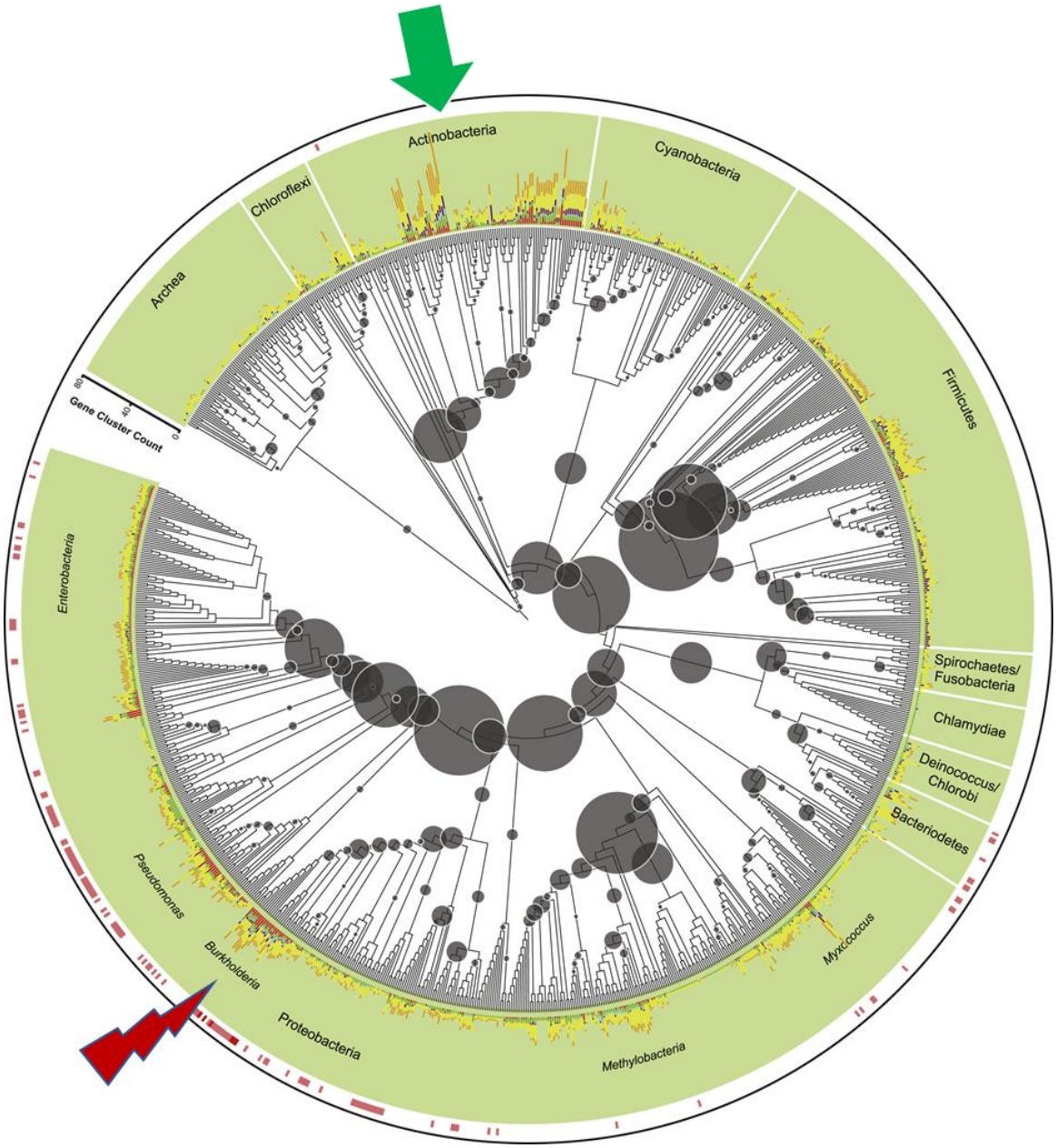

Figure 1-2 Distribution of BGC diversity among all sequenced prokaryotic genomes[23]. The green arrow points to the actinobacterial BGCs, while the red lightning bolt highlights the BGC count of *Burkholderia* bacteria.

1.1.2 The Microbiological Background and Taxonomy of *Burkholderia*

The genus *Burkholderia* is a group of β-proteobacteria. Morphologically, they are straight or slightly curved, non-sporulating rods. They are aerobic gram-negative and motile bacteria with one or more flagella, with the exception of *B. mallei* (Figure 1-3). They have a variable genome size ranging from 2.4 to 11.5 Mb, with high G+C contents varying from 62 to 68%[24-26]. It is not unusual for them to possess multiple replicons which can be defined as chromosomes, and they are rich in insertion sequences. These kinds of features may be the crucial factors in the evolution of the unusual adaptability of this bacterium[27]. As a matter of fact, *Burkholderia* species are able to occupy diverse ecological niches, such as soil, water, the rhizosphere, the phyllosphere and even the respiratory tract of humans[28,29].

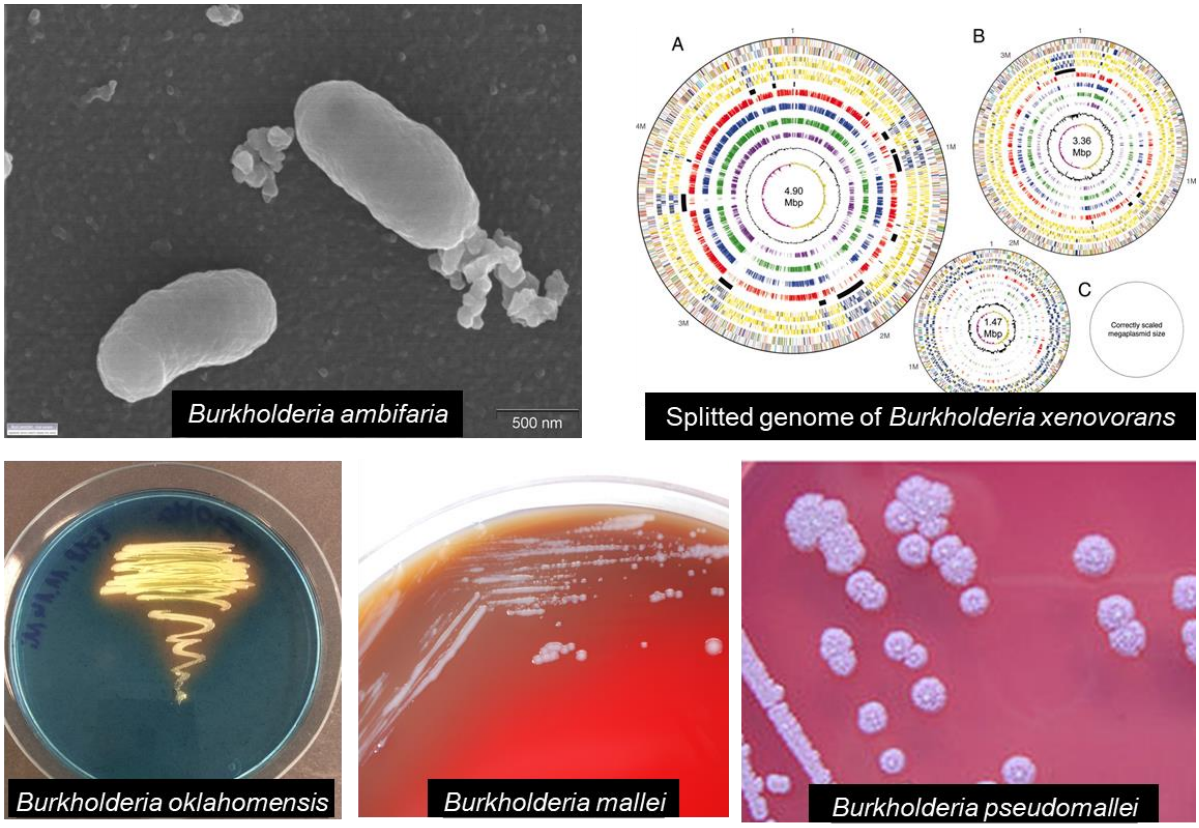

Figure 1-3 *Burkholderia* morphology and distribution of chromosomes[30]. Photo source: Wikipedia, JGI and reference 30.

Burkholderia species were originally described as *Pseudomonas* species in 1950 by Walter H. Burkholder, who firstly reported *Pseudomonas cepacia* as the causative agent for the occurrence of 'sour skin' in onions. Until 1992, Yabuuchi *et al*. named this genus *Burkholderia* to honor the former´s seminal work[31,32]. Among these species, *B. pseudomallei* and *B. mallei* belong to the pathogenic species, which are the causative agents of melioidosis, a serious and

often fatal disease of humans and animals, and glanders, respectively[33]. The other famous group is termed the *Burkholderia cepacia* complex (Bcc). Their members were originally recognized as pathogens of onions, and are now known as an important group of opportunistic human pathogens that can infect cystic fibrosis (CF) or immunocompromised patients as shown in Figure 1-4[34]. However, on the other hand, the Bcc group also exerts some positive environmental effects, such as plant growth promotion and the degradation of a wide variety of compounds, including pollutants.

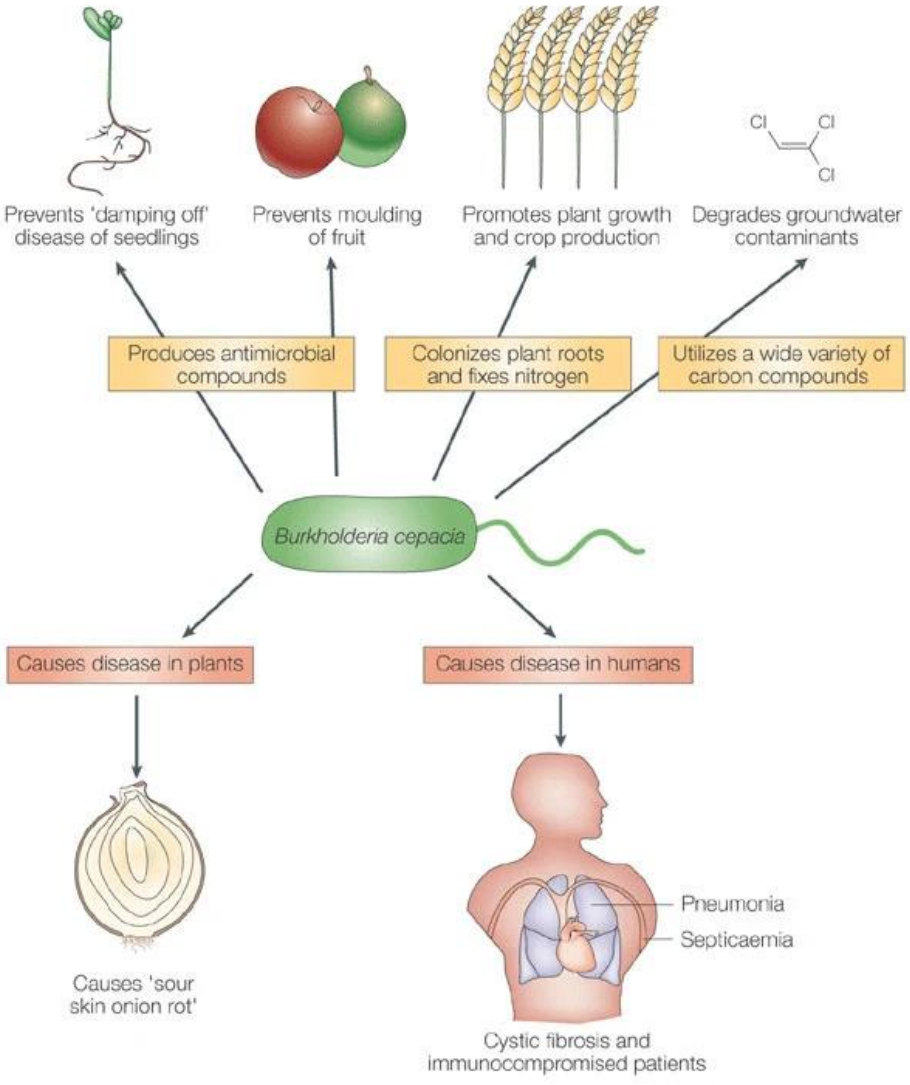

Figure 1-4 Beneficial and detrimental effects of the *Burkholderia cepacia* complex[34].

After the creation of this new genus, several other *Pseudomonas* species were also reclassified as *Burkholderia*, while two of the already named *Burkholderia* species, including *B. picketti* and *B. solanacearum*, were further transferred into the new and distinct genus *Ralstonia*[35,36]. In the following years, *Burkholderia* drew increased attention, as more and more novel species

were isolated and described[37-48], which heavily enriched the diversity of the *Burkholderia* community. To date, this genus consists of more than 100 species. However, with the expanded group numbers within this genus, several taxonomic rearrangements were carried out. In 2005, Payne *et al.* performed 16S rRNA and *recA* gene-based phylogeny analyses, which supported the division of the *Burkholderia* into two clades. One clade included human, animal, and plant pathogens or opportunistic pathogens, while the other consists of plant-beneficial and environmental species[49]. Over the next few years, more major rearrangements and updates in the taxonomy of *Burkholderia* were conducted, and new genera were suggested and divided from *Burkholderia* according to these investigations[50-55]. Thus, the new term "*Burkholderia* sensu lato" was suggested for covering all the six *Burkholderia* related genera, which currently comprise *Burkholderia* sensu stricto, *Caballeronia*, *Paraburkholderia*, *Robbsia*, *Mycetohabitans*, and *Trinickia* as illustrated in Figure 1-5[56]. To avoid confusion, if not specified, the term *Burkholderia* is used to mean *Burkholderia* sensu lato in the following chapters.

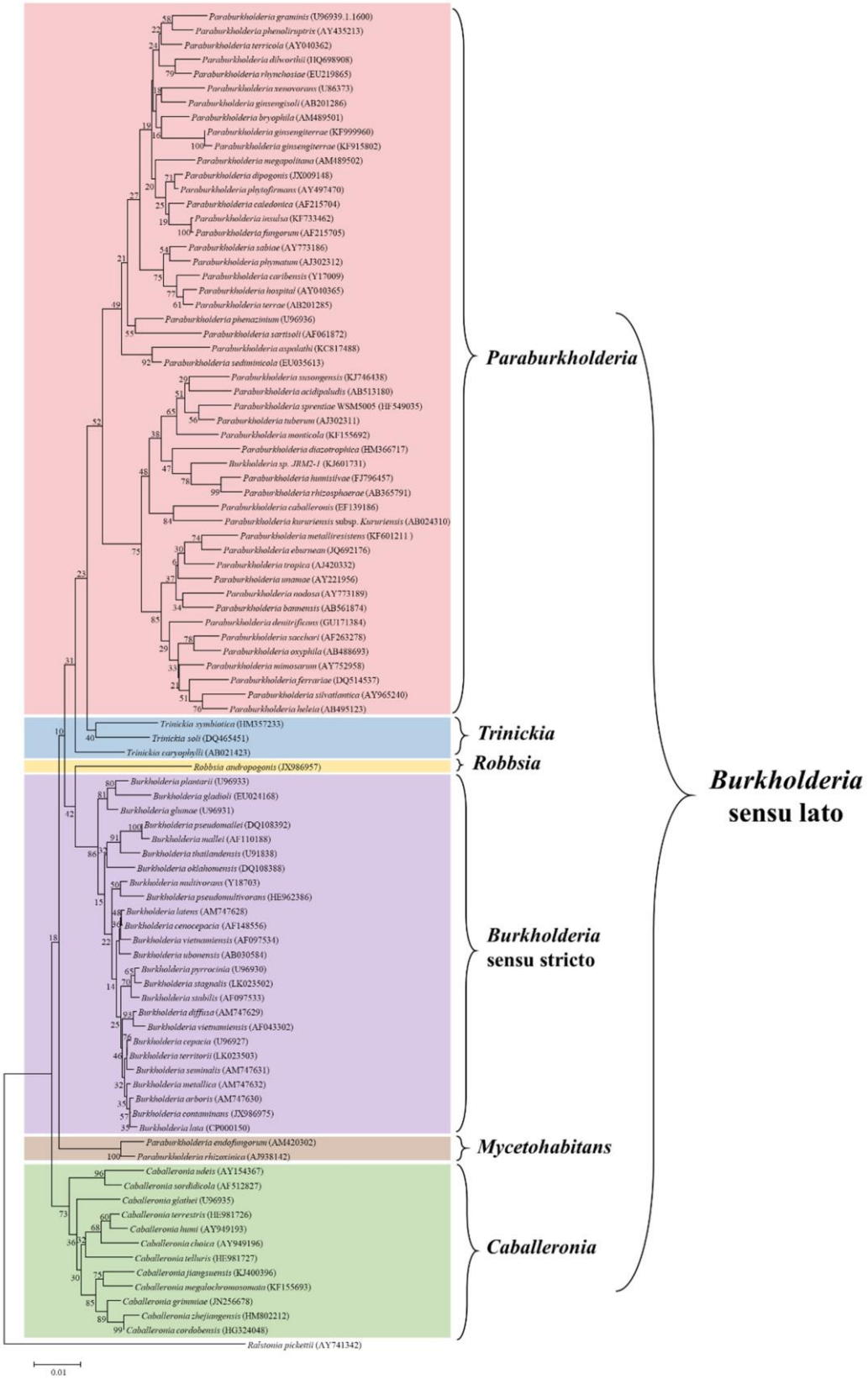

Figure 1-5 Phylogeny of constructed by the neighbor-joining method using 16S rRNA sequences of representative strains from *Burkholderia* related genera[56]. The 16S rRNA sequences were retrieved from the SILVA database (https://www.arb-silva.de/). Species names were corrected based on the current taxonomic positions. The updated genera and their phylogenetic relationships are also shown. *Ralstonia pickettii* (AY741342) was used as an outgroup.

1.1.3 *Burkholderia*: An Attractive and Fruitful Resource for Natural Product Isolation

Burkholderia species are considered to be a new rich source and have received incremental attention from different fields, especially in the natural products area. To date, several reviews focusing on genome mining in *Burkholderia* species gave a comprehensive overview and supported the statement that the genus *Burkholderia* has been found to be a promising source of natural products[7,57-60]. These published findings of the last decade reshaped the chemistry map of *Burkholderia* species. In total, more than 60 structures could be added, and many novel biosynthetic details were unveiled[61].

Recently, more and more research groups moved onto the playground of this attractive secondary metabolite pool. For example, only in 2018, several novel compounds like fragin together with valdiazen (a rare diazeniumdiolate class from nature[62]), icosalides (possessing tandem condensation domains within its biosynthetic pathway[63]) and burriogladins as well as haereogladins (which represent threonine-tagged lipopeptides[64]) were extracted one after the other. From then until now, several other unusual compounds, like gramibactin[65], plantaribactin[66], thailandenes[67], gladiofungin[68] and necroxime[69], were isolated at breakneck speed (Figure 1-6).

More interestingly, in the cases of icosalides and bolagladins, they were published by different groups in parallel, which reflects the intense competition pattern in natural product research of *Burkholderia*[63,70-72]. To a great extent, these explorations led to an explosive scene, in which further accelerated the exposure of *Burkholderia* species in the scientific community.

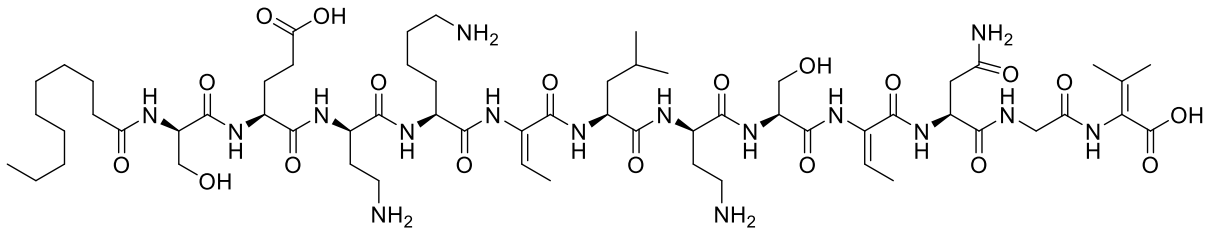

8

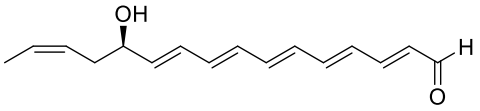

9

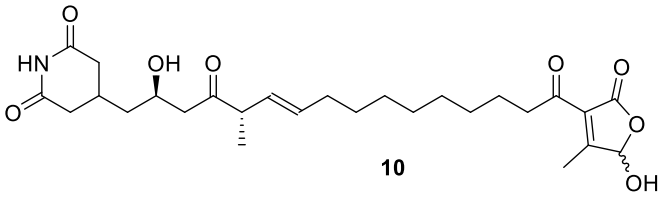

10

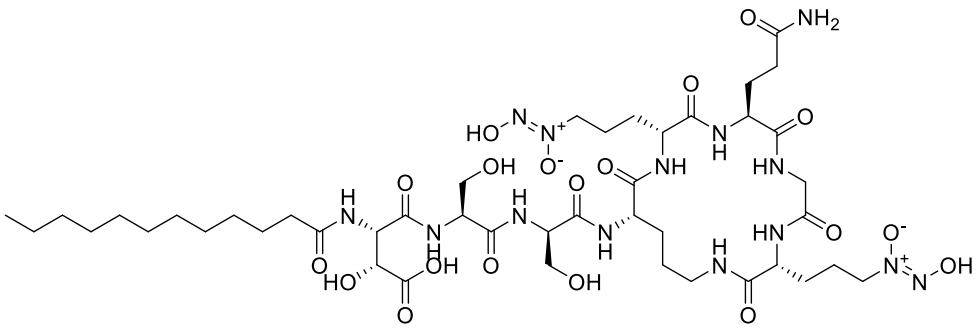

11

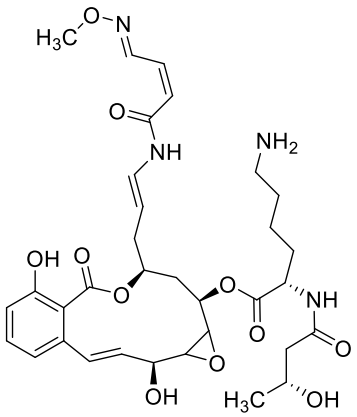

12

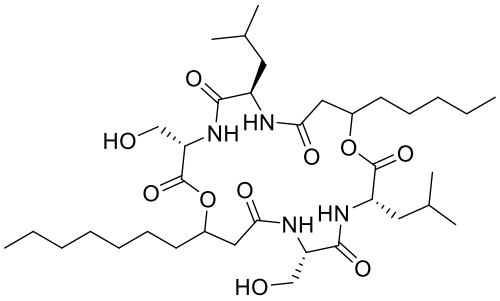

13

Figure 1-6 Recently reported natural products isolated from *Burkholderia* species. Glidopeptin A (**8**), gladiofungin A (**9**), thailandene A (**10**), plantaribactin (**11**), necroxime A (**12**) and icosalide A1 (**13**).

Most notably, the overwhelming majority of the secondary metabolites from *Burkholderia* are of peptidic and polyketidic origin (Figure 1-7). Concerning their bioactivity, most of the metabolites are either antibacterial, antifungal or cytotoxic[61]. So far, most of the compounds from *Burkholderia* species have been discovered by a classic, bioactivity-guided approach based on statistics. However, the majority of the recently discovered compounds were isolated

via genome mining approaches[62-66,68,69]. With the increased number of available sequenced genomes and rapid development of bioinformatic tools, such as AntiSMASH, ClusterFinder, NaPDoS, NRPSPredictor[23,73-75], progressively, more biosynthetic genes are understood. Therefore, it could be predicted that more investigations of *Burkholderia* sensu lato will be genome-driven.

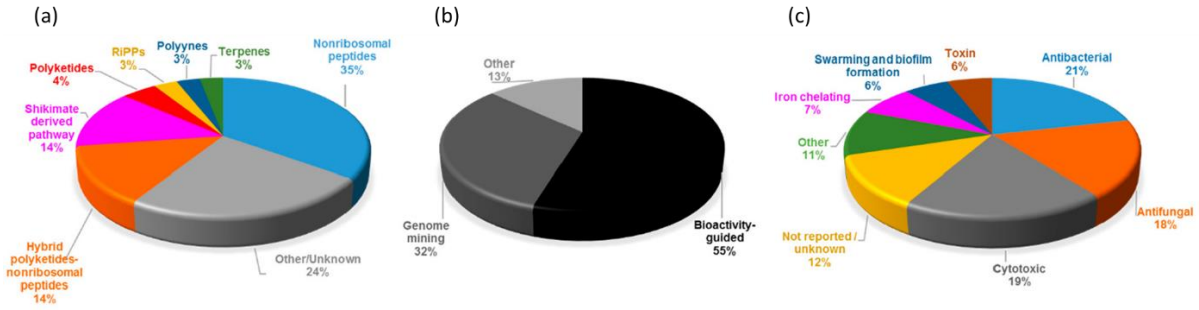

Figure 1-7 Analyses of natural products isolated from *Burkholderia* sensu lato[61]. (a) Pie chart depicting the biosynthetic classes. Compounds belonging to the same structural class (defined as known or expected to be encoded in the same or very similar BGC) were counted as one. The 66 structural classes were then classified into seven biosynthetic classes as shown. (b) Natural product isolation via different approaches. "Other" includes structure-guided isolation. (c) Reported bioactivity of the reported compounds from *Burkholderia* sensu lato (adapted from reference 61).

1.2 Genome Mining Approaches to Access the *Burkholderia* Metabolic Pool

In the early 2000s, with the sequencing of the first genomes of *Streptomyces coelicolor* [76] and *Streptomyces avermitilis*[77], it became apparent that there is a much higher capacity to produce secondary metabolites is given, than formerly anticipated. This initiated a new idea of digging for microbial metabolites with the help of genomic data, which then became a popular discovery approach and which was coined "microbial genome mining"[78]. In the case of genome mining, the microbial whole genome sequencing data is analyzed by bioinformatics to search for new chemical features[79]. With the dropping price of genome sequencing, more available sequencing data, and the rapidly developed bioinformatic methods, this approach has been integrated deeply into the current research process. In this scenario, a huge number of novel secondary metabolites, together with their biosynthetic pathways, have been successfully elucidated. Thus, it is of utmost importance to have a comprehensive understanding of biosynthetic pathways, in order to enter the next stage of the *Burkholderia* metabolome world.

Given that the *Burkholderia* metabolite pool is quite rich in peptidic and polyketidic products, the thiothemplate-based machineries producing these intriguing compounds shall be highlighted in the following chapter.

1.2.1 Nonribosomal Peptide Synthetases

Several peptides produced by *Burkholderia* strains are formed by an exceptional machinery, termed non-ribosomal peptide synthetase (NRPS). In contrast to the regular ribosomal peptides synthetase, NRPSs ultilize not only the 20 proteinogenic amino acids, but also employ more than 500 nonproteinogenic amino acids, fatty acids, and α-hydroxy acids as building blocks [80]. Thus, they can generate an extended chemical space with high structural diversity. Indeed, there are already some derived candidates, such as the hepatotoxic cyclopeptide rhizonin A, the cytotoxic rhizomide A and the selective Gq-signaling inhibitor FR900359 as shown in Figure 1-8[29,81-83].

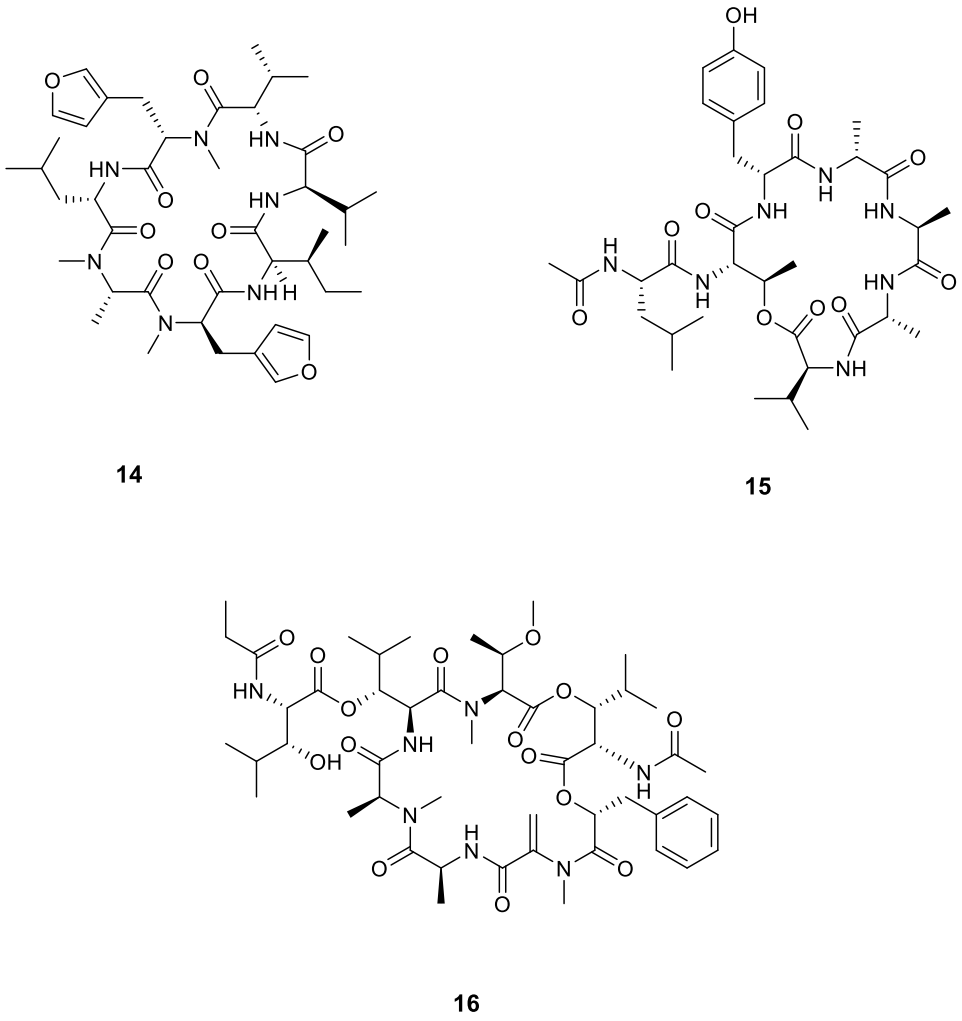

Figure 1-8 Structures of selected nonribosomal peptides produced by *Burkholderia*. Rhizonin A (**14**), rhizomide A (**15**) and FR900359 (**16**).

Generally, NRPS enzymes act together as an assembly line consisting of multiple modules that catalyze the integration of single amino acids into a growing peptide chain regulated by the collinearity rule[84]. Normally, each NRPS module typically comprises three domains, namely an adenylation (A), a thiolation (T) and a condensation (C) domain as reflected in Figure 1-9.

The A domain, with a size of around 60 kDa, consists of an N-terminal subdomain and a small C-terminal subdomain. It contains a hydrophobic active site for binding the amino acid and ATP substrates. Since the C-terminal subdomain is relatively flexible, its rotation around 140 ° to the large N-terminal subdomain led to two distinct conformational states that are specific for the adenylation and thiolation, respectively[85]. In silico studies revealed the power of the A domain code in predicting the substrate specificity of uncharacterized A domains[86]. Since bacterial A domains are highly conserved structures, their sequences can generally be used to predict the amino acid sequence of the NRPS products[87].

The small T domain (also called **P**eptidyl **C**arrier **P**rotein domain, PCP), with a size of about 10 kDa, contains a highly conserved serine residue which could be modified by a phosphopantetheine transferase (Ppant), following the transition from the apo- to the holo-form, which allows the thiolation loading steps[88].

The third essential NRPS domain, is the C domain with a size of about 45 kDa, which performs the peptide bond formation of two adjacent activated amino acids. The C domain is comprised of two related subdomains of the CAT (chloramphenicol acetyl transferase) fold, a conserved active site motive that could be found at the interface. This active site is reached by the Ppant arm through the interface to transfer the activated amino acid substrate from upstream to dock to the acceptor site. Furthermore, C domains are also selective in terms of stereochemistry, with $^{L}C_{L}$ domains connecting two L-amino acids, and $^{D}C_{L}$ domains fusing an upstream D-amino acid with a downstream L-amino acid. Further, the $C_{starter}$ domain catalyzes the condensation of a (β-hydroxy) fatty acid and the first activated amino acid, which represent a special label for a lipopeptide biosynthesis[89].

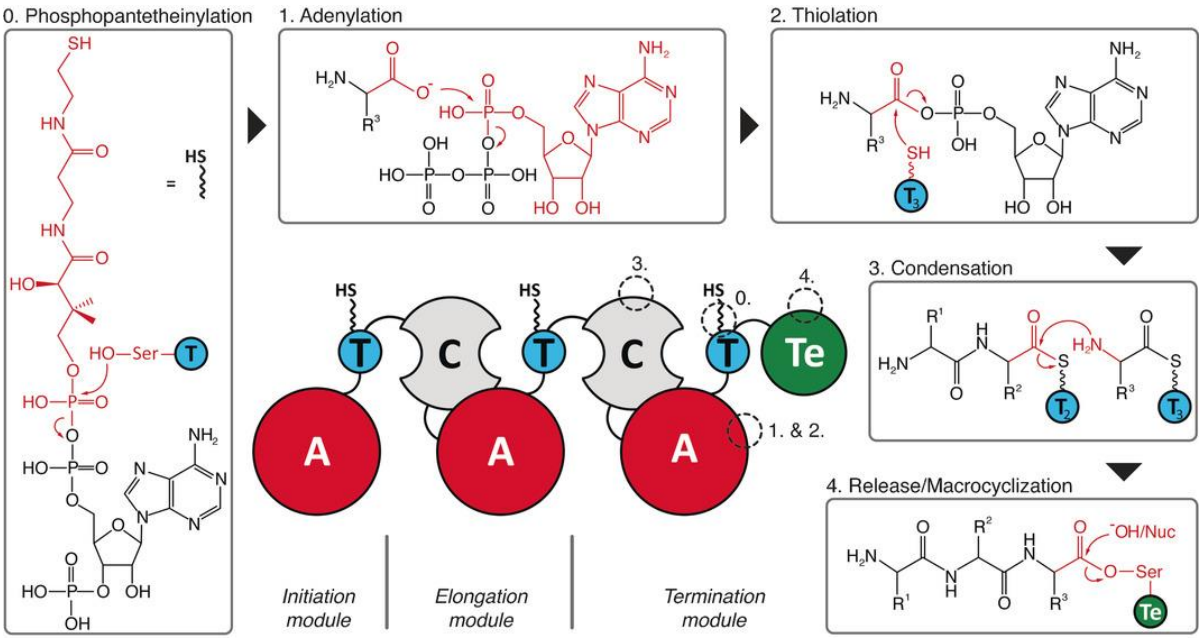

Figure 1-9 Domain arrangement of bacterial NRPSs, including the involved reactions[90]. 0) Phosphopantetheinylation: The Ppant tail is attached to conserved serine residue in the T-domain. 1) The amino acid is selected and adenylated by the A domain and generates an aminoacyl-AMP moiety. 2) Thiolation: The activated amino acid is attached to the Ppant of the holo-T domain. 3) The C domain combined the activated amino acid to the previous amino acid or the growing peptide attaches to the upstream module to produce an amide bond. 4) The Te domain releases the peptide chain through hydrolysis or macrocyclization. R1, R2 and R3 refer to the amino acid residues selected by A domains A: adenylation, C: condensation, T: thiolation, Te: Thioesterase (adapted from reference 90).

To terminate the NRPS assembly line, the thioesterase (Te) domain is normally required. Thioesterase domains are approximately 30 kD in size and act as either hydrolases or as cyclases, where they can catalyze cleavage of the assembled peptide product from the T domain in the last module[84].

Briefly, the A-domain determines which amino acid should be selected for incorporation into the growing peptide chain. First of all, the selected amino acid monomer is activated by using ATP and then loaded onto the T domain next to it. Then the T domain will transfer the activated amino acid to the C domain. Subsequently, the C domain will condensate the received amino acids both from upstream and downstream modules to generate the amide bond until at the last NRPS domain, after condensation, the growing peptide chain will be released through hydrolysis or macrocyclization as reflected in Figure 1-9.

Apart from these three core domains (A, T and C), further domains such as epimerization domains (E) are existant, which are responsible for the conversion of regular L- amino acids into the corresponding D-configuration. Further specific domains including heterocyclization (Cy), formylation (F), methylation (Mt) and oxidation (Ox) domains play different roles for modifications, which could also lead to the chemical diversity of the peptides in this scenario[84,90-92].

In the classical definition of NRPS modules, the C-A-T domains are considered a standard structural unit[87]. Within the framework of a NRPS reprogrammng study, the Bode group reported a new concept for the modification of NRPSs that uses differently defined exchange units (XUs, A-T-C or A-T-C/E domains are defined as XUs) and not modules as functional units (Figure 1-10). This allows up to five XUs from four different natural NRPSs to be assembled, resulting functional de novo NRPSs to synthesize novel peptides[93]. Due to the limitation of the downstream C domain specificities, a further complemented XUC concept was developed. Based on this new concept, $C_{Acceptor}$-A-T-$C_{Donator}$ (XUC) units represent a self-contained active unit for catalytic activity, without interfering in major domain-domain interfaces/interactions during the NRPS catalytic cycle[94]. The generation of random natural-peptide-like peptide libaries for bioactivity screening could also be performed, which will inspire the further bioengineering work and facilitate the generation of more diverse peptide natural products in future.

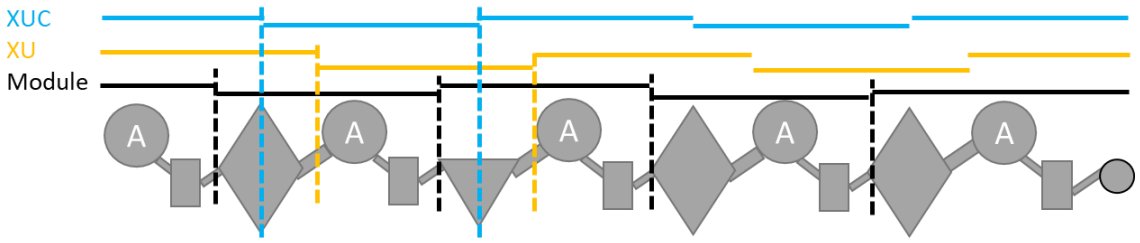

Figure 1-10 A schematic representation of a fictional NRPS assembly line with modules, XUs and the XUCs highlighted[94]. For domain assignment the following symbols are used: A, adenylation domain, large circles; T, thiolation domain, rectangle; C, condensation domain, triangle; C/E, dual condensation/epimerization domain, diamond; Te, thioesterase domain, C-terminal small circle. XU, A-T-C swapping strategy, denoted as the concept of exchange units, XUC, the concept of exchange unit condensation domain (adapted from reference 94).

1.2.2 Polyketide Synthases

Polyketide synthases (PKSs) are another class of multifunctional enzymes, which are responsible for the biosynthesis of various natural products. These PKS assembly lines are widely found in nature, and especially well studied in microbes including bacteria. Numerous secondary metabolites were produced via the complex PKS machinery and some of them even play important roles in clinical applications. Prominent examples of PKS-products from *Burkholderia* are the antibacterial agent gladiolin, the respiratory toxin bongkrekic acid and the antibacterial lagriene (Figure 1-11)[95-97].

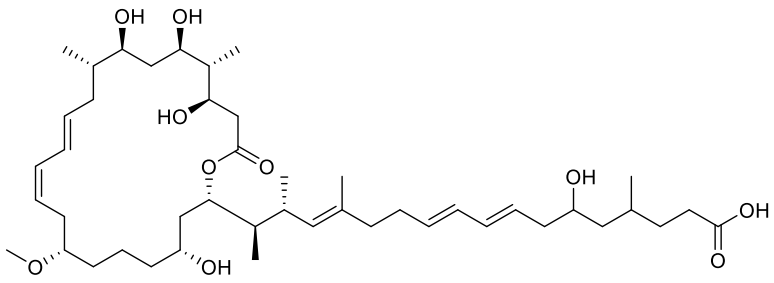

17

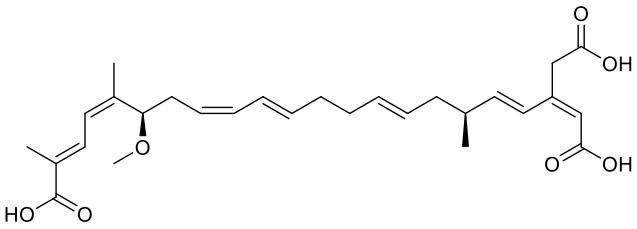

18

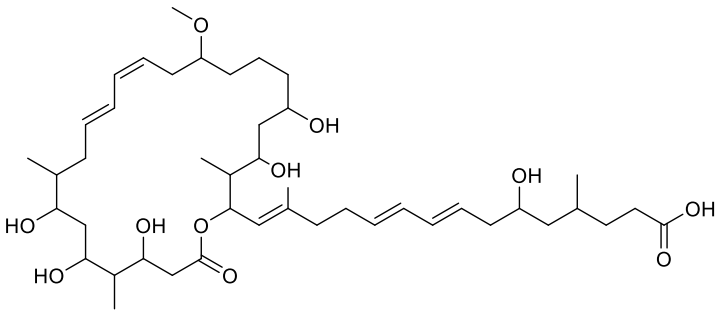

19

Figure 1-11 Representative polyketide structures produced by *Burkholderia*. Gladiolin (**17**), bongkrekic acid (**18**) and lagriene (**19**).

To date, three types of PKSs have been classified so. Type I PKSs are multifunctional proteins consisting of modularized domains, and each module harbors a set of distinct, non-iteratively

acting domains that could catalyze one cycle of polyketide chain elongation. In comparison to type I PKSs, type II PKSs are also multienzyme complexes, but carry a single set of catalytic domains, which act iteratively. Type III PKSs, also known as simpler chalcone synthase-like enzymes, function iteratively and catalyze the formation of the product within a single active site[98].

As a prototypical Type I PKS assembly line, the erythromycin PKS biosynthesis is usually exemplified as a textbook model to understand their mechanism[99]. Within the multienzyme, each module contains at least three essential domains: the ketosynthase (KS) domain, the acyltransferase (AT) domain and the acyl carrier protein (ACP) domain, except the di-domain containing loading module. In contrast to this type of PKS, an unexpected multimodular PKS type was also discovered. These enzymes lacked the AT domain, however, a freestanding AT domain donated the building blocks during the biosynthsis instead. Hence, the new terms *cis*-AT PKS and the *trans*-AT PKS were given to the former and the latter were given, respectively, as seen in Figure 1-12.

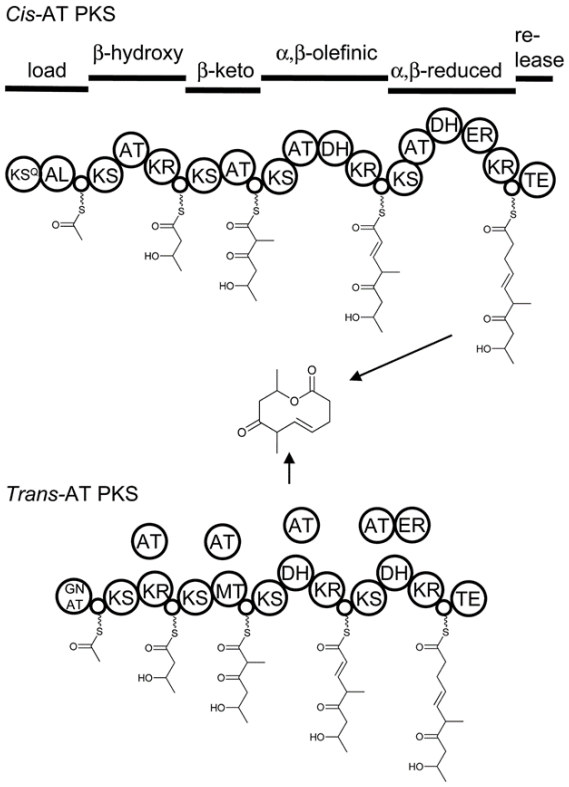

Figure 1-12 Biosynthesis of a fictional complex polyketide by a textbook (*cis*-AT) PKS and a *trans*-AT PKS[100]**.** The location of modules is shown above in the *cis*-AT PKS. For the *cis*- AT PKS, the methyl group was generated either by an incorporated methylmalonyl-CoA, selected by the corresponding AT domain or introduced by MT-catalyzed α-methylation. For the *trans*-AT PKS, the architecture can differ substantially from the one shown. KS^Q: decarboxylating KS, GNAT: acetyl-loading AT of the GCN5-related N-acetyl transferase superfamily. The circles represent ACP domains.

On closer inspection of these modular domains in *cis*-AT PKS, the ACP is post-translationally equipped with a phosphopantetheinyl (Ppant) arm by a Ppant transferase (PPTase). The KS takes over the growing polyketide chain from the ACP of the upstream module, while the AT domain captures an α-carboxyacyl extender unit via trans-esterification from an optional acyl-CoA metabolite onto the ACP. Then, the KS catalyzes a decarboxylative Claisen-like condensation between the polyketide chain and the extender unit[101]. Before being transferred onto the next module, the ACP-tethered β-ketothioester intermediate can be further modified by additional domains, such as a ketoreductase (KR) domain, converting the β-keto function to a hydroxylgroup, a dehydratase (DH) domain, which removes water to generate olefinic moieties, and an enoylreductase (ER) domain, which reduces double bonds to a saturated intermediate, or some other functionality could be introduced as well. The TE domain, located in the last module, catalyzes the off-loading by hydrolysis or macrocyclization[100]. In comparison to the *cis*-AT PKS, the AT domain in *trans*-AT PKS is seperately located outside of the module and the ACP domains are loaded with malonyl units in trans by interatively acting AT domains.

1.2.3 NRPS-PKS Hybrid Systems

After thousands of years of bacterial evolution, the equipment of NRPS-PKS genes and their encoded enzymes give them more possibilities of synthesizing numerous diverse beneficial metabolites. NRPSs and PKSs share a similar strategy for the biosynthesis of two distinct classes of natural products. Both systems not only have well-organized modules, but also use carrier proteins (PCP for NRPS and ACP for PKS) to tether the growing chain. Both PCP and ACP are posttranslationally modified by a 4'-phosphopantetheine group, which is catalyzed by a family of 4'-phosphopantetheinyl transferases (PPTases). Furthermore, if they reach the final full length, the peptide or polyketide product will be released from the corresponding assembly line by a thioesterase (TE) domain[102]. Thus, they can interact with each other and form a combined assembly line.

Generally, two types of NRPS-PKS hybrid system can be distinguished. If the NRPS module is upstream of the PKS module, this combination will generate a C-C bond formation, while the C-N bond will be formed if the NRPS module is downstream of the PKS module as shown in Figure 1-13.

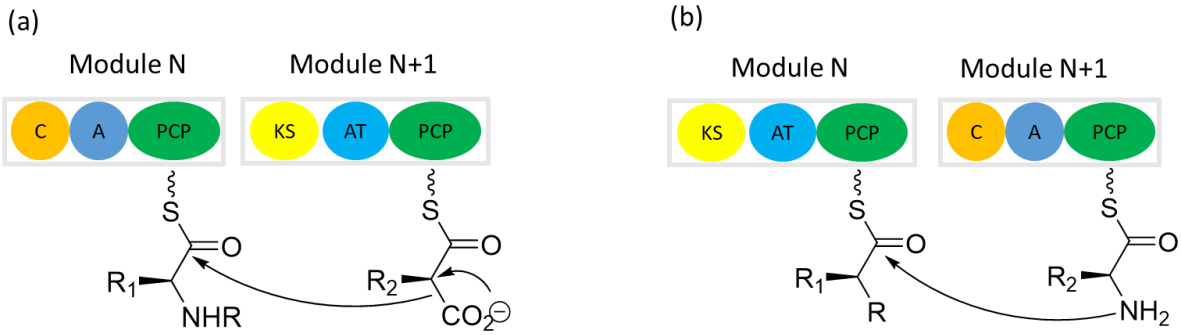

Figure 1-13 Modular organization of hybrid NRPS-PKS and PKS-NRPS[102]. (a) C-C bond formation for hybrid peptide-polyketide biosynthesis catalyzed by a hypothetical NRPS-PKS hybrid. (b) C-N bond formation for hybrid polyketide-peptide biosynthesis.

Since the first elucidation of a hybrid megasynthase in the bleomycin biosynthetic pathway[103], more and more hybrid compounds were later discovered. Commonly, these pathways often contain an impressive biosynthetic machinery due to the hybridization. Structurally, they are derived from amino acids and short carboxylic acids through a rational combination. Being a rich source of NRPS-PKS natural products, *Burkholderia* species have delivered plentiful compounds of this class. Many compounds showed a good prospect in drug discovery[104-107], for example, the cytotoxic thailanstatin A, a mRNA splicing inhibitor, the antibiotically active compounds thailandamide A and enacyloxin IIa as illustrated in Figure 1-14.

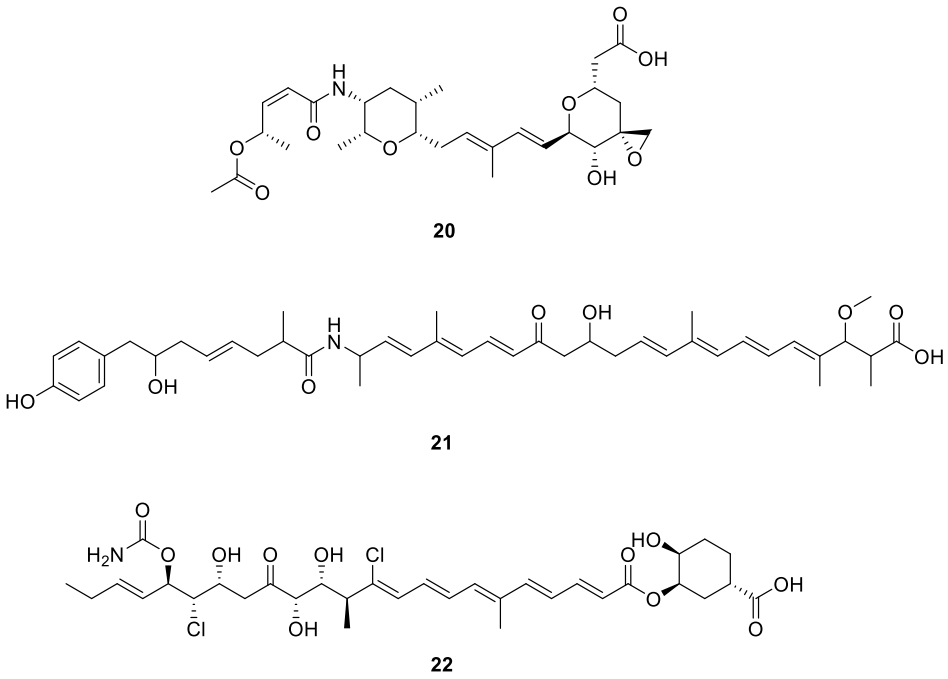

Figure 1-14 NPRS-PKS hybrid natural products isolated from *Burkholderia* species. Thailanstatin A (**20**), thailandamide A (**21**) and enacyloxin IIa (**22**).

2 Aim of the Present Study

As discussed in the introduction chapter, because *Burkholderia* sensu lato represent prolific producers of novel compounds with ingenious scaffolds, an intensive investigation of our collected *Burkholderia* strain library is worthwhile to conduct, aiming to discover some potent bioactive secondary metabolites.

First and foremost, the collected bacteria should be evaluated with multiple approaches to priorize some candidate strains for further investigation. To satisfy this purpose, chemical pre-screening efforts under genomic guidance will be utilized.

Once the detected target compounds produced by the prioritized strains are bioinformatically confirmed, the strain will be cultivated in the most productive medium on a large scale. Then, the crude extracts will be generated via suitable extraction procedures based on the chemical properties of target compounds. Subsequently, the targeted compound will be fractionated and isolated using various chromatographic methods. In parallel, LC-MS investigations will also be integrated to monitor the whole procedure. The target compounds of interest will be structurally elucidated using a set of analytical methods including 1D-, and 2D-NMR, in addition to HR-MS analysis.

Given that the bacterial secondary metabolites often appear with novel bioactivity in a high frequency, and later may serve as new lead structures for new drugs, the isolated new compounds will be tested for biological activities, such as antibacterial, antifungal, antitumor or other specific assays depending on their chemical scaffolds.

3 Materials and Methods

3.1 Materials

3.1.1 Chemicals and Auxiliary Materials

Table 3-1 Chemicals utilized in the studies.

Chemical name	Supplier
Methanol for HPLC	Merck
Methanol for LC-MS	TH. GEYER
Acetonitrile for HPLC	Fisher Chemical
Acetonitrile for LC-MS	TH. GEYER
Butan-1-ol	Fisher Chemical
Sephadex™ LH-20	GE Healthcare
Amberlite® XAD-16N	Sigma
Ethyl acetate	Chemical dispensary (Bulk material)
Formic acid	Sigma Aldrich
Trifluoroacetic acid	Sigma Aldrich
Gallium(III) sulfate	Sigma Aldrich
Marfey's Reagent (FDAA)	Thermo Fischer
Potato Dextrose Broth	Becton Dickinson
(±)-3-hydroxy-hexanoic (octanoic) acid	Sigma Aldrich
DMSO-d_6	Sigma Aldrich
Deuterium oxide (D_2O)	Merck
Methanol-d_4	Sigma Aldrich
DMF-d_7	Sigma Aldrich
Aceton-d_6	Sigma Aldrich
Pyridin-d_5	Sigma Aldrich
Dichlormethan-d_2	Eurisotop

Table 3-2 Auxiliary materials.

Materials	Supplier
Eppendorf tubes (20/200/1500 µl)	Systec
Falcon tubes (50/15 mL)	Eppendorf
Filter papers (MN 615 Ø55mm)	MACHEREY-NAGEL
Filter papers (MN 615 1/4 Ø320mm)	MACHEREY-NAGEL
Syringe (2.5 mL, 250/100 µl)	HAMILTON

3.1.2 Medium Recipes

Table 3-3 Modified M9 medium.

Ingredients	Composition	
5×salt solution	200 mL/L	Na_2HPO_4 33.9 g/L (Merck)
		KH_2PO_4 15 g/L (Sigma Aldrich)
		NH_4Cl 5 g/L (AppliChem)
		NaCl 2.5 g/L (Sigma Aldrich)
		MilliQ Water added up to 1L
1M $MgSO_4$	2 mL/L	$MgSO_4 \cdot 7H_2O$ 246.5 g/L (AppliChem)
		MilliQ Water added up to 1L
20% Glucose	25 mL/L	Glucose 200 g/L (Merck)
		MilliQ Water added up to 1L
10% Casamino acid	10 mL/L	Casamino acid 100 g/L (MP Biomedicals)
1000×TES solution	250 µL/L	$ZnSO_4 \cdot 7H_2O$ 0.1 g/L (AppliChem)
		H_3BO_3 0.1 g/L (Merck)
		$MnSO_4 \cdot 4H_2O$ 0.03 g/L (Alfa Aesar)
		$CaCl_2 \cdot 2H_2O$ 0.02 g/L (Carl Roth)
		$CuSO_4$ 0.004 g/L (AppliChem)
		MilliQ Water added up to 1L
1M $CaCl_2$	100 µL/L	$CaCl_2 \cdot 2H_2O$ 147 g/L (Carl Roth)
		MilliQ Water added up to 1L
MilliQ Water	add up to 1L	

Table 3-4 SRM_{HG} Medium.

Ingredients	Composition	Supplier
L-Histidine	4 g/L	Sigma Aldrich
$MgSO_4.7H_2O$	197.1 mg/L	AppliChem
KH_2PO_4	0.8 g/L	Sigma Aldrich
K_2HPO_4	0.8 g/L	Sigma Aldrich
Dissolve in 900 mL water		
$FeCl_3$	1.6 mg/L	ROTH
Glucose	10 g/L	Sigma
Fructose	1 g/L	Sigma
Arbutin	27 mg/L	Sigma
Dissolve in 100 mL water, sterile filtrated into the 900 mL solutions described above		

Table 3-5 LB Medium.

Ingredients	Composition	Supplier
Tryptone	10 g/L	Becton Dickinson
Yeast Extract	10 g/L	Becton Dickinson
NaCl	10 g/L	Sigma Aldrich
(Agar)*	(15 g/L)	Sigma Aldrich
MilliQ Water	add up to 1L	PURELAB

*Agar is only added for LB medium agar plate preparation

Table 3-6 CPG medium.

Ingredients	Composition	Supplier
Casamino Acid	0.5 g/L	MP Biomedicals
Peptone	5 g/L	Becton Dickinson
Glucose	5 g/L	Merck
MilliQ Water	add up to 1L	PURELAB

Table 3-7 King´s B medium.

Ingredients	Composition	Supplier
Proteose Peptone	20 g/L	Becton Dickinson
Glycerol	15 g/L	Sigma-Aldrich
K_2HPO_4	1.5 g/L	Sigma Aldrich
$MgSO_4 \cdot 7H_2O$	1.5 g/L	AppliChem
MilliQ Water	add up to 1L	PURELAB

Table 3-8 YM medium.

Ingredients	Composition	Supplier
Yeast Extract	2 g/L	Becton Dickinson
Malt Extract	5 g/L	Sigma Aldrich
Glucose	2 g/L	Merck
MilliQ Water	add up to 1L	PURELAB

Table 3-9 Modified TSB medium.

Ingredients	Composition	Supplier
Tryptic soy broth	15 g/L	Becton Dickinson
Sucrose	2 g/L	Sigma Aldrich
K_2HPO_4	2.5 g/L	Merck
NH_4Cl	5 g/L	AppliChem
MilliQ Water	add up to 1L	PURELAB

Table 3-10 Nutrient broth medium.

Ingredients	Composition	Supplier
Glucose	1 g/L	Sigma-Aldrich
Pepton	15 g/L	Becton Dickinson
NaCl	6 g/L	Sigma Aldrich
Yeast Extract	3 g/L	Becton Dickinson
MilliQ Water	add up to 1L	PURELAB

Table 3-11 Modified Pharmamedia.

Ingredients	Composition	Supplier
Glycerol	40 g/L	Sigma-Aldrich
NZ-case	5 g/L	Fluka
Pharmamedia	20 g/L	AMD
$CaCO_3$	5 g/L	CHEMSOLUTE®
MilliQ Water	add up to 1L	PURELAB

Table 3-12 DMBg medium.

Ingredients	Composition	Supplier
Minimal broth Davis	10.6 g/L	Becton Dickinson
Glycerol	1.83 mL	Sigma-Aldrich
MilliQ Water	add up to 1L	PURELAB

3.1.3 Bacterial Strains

Table 3-13 The investigated strains and their strain numbers.

Organism	Strain No.
Paraburkholderia phenazinium	DSM 10684
Paraburkholderia caribensis	DSM 13236
Paraburkholderia fungorum	DSM 17061
Paraburkholderia phymatum	DSM 17167
Paraburkholderia unamae	DSM 17197
Paraburkholderia xenovorans	DSM 17367
Paraburkholderia ferrariae	DSM 18251
Paraburkholderia mimosarum	DSM 21841
Paraburkholderia caledonica	LMG 19076
Paraburkholderia phytofirmans	LMG 22487
Paraburkholderia silvatlantica	LMG 23149
Paraburkholderia tuberum	LMG 21444
Paraburkholderia unamae	LMG 22722
Burkholderia glumae	DSM 9512
Burkholderia glumae	ICMP 3729
Burkholderia cenocepacia	K56-2
Burkholderia cepacia	JKB9
Burkholderia ambifaria	DSM 16087
Burkholderia ubonensis	MSMB1189WGS
Burkholderia oklahomensis	DSM 21774
Trinickia caryophylli	DSM 50341

All the strains involved in this study were obtained either from the DSMZ - German Collection of Microorganisms and Cell Cultures GmbH, Braunschweig, Germany, from the BCCM/LMG-Belgian Coordinated Collections of Microorganisms, from the ATCC - American Type Culture Collection, Manassas, USA or from the ICMP - International Collection of Microorganisms from Plants, New Zealand and treated according to the given instructions.

The strains *Burkholderia cenocepacia* K56-2 and *Burkholderia cepacia* JKB9 were provided by Prof. Leo Eberl (University of Zurich) and Prof. Jae-Ho Shin (Kyungpook National University), respectively. *Burkholderia ubonensis* MSMB1189WGS was provied by Menzies School of Health Research (Australia).

For antibacterial assays, the reference strain *E. coli* DH5-α was purchased from Stratagene, while the strain *Yersinia pseudotuberculosis* YPIII was kindly provided by Prof. P. Dersch (Institute of Infectiology, University of Münster).

Table 3-14 Employed instruments for the studies.

Instruments	**Supplier**
Scale (2200 g, 10 mg)	AND Company
Special accuracy weighing scale (BP210D)	Sartorius
Autoclave	Systec VX-150
Clean bench (safe 2020)	Thermo
Incubator	Memmert
Shaker for pre-cultivation	VWR
Shaker for large scale cultivation	Infors HT
Centrifuge	Thermo
HPLC	Waters
LC-MS	Agilent, AB SCIEX
Vacuum freeze dryer (Alpha 3-4 LSC basic)	Martin Christ
NMR	Bruker
Lab water purifier	Elga
Rotary evaporator	Heidolph
Vacuum pump	Welch
Unichiller	Huber
Sonicator	Bandelin

3.2 Methods

3.2.1 Cultivation Methods

3.2.1.1 Preculture Preparation

20 µL bacterial cryoculture was inoculated on an LB medium agar plate with streaking and then grown in the inoculator at 30 ℃ for 3 days. After that, a single colony of *Burkholderia* strain from the LB medium agar plate was inoculated in a falcon tube containing 15 mL of LB medium and the pre-cultivation was carried out on a shaker at 30 ℃ and 220 rpm for 24 hours. This applied for all the *Burkholderia* strains involved in this study.

3.2.1.2 Cultivation of Selected Strains for Screening Using Different Media

A 300 mL Erlenmeyer flask containing 100 mL of used media was inoculated with 1 mL of the overnight preculture of the selected strains and subsequently grown on a shaker at 30 ℃ and 120 rpm for 4 days. In parallel, 100 mL of each used medium was prepared as control and treated in the same way, which later served as a control for further analytical work. The same method applied for different media including modified M9, SRM_{HG}, modified TSB, CPG, NB, LB, YM, modified Pharmamedia, DMBg, and King´s B during screening cultivation.

3.2.1.3 Upscaled Cultivation in MM9 Medium for Target Compounds Isolation

Each of seven 3 L Erlenmeyer flasks containing 1 L of MM9 medium (for hybridobactins and acybolins production) or SRM_{HG} medium (for trinickiabactin production) was inoculated with 1 mL of the overnight pre-cultivation on a shaker at 30℃ and 120 rpm for 4 to 5 days, while another 1 L of MM9 medium or SRM_{HG} medium without inoculum in a 3 L Erlenmeyer flask was also prepared as a control and incubated under the same condition. The cultivation was repeated until enough raw material could be obtained for final purification.

3.2.2 Extraction Methods

3.2.2.1 Liquid-Liquid Extraction for Chemical Screening

100 mL of different bacterial cultures from various applied media for pre-screening were extracted twice with ethyl acetate (1:1, v/v) and the supernatant was concentrated to dryness under reduced pressure until a crude extract was obtained. The crude extract was then dissolved

in 80% aqueous methanol and the dissolvable portion was transferred into a vial for LC-MS analysis. 100 mL of each corresponding medium was prepared and treated in the same way.

3.2.2.2 Extraction Using Resin for Large Scale Cultivation

The 4 to 5 days fermented cultivation (in line with the cultivation section) in 3 L Erlenmeyer flasks was centrifuged at room temperature and 4,000 rpm for 15 min to yield the supernatant. To obtain sufficient extract from the supernatant, 40 g preswollen resin Amberlite® XAD 16N was added to each 1 L supernatant and stirred for 30 min. After filtration, the resin from each 1 L supernatant was eluted once with 100 mL 50% aqueous methanol and twice with 100 mL 100% methanol, respectively. Subsequently, all the eluates were combined and concentrated under reduced pressure to obtain the crude extracts for further analysis. 1 L of MM9 medium or SRM_{HG} medium was prepared as control and processed with the same steps.

3.2.3 CAS Assays

The CAS assay is a universal assay developed by Schwyn and Neiland in 1987[108]. CAS is short for chrome azurol S, which is a dye applied to detect the presence of siderophores in a quick and easy way.

CAS assay agar plates for the detection of siderophores were prepared on a 100 mL scale as follows:

Firstly, 60.5 mg chrome azurol S was dissolved in 50 mL ddH_2O to give solution 1. Then, a solution 2 consisting of 27 mg $FeCl_3 \cdot 6H_2O$ and 83.3 µL concentrated HCl in 100 mL was prepared. Then 10 mL of solution 2 was added into the CAS solution. After that 73 mg HDTMA was dissolved in 40 mL ddH_2O as solution 3 and added slowly to the CAS solution with stirring, forming a dark blue solution. Subsequently, the solution was autoclaved.

A basal agar medium was prepared, to which the CAS solution would later be added: 3 g MOPS, 0.05 g NaCl, 0.03 g KH_2PO_4, 0.01 g NH_4Cl and 0.05 g L-asparagine were dissolved in 83 mL ddH_2O. The pH was adjusted to 6.8, ddH_2O added until the total volume reached 88 mL, and 1.5 g agar added with stirring and heating until it became homogeneous. Both this solution and the CAS solution were autoclaved.

10 mL of a 50% solution of glucose was prepared by sterile filtration. Once the other solutions were autoclaved and cooled down to around 50 °C, 2 mL of the glucose solution was slowly

added to the basal agar medium with stirring, followed by 10 mL of the CAS solution. The resulting mixture was poured onto sterile agar plates (~25 mL per plate).

The iron-binding activity of samples of interest was conducted by dropping 10 µL of concentrated samples directly onto CAS agar plates and incubating at room temperature; positive results were typically discernible within six hours of incubation.

3.2.4 Mass Spectrometry

3.2.4.1 LC-MS

An 1100 Series HPLC system (Agilent Technologies, Waldbronn, Germany) connected with an ABSCIEX 3200 Q TRAP LC/MS/MS mass spectrometer (AB Sciex, Germany GmbH, Darmstadt, Germany) was used. The HPLC system is equipped with a G1322A degasser, G1312A binary pump, G1329A autosampler and G1315A diode array detector. A Phenomenex Luna C18 (2) column (250 x 2.0 mm, 5 µm) was used, and the injection volume was 5 µL. Acetonitrile was used as mobile phase A and 0.1% TFA in ddH_2O as mobile phase B. The following gradient was applied during pre-screening and LC-MS guided isolation and purification in Q1 positive and negative scan mode, and the mass range was set from 100 to 1,600 Da.

Table 3-15 The gradient for LC-MS.

Total Time (min)	Flow Rate (µL/min)	A (%)	B (%)
0	200	10	90
8	200	30	70
16	200	50	50
22	200	100	0
30	200	100	0
36	200	10	90
45	200	10	90

3.2.4.2 HR-LC-ESI-MS

HR-HPLC-ESI-MS, Infusion ESI-MS and MS/MS experiments were performed by Dr. Dorothee Wistuba (University of Tuebingen, Department of Mass Spectrometry) on a Bruker QTOF-MS maXis Impact ESI-HR-MS.

3.2.5 Chromatographic Methods

3.2.5.1 Size exclusion chromatography (SEC)

The crude extracts from above were resuspended in 70% aqueous methanol and the supernatant obtained after centrifugation (4,000 rpm, 15 min, rt.) was loaded onto an open column, which was filled with Sephadex^{TM} LH-20 (d=3 cm, l=32 cm) and equilibrated with 70% aqueous methanol overnight at room temperature before use to assure that the filling materials was swollen entirely. The subfractions were eluted isocratically with 70% aqueous methanol and collected based on the color bands. Afterwards, all the fractions were concentrated to dryness for LC-MS guided isolation and purification.

3.2.5.2 High performance liquid chromatography (HPLC)

The isolation procedure by preparative HPLC was carried out with a Waters system, which consists of a internal degasser, Waters binary pump 2545, Rheodyne 3725i-119 injector and Waters photodiode array detector 2489 and is controlled by ChromScope IE software. An Agela Unisol C18 (2) column (250 x 21.2 mm, 5µm) was used to profile fractions obtained after SEC.

A Waters system consisting of a Kromega 1210 degasser, Waters binary pump 1525 and Rheodyne 7725i injector integrated with a Waters photodiode array detector 996 controlled by Millennium32 software was used for isolation and purification procedures by semipreparative and analytical HPLC. Utilized columns during this procedure are listed in Table 3-16.

Table 3-16 Applied columns during isolation procedure.

Columns used for semipreparative HPLC	Columns used for analytical HPLC
Phenomenex Synergi Hydro-RP C18 (250 x 10 mm, 4 µm)	Phenomenex Luna Omega Polar C18 (250 x 4.6 mm, 5 µm)
Phenomenex Luna Omega Polar C18 (250 x 10 mm, 5 µm)	Phenomenex Aeris PEPTIDE XB-C18 (250 x 4.6 mm, 3.6 µm)
Phenomenex Luna Polar C18 (250 x 10 mm, 5 µm)	Phenomenex Luna C5 (250 x 4.6 mm, 5 µm)
Knauer Eurospher II C18 P (250 x 8 mm, 5 µm)	Phenomenex Kinetex EVO C18 (250 x 4.6 mm, 5 µm)
Knauer Eurospher II C8 (250 x 8 mm, 5 µm)	Phenomenex Kinetex PFP5 (250 x 4.6 mm, 5 µm)

3.2.6 Marfey's Analysis with the Amino Acid Constituents of Compounds

2 mg of the sample was hydrolyzed with 6 M DCl overnight at 105 °C. The solvent was removed by reduced pressure and 50 µL 1 M $NaHCO_3$ along with 100 µL L-FDAA (10 mg/mL in acetone) were added to the reaction that was heated at 37 °C for 1 h. Then, 25 µL 2 M HCl was added, and the reaction mixture was resuspended in 200 uL 50% (vol/vol) DMSO. The derivatized samples were analysed via analytical HPLC with a Waters system, consisting of a Waters 1525 pump with an integrated degasser, a Waters 996 photodiode array detector, and a Phenomenex Aeris PEPTIDE XB-C18 column. The HPLC run was performed in gradient elution mode with methanol (A) and 0.1%TFA containing water (B) as mobile phases. The gradient started at 20% A with a flow rate of 0.8 mL/min, increasing the percentage of A to 50% within 8 min, followed by isocratic conditions until 16 min, increasing the percentage of A to 100% in 6 min which was held for another 3 min, followed by reequilibration at 20% A for 5 min.

3.2.7 Determination of the Sidechain Stereochemistry

An aliquot of 50 µL of the samples dissolved in MeOH (corresponding to 500 µg) was added up to 1 mL with a solution of 6N deuterated hydrochloric acid (DCl/D_2O, 1:1, v/v) in a screw-capped glass vial and heated for 24 h at 110 °C. The reaction mixture was evaporated to dryness and extracted with chloroform. The chloroform layer was evaporated and reconstituted with MeOH-water (10:90; v/v) for injection to the CHIRALPAK IA-U column.

Chromatographic enantiomer separation of 3-hydroxy fatty acids was performed on a CHIRALPAK IA-U column (3.0 mm x 100 mm, sub-2 µm) (Daicel, purchased from Chiral Technologies Europe, Illkirch, France). Gradient elution was carried out with the mobile phase comprising water (A) and acetonitrile (B), both containing 0.1% (v/v) acetic acid. The following gradient profile was used: 0–2 min 10% B, 2–20 min 10-100% B, 20–22 min 100% B, 22–22.1 min 100-10% B and 22.1–25 min 10% B. The flow rate was 300 µL/min, the column temperature 40 °C and the injection volume 10 µL.

For the generation of an enantiomeric reference compound of 3-hydroxy-octanoic acid Rhamnolipid (R-95) was hydrolyzed with 2N NaOH solution in THF/MeOH (9:1, v/v) and stirred for 2 h at room temperature ($\approx$ 25 °C). After the reaction, solvents were removed, the residue acidified with 0.1 M HCl, and extracted with ethyl acetate. After evaporation of the

organic solvent, the residue was reconstituted with 100 µL MeOH/H_2O (3:7, v/v) for LC-MS analysis on the CHIRALPAK IA-U column[109].

3.2.8 Nuclear Magnetic Resonance (NMR) Spectroscopy

The final purified compounds were analysed via NMR with a Bruker Avance III 400 HD instrument, at 400 MHz. A series of 1D-/2D- NMR experiments, including ^{1}H-NMR, ^{13}C-NMR, DEPT 135, ^{1}H-^{1}H COSY, ^{1}H-^{1}H NOESY, ^{1}H-^{13}C HSQC, ^{1}H-^{13}C HMBC, ^{1}H-^{13}C HSQC-TOCSY, ^{1}H-^{15}N HSQC and ^{1}H-^{15}N HMBC were peformed.

Prior to NMR mesurements, the pure compounds were firstly freeze-dryed overnight and then dissolved in adapted solutions. The dissolved samples were measured in 5 mm NMR tubes. All the acquired spectra were processed and analyzed with the help of MestReNova 11.0. Spectra were referenced to the residual solvent signals with resonances as listed in Table 3-17.

Table 3-17 Compounds measured by NMR and ultilized solvents.

Compound name	Referenced solvent signals
Trinickiabactin	H/C 2.50/39.5 (DMSO-d_6)
Hybridobactin A	H/C 2.50/39.5 (DMSO-d_6)
Hybridobactin B	H/C 2.50/39.5 (DMSO-d_6)
Hybridobactin C	H/C 2.50/39.5 (DMSO-d_6)
Hybridobactin D	H/C 2.50/39.5 (DMSO-d_6)
Bactobolin B/E	D_2O+0.02% TFA
Acybolin A/J	H/C 2.75/29.76 (DMF-d_7)

3.2.9 Ultraviolet/Vis (UV) Spectroscopy

UV measurements were performed on a Perkin-Elmer 25 UV/VIS spectrometer, using 1 cm quartz cells and dissolving samples either in ddH_2O, MeOH or DMF. UV scans were recorded over the range 400 to 190 nm. The molar absorption coefficient ε was calculated based on the Beer–Lambert law:

$$\varepsilon = \frac{A}{c * d} \; [\, L * mol^{-1} * cm^{-1}]$$

A = absorption at peak maximum (nondimensional)
c = concentration in mol / L
d = layer thickness of solution in cm

3.2.10 Optical Rotation

Specific optical rotation measurements were performed on a Jasco P-2000 polarimeter, using a 10 mm micro cell, and measuring at λ = 589 nm (sodium D-line). Optical rotation was calculated by use of the following equation:

$$[\alpha]_D^T = \frac{\alpha}{c * l} \times 10^4$$

$[\alpha]_D^T$= specific optical rotation
T = temperature (°C)
D = sodium D-line (λ = 589 nm)
α = rotation (°)
c = concentration (g/100 mL)
l = cell length (mm)

3.2.11 Infrared (IR) Spectroscopy

IR spectrometry was performed with a Jasco FT/IR-4200 series spectrometer, comprising a ZnSe optical window and processed with the software Spectra Manager 2.10.01.

3.2.12 Bioinformatics

Identification and characterisation of relevant gene clusters were analyzed with the web-based software antiSMASH (4.0 and 5.0 versions)[73,110]. Percentage identities and coverages between homologous genes were obtained through the NCBI GenBank blastP search algorithm.

For phylogenetic analysis, amino acid sequences of 90 A domains of known NRPS and NRPS-PKS natural products were aligned using MEGA-X software with default settings (algorithm: MUSCLE).

Neighbor-joining trees were reconstructed using the Jones-Taylor-Thornton (JTT) model and 1,000 bootstrap replicates. Refinement of the tree was visualized using the web-based software Interactive Tree of life (iTOL, https://itol.embl.de/).

3.2.13 Antibacterial Assay

The antibacterial activity analysis of trinickiabactin against *Escherichia coli* DH5-Alpha, *Pseudomonas aeruginosa* PA14 (DSM 19882), *Burkholderia thailandensis* DSM 13276, *Yersinia pseudotuberculosis* YPIII, *Bacillus subtilis* ATCC 6633, methicillin-resistant

Staphylococcus aureus DSM 25691, and *Streptococcus pneumoniae* ATCC 49619, was performed in a 96-well plate format using the broth dilution method according to The European Committee on Antimicrobial Testing (EUCAST) guideline[111]. In brief, 190 µL of Mueller-Hinton (MH) broth and 10 µL of each bacterial pathogen (OD_{600}= 0.2) were cultured in each well. For fastidious organisms (*S. pneumoniae* ATCC 49619) MH broth was supplemented using mechanically defibrinated horse blood and β-nicotinamide adenine dinucleotide. A total of 200 µL from the solution of 1000 µg/mL of trinickiabactin and two positive controls (kanamycin and rifampicin), previously dissolved in MeOH 10%, were applied in the first vertical line of the 96-well plate. Subsequently, serial dilutions were constructed to obtain ten different concentrations in each well: 500, 250, 125, 62.50, 31.50, 15.63, 7.81, 3.91, 1.95 and 0.98 µg/mL. MeOH 10% served as negative control. The 96-well plates were then incubated for 24 h at 37 ^{o}C and growth inhibition was measured at 600 nm using a Tecan Infinite M200 plate reader. The MIC was determined in independent triplicates for each bacterial pathogen. OD_{600} data that represented bacterial growth were adjusted employing the Gompertz equation to calculate the MIC[112].

3.2.14 20S Proteasome Inhibition Assays

The hybridobactins A-D were applied in an established human 20S proteasome assay to probe inhibitory activity against the β5-subunit. To monitor the conversion of the β5-specific chymotryptic substrate LLVY-AMC (Bachem) a concentration of 0.4 µg/mL of the human proteasome (Enzo Life Sciences: BML-PW8720-0050) was employed in assay buffer (20 mM HEPES pH 7.8, 0.5 mM EDTA/ 0.035% SDS). The assay set up for the inhibition was validated with the well investigated proteasome inhibitor epoxomicin (Sigma) as a commercial standard.

3.2.15 Determination of k_{assoc}

To calculate the rate of covalent inhibition (k_{assoc}) against the human proteasome using $k_{obs}/[I]$ ($M^{-1}s^{-1}$), the pseudo-first-order association rate constant k_{obs} was determined for hybridobactins A-D. Therefore, the human 20S proteasome was incubated with inhibitors at varying concentrations ranging from 5 to 160 nM and a fixed substrate concentration of 50 µM LLVY-AMC, pre-diluted in assay buffer without pre-incubation of the enzyme with inhibitors. The reaction was initialized by adding the proteasome as the last reagent to the wells. The substrate conversion into the fluorescent product was measured every minute over an hour in a Tecan Infinite 200 Pro Instrument at an excitation wavelength of 360 nm and an emission wavelength

of 460 nm. All inhibitor concentrations were measured in triplicates. Side by side, control wells included a no-inhibitor control with maximum conversion, a DMSO control and a no-enzyme control to record the substrates basic fluorescence over time. Using GraphPad Prism software, k_{obs} values were calculated and plotted over the inhibitor concentration. At least three independent experiments were performed for the hybridobactins. Commercially available epoxomicin and isolated glidobactin C from cultures of *Polyangium brachysporum* were used as references and measured under the same conditions as described above.

3.2.16 Cell Proliferation Assays

Inhibition of cell proliferation was determined using a CyQuant NF assay (Invitrogen) according to the manufacturer's instructions. Human multiple myeloma U-266 cells (DSM ACC 9) in RPMI1640/10%FCS medium were seeded at 500 cells/cavity in 96-well plates and treated with inhibitors for 5 days. Measurement of fluorescence was taken after 30 min incubation with the natural product of interest in HBSS on a Tecan Infinite 200 Pro instrument. Data were analyzed by nonlinear regression using Prism from GraphPad Software, Inc. (San Diego, CA). Mean ± SEM was used for error bars.

4 Results and Discussion

4.1 Chemical Screening and Priorization of Investigated Strains

Our in-house *Burkholderia* strain library comprised around 30 *Burkholderia* sensu lato strains. A literature search focused on secondary metabolites from *Burkholderia*-related strains was performed at the beginning, to exclude relatively overexplored species such as *B. thailandensis* and *B. gladioli*. Since they are ubiquitous model species, several research groups investigated them heavily. Thailanstatins, thailandamide and malleilactone from the former species and gladiolin, bongkrekic acid and lagriene from the latter have been both structurally and biosynthetically fully elucidated. Furthermore, along with the literature search, a small MS-based database, containing around 100 structures including all derivatives from *Burkholderia*, was constructed as well, which will facilitate the analysis of the LC-MS screening results, particularly concerning the dereplication of secondary metabolites.

For chemical screening, the OSMAC strategy was applied. The term OSMAC (One Strain, Many Compounds) was coined by Zeeck and coworkers[113]. They showed empirically that, each microbial strain appears to have the potential to produce a various number of compounds, but only subsets of these compounds are produced under specific growth conditions. Thus, a cultivation-based approach via changing the medium can elicit the production of new secondary metabolites. Here, two groups of the *Burkholderia* strains were screened seperately. The first group belongs to the so called *Burkholderia* sensu stricto clade and the other group contains mainly plant-associated *Burkholderia* species, including *Paraburkholderia* species and plant pathogens.

Besides the commonly used LB and DMBg media, further media for screening were collected from the literature, whenever they have been used for the successful isolation of secondary metabolites. In total, ten media for the four selected strains from the *Burkholderia* sensu stricto clade, and two media for the 16 plant-associated *Burkholderia* strains were utilized for chemical screening, respectively. The corresponding cultivation conditions and sample preparation procedures were described in chapter 3.2.1. The media in which the metabolites could not be dectected are not shown. The masses from the media control were also excluded. After analysis of LC-MS data (in positive mode), all the investigated strains and their detected products were listed (Table 4-1 and Table 4-2). The dereplicated compounds are labeled in brackets, while the unknown compounds are indicated in red.

Table 4-1 Results of LC-MS screening from *Burkholderia* sensu stricto related strains.

Organism	PDB	Pharmamedia	DMBg	MM9
B. cenocepacia K56-2	734.6 (AFC-BC11)/ 748.6	-	-	-
B. cepacia JKB9	-	685.5 (icosalide B)/ 713.6 (icosalide A1 or A2)	-	325.1 (pyochelin)/ 685.5 (icosalide B)/ 713.6 (icosalide A1 or A2)/ 737.7 (ornibactin C8)/ 709.3 (ornibactin C6)/ 448.3/474.3/394.6
B. oklahomensis DSM 21774	-	-	-	485.4/499.5/513.5/526.5/ 968.5/894.8
B. ubonensis MSMB1189WGS	-	-	156.2 (cepabactin)	737.7 (ornibactin C8)

*Mass detection *m/z* in positive mode.

These four *Burkholderia* sensu stricto related strains behaved quite differently in the ten selected media: most of the produced secondary metabolites could only be detected in the listed four media (Table 4-1). *B. cenocepacia* K56-2 was able to produce the compound AFC-BC11 and a new derivative in PDB medium. However, fast degradation was observed during the isolation procedure. Hence, it could not be followed-up for further isolation. The most productive strain was *B. cepacia* JKB9 in MM9 medium. Several compounds were detectable and dereplicated. Because its non-dereplicable compounds were present only in low amounts, these findings were also not included in follow-up studies. In contrast to *B. ubonensis*, *B. oklahomensis* produced more unknown targets in a relatively high concentration, which could not be dereplicated with databases. Therefore, a further cultivation and investigation of the strain *B. oklahomensis* DSM 21774 was considered to be worthwhile pursuing.

Table 4-2 Results of LC-MS screening from plant-associated *Burkholderia* strains.

Organism	MM9 medium	SRM_{HG} medium
B. glumae DSM 9512	466.3/667.7/681.7	350.6/376.6/ 667.6/693.8
B. glumae ICMP 3729	325.3 (pyochelin)/1105.5 (plantaribactin)/ 454.1 (bactobolin B)/525.2 (bactobolin E)/ 1077.5/1121.5/466.3/313.2/667.6/681.7/353.3/702.3	667.6
P. phenazinium DSM 10684	196.1 (phenazine-N-oxide)/239.3	207.1
P. caribensis DSM 13236	-	-
P. fungorum DSM 17061	-	316.2
P. phymatum DSM 17167	304.3	610.2/355.3
P. unamae DSM 17197	325.3 (pyochelin)/466.3/454.4	-
P. xenovorans DSM 17367	-	-
P. ferrariae DSM 18251	-	-
P. mimosarum DSM 21841	708.7	-
P. caledonica LMG 19076	-	-
P. phytofirmans LMG 22487	-	-
P. silvatlantica LMG 23149	284.3 (quinolone)	-
P. tuberum LMG 21444	-	-
T. caryophylli DSM 50341	139.05 (urocanic acid)/667.7	437.2/853.8
P. unamae LMG 22722	325.5 (pyochelin)/466.3/470.2/454.3	-

*Mass detection *m/z* in positive mode. *B= Burkholderia, P= Paraburkholderia, T= Trinickia.*

In comparison to the *Burkholderia* sensu stricto strains, plant-associated *Burkholderia* strains were predominant in our strain collection. Here, minimal media were prefered for cultivation of these plant-associated *Burkholderia* strains. One reason is that the minimal media may stress these strains to produce more secondary metabolites. On the other hand, the downstream analytical work can also be simplified due to less disturbance of media components. An impressive example is the isolation of syringolins: these compounds were only secreted by *P. syringae* pv. *syringae* by using a mininal medium under appropriate conditions[114]. Thus, the MM9 and SRM_{HG} media, which were frequently used for isolation of secondary metabolites from *Burkholderia* related strains, were chosen for chemical screening. It can be seen from Table 4-2 that seven out of the 16 strains are silent in both media after cultivation and no obvious peaks could be detected except media components. *P. phenazinium* DSM 10684 is able to produce phenazine-related compounds, which may help their host to fight against fungal infection[115]. Pyochelin[116], a siderophore assisting bacteria in aquiring iron, was also observed from both *P. unamae* strains. The plant pathogenic strains, *B. glumae* DSM 9512 and *B. glumae* ICMP 3729, shared a high similarity on the metabolic level. Besides these two strains, *T. caryophylli* DSM 50341 also produced some intriguing compounds. Especially one compound, showing a mass ion at *m/z* 853.8, which was produced in SRM_{HG} medium at a high concentration, deserved a deeper investigation.

Upon LC-MS screening results, bioinformatic analyses were also taken into consideration. The candidate strains from LC-MS screening, whose genomes were accessible, were processed with AntiSMASH 4.0. Based on the bioinformatical analysis, the encoded biosynthetic gene clusters and indicated compound classes were predicted. In combination with the LC-MS screening results, some of the targets were deduced via their defined masses or mass ranges, or other physico-chemical properities. The integration of bioinformatics corroborated the MS-based findings and clearly indicated which target should be followed-up.

As an initial step to access the bacterial metabolites, OSMAC was proven to be an effective tool. Although it is undirected, a broader metabolic spectrum can be obtained. Recently, an extended OSMAC concept using a high-throughput screening approach to discover small molecule elicitors of silent biosynthetic gene clusters was reported. A library containing up to 640 compounds was applied to the model strain *Burkholderia thailandensis*[117]. This led to the discovery of a potent trigger—trimethoprim. With the applying of trimethoprim at a subinhibitory concentration, over 100 compounds were triggered from *Burkholderia thailandensis* under standard laboratory conditions[118].

In our study, a similar concept was applied to the selected *Burkholderia* strains during the chemical screening. In response to the varying media components, the metabolite spectra of 14 out of 20 selected strains were changed accordingly. Depite its random nature, this strategy is still widely applied as an integral part of genomics-guided strategies[119]. With genomics, the full spectrum of the bacterial potential could be evaluated. However, due to the issue of silent genes, the full metabolic map of bacteria can not be realized under standard laboratory conditions. Thus, pairing these two tools will reinforce the power of genome mining for new secondary metabolites.

In this study, three strains, *B. oklahomensis* DSM 21774, *B. glumae* ICMP 3729 and *T. caryophylli* DSM 50341, showed notable masses that stood out from the 20 selected strains. Thus, these three strains were priorized and further investigated.

4.2 *Trinickia caryophylli* DSM 50341

4.2.1 Genome Mining and Bioinformatic Analysis

A bioinformatic analysis was performed based on the LC-MS screening results of the strain *T. caryophylli* DSM 50341. The whole genome shotgun project for *T. caryophylli* DSM 50341 has been deposited at DDBJ/ENA/GenBank under the accession VJZF00000000. The sequence of this strain was then uploaded in AntiSMASH 5.0.0, and a prediction of possible secondary metabolites from the identified biosynthetic gene clusters (BGCs) was obtained. In total, 13 BGCs have been identified from the strain *T. caryophylli* DSM 50341. At the time that this bioinformatic analysis was performed, the BGC of gramibactin was still unknown. The analysis unveiled a NRPS BGC (*trbA-trbN*) sharing 26% similarity with that of ornibactin and represented a convincing candidate, encoding the target compounds with a mass ion at *m/z* 853 (termed trinickiabactin). However, a closer look revealed that this BGC codes for the assembly of six amino acids. Since ornibactin contains only four amino acids, it was concluded that ornibactin can not be the product. An extended literature search indicated that this attractive BGC possesses high similarity with gramibactin, a new class of lipopeptide-derived siderophores as mentioned in the previous chapter[65]. A BlastP-based comparison of gramibactin and trinickiabactin BGCs indicated a highly similar NRPS machinery (Figure 4-1). Both of these two BGCs consist of three core NPRS genes (*grb HIJ* vs. *trb HIJ*) that were flanked by a number of putative accessory genes (Figure 4-1). Further, most of their encoded genes could be correlated with each other with relatively high similarity (Table 4-3).

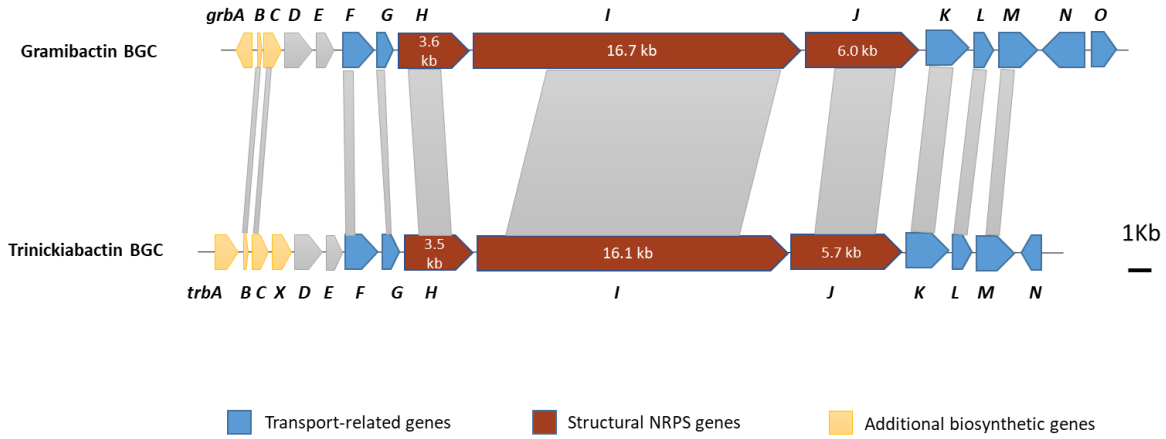

Figure 4-1 Comparison of gene clusters coding for the NRPS product machinery (red) and transport-related proteins (blue) between *P. graminis* C4D1M and *T. caryophylli* DSM 50341. Top: Gramibactin biosynthetic gene cluster; bottom: Trinickiabactin biosynthetic gene cluster.

Table 4-3 Comparison of genes involved in grambactin and trinickiabactin BGCs.

Gramibactin Biosynthetic Gene Cluster				Trinickiabactin Biosynthetic Gene Cluster		
Protein	Size (aa)	Putative Function	Identity [%]	**Protein**	Size (aa)	Putative Function
GrbA	207	Nitroreductase	/			Not observed
		Not observed	/	**TrbA**	399	formaldehyde dehydrogenase
GrbB	77	MbtH-like protein	83.56	**TrbB**	80	MbtH-like protein
GrbC	292	Thioesterase	58.73	**TrbC**	273	Thioesterase
		n.o.	/	**TrbX**	339	TauD/TfdA family dioxygenase
GrbD	478	Unknown function	79.11	**TrbD**	478	Putative peptide synthetase
GrbE	294	Unknown function	79.76	**TrbE**	324	Unknown function
GrbF	548	ABC transporter	80.21	**TrbF**	559	ABC transporter
GrbG	274	Transporter	80.75	**TrbG**	301	ABC transporter
GrbH	1197	NRPS (CAL-T-C)	66.47	**TrbH**	1179	NRPS (CAL-T-C)
GrbI	5574	NRPS (A-T-C-A-T-C-A-T-C-A-T-E-C-A-T)	58.16	**TrbI**	5353	NRPS (A-T-C-A-T-C-A-T-C-A-T-E-C-A-T)
GrbJ	1933	NRPS (C-A-T-)	67.15	**TrbJ**	1903	NRPS (C-A-T-E-TE)
GrbK	730	TonB-dependent transporter	81.49	**TrbK**	737	TonB-dependent transporter
GrbL	322	ABC transporter substrate-binding protein	74.03	**TrbL**	346	ABC transporter substrate-binding protein
GrbM	663	Transporter	73.73	**TrbM**	657	Transporter
GrbN	718	TonB-dependent transporter	/	**TrbN**	304	MSF Transporter
GrbO	423	Unknown function	/			Not observed

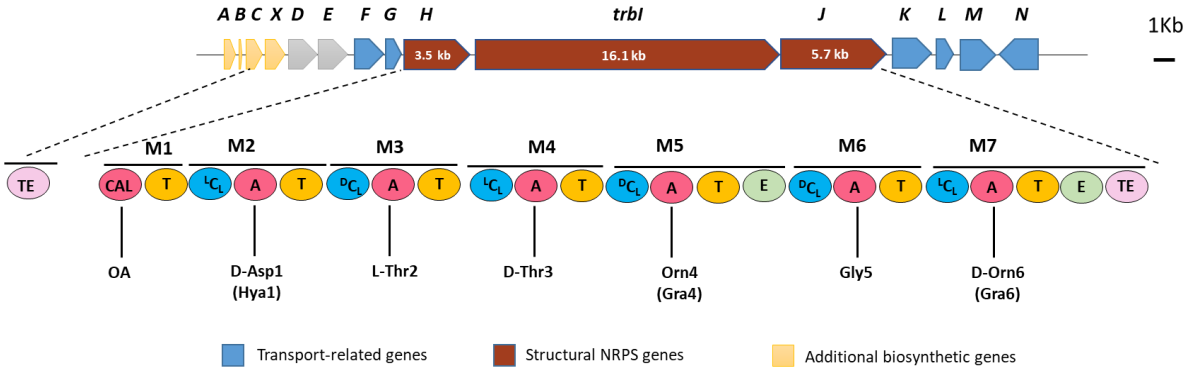

Figure 4-2 The putative gene cluster of trinickiabactin. Underneath the genes are the module and domain organization of TrbC and TrbH, Trb I and Trb J. Underneath the domains are the amino acids that are incorporated into the lipopeptide moiety. The number associated with the amino acid refers to the position of the amino acid in the peptide chain. OA stands for octanoic acid and Gra stands for graminine, respectively.

The trinickiabactin biosynthetic gene cluster consists of three central NRPS genes (*trbHIJ*). Several transporter genes are located directly adjacent downstream and upstream of the NRPS core genes (Figure 4-1, Figure 4-2). Further NRPS accessory and putative amino acid tailoring genes are present particularly upstream of *trbH* and comprise genes encoding an MbtH protein

(TrbB), a further NRPS-TE domain (TrbC) and a dioxygenase (TrbX). Except the first module, all the other NRPS modudes within the NRPS genes consisted of a condensation (C), adenylation (A), epimerization (E) and thiolation (T) domain. Addtionally, a terminal thioesterase (TE) domain was located at the carboxy terminus of *trbJ*. The first module consisted of a coenzyme A ligase (CAL) and a T-domain, which possesses fatty acid adenylating activity and is responsible for the lipo-initiation[120,121]. Analysis of all A and C domains, employing automated web-based software tools in combination with a phylogenetic approach (Figure 4-3), led to the prediction of the sequence Asp1-Thr2-Thr3-Orn4-Gly5-Orn6.

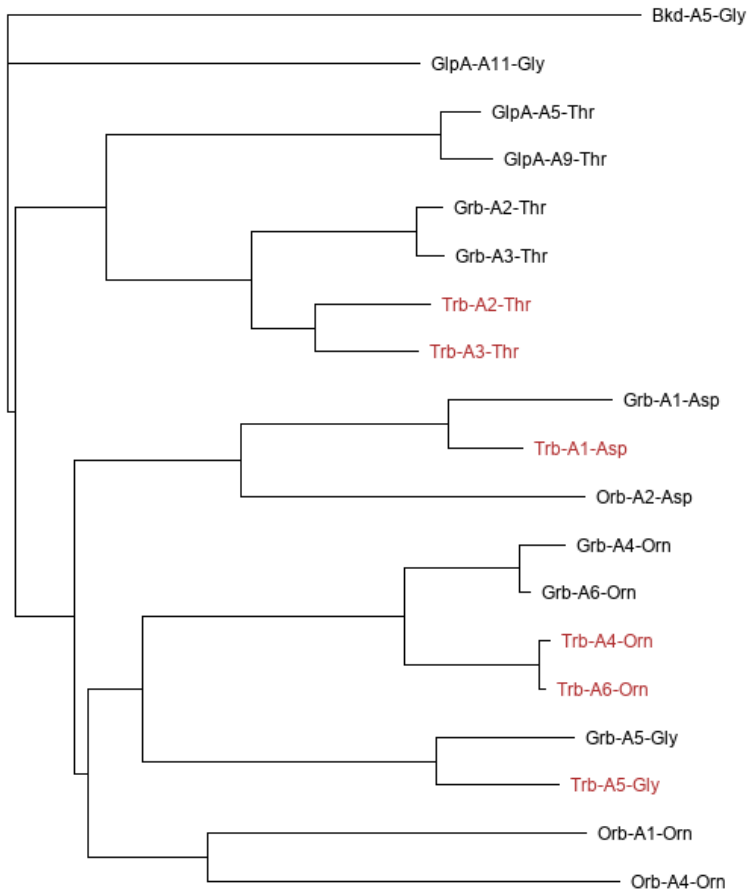

Figure 4-3 Phylogenetic analysis of selected A domains. These A domains were extracted from the modules of the gene clusters encoding NRP synthetases involved in burkholdine (*B. ambifaria* AMMD), ornibactin (Orb, *B. cenocepacia* J2315), glidopeptin A (GlpA, *B.* sp. DSM 7029), gramibactin (Grb, *P. graminis* C4D1M) and trinickiabactin (Trb, *T. caryophylli* DSM 50341).

4.2.2 Isolation of Trinickiabactin

To get more structural information of this compound, a sufficient amount and purity was demanded, hence the following procedure was carried out. Figure 4-4 features the whole procedure for isolation of pure trinickiabactin.

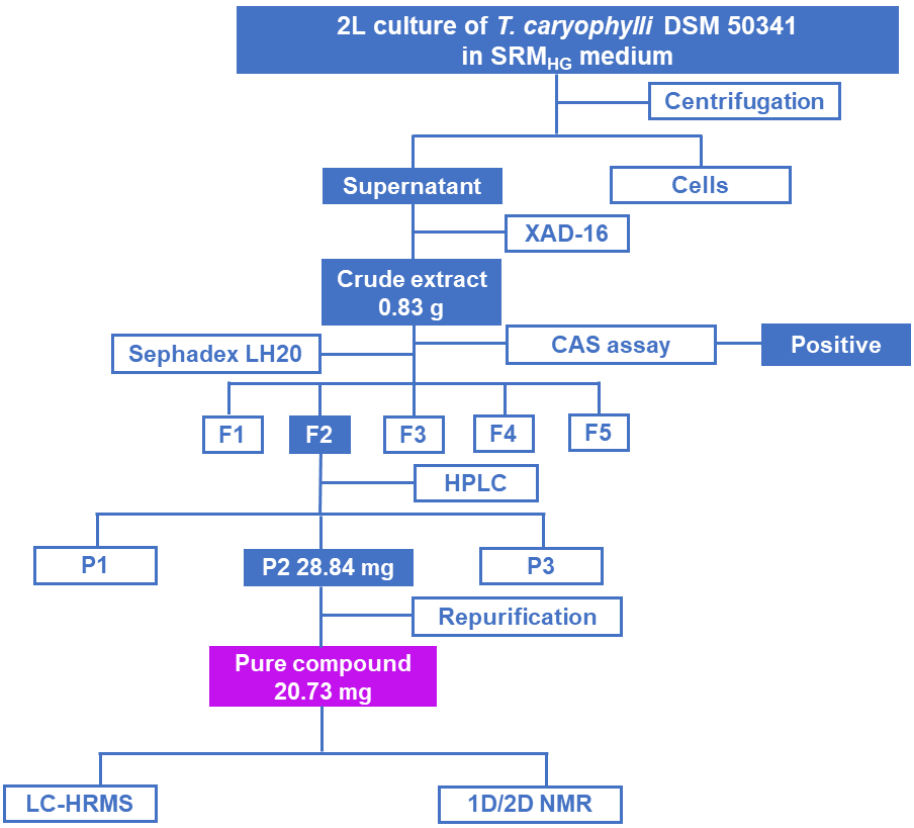

Figure 4-4 Fractionation scheme for the isolation of trinickiabactin.

A total of 0.83g crude extract was obtained from 2 L *T. caryophylli* culture, which was resuspended in 70% MeOH and further fractionated by open column chromatography with Sephadex^{TM} LH-20 beads (32 cm x 3 cm). The sample was loaded stepwise and eluted with an isocratic gradient with 500 mL 7:3 water/methanol (v/v). Afterwards, different fractions appeared according to the color bands, thus five fractions (F1-F5) were collected in round bottom flasks. The dried subfractions weighted 0.16, 0.22, 0.12, 0.103 and 0.096 g, respectively. LC–MS screening of the LH-20 fractions, showed fraction 2 to be of further interest, since it contained the target ion *m/z* 853.6.

Separation of this fraction by RP-HPLC was performed in gradient elution mode with deionized H_2O containing 0.1% TFA (A) and methanol (B) as mobile phases, and provided this compound in a semipure form (Figure 4-5). The gradient started at 40% B, increasing the percentage of B

in 3 min to 60%, increasing the percentage of B to 90% in 5 min and from 90 to 100% in 5 min, followed by isocratic elution of 100% B for an additional 4 min (Phenomenex Luna C18 column, 10 × 250 mm, 5 µm in combination with a Phenomenex SecurityGuard Luna C18(2) 10 × 10 mm precolumn; 4 mL/min flow rate; UV monitoring at 210 and 254 nm). Rechromatography of the obtained material eluting at t_R = 9.5 min using the same RP-HPLC conditions yielded 20.7 mg of this pure target compound (Figure 4-5).

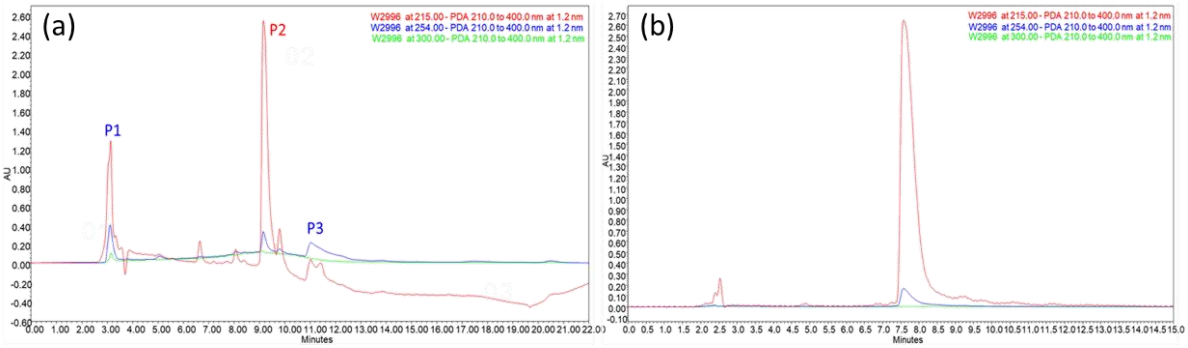

Figure 4-5 HPLC profiling runs during the isolation of the target compound. (a) HPLC run of subfraction 2. (b) HPLC run of the pure compound. Red, blue and green traces represent the UV absorption at 215, 254 and 300 nm, respectively.

4.2.3 Structure Elucidation of Trinickiabactin

To confirm the accurate mass of this unknown compound, the samples were submitted to HR-MS measurements both in positive and negative mode. Analyzing the LC–HRMS profile of *T. caryophylli* DSM 50341 identified two co-eluting singly charged ions with *m/z* of 853.6 and 906.5 in SRG_{HG} medium (Figure 4-6). The mass difference of 53 indicated a loss of Fe(III), a typical iron binding siderophore, which is in agreement with our previous bioinformatical analysis[122]. Since some other trivalent metals like Ga(III) are capable of displacing iron from siderophores[123], the effect of gallium was investigated. From the Ga(III) treated crude extract, a gallium-adduct ion at *m/z* 919 ($[M-2H+Ga(III)]^+$) was clearly observed (Figure 4-6).

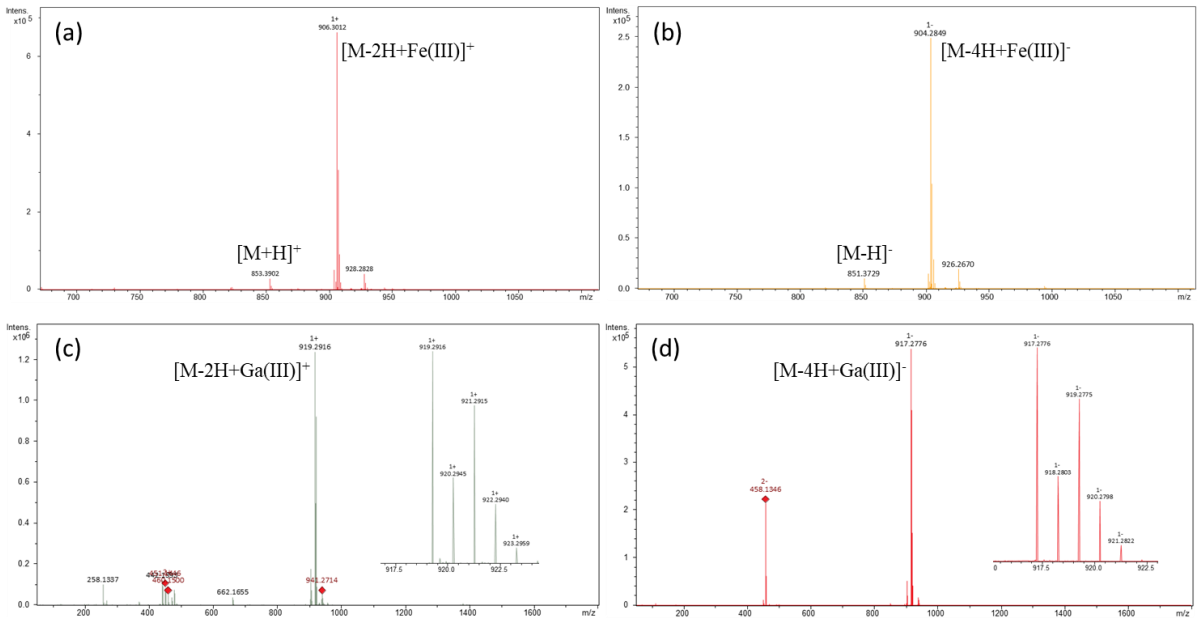

Figure 4-6 High-resolution ESI-MS spectra of trinickiabactin. (a) HR-ESI-MS spectrum of ferrated trinickiabactin in positive mode. (b) HR-ESI-MS spectrum of ferrated trinickiabactin in negative mode. (c) HR-ESI-MS spectrum of trinickiabactin with gallium in positive mode and magnification of the pseudomolecular ion peak. (d) HR-ESI-MS spectrum of trinickiabactin with gallium in negative mode and magnification of the pseudomolecular ion peak.

All these analyzed results were summarized in Table 4-4. Employing the MS database of *Burkholderia* and based on these HRMS results, it can be deduced that the compound of interest represents a new siderophore with the molecular formula $C_{32}H_{56}N_{10}O_{17}$, which was given the common name trinickiabactin.

Table 4-4 HR-MS results of trinickiabactin.

Pseudo-molecular Ion	Calculated [*m/z*]	Measurement [*m/z*]	Err. [ppm]	Molecular Formula
$[M+H]^+$	853.3898	853.3899	-0.2	$C_{32}H_{57}N_{10}O_{17}$
$[M-2H+Fe(III)]^+$	906.3018	906.3012	0.8	$C_{32}H_{54}FeN_{10}O_{17}$
$[M-2H+Ga(III)]^+$	919.2924	919.2919	0.3	$C_{32}H_{54}GaN_{10}O_{17}$
$[M-H]^-$	851.3752	851.3752	-0.3	$C_{32}H_{55}N_{10}O_{17}$
$[M-4H+Fe(III)]^-$	904.2861	904.2863	0.5	$C_{32}H_{52}FeN_{10}O_{17}$
$[M-4H+Ga(III)]^-$	917.2768	917.2773	-0.3	$C_{32}H_{52}GaN_{10}O_{17}$

For the full structure elucidation of trinickiabactin, NMR spectroscopy was integrated into the analysis, too. The isolated pure trinickiabactin was recorded with 1D and 2D NMR measurements. In NMR analysis, 1D NMR experiments, including ^1H, ^{13}C and DEPT135, and 2D NMR experiments, such as HSQC, COSY, HSQC-TOCSY, HMBC and NOESY were performed.

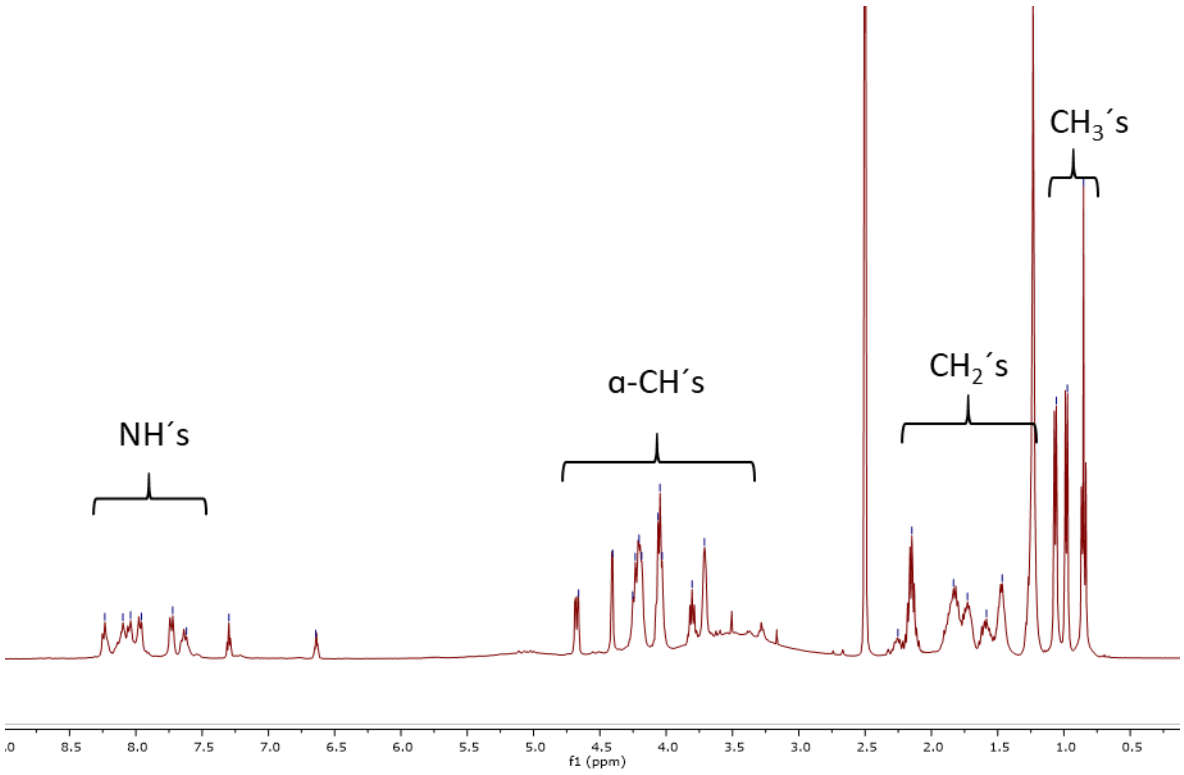

Figure 4-7 ^1H NMR spectrum of trinickiabactin (400 MHz, DMSO-d_6).

The ^1H NMR spectrum of trinickiabactin in DMSO-d_6 displayed resonances for exchangeable amide protons (NH) at δ_H 7.5 to 8.5, partially overlapped signals of α-protons ranging from δH 3.60 to 4.80, a large envelope of CH_2 protons at δ_H 1.2 to 2.4 and three methyl group signals at δ_H 0.85, 0.97 and 1.07, respectively (Figure 4-7). Combining ^{13}C- and DEPT135 spectra (Figure

4-8), the number of CH, CH_2 and CH_3 groups could be confirmed. In total, 3 CH_3-, 13 CH_2- and 8 CH- groups could be detected within the structure, in addition to the 8 carbonyl groups. Overlapping methylene signals in the high magnetic field, together with a terminal methyl resonance at δ_H 0.85, suggested that trinickiabactin contained an alkyl chain. Therefore, these data suggested that trinickiabctin bears a typical lipopeptide scaffold.

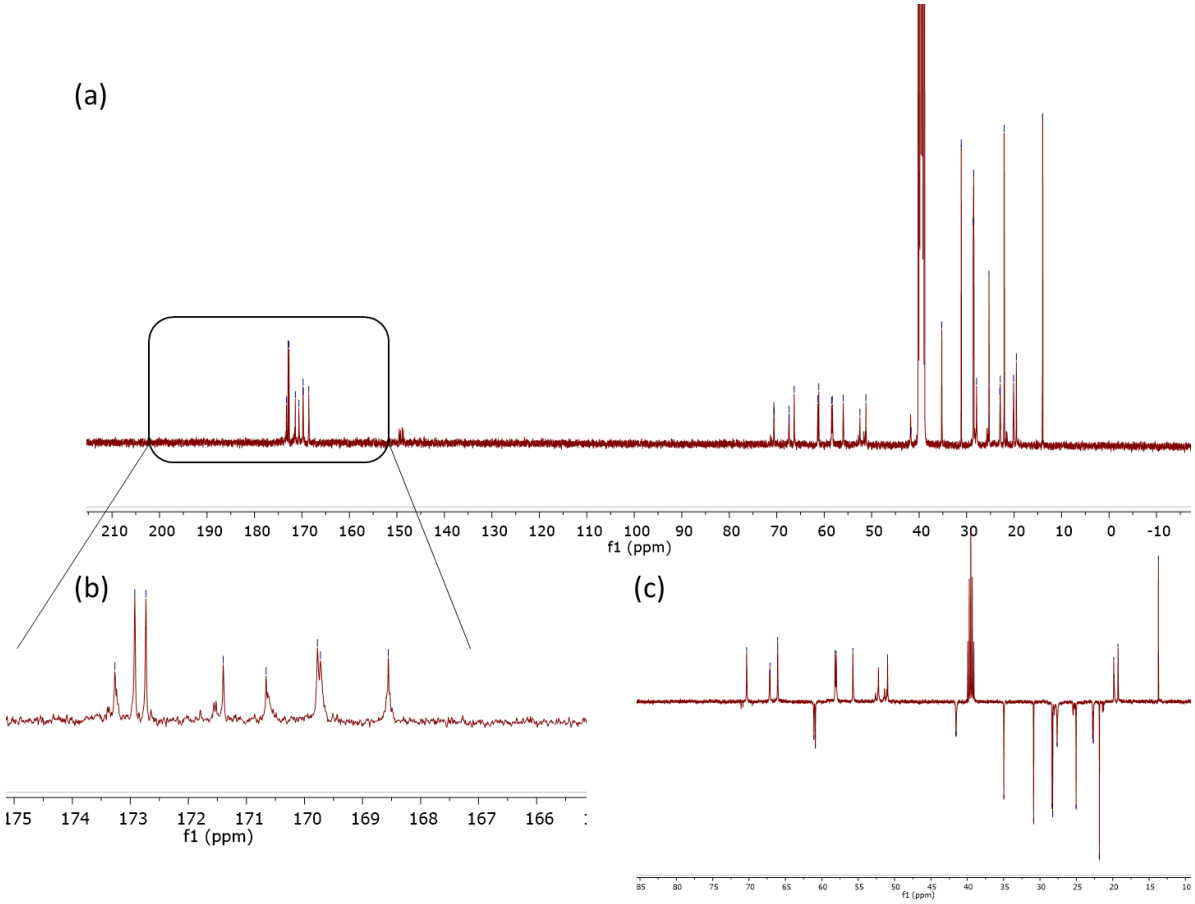

Figure 4-8 ^{13}C and DEPT135 NMR spectra of trinickiabactin. (a) ^{13}C NMR spectrum of trinickiabactin. (b) Expanded region of ^{13}C NMR spectrum of trinickiabactin. (c) DEPT135 NMR spectrum of trinickabactin.

Initial NMR analysis of the ^{1}H-^{13}C HSQC-TOCSY and ^{1}H-^{1}H COSY spectra indicated that there are seven spin systems present. Examplified is the elucidation of one of the spin systems (Figure 4-9). The proton at position 2 with a chemical shift δ_H at 4.03 is connected to carbon 2 (δ_C at 66.3) according to ^{1}H-^{13}C HSQC spectrum. Besides, it can be observed from the ^{1}H-^{13}C HSQC-TOCSY spectrum that this proton was correlated to carbons with δ_C at 58.3 and 19.5. The protons at position 3 and position 4 (with δ_H at 4.23 and 0.97, respectively) were also correlated with these three carbons. Hence, this residue can be determined to threonine.

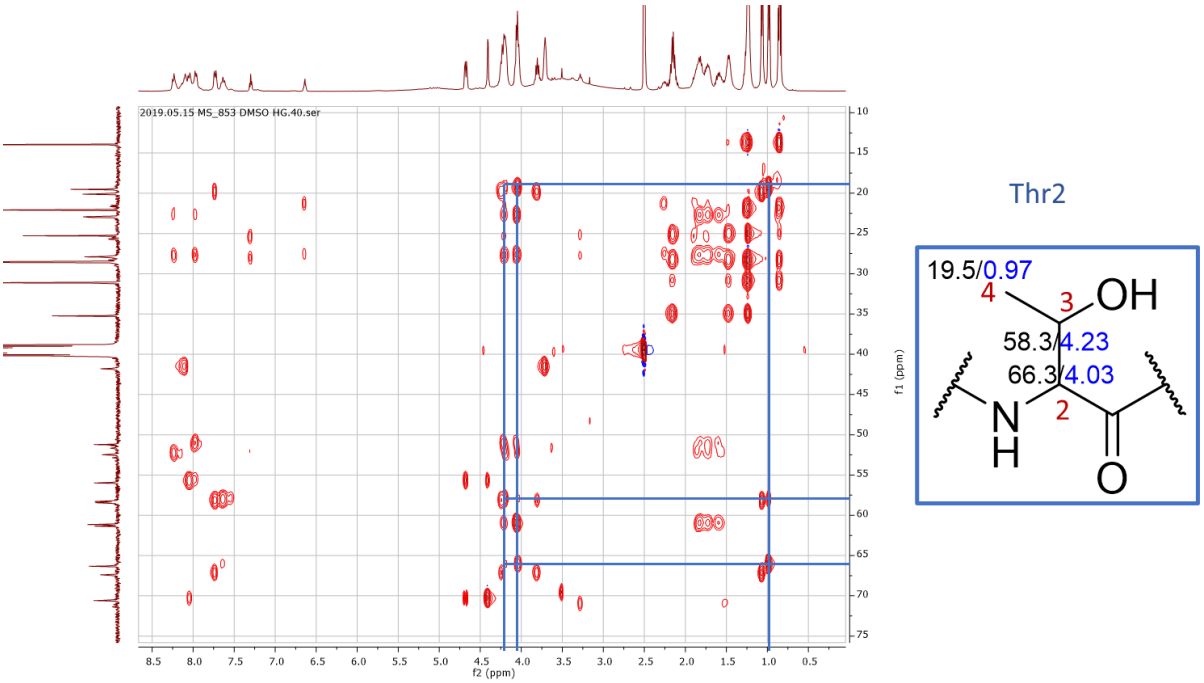

Figure 4-9 ^{1}H-^{13}C HSQC-TOCSY NMR spectrum of trinickiabactin (400 MHz, DMSO-*d*$_6$). The blue box depicts the structure of threonine (the number of the carbons are colored in red, the chemical shift of δ_C is colored in black, and the chemical shift of δ_H is in blue).

In a similar manner, the remaining signals of the other six spin systems together with the examplified threonine were summarized in Table 4-5. This included the amino acids 2× threonine (Thr), 1× β- hydroxyaspartic acid (Hya), 1× glycine (Gly), 2× putative ornithine residues, and a fatty acid. HMBC cross correlations between the α- or β-hydrogens and their corresponding carbonyl groups complemented each amino acid moiety. As the chemical shifts of the *δ*-atoms of the putative ornithine residues were relatively downfield (δ_H 4.05/δ_C 61.1–61.3), the nitrogen atom was estimated to be further functionalized. An in-depth analysis of the ^{1}H-^{15}N HMBC spectrum demonstrated coupling between each *δ*-hydrogen of the putative ornithine residues and a hydroxylamine and a nitroso group (Figure 4-10), respectively. The presence of two nitroso groups was also corroborated by a LR-MS spectrum, which showed twice the typical loss of 30 Da (Figure 4-10). Therefore, the assumed regular ornithine residues were revised to be 2× N$^{\delta}$-nitroso-N$^{\delta}$-hydroxy-D-Orn, also known as graminines (Gra)[65].

Table 4-5 NMR spectroscopic data (DMSO-d_6) for trinickiabactin.

Position		$\delta_{C/N}$ in ppm (mult.)	δ_H in ppm (mult. *J* in Hz)
Octanoic acid	C=O	172.7, qC	-
C2		35.2, CH_2	2.15, 2H (m)
C3		25.3, CH2	1.47, 2H (m)
C4		28.6, CH2	1.23, 2H (m)
C5		28.5, CH2	1.23, 2H (m)
C6		31.1, CH2	1.22, 2H (m)
C7		22.1, CH2	1.26, 2H (m)
C8		14.0, CH_3	0.85, 3H (t, 7.1)
Hya1	C=O	169.7, qC	-
C2		56.0, CH	4.67, 1H (dd, 8.6, 2.6)
C3		70.6, CH	4.41, 1H (d, 2.6)
COOH		172.9, qC	-
NH		112.2	8.04, 1H (d, 8.6)
Thr2	C=O	169.8, qC	-
C2		58.3, CH	4.20, 1H (m)
C3		66.3, CH	4.04, 1H (m)
C4		19.5*, CH_3	0.97, 3H (d, 6.2)
NH		109.1	7.64, 1H (m)
Thr3	C=O	170.6, qC	-
C2		58.4, CH	4.24, 1H (m)
C3		67.4, CH	3.80, 1H (m)
C4		20.1*, CH_3	1.07, 3H (d 6.1)
NH		114.2	7.73, 1H (d, 8.4)
Gra4	C=O	171.4, qC	-
C2		52.5, CH	4.19, 1H (m)
C3		23.0*, CH_2	1.83, 2H (m)
C4		27.9*, CH2	1.72, 2H (m)
C5		61.3, CH2	4.05, 2H (m)
NH		121.0	8.23, 1H (m)
N-OH		-32.7	-
N=O		315.7	-
Gly5	C=O	168.5, qC	-
C2		41.8, CH_2	3.71, 2H (brs)
NH		112.2	8.10, 1H (m)
Gra6	COOH	173.3, qC	n.d.
C2		51.2, CH	4.22, 1H (m)
C3		22.9*, CH_2	1.82, 2H (m)
C4		27.9*, CH_2	1.72, 2H (m)
C5		61.1, CH2	4.05, 2H (m)
NH		116.0	7.97, 1H (brd)
N-OH		-32.7	
N=O		315.7	

* carbon chemical shifts are interchangable.

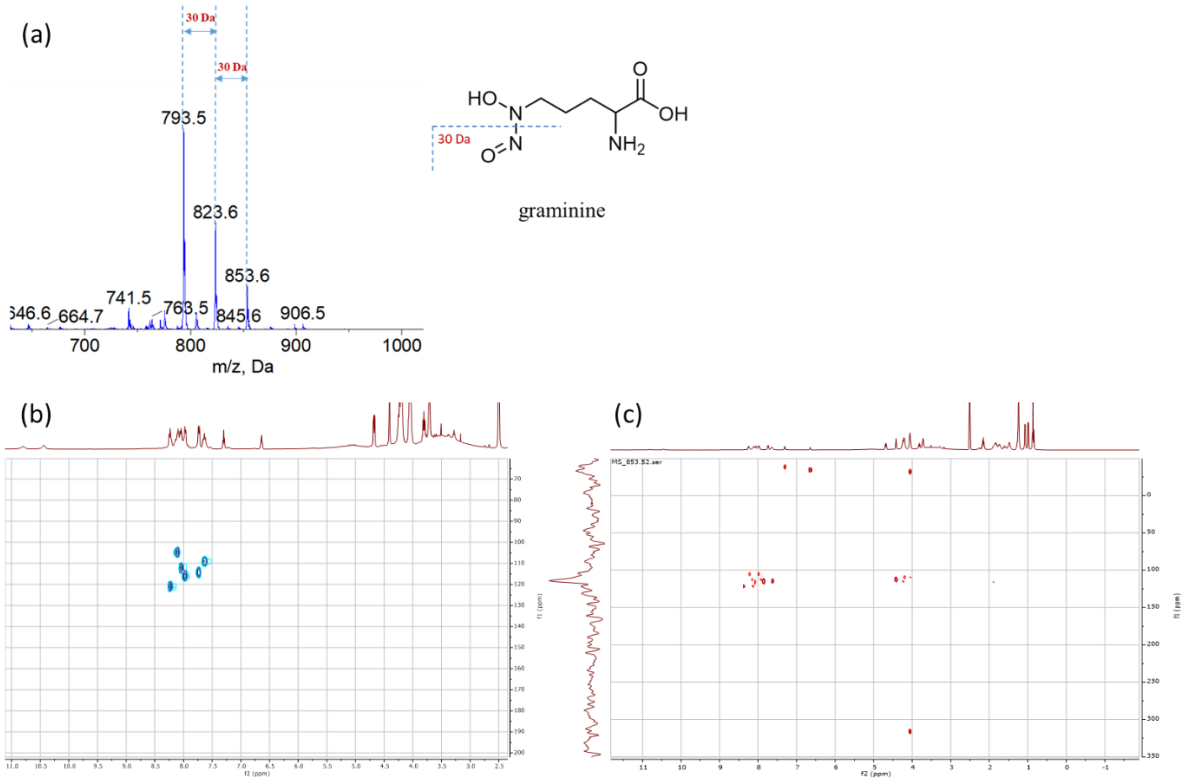

Figure 4-10 MS and NMR measurements of trinickiabactin. (a) MS-fragmentation pattern due to a tandem loss of NO. (b) ^{1}H-^{15}N HSQC NMR spectrum of trinickiabactin (400 MHz, DMSO-d_6). (c) ^{1}H-^{15}N HMBC NMR spectrum of trinickiabactin (400 MHz, DMSO-d_6).

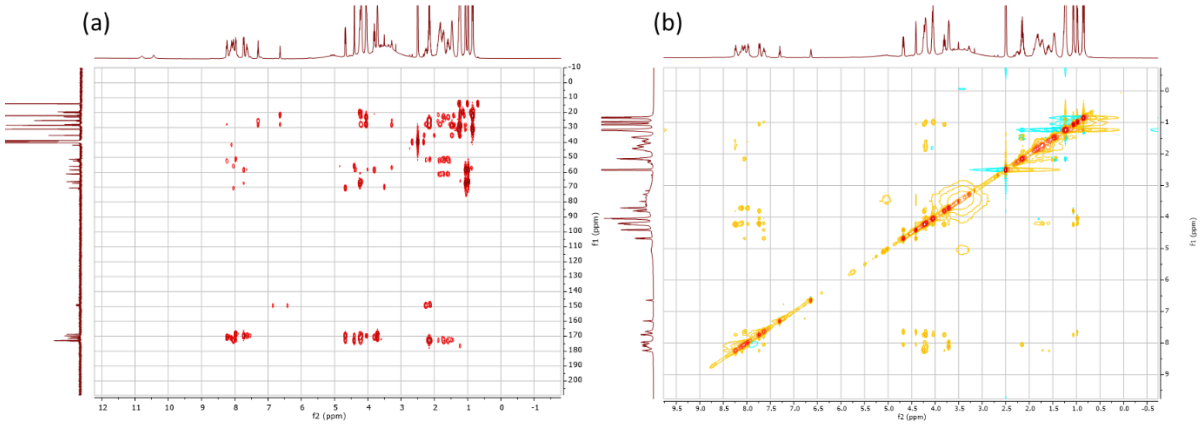

Figure 4-11 2D NMR spectra of trinickiabactin. (a)^{1}H-^{13}C-HMBC NMR spectrum of trinickiabactin (400 MHz, DMSO-d_6). (b)^{1}H-^{1}H-NOESY NMR spectrum of trinickiabactin (400 MHz, DMSO-d_6).

Employing ^{1}H-^{13}C-HMBC through bond as well as ^{1}H-^{1}H-NOESY through space interactions (Figure 4-11) observed between the amide protons and the α-atoms of the adjacent amino acid residue identified the linear peptide sequence as OA-Hya1-Thr2-Thr3-Gra4-Gly5-Gra6 (Figure 4-12). This sequence was also in alignment with tandem MS data (Figure 4-13), of which the chemical formula is in agreement with $C_{32}H_{56}N_{10}O_{17}$ as discussed above.

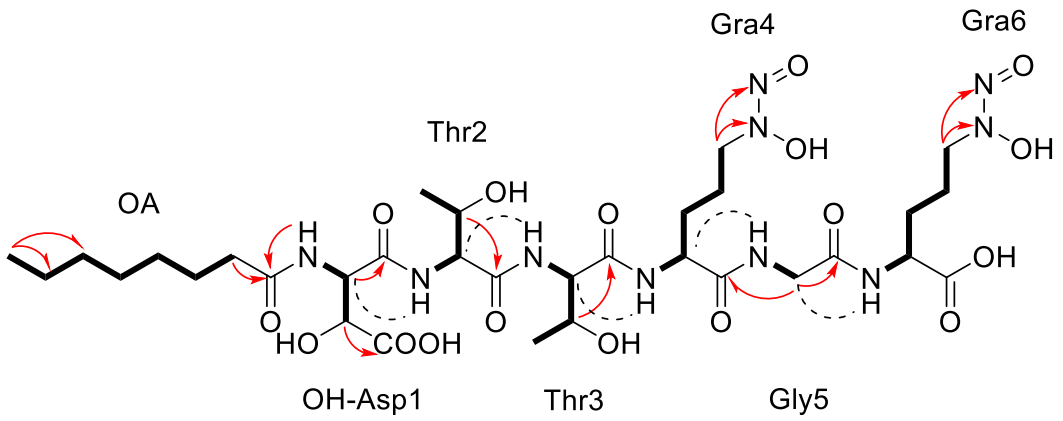

Figure 4-12 Key spin systems and selected long-range correlations leading to the identification of the planar structure of trinickiabactin. Bold lines indicate ^{1}H-^{1}H COSY or ^{1}H-^{13}C HSQC-TOCSY correlations, arrows indicate ^{1}H-^{13}C or ^{1}H-^{15}N HMBC correlations.

The product ions at *m/z* 793.3989 exhibited the tandem loss of NO (30 Da) from the precursor ions, which could be explained by the characteristic M-30 fragment ions (-NO) caused by the cleavage of diazeniumdiolate moieties from graminine. The ion at *m/z* 460.2298 shows the loss of (Gra-Gly-Gra) from trinickiabactin and 359.1821 represents an additional obliteration of threonine. The relatively small fragment at *m/z* 258.1342 indicates the absence of another Thr from 359.1821, and corresponds to the mass of octanoic acid-hydroxylated aspartic acid.

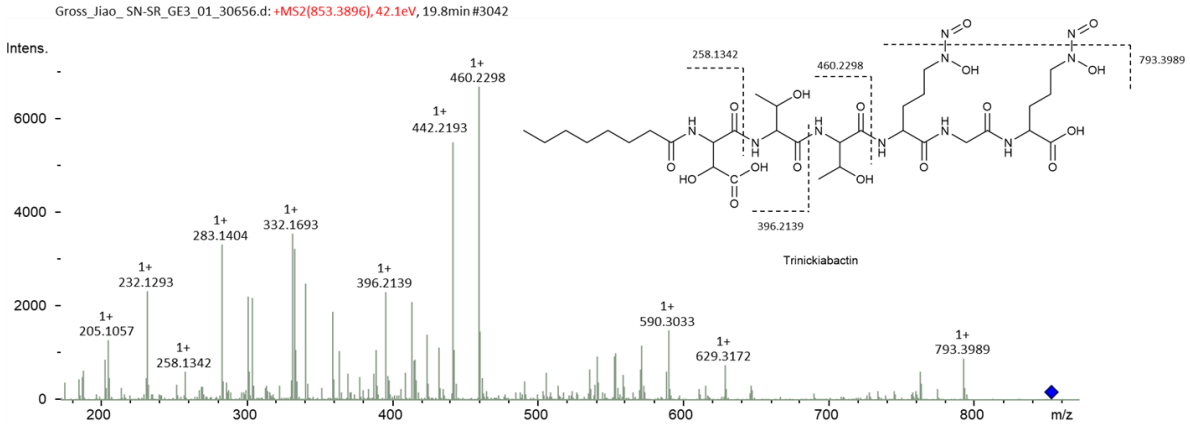

Figure 4-13 MS/MS spectrum of trinickiabactin in positive mode.

The absolute configuration of the amino acids in trinickiabactin was deduced in silico from its BGC, since the whole genome of the producer strain was sequenced and the corresponding BGC readily identified using antiSMASH 5.0 and PRISM 3[124]. These results led to the prediction of the sequence D-Asp1-L-Thr2-D-Thr3-D-Orn4-Gly5-D-Orn6 (Figure 4-14). It is noteworthy that the epimerization of the Asp1 and Thr3 must be performed by epimerases that are located elsewhere in the genome. Considering that tailoring enzymes will convert Asp1 into Hya1 (possibly mediated by dioxygenase TrbX) and Orn4/Orn6 into Gra4/Gra6, the gene

cluster was in full agreement with the discovered planar structure and the data allowed the suggestion of the absolute configuration of trinickiabactin with the exception of the stereochemistry at the β-atoms of Hya1, Thr2 and Thr3.

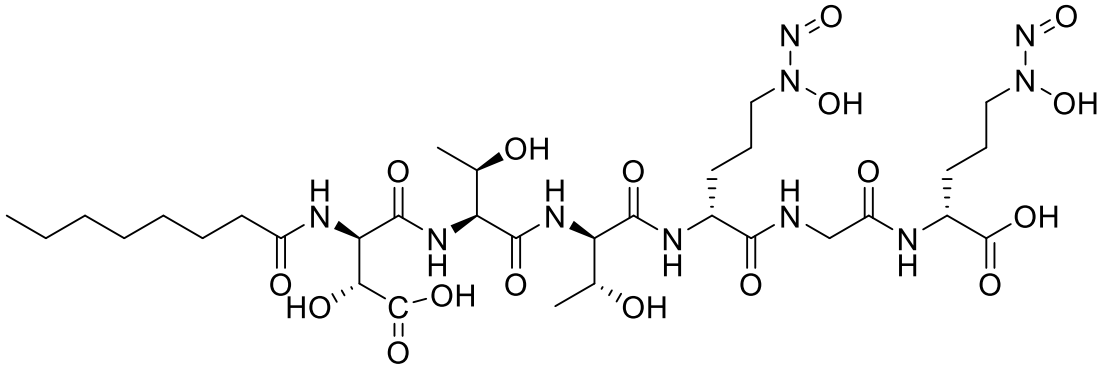

Figure 4-14 Chemical structure of trinickiabactin.

4.2.4 Biological Activity of Trinickabactin

Purified trinickiabactin was profiled in an antibacterial assay comprising seven bacterial pathogens (Table 4-6). In general, only gram-negative bacteria were affected by trinickiabactin. With a MIC value of 0.004 mM, trinickiabactin exhibited the highest activity towards *Yersinia pseudotuberculosis* YPIII, followed by moderate to low activities towards kanamycin-resistant and rifampicin-resistant *Burkholderia thailandensis* DSM 13276 and *Pseudomonas aeruginosa* PA14, respectively.

Table 4-6 Antibacterial activity of the isolated trinickiabactin.

	Trinickiabactin[a]	**Kanamycin[a] (+)**	**Rifampicin[a] (+)**
E. coli DH5-α	0.036	0.004	0.035
P. aeruginosa PA14	0.040	NA[b]	NA[b]
Burkholderia thailandensis DSM 13276	0.012	0.010	0.007
Yersinia pseudotuberculosis YPIII	0.004	0.031	0.014
Bacillus subtilis ATCC 6633	NA[b]	0.007	0.004
Staphylococcus aureus DSM 25691	NA[b]	0.018	0.011
Streptococcus pneumoniae ATCC 49619	NA[b]	0.079	0.040

[a]Antibacterial activity is expressed as MIC (mM). [b]NA: no activity observed (threshold: MIC > 0.07 mM). The negative control MeOH 10% exhibited an MIC > 0.18 mM.

4.2.5 Discussion and Outlook

4.2.5.1 Lipopeptide Derived Siderophores

Lipopeptides are a class of surface-active compounds produced by a large number of bacteria, fungi or yeast[125]. Structurally, they contain a fatty acyl residue ranging from C_5–C_{16} in length and chains of 7–25 amino acids[126]. Because of their diverse structure compositions, lipopeptides have amphipathic features that allow a wide range of biological activities. Representative compounds from this class are the antibacterial surfactin, the antifungal iturin and the antitumoral fengycin[127]. In addition to these bioactive lipopeptides, further lipopeptides have been reported to act as siderophores, such as ornibactins, corrugatin[128,129], as well as the recently isolated serobactins and variochelins[130,131], which occur frequently in *Pseudomonas*, *Burkholderia* or other closely related bacteria.

Siderophores (from the Greek: "iron carriers") are low-molecular-weight iron chelators that ensure the iron-supply for microorganisms[132]. In the natural environment, the number of soluble iron (Fe^{2+}) sources is limited, and in order to satisfy iron requirements, bacteria synthesize one to two siderophores, which have a high affinity to ferric iron (Fe^{3+}). Afterwards, these ferric iron-siderophore complexes will be transferred into the cell. There, the ferric iron is reduced into the ferrous iron and becomes bioavailable for bacteria[129,133]. In *Burkholderia*, this step requires an outer membrane receptor with a size ranging from 75 to 85 kDa. This receptor is a polypeptide that folds into a β-barrel containing a central plug domain. The entry of the ferric-siderophore complexes to the periplasmic space is allowed by binding of the complex to the external face of the receptor, which triggers a conformational change in the gated receptor (Figure 4-15)[116]. The required energy is translated through the periplasm by the TonB protein complex, composed of TonB, ExbB and ExbD proteins and which are all located in the cytoplasmic membrane. It uses the proton motive force at the inner membrane to transduce energy to the outer membrane via TonB. Thus, ferric-siderophore receptors involved in this process are referred to as TonB-dependent receptors (TBDRs) or TonB-dependent transporters (TBDTs).

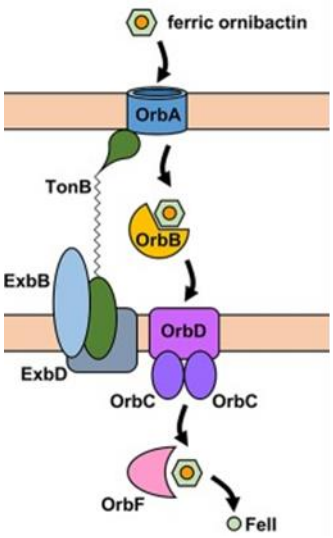

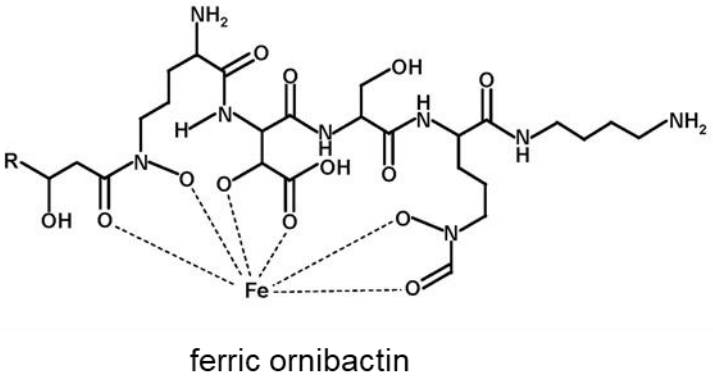

Figure 4-15 Ferric-ornibactin and proposed ornibactin uptake pathways into the *Burkholderia* bacterium[116,134]. Ferric-ornibactin is recognized by the OrbA TBDR and is translocated into the periplasmic space through a conformational change in the plug domain of the TBDR that requires energy transduction by the TonB complex (TonB-ExbB-ExbD). The iron-siderophore complex is then transported across the cytoplasmic membrane by a periplasmic binding protein-dependent ABC transporter (OrbBCD). Once the ferric-siderophore complex has been internalized, iron is released from ornibactin through its reduction to the ferrous form by OrbF.

Briefly, two general biosynthetic pathways for siderophores can be classified. The first is the well-characterized NRPS-dependent pathway and the other is the NRPS-independent siderophore (NIS) pathway, which relies on a different family of sparsely investigated synthetases[135]. In the bacterial world, NRPSs play a dominant role in siderophore production. So far, the majority of siderophores coming from *Burkholderia* are biosynthesized using these thiotemplate mechanisms (e.g., for the production of ornibactins or malleobactins[134,136]).

In the medical field, siderophores have been applied to fight against antibiotic-resistant bacteria and in the treatment of several human diseases[133]. They can mediate the selective delivery of antibiotics to antibiotic-resistant bacteria by the Trojan horse strategy[137]. This strategy exploits the iron transport abilities of siderophores to carry drugs into cells by preparation of conjugates between siderophores and antimicrobial agents. Furthurmore, the siderophores show bright prospects in other fields as well, in agricuture, for examples. Here, they are used for promoting plant growth or biological control. In addition, they can contribute to the soil environment for bioremediation of heavy metals[133].

Burkholderia species are talented producers of lipopetide-derived siderophores. A common feature of this class of compounds is that the polar amino acids like ornithine, lysine, serine, threonine, or aspartic acids are usually inserted into the peptide backbone. These polar amino acids are rich in hydroxy groups and therefore will facilite the iron-chelating ability of the final

product. Another hint for encoded siderophores on the genomic level can be the presence of genes coding for lysine/ornithine-N-monooxygenases and TonB-dependent receptors[138,139]. Besides the well studied ornibactins and malleobactins, a new group of siderophores that contain unique amino acid with diazeniumdiolate moiety was recently reported from *Burkholderia* as shown in Figure 4-16.

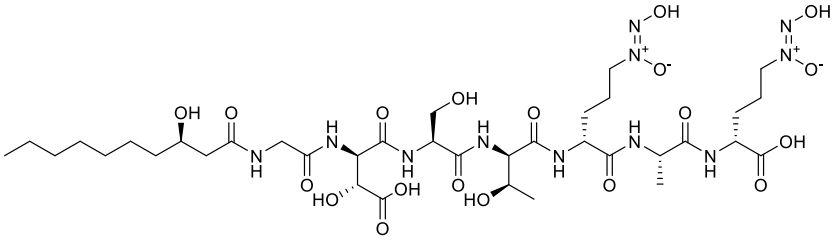

23

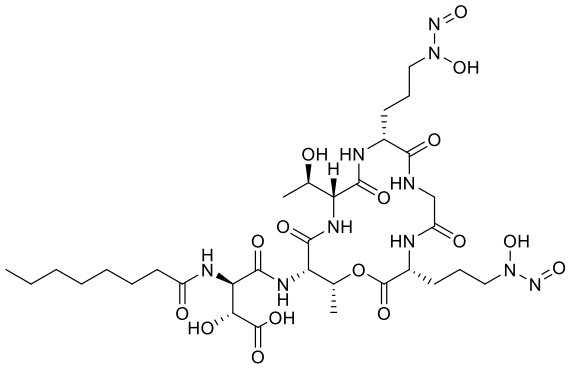

24

Figure 4-16 Chemical structures of megapolibactin A (23) and gramibactin (24).

This new class of lipopeptide-derived siderophores, megapolibactins and gramibactins, is biosynthesized via the classical NRPS-dependent pathway in a similar manner. They share a high similarity in chemical structures, harboring a lipide chain ranging from C_6 to C_{10} with or without a 3-hydroxy group. Further, all of them possessed the new defined amino acid graminine (a diazeniumdiolate containing amino acid) within their structure. This newly found amino acid played crucial roles in this siderophore. It has also been demonstrated that the diazeniumdiolate siderophore pathways are widespread in plant-associated or pathogenic bacteria, which increases interest in further investigational work[66].

4.2.5.2 Discovery of a New Siderophore Against Gram-Negative Bacteria

The major focus of this work was the isolation and structure elucidation of new chemistry from *Trinickia caryophylli* DSM 50341 based on screening results. The whole genome sequencing allowed the identification of its biosynthetic gene cluster. As a result, the structure was elucidated by a combination of NMR- and MS-spectroscopic techniques and bioinformatics.

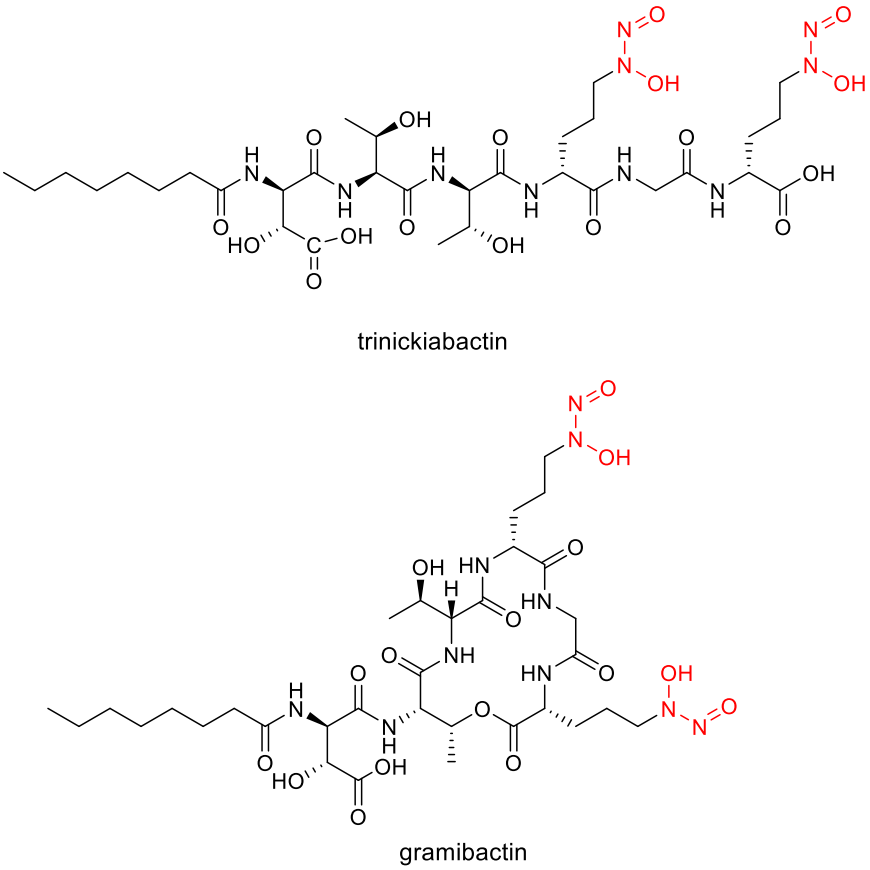

Figure 4-17 Chemical structures of trinickiabactin and gramibactin.

It was proven that trinickiabactin bears a rare diazeniumdiolate ligand as well. Structurally, trinickiabactin could be considered a linearized form of gramibactin, which was recently published by the Hertweck group. According to their publication, gramibactin ($C_{32}H_{54}N_{10}O_{16}$, exact mass of 834.37 Da, 18 Da less than the mass of the compound detected in our study) is a bacterial siderophore with a diazeniumdiolate ligand system produced by *Paraburkholderia graminis* C4D1M (Figure 4-17). This new discovery led to the extension of the type of siderophore because of its novel diazeniumdiolate (N-nitroso-N-hydroxylamine) chelators found in two graminine (Gra) moieties of the cyclopeptide. They introduced a new amino acid-graminine from natural origin and confirmed its structure via chemical synthesis[65]. As mentioned before, graminine may play crucial roles in this siderophore. The strong iron

chelating ability could be observed even during the isolation procedure when monitored with a CAS assay as reflected in Figure 4-19 (even 20 µL of diluted crude extract dissolved in methanol caused an intense orange halo).

Figure 4-18 CAS assay result of the crude extract from *T. caryophylli* DSM 50341.

With a deeper inspection of the ^{13}C NMR spectrum, some of the carbonyl groups were found to be significantly lower in intensity and exhibited minor peak broadness, likely owing to conformational changes or incomplete iron removal, and indicating, in the latter case in turn that Fe(III)-binding might be mediated via Gra4, Gra6, Thr2 and Thr3, which could differ from those of the cyclized gramibactin[140] (Figure 4-19).

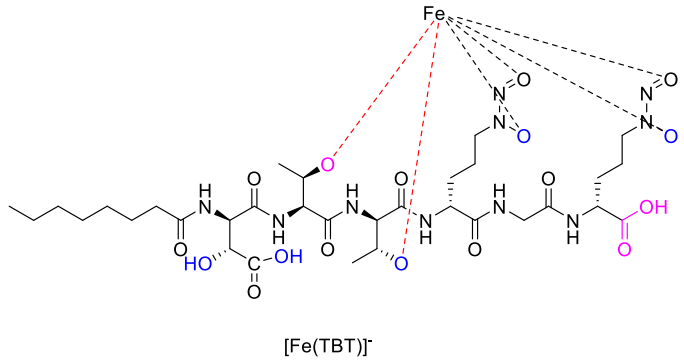

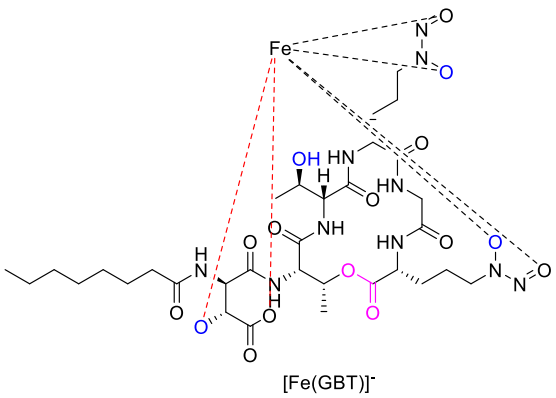

Figure 4-19 Proposed ferric structural form of trinickiabactin ([Fe(TBT)$^-$]) and gramibactin (Fe(GBT)$^-$).

According to the recently reported study, four hydroxyl groups of gramibactin could be involved in various protonation/deprotonation processes, including two hydroxyl groups from hydroxyl-aspartic acid and two N-nitroso-N-hydroxylamine groups[140]. In the case of trinickiabactin, two more hydroxyl groups are available due to the opened lacton ring (labeled in pink). Moreover, due to the linearized form of trinickiabactin, the conformation of the whole molecule should be altered compared to the cyclic gramibactin. Therefore, these two molecules may differ in their iron binding affinity. However, no detailed comparison studies were performed so far.

In brief, the difference between gramibactin and trinickiabactin is that the former has a cyclic form, while the compound in this study is in linear form. However, the genes of the corresponding BGC within *P. graminis C4D1M* and *T. caryophylli* DSM 50341 showed only an average identity of 63.9% and vary significantly in size (*grb HIJ* = 26.3 kb vs. *trb HIJ* = 25.3 kb). The difference between gramibactin and trinickiabactin could be explained by a speculated different activity of the involved TE domains (GrbC and terminal in GrbJ vs. TrbC and terminal in TrbJ), that is, the TE domains of the trinickiabactin BGC possibly lost their cyclase activity during evolution (Figure 4-1,Table 4-3).

In contrast to gramibactin, trinickiabactin was found to be antibacterial toward several gram-negative bacteria (MIC values ranged from 0.007 to 0.040 mM), while the antibacterial activity of gramibactin is unknown. Another example of a bioactive siderophore is serratiochelin A, which inhibited the growth of eukaryotic cells and *Staphylococcus aureus*[141]. Trinickiabactin showed selectively antibacterial activity against gram-negative bacteria, especially, against *Yersinia pseudotuberculosis* YPIII and *Burkholderia thailandensis* DSM 13276 with the highest activity. A plausible explanation could be the iron deprivation as observed for other siderophores, particularly, concerning the intraspecific and interspecific stimulated competition. An example is the case of actinomycete *S. coelicolor* in interaction with five other species of actinomycetes: in the face of fierce competition for iron *S. coelicolor* produced a vast and diverse range of siderophores[142].

To summarize this study, we confirmed that the plant pathogenic *Trinickia caryophylli* DSM 50341 is capable of producing trinickiabactin, a new siderophore that represents the linearized form of gramibactin, which was in turn isolated from a plant-beneficial rhizosphere bacterium *Paraburkholderia graminis* C4D1M. Both strains share a highly similar BGC but produce predominantly either a cyclized or a linearized variant. Assuming that the closed-ring molecule

is the maximal product of the biosynthetic pathway, differences among the detected variants could be explained by a different activity of the involved TE domains (TrbC and terminal in TrbJ vs. GrbC and terminal in GrbJ) in the *Trinickia* isolate or by isolation of artifacts, possibly caused by fermentation, isolation, or analytical conditions used in one of the two studies. Because lactone rings can be cleaved by strongly acidic or basic conditions, pH could be a crucial factor in these experiments. However, we monitored the pH at the start and at the end of the cultivation and noticed a comparable and only mild decrease of the pH value within the cultivation time frame, more specifically from neutral pH down to pH 6.4 in case of *T.caryophylli* in SRM_{HG} medium and down to pH 6.6 in the case of *P. graminis* in modified M9 medium, respectively. Since in each extraction protocol no acid was used and the same parameters were applied for the LC-MS analysis, a work-up- or analytics-related cleavage in the case of trinickiabactin was excluded. We thus speculate that there are differences between the TE domains involved in the respective biosyntheses (i.e., that the TE domains of the trinickiabactin BGC possibly lost their cyclase activity during evolution). If trinickiabactin production represents an ecological advantage for *T. caryophylli* in terms of competition for iron or for the defense of its niche, or if it even influences the virulence of the strain towards plants, are intriguing questions for future studies.

4.3 *Burkholderia oklahomensis* DSM 21774

4.3.1 Identification of the Hybridobactin Biosynthetic Gene Cluster

As one of the most talented producers among *Burkholderia* stricto-related strains during pre-screening, *Burkholderia oklahomensis* DSM 21774 demanded further study. Given that the genome (7.13 Mb, 67.07 GC%) of *B. oklahomensis* DSM 21774 was accessible from the GenBank (NCBI, accession number NZ_CP013358 and NZ_CP013358), a bioinformatical analysis using the web-based software AntiSMASH 4.2.0 was performed. Altogether, two chromosomes containing 20 biosynthetic gene clusters (BGCs) could be observed as reflected in Table 4-7.

Table 4-7 Secondary metabolites biosynthetic gene clusters identified in *Burkholderia oklahomensis* DSM 21774 using AntiSMASH 4.2.0 software.

Chromosome 1	Cluster	Type	Predicted Product	Similarity
	1	Phosphonate	-	5%
	2	T1 PKS	Lipopolysaccaride	5%
	3	Arylpolyene	-	-
	4	NRPS	Azinomycin B	4%
	5	NRPS	Nunapeptin	35%
	6	Terpene	-	-
	7	Lassopeptide_NRPS	Capistruin	100%
	8	Bacteriocin	-	-
Chromosome 2	1	Other	Echosides	23%
	2	Hserlactone	-	-
	3	Pyoverdine	-	-
	4	NRPS	-	-
	5	Bacteriocin	-	-
	6	Herlactone	PM100117/PM10018	10%
	7	Phosphonate	Thailanstatin	10%
	8	TransatT1- PKS-NRPS	Malleilactone	100%
	9	Terpene	-	-
	10	T1 PKS-NRPS	Yersiniabactin	11%
	11	T1 PKS-NRPS	Glidobactin	26%
	12	Terpene-Other KS	-	-

The strain showed a high chemical diversity, including numberous attractive NRPS or NRPS-PKS products, as expected. After an intensive analysis of these selected BGCs and combining the previous screening results, the BGC encoded in the second chromosome sharing 26% similarity with glidobactin was considered to be an intriguing target for further investigation.

This potential biosynthetic gene cluster (*hybA-H*) was 13.5 Mb in size and centrally consisted of NRPS and NRPS-PKS hybrid genes, which were given the designation *hybB* and *hybE*, respectively. Some transporter genes and accessary genes flank the central genes upstream and downstream(Figure 4-20 and Table 4-8). The genes between *hybB* and *hybE* represent an MFS transporter and an MbtH-like gene, respectively. The gene *hybA* that encodes a dioxygenase shares 59% similarity with the *glbB* gene of the glidobactin BGC, which was recently identified as a lysine 4-hydroxylase, allowing the hydroxylation of the lysine residue during the biosynthesis[143].

The genes *hybB* and *hybE* build up the core assembly line: *hybE* encodes a C-A-T module and the $C_{starter}$ domain initiates the fusion of the fatty acid chain with the first activated threonine. Afterwards, the acylated threonine should be extended by the other two NRPS and single PKS modules encoded by *hybB*. Therefore, a Thr1-Lys/Orn2-X3 sequence could be deduced from this biosynthetic pathway, in which X3 represents an unknown amino acid-based unit.

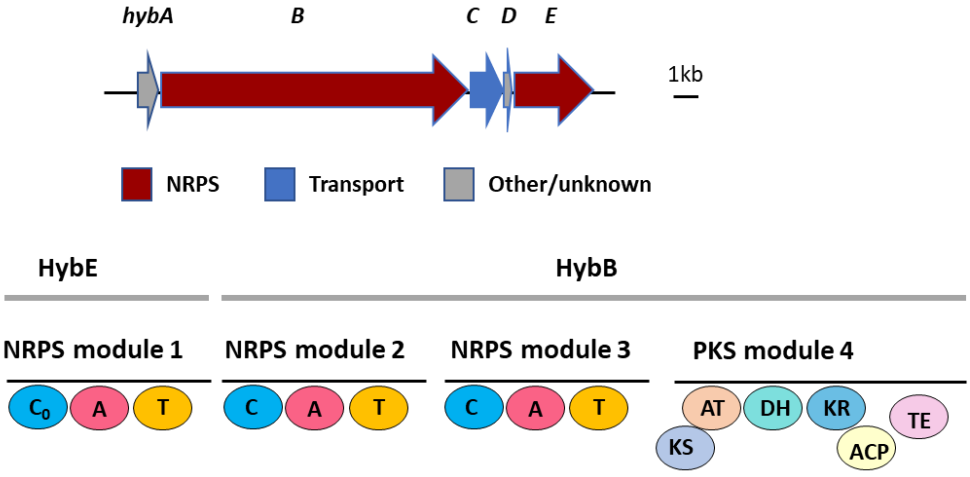

Figure 4-20 Proposed hybridobactin biosynthetic gene cluster.

Table 4-8 Encoded enzymes and their putative functions within the proposed (hybridobactin) biosynthetic gene cluster.

Protein	Size [aa]	Putative Function
HybA	263	2OG-Fe dioxygenase
HybB	4203	NRPS-PKS
HybC	416	MFS transporter
HybD	66	MbtH-like
HybE	1070	NRPS

4.3.2 Isolation of Hybridobactins

To get a sufficient amount of the target compounds (termed hybridobactins A-D), an upscaled bacterial culture of 24 liters was fermented. The supernatant was extracted with XAD-16N resin and subsequently eluted with MeOH and evaporated under reduced pressure to yield 6.8 g crude extract. The resulting residue was resuspended in a mixture of MeOH-H_2O (70:30) and fractionated by LH-20 size exclusion chromatography (SEC) to afford six subfractions, which were collected according to the occurence of the colored bands. LC-MS monitoring of the obtained subfractions showed the third fraction to be of further interest, since it contained the targeted hybridobactins (Figure 4-21). Then, the third fraction was subjected to semi-preparative RP-HPLC to obtain the hybridobactins in a semi-pure form. The separation was then further performed in gradient elution mode using MeOH (A) and deionized H_2O containing 0.1% TFA (B) as mobile phases. The gradient started at 30% A, holding for 5 min, increasing the percentage of A in 10 min to 60%, increasing the percentage of A to 100% in 5 min, followed by isocratic elution of 100% A for an additional 3 min (Phenomenex Luna Omega Polar C_{18} column, 10 x 250 mm, 5 µm in combination with a Phenomenex SecurityGuard RP C_{18} 10 x 10 mm precolumn; 4 mL/min flow rate; UV monitoring at 254 nm).

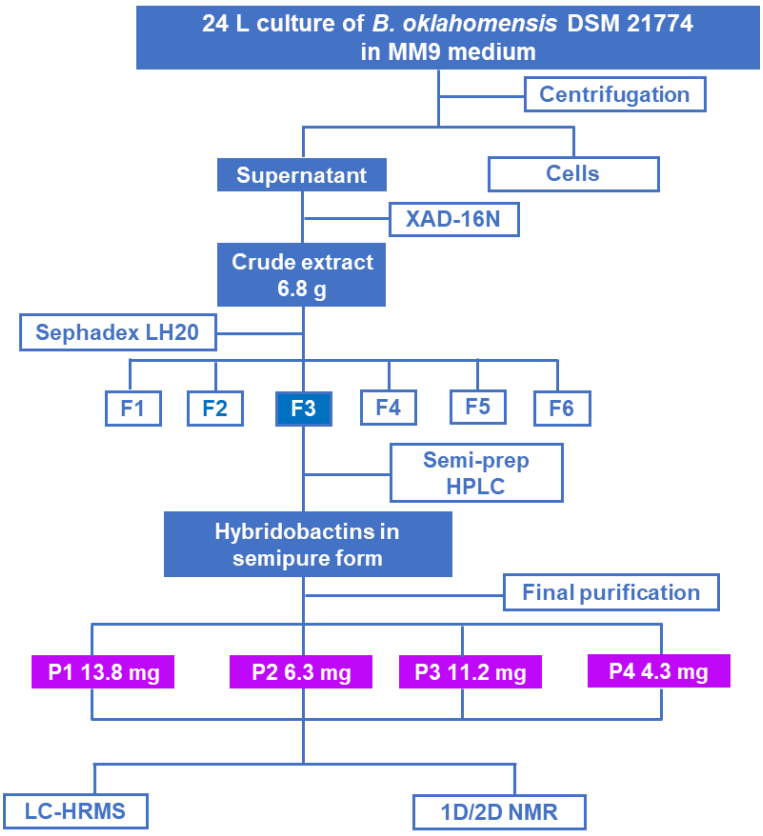

Figure 4-21 Fractionation scheme for the isolation of hybridobactins.

Final purification was performed with an Aeris^{TM} Peptide XB-C18 column (250 x 4.6 mm, 3.6 µm), flow rate 0.8 mL/min, UV monitored at 254 nm (Figure 4-22). The gradient started at 10% A, holding on for 3 min, increasing the percentage of A in 7 min to 50%, increasing the percentage of A to 100% in 10 min, followed by isocratic elution of 100% A for an additional 3 min. Hybridobactins A-D were eluted at 12.7 min, 13.8 min, 14.9 min and 15.7 min, respectively. Rechromatography of the obtained material yielded 13.8 mg hybridobactin A, 6.3 mg hybridobactin B, 11.2 mg hybridobactin C and 4.3 mg hybridobactin D.

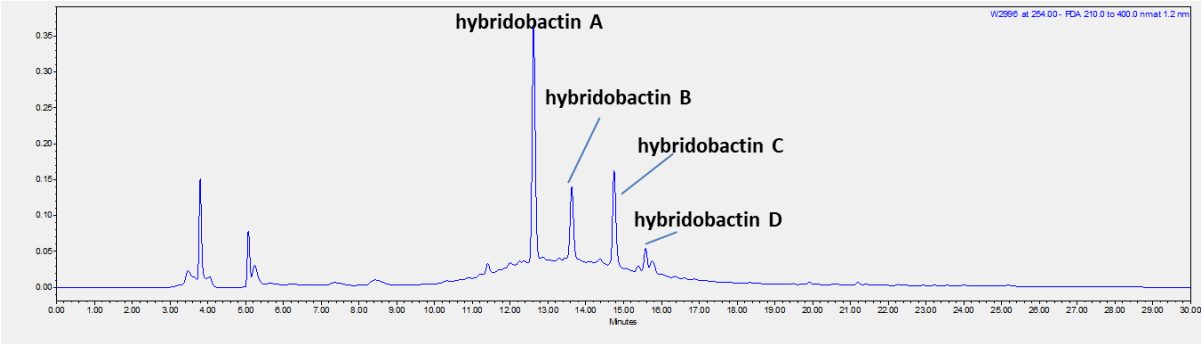

Figure 4-22 HPLC chromatogram of the purification of hybridobactins. UV monitored at 254 nm.

4.3.3 Structure Elucidation of Hybridobactins

To determine their planar structures, ESI-HR-MS, MS/MS, and 1D and 2D NMR experiments were performed. For hybridobactin A, HR-MS analysis in positive mode with an *m/z* of 485.2976 $[M+H]^+$ (Figure 4-23) suggested a molecular formula of $C_{23}H_{41}N_4O_7$ (calc. for 485.2970, Δ 0.6 ppm, 6 degrees of unsaturation).

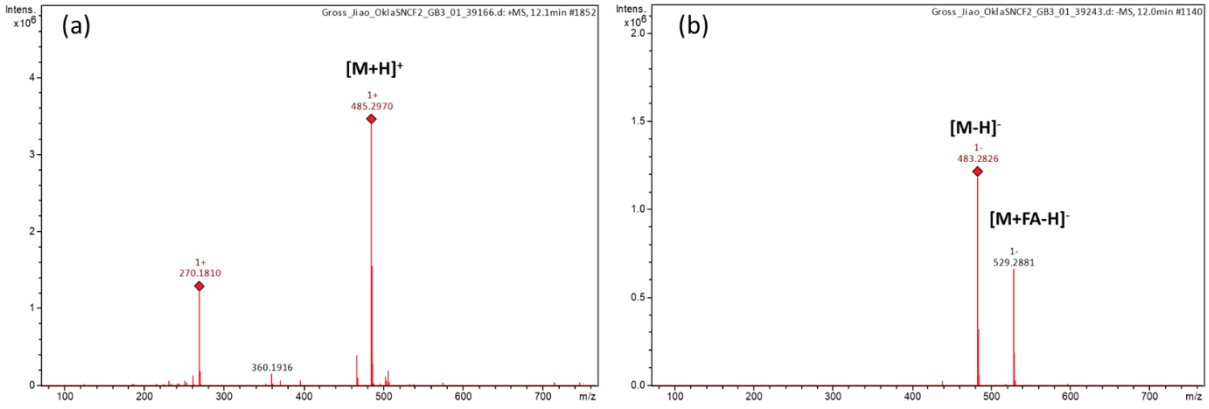

Figure 4-23 High-resolution ESI-MS spectra of Hybridobactin A. (a) Positive mode. (b) Negative mode. FA is abbreviated for formic acid.

All ^{13}C NMR and ^{1}H NMR signals were assigned using DEPT135, COSY, HSQC, HSQC-TOCSY and HMBC spectroscopy experiments (Table 4-9).

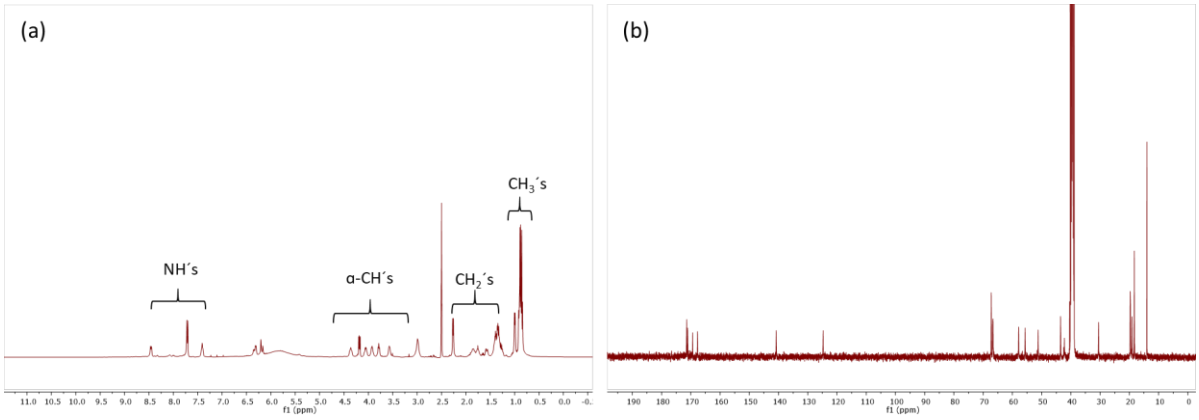

Figure 4-24 1D NMR spectra of hybridobactin A. (a) ^{1}H NMR spectrum of hybridobactin A (400 MHz, DMSO-d_6). (b) ^{13}C NMR spectrum of hybridobactin A (100 MHz, DMSO-d_6).

In ^{1}H NMR spectrum exchangeable downfield amide signals at δ_H 7.40–8.50 and α-proton resonances between δ_H 3.50 and 4.50 were observed (Figure 4-24). Overlapping methylene signals in the high magnetic field, together with a terminal methyl resonance at δ_H 0.85 suggested that hybridobactin A contained an alkyl chain. The ^{13}C NMR spectrum detected four

carbonyl carbons in the range of δ_C 167–172. These data suggested that hybridobactin A was likely to feature a typical lipopeptide structure.

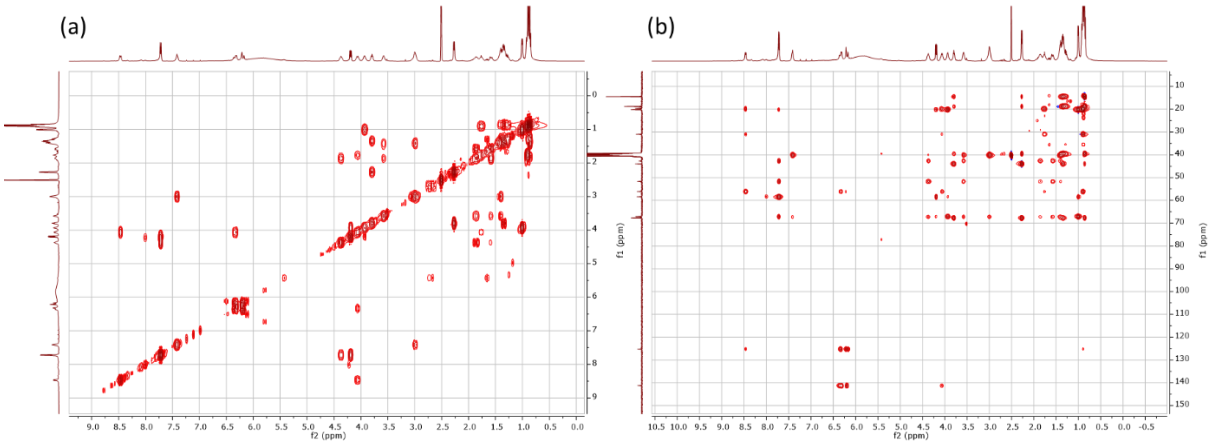

Figure 4-25 2D NMR spectra of hybridobactin A. (a) ^{1}H-^{1}H COSY NMR spectrum of hybridobactin A (400 MHz, DMSO-d_6) (b) ^{1}H-^{13}C HSQC-TOCSY NMR spectrum of hybridobactin A (400 MHz, DMSO-d_6).

Based on an HSQC-TOCSY spectrum, one spin system was interpreted as a 5-methyl-4-amino-2-hexenoic acid moiety derived from valine incorporating a double bond, a vicinal coupling constant of 16 Hz indicated that this double bond harbored an *E*-configuration. A deeper analysis of the HSQC-TOCSY and COSY spectra revealed the presence of another three spin systems (Figure 4-25 and Table 4-9). Therefore, hybridobactin A posssessed one threonine (Thr), one 4-hydroxy-lysine (4-OH-Lys), one 5-methyl-4-amino-2-hexenoic acid (5-Mah) moiety and a fatty acid chain.

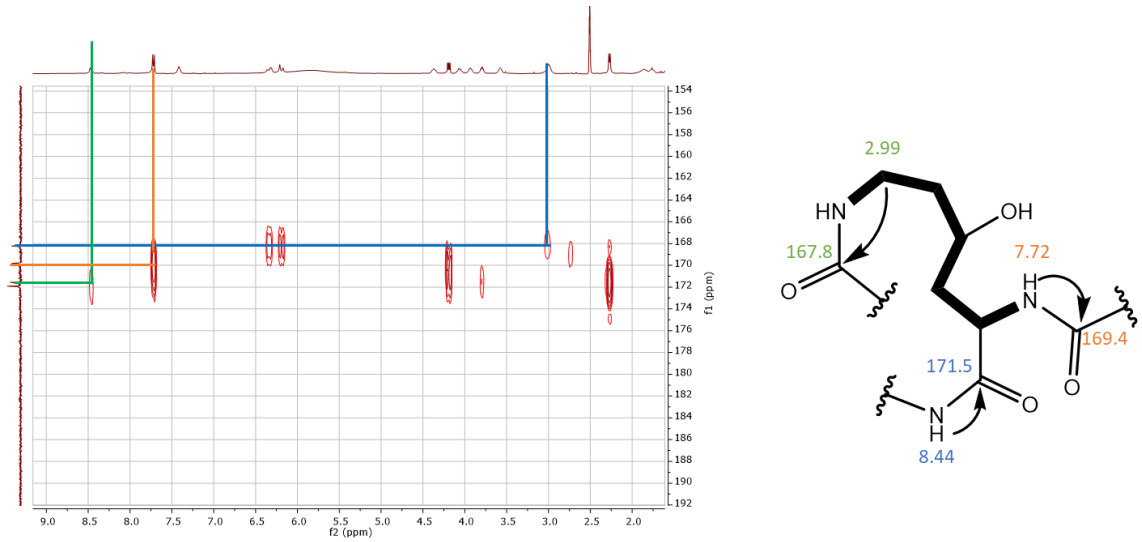

Figure 4-26 Enlarged ^{1}H-^{13}C HMBC spectrum of hybridobactin A and key correlations. Signals in different colors are reflected on the partial planar structure at right side.

Analysis of the HBMC spectrum revealed that both the amide groups and its carbonyl group of the 4-hydroxy-lysine were involved in the ring closure (Figure 4-26). Moreover, its α-amino group was connected with an N-acylated threonine, followed by the fatty acid chain. The remaining unassigned six carbon and two oxygen atoms that were not accounted for by amino acids, including one methyl, one carbonyl carbon and one carbinol methine and three aliphatic methylene carbons (Table 4-9), suggested the presence of a linear hydroxy-hexanoic acid (OA). Summarizing all the information above, the linear peptide sequence of hybridobactin A was identified as HHA-Thr1-(4-OH-Lys2)-Mah3 (Figure 4-27).

Table 4-9 NMR spectroscopic data (DMSO-d_6) of hybridobactin A

Unit	Position	$\delta_{C/N}$, mult.	δ_H,mult. (*J* in Hz)
3-hydorxy-hexanoic acid (HHA)	1	171.1, qC	-
	2	43.5, CH_2	2.26, 2H (d, 6.7)
	3	67.2, CH	3.79, 1H (m)
	4	38.6, CH_2	1.34*, 1.27*, 2H (m)
	5	18.3, CH_2	1.34*, 1,27*, 2H (m)
	6	14.0, CH_3	0.85, 3H (d, 6.8)
Thr1	C=O	169.4, qC	-
	α	57.9, CH	4.18, 1H (dd, 8.6, 4.3)
	β	66.6, CH	3.92, 1H (m)
	γ	19.7, CH_3	1.00, 3H (d, 6.0)
	NH	121.2	7.72, 1H (d, 7.5)
4-OH Lys2	C=O	171.5, qC	-
	α	51.2, CH	4.36, 1H (t, 8.7)
	β	42.4, CH_2	1.86, 1.56, 2H (m)
	γ	66.7, CH	3.57, 1H (Broad s)
	δ	39.2	1.39, 2H (m)
	ε	39.6	2.99, 2H (Broad s)
	α-NH	118.1	7.72, 1H (d, 7.5)
	NH	118.1	7.41, 1H (Broad s)
5-Mah3	C=O	167.8, qC	-
	α	124.7, CH	6.20, 1H (d, 16.2)
	β	140.7, CH	6.32, 1H (dd, 16.4, 6.7)
	γ	55.7, CH	4.05, 1H (q, 7.6)
	δ	30.5, CH	1.75, 1H (m)
	ε	19.1, CH_3	0.89, 3H (d, 7.1)
	ζ	19.6, CH_3	0.86, 3H (d, 7.0)
	NH	132.6	8.45, 1H (d, 8.1)

*Overlapped signals.

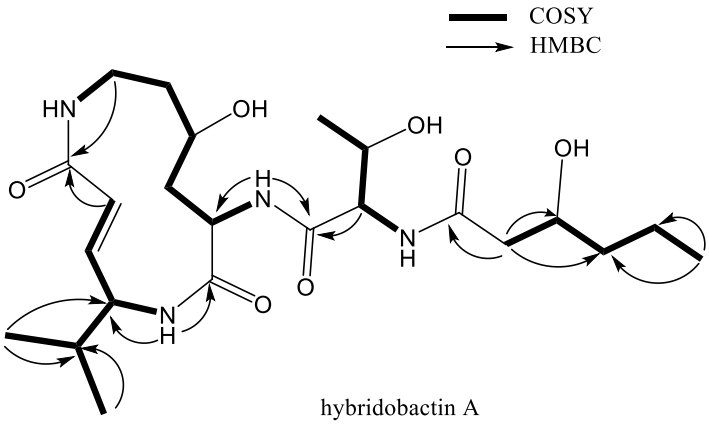

Figure 4-27 Key spin systems and selected long-range correlations leading to the identification of the planar structure of hybridobactin A. Bold lines indicate ^{1}H-^{1}H COSY or ^{1}H-^{13}C HSQC-TOCSY correlations, arrows indicate ^{1}H-^{13}C correlations.

To acquire more information and to confirm the building block composition and their connectivity, ESI-MS/MS experiments were also carried out. For this analysis, the pseudo-molecular ion $[M+H]^{+}$ was selected and fragmented. The fragmentation occurred mainly in the amide bond, which is common in peptides. The combination of b and y fragments from MS/MS was in agreement with the proposed peptide sequence derived from NMR and bioinformatics (Figure 4-28).

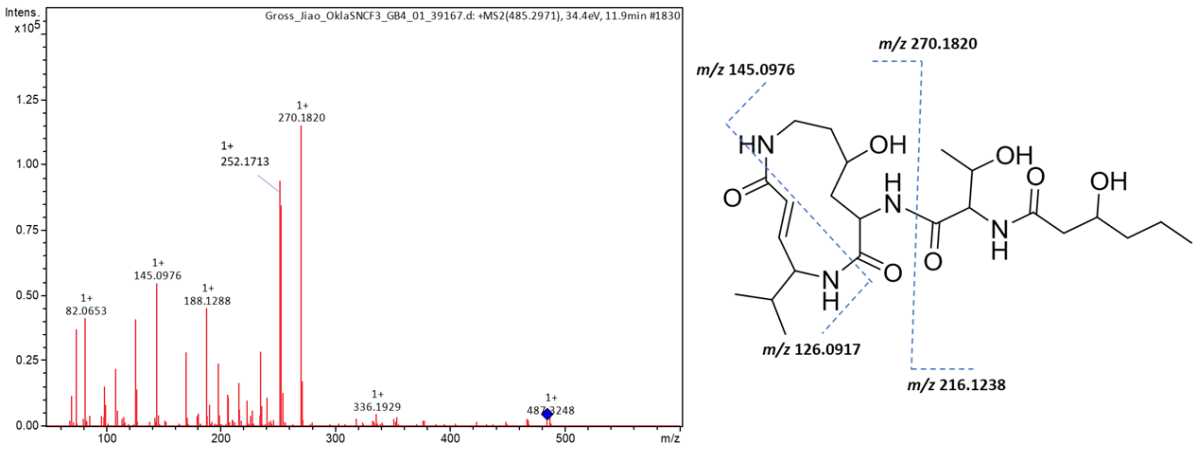

Figure 4-28 MS/MS spectrum of hybridobactin A in positive mode.

Based on HR-MS analysis, hybridobactins B-D represent derivatives which successively increased 14 Da in their masses in comparison to hybridobactin A. Hybridobactin B bears one more methylene group than hybridobactin A, located at the double bond-containing residue based on MS/MS fragmentation. This assignment could be confirmed with 1D and 2D NMR analysis. Hence, hybridobactin B habors a 6-methyl-4-amino-2-heptenoic acid (6-Mah) instead of 5- methyl-4-amino-2-hexenoic acid (Table 4-10 and Figure 4-29).

Table 4-10 NMR spectroscopic data (DMSO-d_6) for hybridobactin B.

Unit	Position	$\delta_{C/N}$, mult.	δ_H, mult. (*J* in Hz)
3-hydroxy-octanoic acid (HOA)	1	171.1, qC	-
	2	43.5, CH_2	2.25, 2H (d, 6.4)
	3	67.2, CH	3.79, 1H (m)
	4	39.3, CH_2	1.36*, 2H (m)
	5	18.3, CH_2	1.27, 1,33*, 2H (m)
	6	14.0, CH_3	0.86, 3H (t, 7.5)
Thr1	C=O	169.4, qC	-
	α	57.9, CH	4.17, 1H (dd, 8.6, 4.3)
	β	66.6, CH	3.92, 1H (m)
	γ	19.7, CH_3	1.00, 3H (d, 6.0)
4-OH Lys2	C=O	171.2, qC	-
	α	51.2, CH	4.31, 1H (t, 8.7)
	β	42.2, CH_2	1.84, 1.62, 2H (m)
	γ	66.9, CH	3.57, 1H (Broad s)
	δ	39.1	1.39, 2H (m)
	ε	39.7	2.98, 2H (Broad s)
6-Mah3	C=O	167.7, qC	-
	α	124.2, CH	6.22, 1H (d, 16.0)
	β	140.0, CH	6.32, 1H (dd, 16.4, 6.0)
	γ	47.6, CH	4.34, 1H (m)
	δ	41.5, CH_2	1.41, 2H (m)
	ε	24.6, CH	1.57, 2H (m)
	ζ	21.9, CH_3	0.84, 3H (d, 7.1)
	η	22.4, CH_3	0.89, 3H (d, 7.2)

*overlapped signals.

Furthermore, hybridobactin C carries two methylene groups more than hybridobactin A due to a longer fatty acid chain (C_8), while the same situation occurs in hybridobactin B and D.

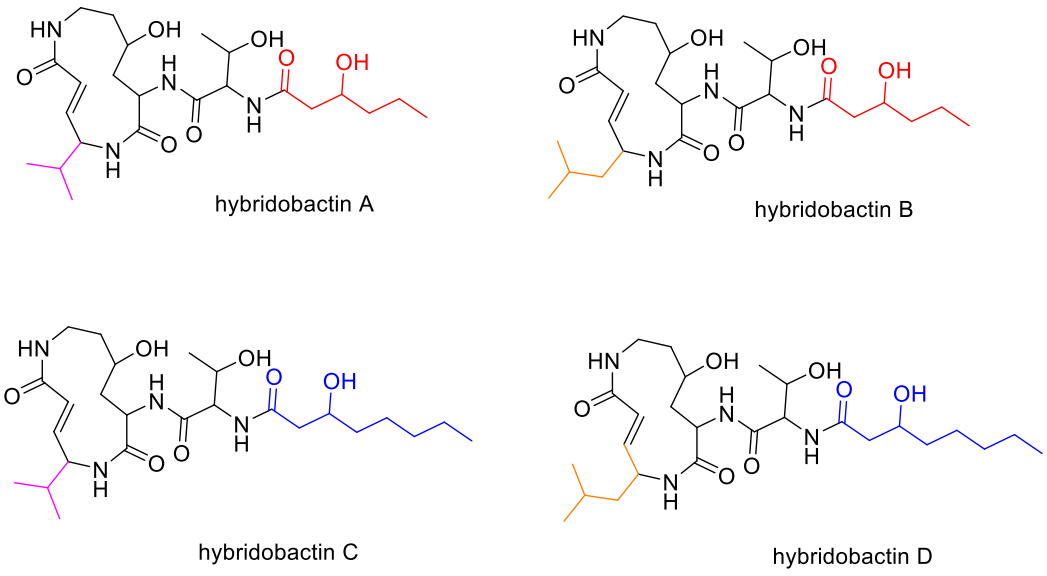

Figure 4-29 Planar structures of hybridobactins A-D. The same color represents the same chemical moiety.

4.3.4 Determination of the Absolute Configurations

To confirm the configuration of the threonine unit within hybridobactins, Marfey´s method was performed as described in chapter 3.2.6. Comparing with all four threonine standards, the absolute configuration of the threonine in hybridobactin A was determined to be L-configured. Since the other two amino acid-containing portions were relatively rare, no standards were commercially available. Thus, Marfey´s method could not be applied in this case. Given that neither epimerization domains nor dual C/E domains[144] were present within the corresponding BGC, all amino acids were considered to be L-configured. Due to the high structural similarities and the existence of only one biosynthetic gene cluster, we inferred that hybridobactin A-D confers the same configuration in the peptide sequence.

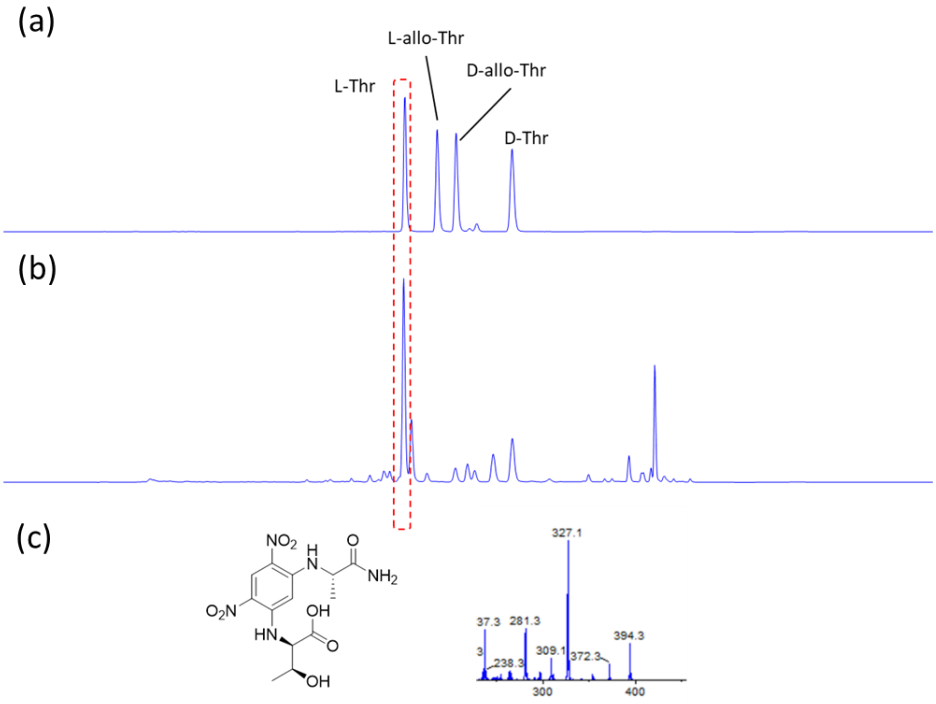

Figure 4-30 Determination of the threonine configuration within hybridobactin A using Marfey´s method. (a) HPLC run of amino acids standard derivatized with L-FDAA. (b) HPLC run of hybridobactin A hydrolyzate derivatized with L-FDAA. (c) Derivatized threonine and its mass ion in postive mode.

To determine the stereocenter at the side chain of all hybridobactins, a stereo-analysis was accomplished by enantioselective UPLC-ESI-MS analysis with a CHIRALPAK® IA-U column as chiral stationary phase. Racemization of the obtained fatty acids residue was detected during sample analysis, possibly due to the hydrolysis. This could also be confirmed through isotopologue correction. However, the major components remained *R*-configured. Thus, the 3-hydroxy-hexanoic acid of hybridobactins A and C matched the 3*R*-hydroxy-hexanoic acid, while hybridobactin B and D were confirmed as 3*R*-hydroxy-octanoic acid[109] (Table 4-11).

Table 4-11 Results of the stereoseparation of the chiral side chains from hybridobactins A-D

Sample Name	**t_R in [min]**	**t_R in [min]**
	S	**R**
HHA standard	2.97	3.14
Hybridobactin A	-	3.15
Hybridobactin C	-	3.15
HOA standard	7.27	7.49
Hybridobactin B	-	7.50
Hybridobactin D	-	7.50

To sum up, applying the bioinformatics and chemical analytical methods in combination allowed the suggestion of the absolute configuration of hybridobactin A-D with the exception of the stereocenter given at the γ-position of 4-hydroxy-lysine.

4.3.5 20S Proteasome Inhibition Assay and Cell Proliferation Assay of Hybridobactins

The syrbactins are known as irreversible proteasome inhibitors, so we performed 20S proteasome inhibition assays to test hybridobactin A–D (Figure 4-31). In order to have a comprehensive comparison with other known subgroups of syrbactins, syringolin A and glidobactin C were isolated as standards, in addition to epoxomicin. In general, hybridobactin A-D exhibited proteasome inhibition ability in varying degrees, as expected. Out of the four hybridobactins, hybridobactin D showed particularly strong activity that could even compete with epoxomicin on the same level (Table 4-12 and Figure 4-31).

Table 4-12 Proteasome inhibition assay results of different inhibitors.

Compounds	Value Based on kobs/I
Epoxomicin	0.12 ± 0.00008573
Hybridobactin A	0.01818 ± 0.009448
Hybridobactin B	0.03518 ± 0.002098
Hybridobactin C	0.03766 ± 0.00546
Hybridobactin D	0.121 ±0.01671
Glidobactin C	0.04847 ± 0.003994
Syringolin A	No inhibition observed

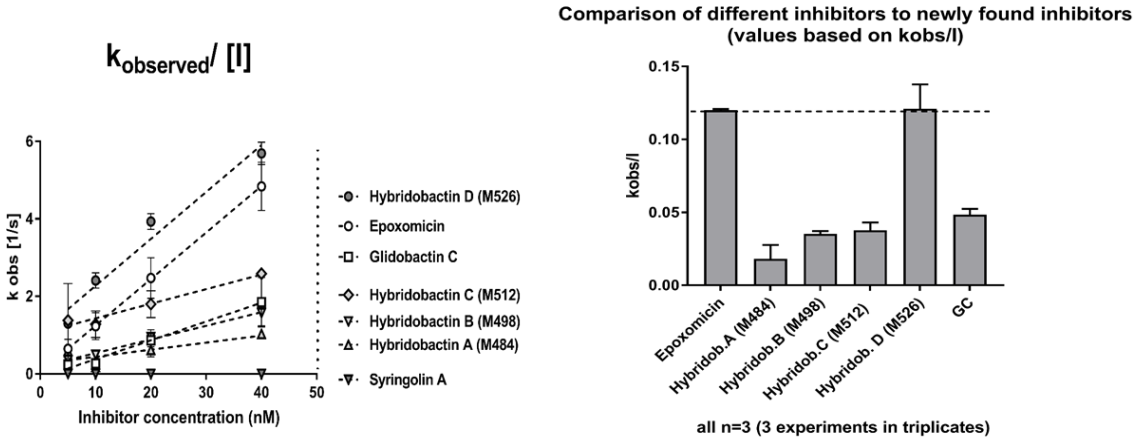

Figure 4-31 Results of the proteasome inhibition assays.

In parallel, the proliferation assay was also carried out to evaluate the in vitro cytotoxicity of hybridobactin D. Due to insufficient amounts of glidobactin C, only duplicates were performed, in which only an approximate IC_{50} value was obtained (Figure 4-32). Hybridobactin D presented a weaker activity (473.3 nM) in comparison to epoxomicin (1.962 nM).

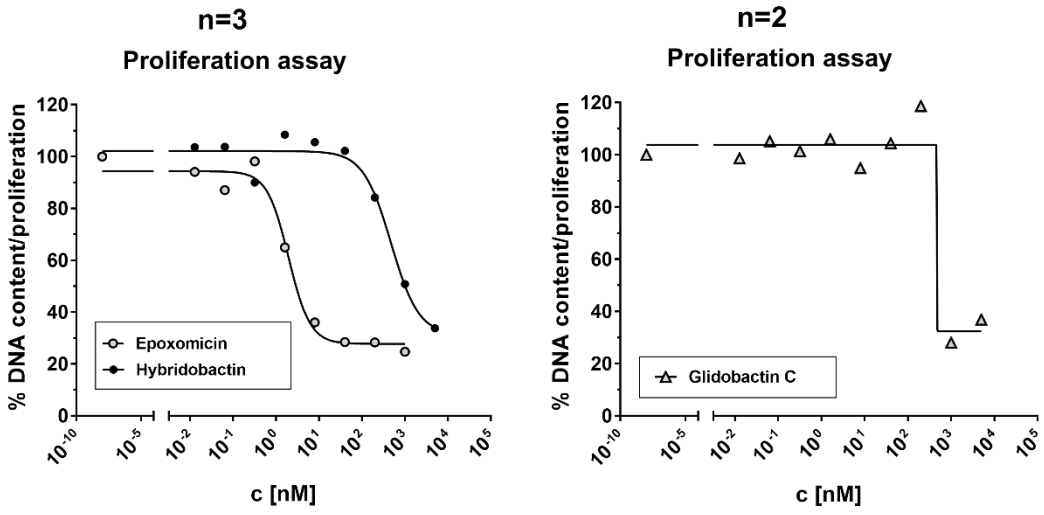

	Epoxomicin	Hybridobactin	Glidobactin C neu
IC50	1.962	473.3	~ 466.7

Figure 4-32 In vitro proliferation assay results of hybridobactin D and glidobactin C.

4.3.6 Discussion and Outlook

4.3.6.1 Proteasome Inhibitors from Syrbactins

The class of syrbactins is composed of syringolins, glidobactins and cepafungins compound families. They not only display a common mode of action, but also share a high similarity on the structural and biosynthetic level. To reflect these facts, the subordinate natural product class of 'syrbactins' was coined from the combination of the names 'syringolins' and 'glidobactins'[145].

Cepafungins and glidobactins exhibit antifungal and antitumor activity and were the first compounds to be isolated from the syrbactin family. Later on, it was reported that syringolins induced resistance to the rice pathogen *Pyricularia oryzae*. Subsquently, further glidobactin derivatives were discovered, such as luminmycins, whose BGC from *Photorhabdus luminescens* was cloned into a vector by using the newly established linear–linear homologous recombination and successfully expressed in *Escherichia coli*. This led to the discovery of luminmycins A-C[146].

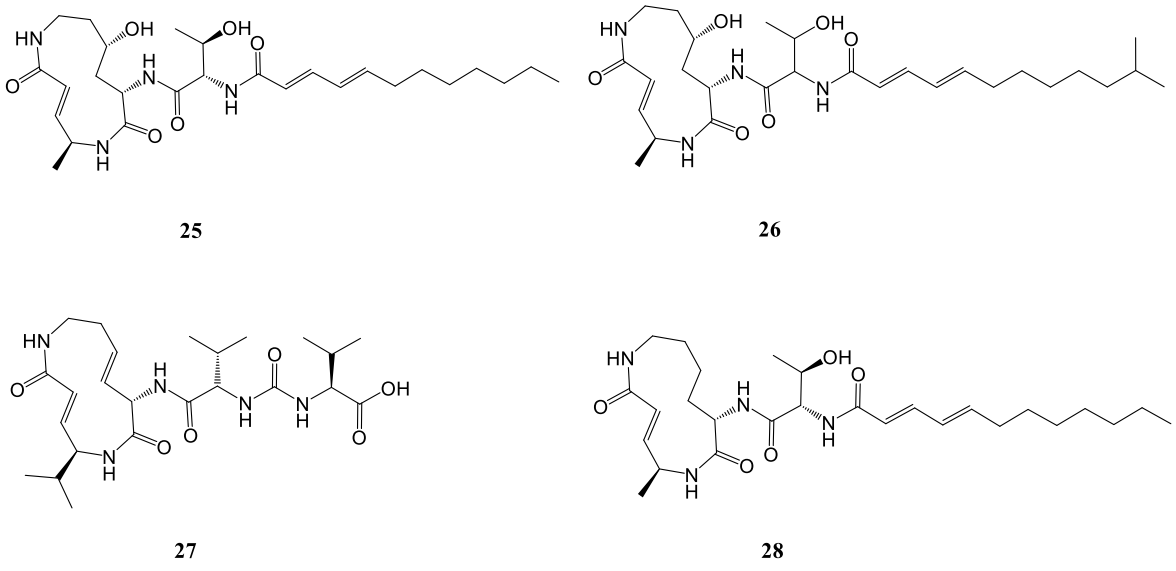

Figure 4-33 Representative compounds from the syrbactin compound family. Glidobactin A(**25**), cepafungin II (**26**), syringolin A (**27**) and luminmycin A (**28**).

As a unifying feature, all syrbactins are framed based on a 12-membered dipeptide-macrolactam ring system, resulting from linkage of a vinylogous amino acid and a modified lysine moiety. Additionally, the α-amino group of the lysine residue is coupled with an exocyclic chain. In the case of syringolins, this exocyclic residue is an ureido dipeptide moiety, while glidobactins and cepafungins possess an N-acylated threonine residue instead (Figure

4-33). Moreover, all amino acids from glidobactins and syringolins feature an (L)-configuration. Luminmycin A is a desoxylated glidobactin A, while other lumininmycins are acyclic derivatives. Due to the unprecedented novelty of the syrbactins, they were turned to an unique natural product class with special chemical and biological properties[145].

However, the bridge of these syrbactin-subgroups was constructed by Groll and coworkers through elucidation of their molecular mechanism. Both glidobactins and syringolins have been proven to act as 20S proteasome inhibitors. Their structural studies revealed that the observed irreversible inhibition resulted from an oxa-Michael-type addition of the hydroxyl group of the active site threonine residue of the 20S proteasome[147]. This study raised the interest of this compound class, particularly in the synthetic field, which led to synthesis of a great number of syrbactin derivatives, aiming to improve their activities, including a lipophilic SylA derivative and a hybrid compound SylA-GlbA exhibiting highly potent activity[148,149].

To have a first insight into the biosynthesis of the structurally unique syrbactins, the Dudler group invested a of efforts identifying and characterizing the biosynthetic gene clusters coding for syringolins and glidobactins[150,151]. The biosynthetic assembly line of both syringolins and glidobactins were proven to be of hybrid NRPS-PKS origin (Figure 4-34). These findings also enabled the discovery of the luminmycin biosynthetic gene cluster through bioinformatic analysis. Recently, Zhao *et al.* found a vast number of glidobactin-like proteasome inhibitors using bioengineering and molecular networking approaches in combination[152]. All these studies enriched the diversity of the syrbactin compound family.

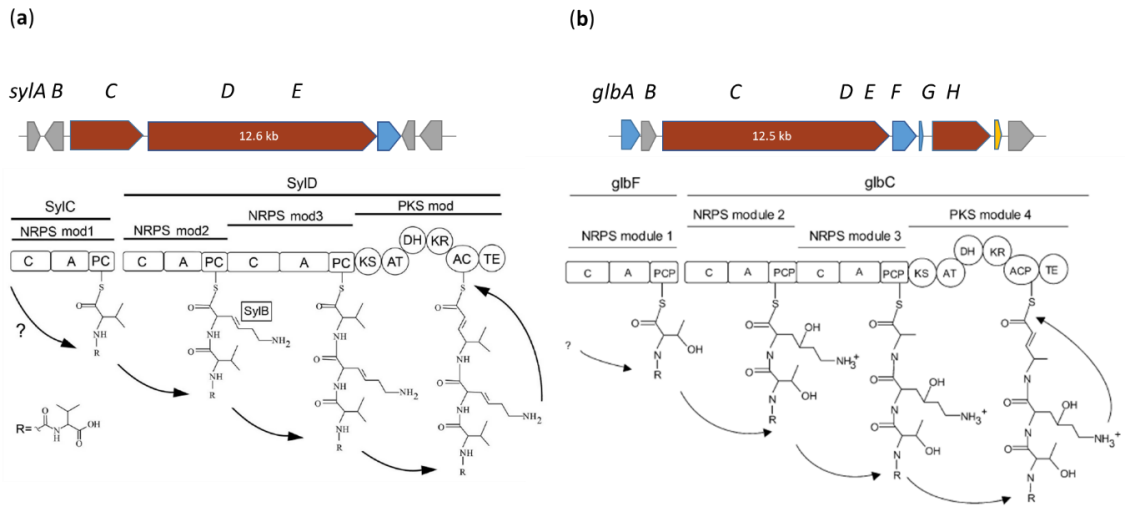

Figure 4-34 The biosynthesis of selected syrbactins. (a) biosynthesis model of syringolin A. (b) biosynthesis model of glidobactin A, R denotes fatty acid moiety. KS, putative β-ketoacyl synthase; AT, acyl transferase; DH, dehydratase; KR, β-ketoreductase; ACP, acyl carrier protein; TE, thioesterase.

4.3.6.2 Discovery of Novel Hybrid Proteasome Inhibitors from the Syrbactin Class

Since the biosynthetic origin of this class of compounds is similar, a comparison of the key enzymes within each of the BGCs was conducted via BlastP (Table 4-13). Two enzymes, HybB and HybE, make up the NRPS-PKS assembly line of the final product as previously predicted, and are conserved both in syringolin and glidobactin BGCs. Another vital transporter like HybC, likely involved in the secretion of the compound, could also be observed. The MbtH-like protein is conserved in both hybridobactin and glidobactin BGCs but could not be detected in syringolin BGC. In general, the hybridobactin correlates more with the glidobactin BGC (approximate identity is 60%) than the syringolin BGC (approximate identity is less than 40%).

Table 4-13 Comparison of encoded enzymes in hybridobactin, syringolin and glidobactin BGCs.

Syringolin BGC *Pseudomonas syringae* pv. *syringae*				**Hybridobactin BGC** *Burkholderia oklahomensis* DSM 27114				**Glidobactin BGC** *Polyangium brachysporum* DSM 7029		
Protein	Length	Encoded putative protein	Identity	Protein	Length	Encoded putative protein	Identity	Protein	Length	Encoded putative protein
SylA	237 aa	LysR-type regulator	-	-	-	-	-	GlbA	337 aa	LysR-type regulator
SylB	350 aa	fatty acid desaturase	-	HybA	263 aa	2OG-Fe dioxygenase	59.09 %	GlbB	286 aa	Conserved protein
SylD	4186 aa	NRPS/PKS	41.11 %	HybB	4203 aa	NRPS/PKS	61.19 %	GlbC	4181 aa	SylD-like NRPS/PKS
SylE	398 aa	permease	39.38 %	HybC	416 aa	MFS transporter	62.65 %	GlbD	436 aa	SylE-like permease
-	-	-	-	HybD	66 aa	MbtH-like	65.57 %	GlbE	73 aa	MbtH-like
SylC	1304 aa	NRPS	33.74 %	HybE	1070 aa	NRPS	61.42 %	GlbF	1083 aa	Sylc-like NRPS
-	-	-	-				-	GlbG	121 aa	Ketosteroid isomerase-related
-	-	-	-				-	GlbH	472 aa	2-Nitrodioxygenase-like

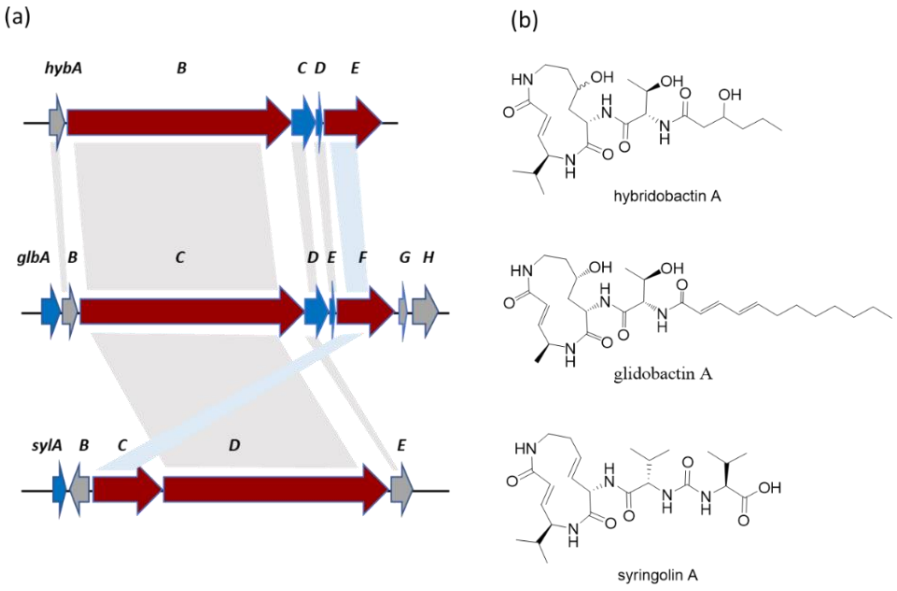

Figure 4-35 Examples of syrbactin BGCs and their encoded secondary metabolites. (a) Biosynthetic gene cluster of hybridobactin (*hyb*) glidobactin (*glb*) and syringolin (*syl*) biosynthetic gene clusters in *B. oklahomensis*, *P. luminescens* and *P. syringae*, respectively. Arrows with the same pattern represent similar functional genes. (b) Chemical structures of selected syrbactins.

This variable identity of these three BGCs from different producers led to the downstream chemical structures variation, in which several subclasses from syrbactins were formed (Figure

4-35). Given that the biosynthetic pathway of both syringolins and glidobactins are relatively clearly understood, the hybridobactin assembly line could also be inferred in a similar fashion after the chemical structure of hybridobactins was fully elucidated.

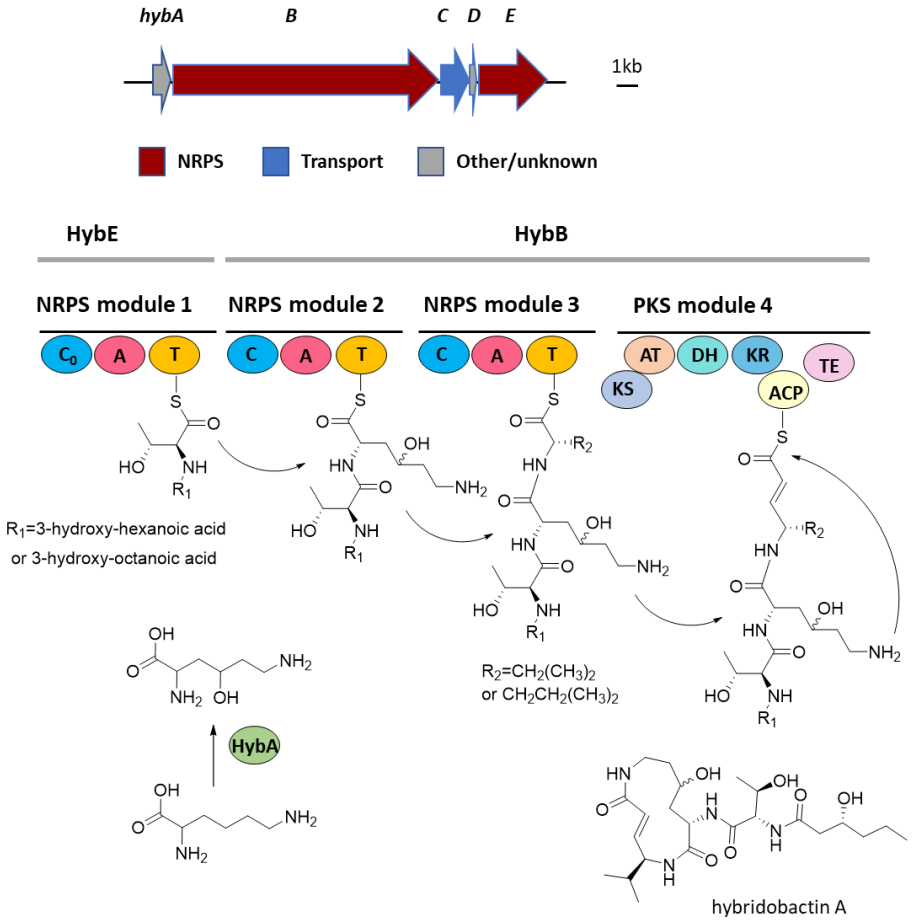

Figure 4-36 Proposed pathway for hybridobactin biosynthesis. Underneath the genes are the module and domain organization of HybE and HybB. C, Condensation domains; A, adenylation domains; T, peptide carrier protein domains; KS, putative β-ketoacyl synthase; AT, acyl transferase domain; DH, dehydratase domain; KR, β-ketoreductase domain; ACP, acyl carrier protein domain; TE, Thioesterase domain.

Here, hybridobactin A was exemplified to introduce the whole biosynthetic pathway (Figure 4-36). The gene *hybA* that encoded a dioxygenase shares 59% similarity with the *glbB* gene in the glidobactin BGC, which was recently identified as a lysine 4-hydroxylase as previously mentioned[143], enabling the hydroxylation of the lysine during the biosynthesis. The gene *hybE* encodes a C-A-T module and the $C_{starter}$ domain initiates the fatty acid chain elongation with the first activated threonine. Subsequently, the acylated threonine continues to be assembled by the NRPS encoded by *hybB*, resulting in a Thr1-Lys2-X3 sequence. X3 is alanine in glidobactin and valine in syringolin, while in hybridobactins, X3 is valine (hybridobactin A and C) or leucine (hybridobactin B and D). Afterwards, the tripeptide chain is elongated by a PKS module,

implementing a malonyl unit via AT and KS. Then, it is reduced through DH and KR to form the double bond. At last, the product is cyclized and relased from the assembly line by a TE domain. Overall, structurally, hybridobactin A and C share the same 5-Mah-moiety like those in syringolins[114] and the 4-OH-Lys portion from glidobactins[153], while the 3-hydroxy-hexanoic (or octanoic) acid chain has never been described in any known syrbactins. Furthermore, hybridobactin B and D that bear a 6-methyl-4-amino-2-heptenoic acid are quite unique and are discovered for first time. Due to the structural hybridity related to glidobactins and syringolin classes (Figure 4-37), these four isolated products were coined hybridobactins A-D, respectively.

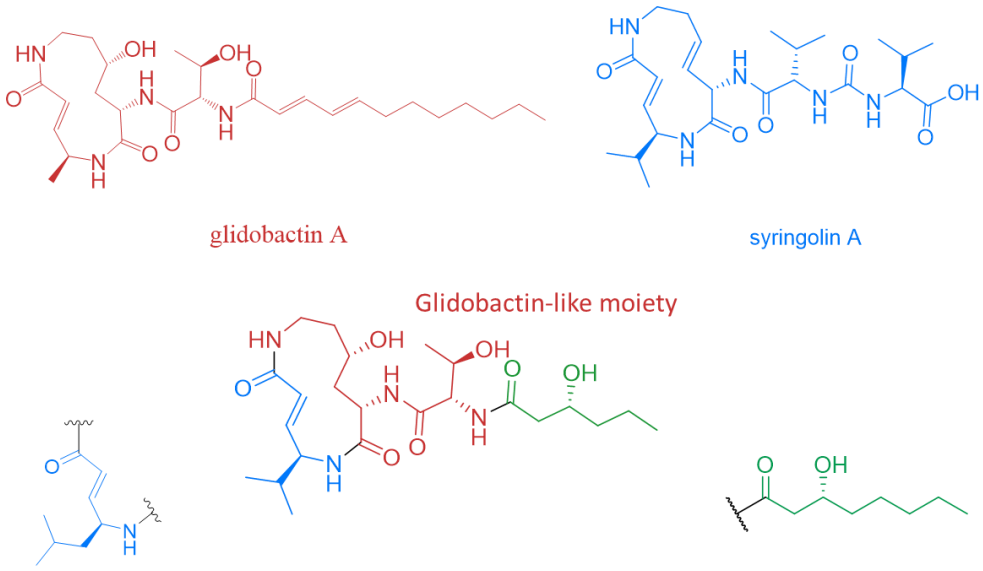

Figure 4-37 Hybridobactin hybridity reflected from syringolin and glidobactin.

To disclose the biosynthetic origin of the structural diversification from the homogeneous BGCs, an in-depth investigation suggested that the A domain specificity plays an important role. Thus, a phylogenetic approach was applied to shed more light on their specificity (Figure 4-38). From this phylogenetic tree, those A domains for Thr1 and Lys2 (color coded in blue and orange) are clustered together in all syrbactin subgroups, which is in line with the chemical investigations. Although the A domains of the third amino acid (colored in red) from different syrbactins BGCs were still clustered together, their specificity is varied in different syrbactin producers, which resulted in the diversification of the peptide-moiety in syrbactins. For example, the A domain in module 3 of HybB from *B. oklahomensis* DSM 21774 could activate both Val (hybridobactin A and C) and Leu (hybridobactin B and D) to generate different hybridobactin derivatives. It suggested that these A domains displayed relaxed substrate specificity for structurally related amino acids. This situation was also frequently visable in cyanobacterial

NRPS pathways. As a characteristic feature of nostopeptolides, the entire families of structurally related compounds were isolated in one specific strain[154]. Similar amino acids such as Val, Ile, and Leu, were found in equivalent positions within the peptides[155].

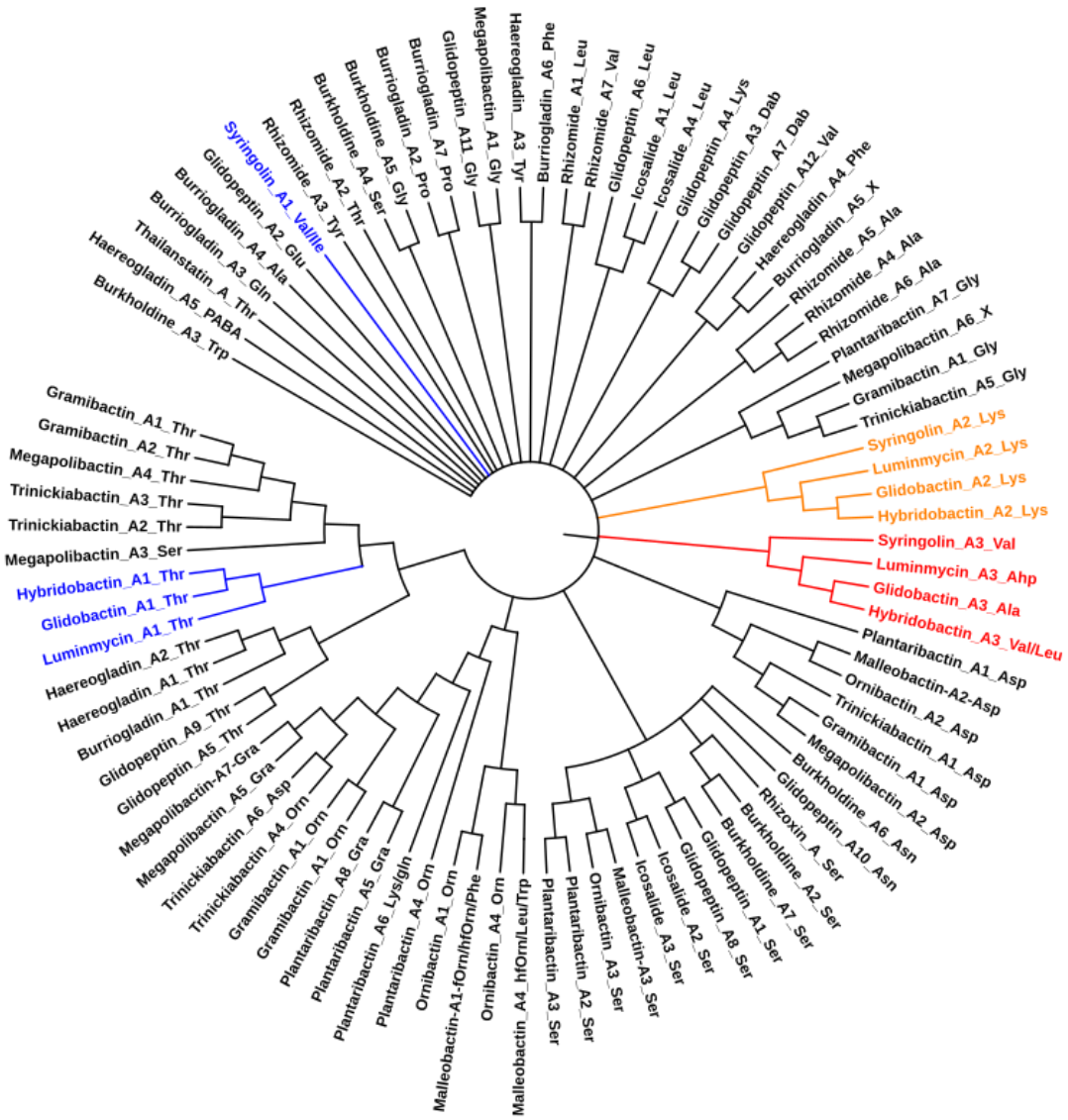

Figure 4-38 Phylogenetic analysis of the A domains extracted from the modules of the NRPS-related biosynthetic gene clusters in genus *Burkholderia*.

Besides the A domains, the lipoinitiation mediated by the $C_{starter}$ domain also contributes to the syrbactin structure diversity. As is already known, the bioactivity of the lipopeptide is normally affected by the attached lipid chain via a process known as lipoinitiation, by which the lipid chain was incorporated into the NRPS peptidyl backbone. A distinct example is the well investigated daptomycin, a component of the A21978C complex. Structural activity relationship (SAR) studies have shown that variations in the lipid side chain caused significant

effects on their bioactivities[156]. For syringolins, which bear an ureido- (from bicarbonate or carbon dioxide) containing amino acid, incorporated by SylC (a special C domain), while the $C_{starter}$ domain in the other syrbactins (glidobactins, cepafungins, lumimycins and hybridobactins) BGCs indicated a variable specificity, resulting in dissimilar types of the acyl chains. A additional BlastP analysis to compare the similarity of these four C domains was also conducted, revealing that the $C_{starter}$ domain of hybridobactin showed an altered identity in glidobactin (50.00%), luminmycin (39.06%) and syringolin (25.57%), respectively. Notably, these levels of identity are significantly lower than the overall identity of the whole BGCs, which ranges between 33-66% (Table 4-13). A compelling research that supported this point was recently published by Bode group[152]. In total, 31 glidobactin-like proteasome inhibitors were identified via heterologous expression and promoter exchange strategies. These derivatives mainly differed in their lipid chains, which in turn reflects the flexible specificity of the $C_{starter}$ domain from the producer strain.

4.3.6.3 Biological Activity and Biological Role of Hybridobactins

As new members of syrbactins, hybridobactins exhibited potent inhibition ability in the performed 20S proteasome inhibition assay. Syringolin was reported as the weakest subclass from the syrbactin family[148], which is in agreement with our experimental results (as described in section 4.3.5). Glidobactin C showed a slightly stronger activity than hybridobactins A-C. However, hybridobactin D displayed an outstanding potency equal to epoxomicin[157]. As previously mentioned, syrbactins mediated an irreversible inhibition via an oxa-Michael-type addition of the hydroxy group of the proteasomal active site residue threonine to the vinylogous amino acid residue[147]. A preliminary model of the structural determinants of syrbactin-mediated proteasome inhibition were suggested based on previous studies (Figure 4-39).

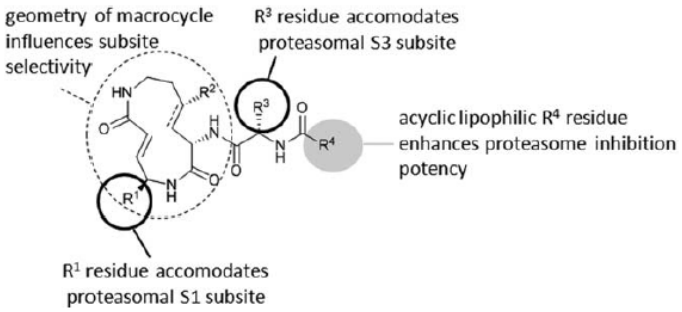

Figure 4-39 Analysis of structural determinants of the syrbactins' proteasome inhibition potency and subsite selectivity as derived from currently available derivatives[145].

As reported, in contrast to hybridobactins, glidobactins bear a longer lipid chain that may occupy the lipid binding pocket in an efficient way, leading to a higher potency of proteasome inhibition. In case of hybridobactins, their lipid chains are only limited to C_6 and C_8, although they have an additional hydroxy group on the side chains. The hybridity properities of hybridobactins enable a structure extension from R^1 residue as reflected in Figure 4-39. This particular alteration may mediate an affinitive binding to the proteasomal S1 subsite. Further, glidobactins and cepafungins were isolated initially through an antifungal screening event. Hence, both the glidobactins and cepafungins are antifungally relevant, while hybridobactins A-D are void of antifungal activity according to antifungal assays (e.g., pure compounds on agar plate with *Aspergillus niger*). It could be determined, that the shorter lipid chain (C_6 or C_8) alters the polarity of hybridobactins, leading to a diminished permeability. Thus, in comparison to glidobactins, hybridobactins lost their antifungal activity. Additionally, this could also explain the reduced cytotoxicity during the cell proliferation assay. To gain a more detailed insight into the molecular mechanism of hybridobactins, a co-crystallization study with the 20S proteasome are on-going as part of a collaboration.

The original producer *Burkholderia oklahomensis* DSM 21774 (C6786) was orignally isolated in 1973 from a 27-year-old farmer with a deep leg wound, which was heavily contaminated with soil during an accident in Oklahoma, USA[47]. Later, another two enviromental isolates C7532 and C7533 were recovered from the soil near the accident site. Due to high similarity based on genomic analysis, these three isolates were grouped as *B. oklahomensis* species[47]. During the identification of the hybridobactin BGC, other secondary metabolite BGCs that could encode several intriguing targets, including some novel siderophores and antifungal compounds, were observed as well. As an opportunistic pathogen, isolated from soil, their potential to produce these cytotoxic compounds are still conserved and silent under normal lab conditions. Once their living enviroment is changed, these hidden weapons are still able to be expressed, which help them to survive in harsh living situations. One interesting example was reported from the isolation of the luminmycin D: an insect might act as a trigger for inducing the production of glidobactins and luminmycins by *Photorhabdus asymbiotica*. Accordingly, *P. asymbiotica* cells were injected into live crickets. A 24-hour postinoculation caused the death of *P. asymbiotica*-infected crickets. All four glidobactins and luminmycins could be detected through an extraction of the insect carcasses[158]. This study coupled with our successful screening and isolation of hybridobactins via fermentaion in selected media, revealed the

admirable ability of the bacteria to adapt to extreme enviroments by secreting diverse secondary metabolites.

4.3.6.4 Distribution of the Syringolin-Like Biosynthetic Gene Clusters.

It was predicted by the Dudler group that syrbactin BGCs are conserved in *Burkholderia* and *Photorhabdus luminescens*[150]. This was later proven based on a series of investigative studies as previously mentioned. However, during the annotation of the hybridobactin BGC, a transposase that is located just downstream of the *hyb* BGC border was noticed (labeled in black, Figure 4-40). This may infer a putative horizontal gene transfer, which commonly occurs in micobes[159-161].

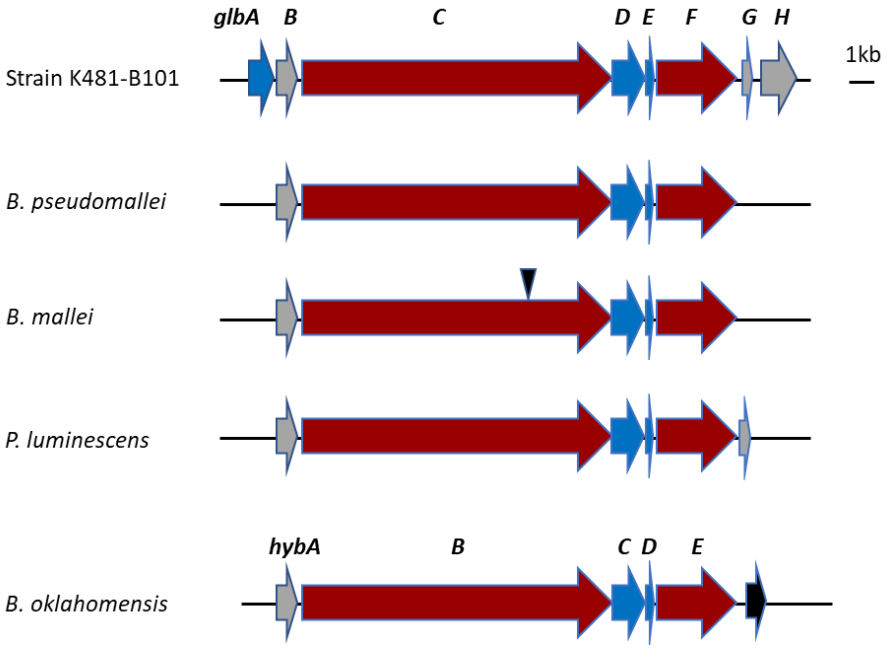

Figure 4-40 Comparison of related BGCs from different strains[150]. Homologous gene clusters of glidobactin producer strain K482-B101, *B. pseudomallei*, *B. mallei* and *P. luminescens* are aligned. The inverted triangle indicates the position of transposon-mediated disruptions in the *glbC* homologues of *B. mallei strains*. The gene labeled in black downstream of the *hyb* BGC represents the transposon IS407.

However, a BlastP search of the genes upstream and downstream of the *hyb* BGC could not locate the other expected transposase (IS407A insertion sequence). The average value of the GC-content of the *hyb* BGC and its adjacent region is around 69%. No obvious fluctuation of the GC-content could be detected, except at the beginning of the gene cluster (highlighted in the red box, Figure 4-41), where a promoter may appear.

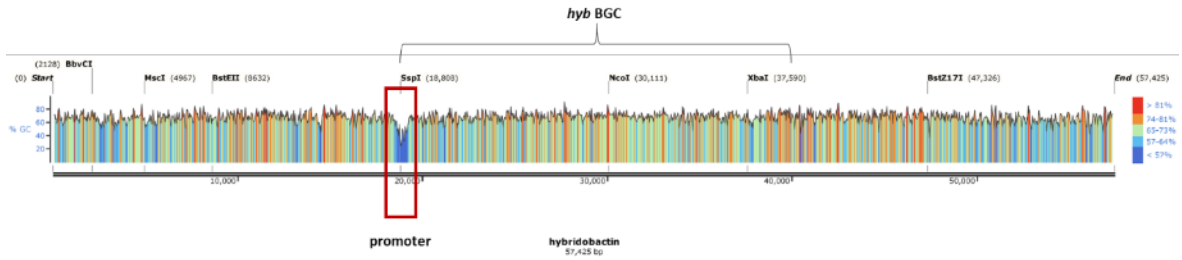

Figure 4-41 Displayed GC-content of the hybridobactin BGC and its nearby genes using SnapGene software.

By coincidence, the Dudler groups compared the syrbactin homologous BGCs from different species. They also demonstrated that except for the *B. mallei* strains, all the syrbactin homologous BGCs in the other strains are executable. Interestingly, in all of the investigated nine *B. mallei* strains, the cluster is disrupted by chromosomal rearrangements including an interruption of the coding region of the *glbC* homolog caused by insertion of the transposons IS407 and ISBm2 as well (Figure 4-40). Based on the fact that the transposon insertion is conserved in all of the nine *B. mallei* strains, they inferred the primary event of the transposition may have happened in a common ancestor[150]. In the case of hybridobactin BGC from *B. oklahomensis*, the cluster is not affected duing the transposition. New hybridobactins could still be synthesized via this complete machinery. Given that the syrbactin BGCs are not so widely conserved in all the *Burkholderia* species, an additional BlastP analysis of the characteristic NRPS-PKS hybrid gene *hybB* was performed. The dominant candidates were detected in *Burkholderia pseudomallei* and several other species (including the known syrbactins producers). These results suggested that functional syrbactin BGCs are limited to certain species. Hence, the spread of these genes may be caused by a horizontal gene transfer as mentioned. Since most of these syrbactin-producing strains are pathogenic, it may raise the question, whether these compounds could contribute to the pathogenicity of these strains.

4.4 *Burkholderia glumae* ICMP 3729

4.4.1 Identification of a Bactobolin-Like Biosynthetic Gene Cluster

The sequenced genome of *Burkholderia glumae* ICMP 3729 (6.62 Mb) was deposited at GenBank under the accession number JABWEA000000000. A total of 15 encoded BGCs were detected using AntiSMASH 5.0, including one NRPS BGC and six NRPS-PKS hybrid BGCs and a few other unknown BGCs. Based on the previous screening results, some chlorine-containing compounds from the bactobolin family were dereplicated. However, a further chlorinated compound with a mass ion at *m/z* 702.3, possibly produced by the same biosynthetic gene cluster, could not be found in databases. This finding reignited our interest in this bactobolin-like BGC (labeled as BGC 1.2), which had a 76% identity to the known BGC *bta* encoded in the *Burkholderia thailandensis* E264 genome. Thus, a further comparative analysis was performed.

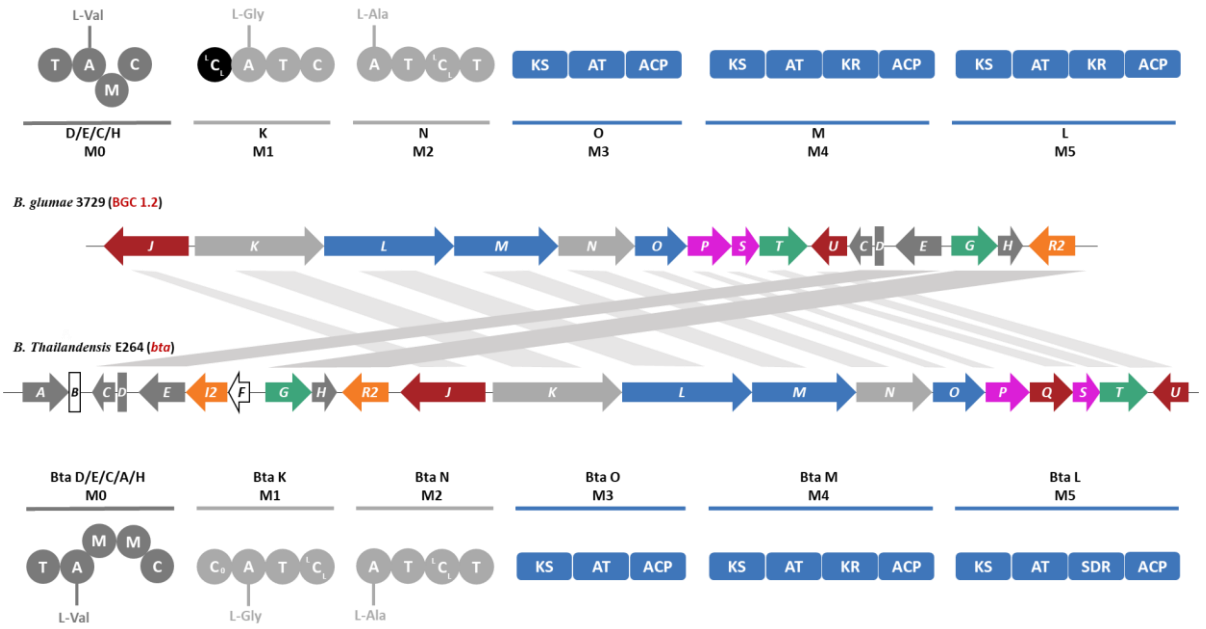

Figure 4-42 Comparison of the bactobolin-like BGC in *B. glumae* 3729 and the BGC *bta* in *B. thailandensis* E264. Two clusters contain distinct elements: synthesis of the unnatural amino acid (gray), Ala-Ala (light gray) and the C6 polyketide (blue), genes involved in regulation (orange), product transporters (green), lactone ring (pink), modification (brown) and genes of unknown functions (white). The "M" domains in module 0 represent modification domains (chlorination and hydroxylation), but their orders are still unclear.

To have an unambiguous overview of both BGCs, all the genes are presented and styled based on the work of Jon Clardy and coworkers[162]. First, detailed domain annotations using BlastP of both BGCs were conducted (Figure 4-42 and Table 4-14). This analysis indicates the presence of a hybrid NRPS-PKS assembly line containing three NRPS modules (module 0/1/2) and three

PKS modules (module 3/4/5) in *B. glumae* 3729 as well. Similarly, the module 0 consists of the free-standing T and A domains, which are coded by genes *D* and *E*, respectively. Additionally, the A domains of module 1 and module 2 possess Gly- and Ala-specificity accordingly. However, there are also some differences between both BGCs. Firstly, the lack of *btaA* in BGC 1.2 may result in the absence of a modification domain in module 0. This modification domain was thought to be responsible for hydroxylation of the unnatural amino acid. In addition, genes *B* and *F* were not found in BGC 1.2 either. These two genes were thought to be inactive, or their functions are still unclear in the BGC *bta*[162,163]. Furthermore, the genes *I2* (regulatory factor) and *Q* (acetyltransferase) are also missing. Besides, the predicted $^{L}C_{L}$ domain of module 1 in *B. glumae* ICMP 3729 (indicated in black in Figure 4-42) was also different from the corresponding C_0 domain in the BGC *bta*.

Table 4-14 Comparison of putative functions of involved enzymes in *B. thailandensis* E264 and *B. glumae* ICMP 3729.

***B. thailandensis* E264**				***B. glumae* ICMP 3729**		
Enz.[a]	Size (nt)	Functions	Similarity	Enz.	Size (nt)	Functions
Biosynthesis of the unnatural amino acid unit						
BtaD	246	Free-standing T	65.01%	D	243	T domain
BtaE	1647	Free-standing A	69.56%	E	1488	A domain
BtaC	924	Dichlorinase	87.62%	C	924	Unknown
BtaA	1146	Hydroxylase	– [f]	–	–	–
BtaH	858	Transacylase	64.03%	H	843	Unknown
Biosynthesis of the peptide linker unit						
BtaK	4341	NRPS	58.84%	K	4542	NRPS
BtaN	3435	NRPS	65.87%	N	3489	NRPS
Biosynthesis of the C6-Polyketides unit						
BtaO	2340	T1PKS	67.01%	O	2313	T1PKS
BtaM	4113	T1PKS	72.32%	M	3963	T1PKS
BtaL[b]	4575	T1PKS	66.52%	L	4500	T1PKS
Modification						
BtaS	843	Thioesterase	70.80%	S	843	Thioesterase
BtaP[c]	1593	ß-lactamase	77.50%	P	2427	Unknown
BtaQ	846	Acetyltransferase	– [f]	–	–	–
BtaJ	2082	Oligopeptidase	55.77%	J	2064	Unknown
BtaU[d]	846	Hydroxylase at C5	77.17%	U	846	Hydroxylase
Others						
BtaG	1233	Transport-related	74.88%	G	1233	Transport-related
BtaT	1227	Transport-related	59.51%	T	1251	Transport-related
BtaI2	621	Regulatory factor	– [f]	–	–	–
BtaR2	705	Transcriptional regulator	70.94%	R2	705	Transcriptional regulator
BtaB[e]	297	Unknown	– [f]	–	–	–
BtaF	408	Unknown	– [f]	–	–	–

Enz.[a]: Enzyme. BtaL[b]/ BtaP[c]: *⊿btaL(SDR)* and *⊿btaP* mutant abrogated completely the biosynthesis of bactobolins. BtaU[d]: *⊿btaU* mutant produced only compounds without OH- group at C5. BtaB[e]: *⊿btaB* mutant did not show any effects on biosynthesis of bactobolins. – [f]: Genes, which could not be found in the BGC 1.2 of *B. glumae* ICMP 3729.

More information about the putative functions of these involved enzymes and their identity were listed in Table 4-14. Based on all the analyses above, it become apparent that several steps in the biosynthesis of the bactobolin compound family (inculding bactobolins and acybolins) are still unclarified. Therefore, the isolation of this new congener (termed acybolin J) from the bactobolin compound family may give more hints to clarify its biosynthesis.

4.4.2 Detection of More Bactobolin Derivatives During Upscaling Using MS

To get a sufficient amount of this new derivative, a fermentation of 31 L bacterial cultures in MM9 medium were performed. Since the LC-MS was also integrated for monitoring the isolation procedure, more bactobolin derivatives were detected, including bactobolin B and E. The following HRMS spectra (Figure 4-44, Figure 4-45 and Figure 4-47) showed the observed bactobolin- or acybolin-related masses in MM9 medium and their MS/MS fragments in positive mode.

To simplify the MS-based dereplication procedure for the bactobolin compound family, all bactobolin-related compounds were divided into four subgroups according to their chemical structure to avoid confusion. The classification depends on the substituents on the position 5 or 3, as well as the side chain variations as reflected in Figure 4-43.

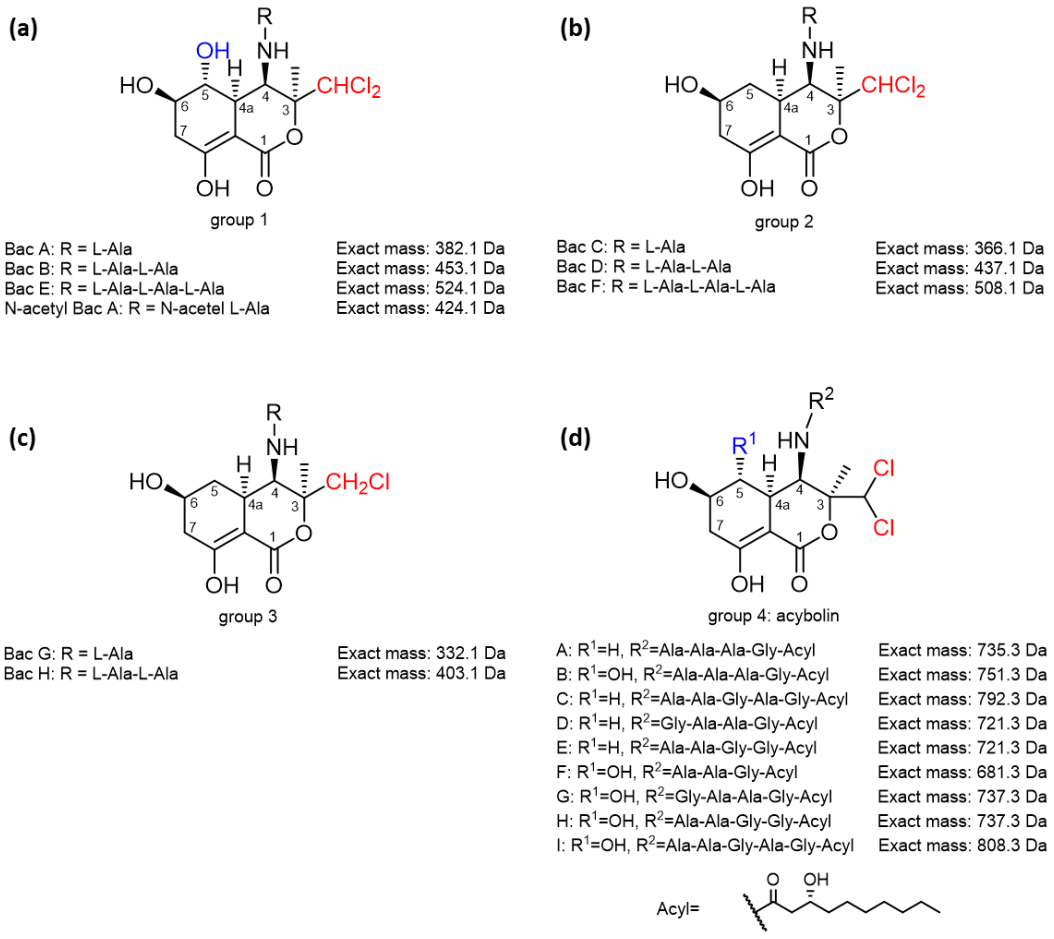

Figure 4-43 The four subgroups of bactobolin-related compounds. (a) Bactobolins of group 1. (b) Bactobolins of group 2. (c) Bactobolins of group 3. (d) Bactobolins of group 4 (acybolins).

For detection of the halogen-containing compounds, MS was proved to be a suitable tool due to the special isotope pattern of these halogens that are present in the compounds[164]. Bactobolin related compounds, which contain one or two chlorine atoms are rare in natural products. When it bears only one chlorine atom, the peak heights of the molecular ion peaks (M^+ and M+2) are in the ratio of 3:1, because chlorine has two principal stable isotopes, ^{35}Cl (75.77%) and ^{37}Cl (24.23%). Likewise, if the molecule carries two chlorine atoms, the ratio of the peak heights of three molecular ion peaks (M^+, M+2 and M+4) will become 9:6:1. Based on the analysis, the bactobolin-related masses in Figure 4-44 and Figure 4-45 contain two chlorine atoms, while the masses described in Figure 4-47 bear only one chlorine atom. Thus, the number of chlorine atoms deduced by the isotope patterns was consistent with the predicted molecular formulas.

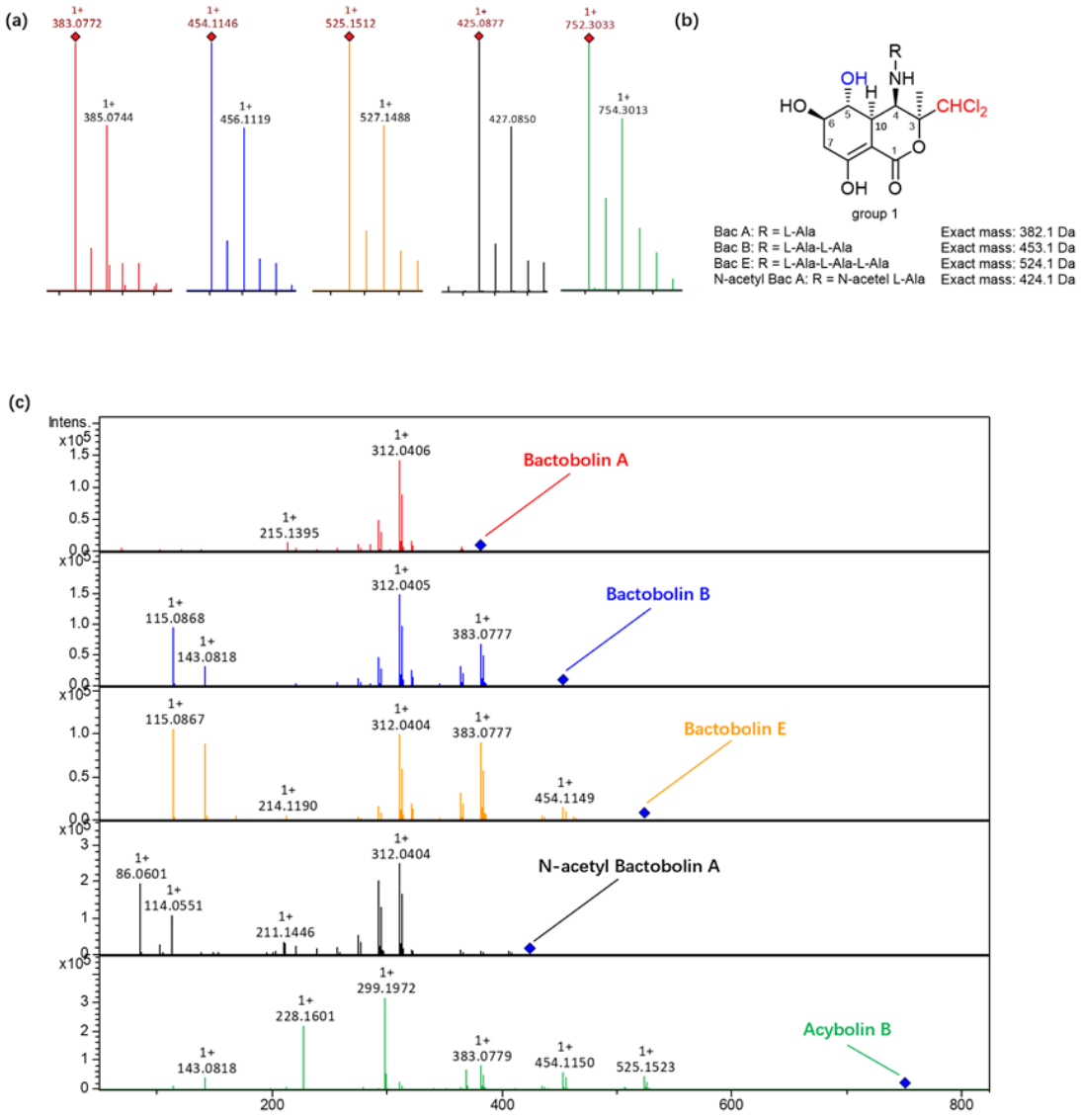

Figure 4-44 Detection of dichlorinated bactobolins with hydroxy group at position C5. (a) The HRMS spectra of bactobolin A, B, E, N-acetyl bactobolin A and acybolin B in positive mode. (b) Group 1 of bactobolins. (c) The MS/MS spectra of their corresponding masses.

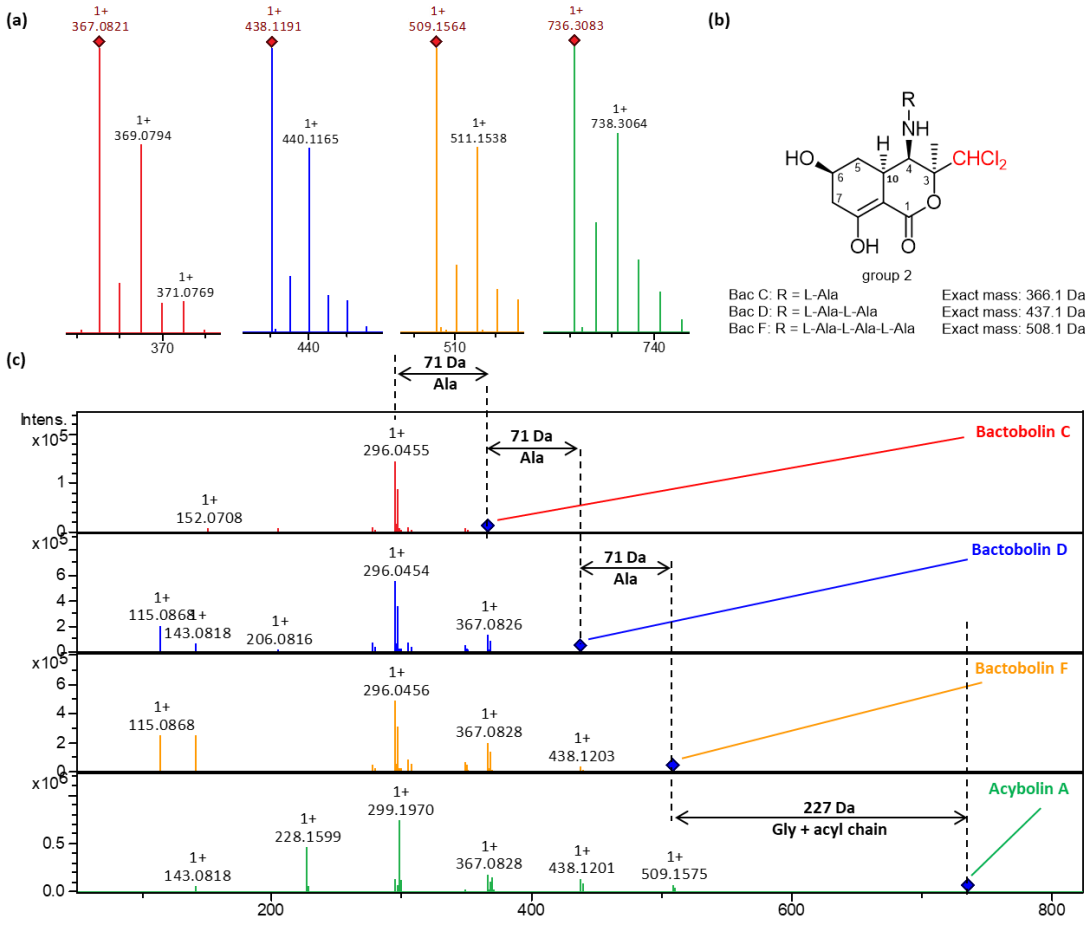

Figure 4-45 Detection of dichlorinated bactobolins without hydroxy group at position C5. (a) The HRMS spectra of bactobolin C, D, F, acybolin A in positive mode. (b) Group 2 of bactobolins. (c) The MS/MS spectra of their corresponding masses.

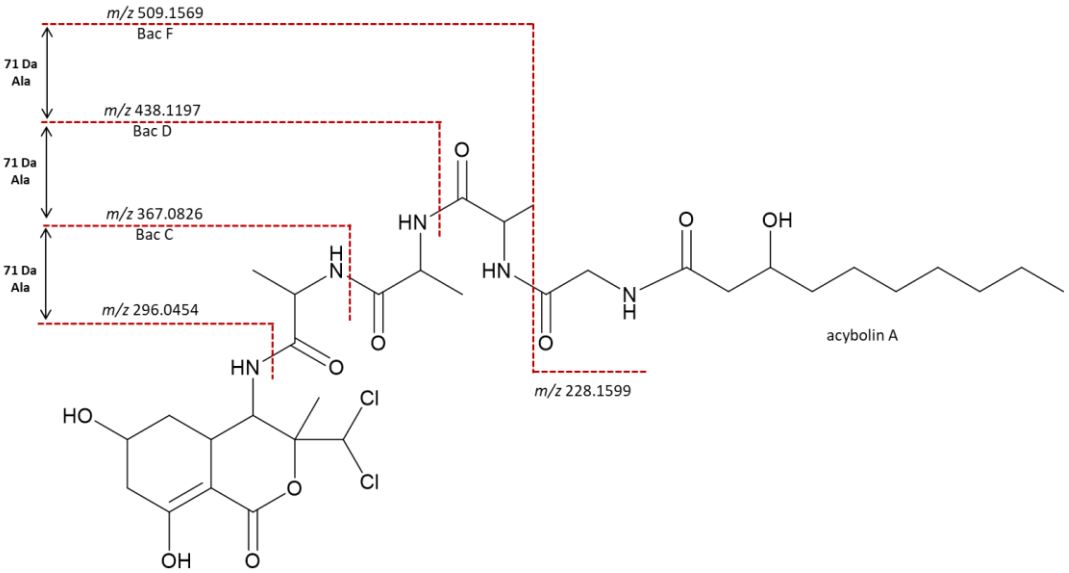

Figure 4-46 MS/MS fragmentation patterns of the compounds described in Figure 4-45.

Additionally, MS/MS fragmentation patterns of precursor ions also provided valuable structural information. Here, the MS/MS fragments from those masses of interest in Figure 4-45 were exemplified to give more insights (Figure 4-46). These compounds shared the same daughter ion at *m/z* 296.0454. The mass difference of 71 Da indicated the tandem loss of the alanyl residues. Additionally, the mass difference between *m/z* 736.3083 and *m/z* 509.1564 represented the mass of the glycyl residue connected with a lipid side chain (3-hydroxy-decanoic acid).

It became apparent that the mass ions at *m/z* 383.0772, 454.1146, 525.1512, and 425.0877 in Figure 4-44 matched bactobolin A, B, E, and N-acetyl bactobolin A, respectively. The similar MS/MS fragmentations were also aligned with each other. In a similar manner, the masses in Figure 4-45 (*m/z* 367.0821, 438.1191 and 509.1564) and the mass in Figure 4-47 (*m/z* 404.1586) matched bactobolins C, D, F and bactobolin H, respectively.

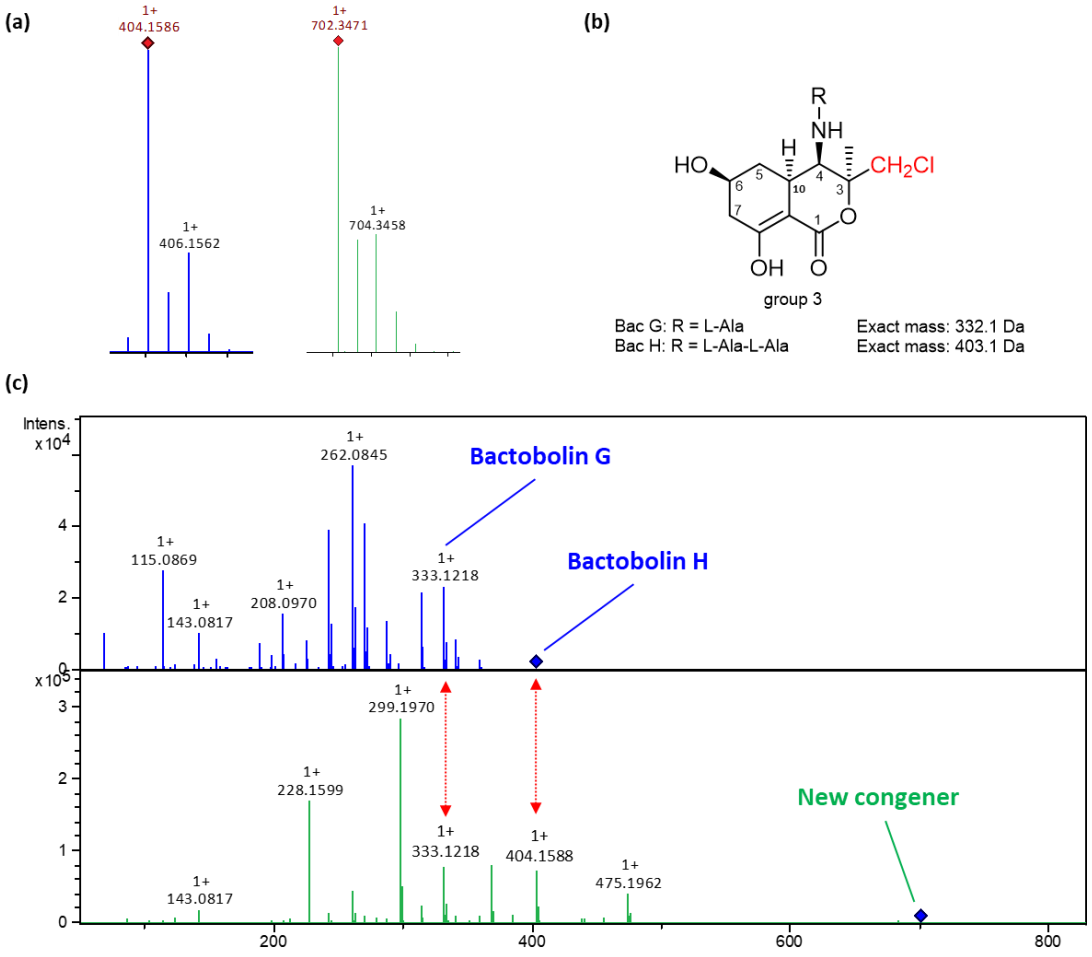

Figure 4-47 Detection of monochlorinated bactobolins. (a) The HRMS spectra of bactobolin H and the new congener in positive mode. (b) Group 3 of bactobolins. (c) The MS/MS spectra of bactobolin H and the new congener.

Furthermore, the mass ions of *m/z* 752.3033 and *m/z* 736.3083 (Figure 4-44 and Figure 4-45) were dereplicated as acybolins B and A, respectively. These findings were also correlated with their molecular formula, molecular mass, and the degree of unsaturation, which were summarized in Table 4-15.

Table 4-15 HRMS data of all bactobolin-related masses in MM9 medium.

Ion Formula $[M+H]^+$	Calculated [Da]	Measurement [Da]	Err. [ppm]	rdb	Retention Time [min]
$C_{14}H_{21}Cl_2N_2O_6$	383.0771	383.0772	-0.2	5	11.1
$C_{17}H_{26}Cl_2N_3O_7$	454.1142	454.1146	-0.8	6	10.9
$C_{20}H_{31}Cl_2N_4O_8$	525.1513	525.1512	0.2	7	11.1
$C_{16}H_{23}Cl_2N_2O_7$	425.0877	425.0877	0.7	6	14.4
$C_{32}H_{52}Cl_2N_5O_{11}$	752.3035	752.3033	0.1	9	21.2
$C_{14}H_{21}Cl_2N_2O_5$	367.0822	367.0821	-0.3	5	12.1
$C_{17}H_{26}Cl_2N_3O_6$	438.1193	438.1191	-0.2	6	12.1
$C_{20}H_{31}Cl_2N_4O_7$	509.1564	509.1564	0.2	7	12.2
$C_{32}H_{52}Cl_2N_5O_{10}$	736.3086	736.3083	0.4	9	21.8
$C_{17}H_{27}ClN_3O_6$	404.1583	404.1586	-1.1	6	10.8
-	-	702.3471	-	-	20.6

The mass of *m/z* 702.3471 was confirmed as a new acybolin congener. First, a typical isotopic pattern of chlorine atoms (3:1) could be observed in its HRMS spectrum (Figure 4-47). On the other hand, the MS/MS fragmentation pattern of this new compound indicated that it structurally belonged to the acybolins group (Figure 4-43). Furthermore, the slightly delayed retention time (Table 4-15) was in agreement with these predictions.

To sum up, eleven bactobolin-related compounds were detected their masses were confirmed using HRMS. Ten out of eleven were dereplicated, while the remaining one was proven to be a new congener based on MS.

4.4.3 Isolation and Purification of The New Bactobolin Congener

To fractionate the 25.5 g crude extract that was obtained from 31 L bacterial cultures, liquid solid size exclusion chromatography using Sephadex^{TM} LH-20, was applied. The whole fractionation and isolation procedure is presented in Figure 4-48. The crude extract was redissolved in 70% aqueous methanol and then loaded on the packed column. Then, the sample was eluted with 70% aqueous methanol. Four fractions were generated and collected based on the observed color bands. Subsequently, the LC-MS analysis showed that the second (F2) and third (F3) fractions contained the target compound. To avoid duplication, these two fractions were combined for further isolation.

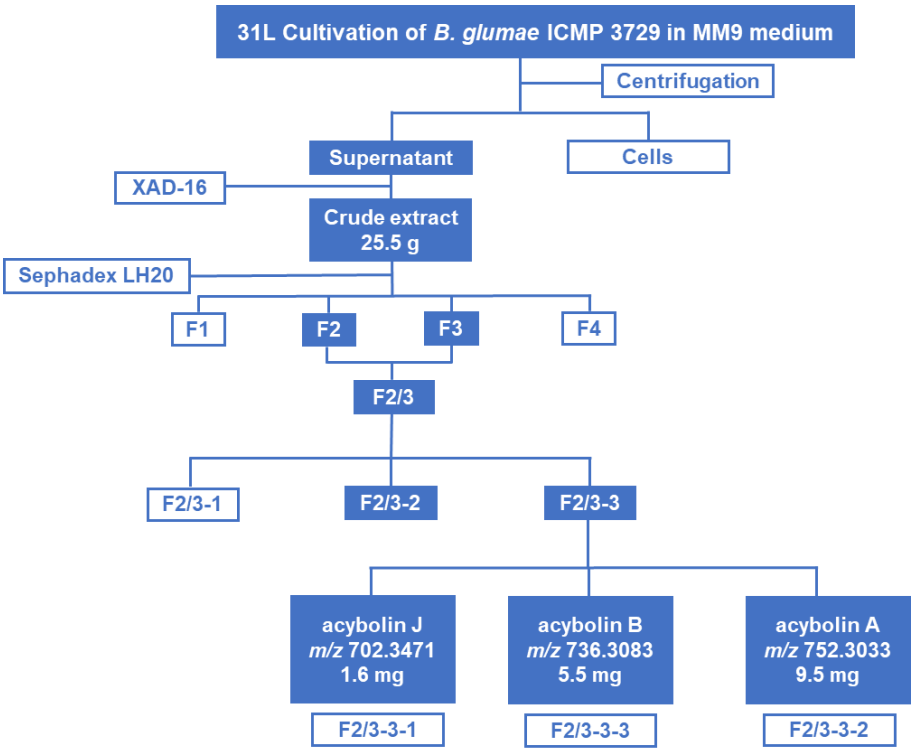

Figure 4-48 Fractionation scheme for the isolation of acybolins.

Due to the complexity of the subfractions, a series of preparative (Agela Unisol C18, 250 x 21.2 mm, 5µm) and semi-preparative columns (Knauer Eurospher II C8, 250 x 8 mm, 5 µm) were used for the following purification procedure. Final separation was carried out employing Phenomenex Kinetex PFP5 column (250 x 4.6 mm, 5 µm), and provided acybolins J and B in a semi-pure form as well as 5.5 mg pure acybolin A.

In order to purify acybolin J and B for NMR analysis, repurification of these two compounds was performed in a gradient mode using methanol (A) and 0.1%TFA containing water (B) as

mobile phases. The gradient started at 35% A, increasing the percentage of A to 50% over 10 min, followed by isocratic conditions for 5 min, increasing the percentage of A to 100% within 1 min and holding for another 2 min, followed by reequilibration at 35% A for 6 min (Phenomenex Luna C5, 250 x 4.6 mm, 5 μm; 0.8 mL/min flow rate; UV monitoring at 215, 250 and 300 nm). Finally, 1.6 mg acybolin J and 9.5 mg acybolin B were obtained for further NMR measurements. Additionally, pure bactobolin B (4.01 mg) and bactobolin E (2.85 mg) were isolated from another subfraction (F2/3-2) obtained above after preparative isolation.

4.4.4 Structure Elucidation of Acybolin J

Out of all five isolated compounds, acybolin B was not able to be submitted to NMR measurement, due to solubility issues (Table 4-16). Obvious precipitation was observed during sample preparation. However, acybolin A and J could be dissolved efficiently in DMF-d_7.

Table 4-16 Applied solvents to dissolve the obtained pure compounds.

Compound	Solvent[a]						
	D_2O	MeOH-d_4	DMSO-d_6	DMF-d_7	Acetone-d_6	CH_2Cl_2-d_2	Pyridine-d_5
Bactobolin B	+ +[b]						
Bactobolin E	+ +						
Acybolin J			+ +	+ +			
Acybolin B	− [d]	−	+[c]	+	−	−	−
Acybolin A				+ +			

Solvent[a]: the volume of all mentioned solvents is 600 µl.
++[b]: completely dissolvable; +[c]: partially dissolvable; − [d]: insoluble.
Relative polarity: D_2O>MeOH-d_4>DMSO-d_6>DMF-d_7>Aceton-d_6> CH_2Cl_2-d_2>Pyridine-d_5.

Acybolin A was isolated in a sufficient amount (5.5 mg) and high-quality NMR spectra of acybolin A were aquired. However, the new congener acybolin J was obtained only in a small amount (1.6 mg) due to its low production. In this case, 600 MHz and 700 MHz instruments were utilized for the measurement of acybolin J, to get improved NMR spectra. To facilitate the structure elucidation procedure, a comparative elucidation strategy was applied for acybolin A and J, due to their structural similarity as predicted using MS analysis. Firstly, acybolin A should be elucidated using 1D-/2D-NMR. Then, the intepretation of the spectra of acybolin J could be referenced from acybolin A to avoid some confusion, except those key signals reflecting the structural variations.

To determine the planar structure of acybolin A, ESI-HR-MS, MS/MS, and 1D and 2D NMR experiments were carried out as mentioned before. The HR-MS analysis of acybolin A in positive mode with *m/z* 736.3083 $[M+H]^+$ suggested a molecular formula of $C_{32}H_{52}Cl_2N_5O_{10}$ (calc. for 736.3086, Δ 0.4 ppm, 9 degrees of unsaturation). In the ^1H NMR spectrum exchangeable downfield amide signals at δ_H 7.40–8.50 and α-proton resonances between δ_H 3.50 and 4.50 were detected (Figure 4-49). Combining ^{13}C NMR and DEPT135 spectra, a total number of 32 carbons, including five CH_3-, ten CH_2-, and eight CH- groups could be delineated. Five carbonyl carbons in the range of δ_C 160 – 180 could be observed, while the remaining three quaternary carbons were supposed to be integrated into the bicyclic ring system typical of

the bactobolin compound family. Overlapping methylene signals in the upfield, together with a terminal methyl resonance at δ_H 0.85, indicated that acybolin A bore an alkyl chain. Based on HSQC-TOCSY and COSY spectra, five further spin systems, including one for glycine and three for alanine together with a typical bactobolin bicyclic component could be confirmed (Figure 4-51).

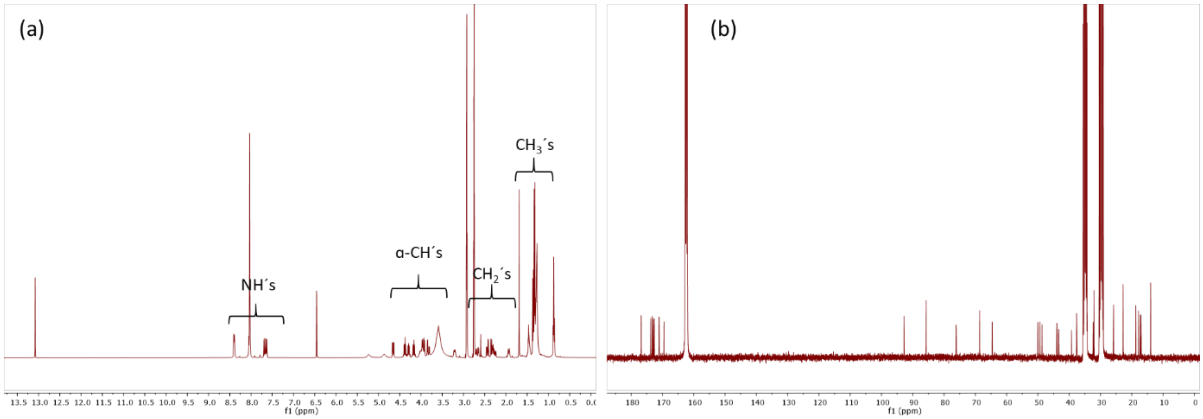

Figure 4-49 1D NMR spectra of acybolin A. (a) ^{1}H NMR spectrum (400 MHz, DMF-d_7). (b) ^{13}C NMR spectrum (100 MHz, DMF-d_7).

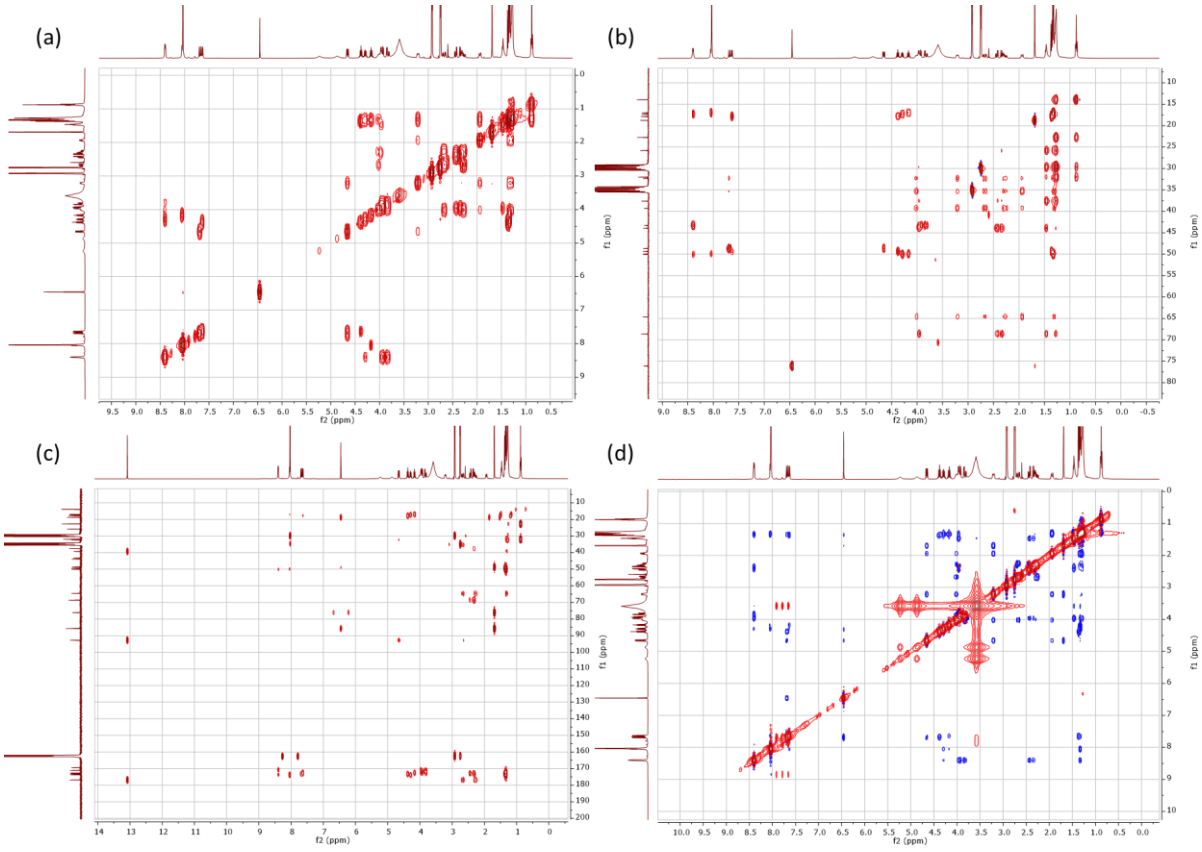

Figure 4-50 2D NMR spectra of acybolin A (400 MHz, DMF-d_7). (a) ^{1}H-^{1}H COSY NMR spectrum. (b) ^{1}H-^{13}C HSQC-TOCSY NMR spectrum. (c) ^{1}H-^{13}C HMBC NMR spectrum. (d) ^{1}H-^{1}H NOESY NMR spectrum.

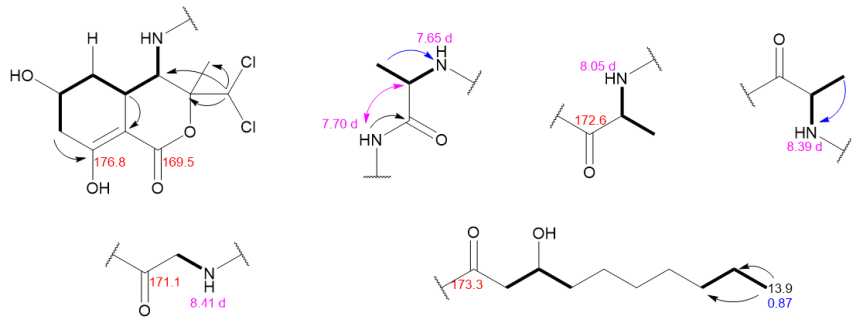

Figure 4-51 Six spin systems of acybolin A.

Subsequently, these spin systems were connected with the help of HMBC and NOESY spectra. All the ^{13}C NMR and ^{1}H NMR signals were assigned and summarized in Table 4-17.

Table 4-17 NMR data of acybolin A (400 MHz, DMF-d_7).

Acybolin A (H/C)	$\delta_{C/N}$ (ppm)	δ_H (ppm) Multiplicity (J/Hz)
1	169.5 qC	
3	85.7 qC	
3a	76.1 CH	6.46, 1H (s)
3b	18.8 CH_3	1.69, 3H (s)
4	48.7 CH	4.65, 1H (dd, 10.33, 3.85)
5	35.3 CH_2	1.95, 1.27, 2H (m)
6	64.6 CH	4.03 m
7	39.3 CH_2	2.69, 1H_e (dd, 18.12, 6.02) 2.28, 1H_a (ddd,18.48, 9.93, 2.41)
8	176.8 qC	
9	92.8 qC	
10	32.4 CH	3.22, 1H (m)
1'	104.2 NH	7.70, 1H (d, 10.42)
2'	173.2 qC	
3'	49.4 CH	4.38, 1H (m)
4'	17.9 CH_3	1.33, 3H (m)
5'	115.8 NH	7.64, 1H (d, 7.24)
6'	172.6 qC	
7'	50.0 CH	4.17, 1H (m)
8'	17.0 CH_3	1.33, 3H (m)
9'	116.8 NH	8.05, 1H (d, 5.15)
10'	173.8 qC	
11'	50.1 CH	4.29, 1H (m)
12'	17.3 CH_3	1.33, 1H (m)
13'	110.6 NH	8.39, 1H (d, 5.62)
14'	171.1 qC	
15'	43.3 CH_2	3.93, 1H (d, 5.84), 3.85, 1H (d, 5.66)
16'	120.7 NH	8.41, 1H (d, 5.62)
17'	173.0 qC	
18'	44.0 CH_2	2.42 d (4.82); 2.36 d (7.89)
19'	68.6 CH	3.97, 1H (m)
20'	37.6 CH_2	1.47, 2H (m)
21'	29.8 CH_2	1.28, 2H (m)
22'	29.5 CH_2	1.28, 2H (m)
23'	25.8 CH_2	1.47, 1.31, 2H (m)
24'	32.0 CH_2	1.26, 2H (m)
25'	22.8 CH_2	1.27, 2H (m)
26'	13.9 CH_3	0.88, 3H (t, 6.92)

The elucidation of acybolin J was performed in a similar manner. HR-MS analysis of acybolin J in positive mode with a mass ion at *m/z* 702.3472 $[M+H]^+$ suggested a molecular formula of $C_{32}H_{53}ClN_5O_{10}$ (calc. for 702.3475, Δ 0.6 ppm, 9 degrees of unsaturation). All ^{13}C NMR and ^{1}H NMR signals were assigned using DEPT135, COSY, HSQC, HSQC-TOCSY and HMBC experiments (Figure 4-52 and Table 4-18). Based on a HSQC-TOCSY spectrum, all the spin systems that were present in acybolin A were also detectable in acybolin J. The number of carbons also matched with those of acybolin A.

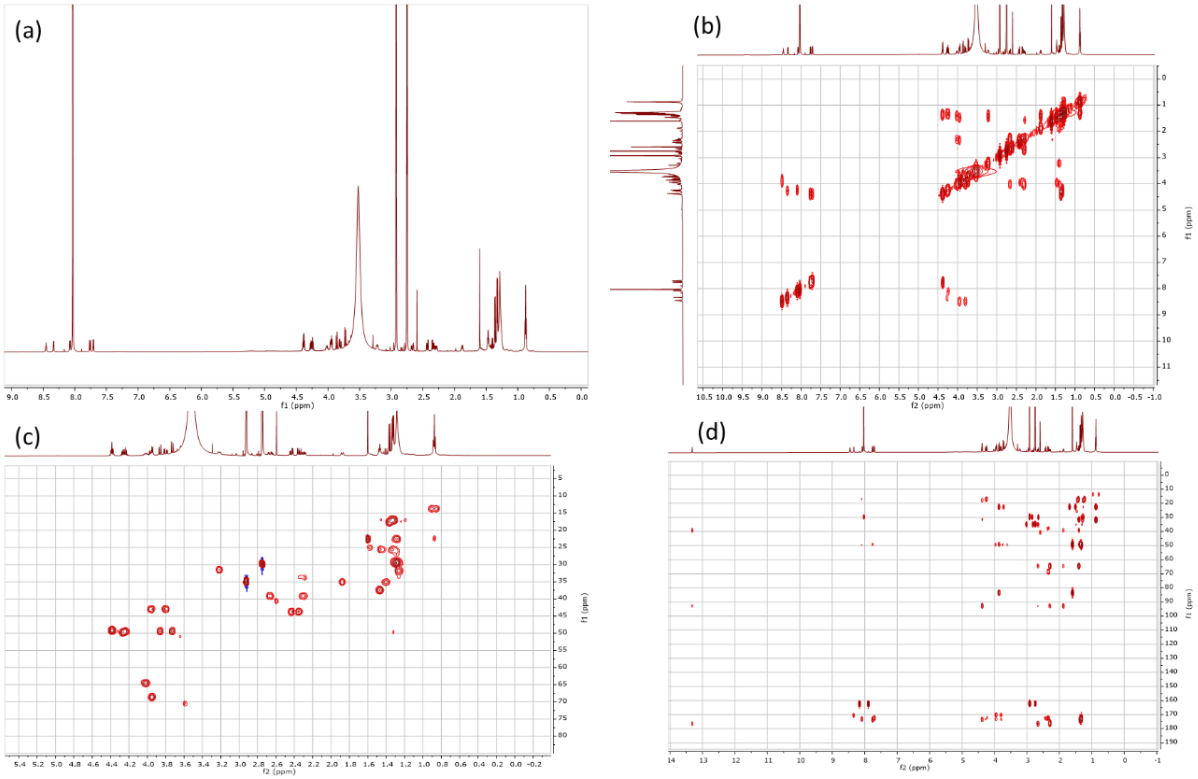

Figure 4-52 NMR spectra of acybolin J. (a) ^{1}H NMR spectrum (700 MHz, DMF-d_7). (b) ^{1}H-^{1}H COSY NMR spectrum (700 MHz, DMF-d_7) (c) ^{1}H-^{13}C HSQC NMR spectrum (600 MHz, DMF-d_7). (d) ^{1}H-^{13}C HMBC NMR spectrum (600 MHz, DMF-d_7).

Since monochlorination instead of dichlorination took place in acybolin J, the carbon and hydrogens at position 3b of acybolin J shifted in comparison with acybolin A upfield due to the decreased deshieding effect of the chlorine atom. Indirectly, it also affected the chemical shift of the carbon at position 3 (Figure 4-53). Other signals were less affected, since they are relatively far from the varied moiety. Summarizing all the above information, all the ^{13}C NMR and ^{1}H NMR signals of acybolin J were compiled in Table 4-18.

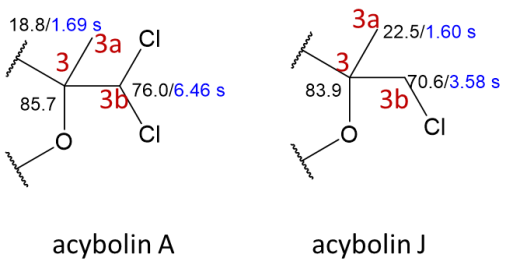

Figure 4-53 Partial structural comparison of NMR values between acybolin A and J.

Table 4-18 NMR data of acybolin J (600 MHz, DMF-d_7).

Acybolin J (H/C)	$\delta_{C/N}$ (ppm)	δ_H (ppm) Multiplicity (*J*/Hz)
1	173.6 qC	
3	83.9 qC	
3a	70.6 CH	3.58, 1H (s)
3b	22.5 CH_3	1.60, 3H (s)
4	49.1 CH	4.38, 1H (m)
5	35.1 CH_2	1.88, 1.40, 2H (m)
6	64.6 CH	4.02 m
7	39.3 CH_2	2.66, 1H_e (dd, 18.57, 2.81)
		2.30, 1H_a (dd, 10.51, 3.02)
8	176.3 qC	
9	92.9 qC	
10	31.5 CH	3.21, 1H (m)
1'	NH	7.75, 1H (d, 10.15)
2'	173.2 qC	
3'	49.4 CH	3.72, 1H (m)
4'	17.8 CH_3	1.36, 3H (d, 7.71)
5'	NH	7.70, 1H (d, 7.67)
6'	173.3 qC	
7'	49.1 CH	4.38, 1H (m)
8'	17.8 CH_3	1.33, 3H (d, 7.36)
9'	NH	8.05, 1H (d, 7.05)
10'	173.4 qC	
11'	49.8 CH	4.27, 1H (m)
12'	17.2 CH_3	1.32, 1H (d, 7.36)
13'	NH	8.34, 1H (d, 6.30)
14'	170.4qC	
15'	43.0 CH_2	3.80, 1H (dd, 16.41, 5.65);
		3.96, 1H (dd. 16.01, 5.97)
16'	NH	8.45, 1H (t, 5.66)
17'	172.7 qC	
18'	43.8 CH_2	2.43 dd (13.8, 4.88); 2.36 (d, 7.89)
19'	68.8 CH	3.95, 1H (m)
20'	37.5 CH_2	1.47, 2H (m)
21'	29.6 CH_2	1.28, 2H (m)
22'	29.3 CH_2	1.28, 2H (m)
23'	25.6 CH_2	1.46, 1H (m); 1.32, 1H (m)
24'	31.9 CH_2	1.26, 2H (m)
25'	22.6 CH_2	1.27, 2H (m)
26'	13.8 CH_3	0.87, 3H (t, 6.92)

A mass difference of 34 Da between acybolin A and J was calculated, which indicated a replacement of a chlorine with a proton. This conclusion was also in agreement with their MS/MS fragmentation patterns (Figure 4-54). Combining these MS data with the previouly interpreted NMR spectra, the planar structure of acybolin J was confirmed together with acybolin A as reflected in Figure 4-55. The absolute configuration of the amino acids in acybolin J was inferred in silico from the biosynthetic gene cluster. Since no epimerase was observed within the biosynthetic gene cluster, we presume that all the amino acids within acybolin J are L-configured and the hydroxy group on the side chain is *R* configured as given in acybolin A.

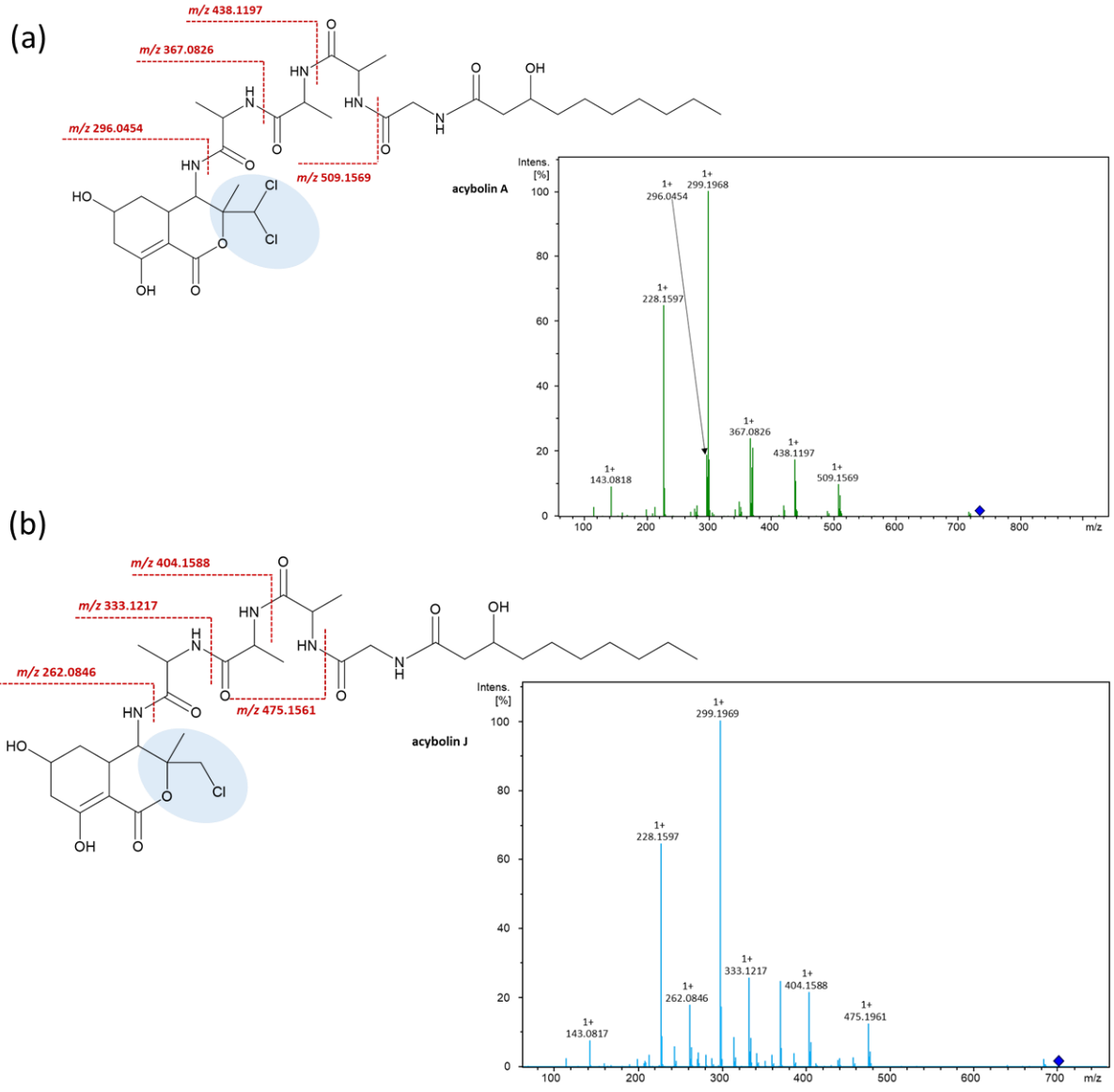

Figure 4-54 MS/MS fragmentation of acybolin J (a) and acybolin A (b).

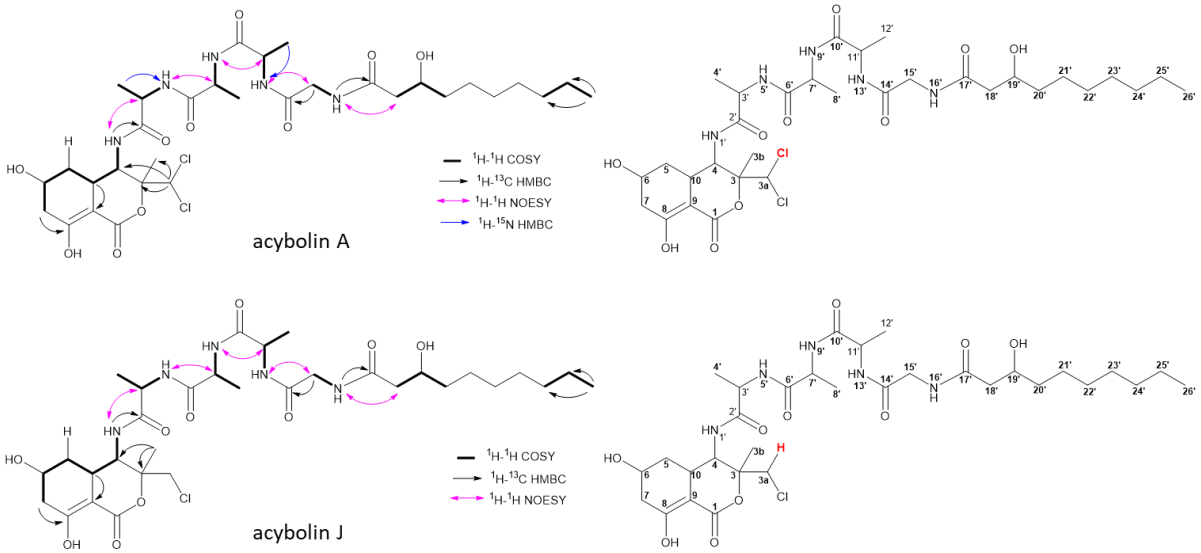

Figure 4-55 Key spin systems and selected long-range correlations leading to the identification of the planar structure of acybolins A and J. Bold lines indicate ^{1}H-^{1}H COSY or ^{1}H-^{13}C HSQC-TOCSY correlations, black arrows indicate ^{1}H-^{13}C HMBC correlations, blue arrows ^{1}H-^{15}N HMBC correlations, and pink arrows indicate ^{1}H-^{1}H NOESY correlations. On the right side, the numbered positions of all the carbon and nitrogen atoms are shown.

4.4.5 Discussion and Outlook

4.4.5.1 Cytotoxic Bactobolin Compound Family

Bactobolins are a class of chlorine-containing secondary metabolites with potent antibacterial and cytotoxic activities. They were firstly isolated from the culture broth of *Pseudomonas* BMG 13-A7 and were later reisolated from the strain *Burkholderia thailandensis* E264, respectively[162,165]. Due to its unique structure and strong activities, a series of follow-up studies were carried out that led to the discovery of its acylated forms, which were named acybolins[118]. Structurally, all these subclasses of the bactobolin compound family share a bicyclic ring moiety. They are extended with various combinations of amino acids from the C4 position via an amide bond. Acybolins have, in comparison with bactobolins, an additional 3-hydroxy-decanoic acid attached to the last amino acid in the peptide linker (Figure 4-56).

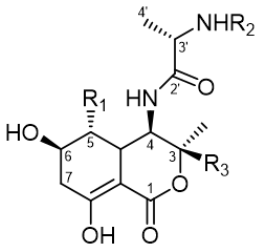

Bactobolin

A: R_1 = OH, R_2 = H, R_3 = $CHCl_2$
B: R_1 = OH, R_2 = L-Ala, R_3 = $CHCl_2$
C: R_1 = H, R_2 = H, R_3 = $CHCl_2$
D: R_1 = H, R_2 = L-Ala, R_3 = $CHCl_2$
E: R_1 = OH, R_2 = L-Ala-L-Ala, R_3 = $CHCl_2$
F: R_1 = H, R_2 = L-Ala-L-Ala, R_3 = $CHCl_2$
G: R_1 = H, R_2 = H, R_3 = CH_2Cl
H: R_1 = H, R_2 = L-Ala, R_3 = CH_2Cl
N-acetyl Bac A: R_1 = OH, R_2 = $COCH_3$, R_3 = $CHCl_2$

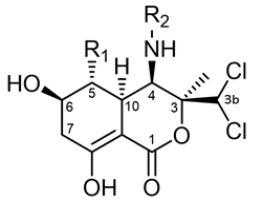

Acybolin

A R^1 = H, R^2 = Ala-Ala-Ala-Gly-*Acyl*
B R^1 = OH, R^2 = Ala-Ala-Ala-Gly-*Acyl*
C R^1 = H, R^2 = Ala-Ala-Gly-Ala-Gly-*Acyl*
D R^1 = H, R^2 = Gly-Ala-Ala-Gly-*Acyl*
E R^1 = H, R^2 = Ala-Ala-Gly-Gly-*Acyl*
F R^1 = OH, R^2 = Ala-Ala-Gly-*Acyl*
G R^1 = OH, R^2 = Gly-Ala-Ala-Gly-*Acyl*
H R^1 = OH, R^2 = Ala-Ala-Gly-Gly-*Acyl*
I R^1 = OH, R^2 = Ala-Ala-Gly-Ala-Gly-*Acyl*

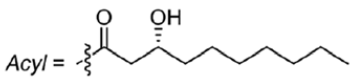

Figure 4-56 Chemical structures of bactobolins and acybolins.

The mode of action of bactobolins have been studied as well. In 2012, Chandler and coworkers have isolated bactobolin-resistant mutants of *B. subtilis* and identified the mutation positions using whole-genome sequencing[166]. With their effort, a 3.4-Å-resolution crystal structure of bactobolin A bound to the 70S ribosome-tRNA complex could be generated. This antibiotic binds at a previously hidden site in the 50S subunit and displaces tRNA bound at the P-site.

Likely, its mode of action is similar to blasticidin S despite binding to a different site, as shown in Figure 4-57. This could explain the potent antibacterial and antitumoral activity of bactobolins[167].

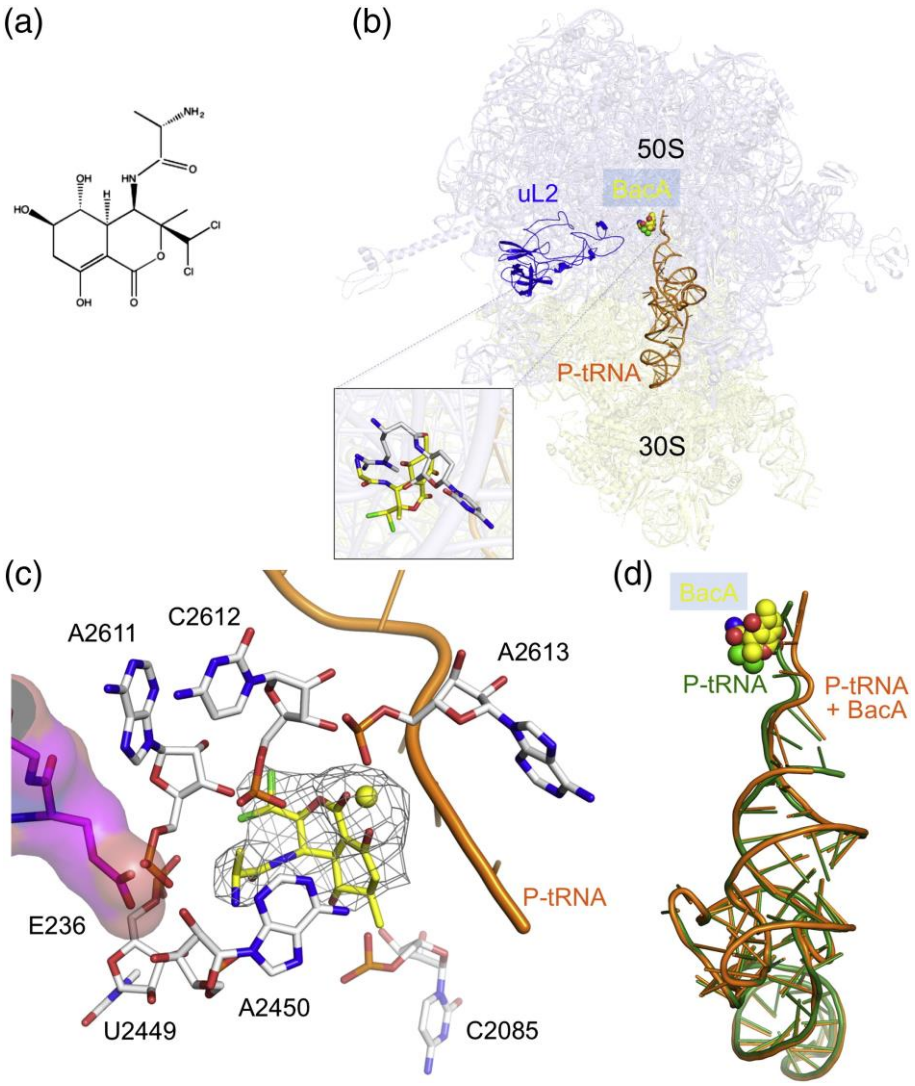

Figure 4-57 Binding of bactobolin A to the ribosome in the presence of P-site tRNA. (a) Chemical structure of bactobolin A. (b) Relative positions of bactobolin, tRNA and uL2; overlapping of the bactobolin and the BlaS binding sites. (c) Unbiased *Fo* − *Fc* difference map corresponding to bactobolin A and adjacent Mg^{2+} (yellow sphere) is contoured at 3σ. rRNA forming contacts with bactobolin is shown. E236 of uL2 stabilizes A2450. (d) Superposition of tRNA in the 70S-tRNA-bactobolin complex with that from antibiotic-free 70S-tRNA, demonstrating the shift of the CCA end of P-site tRNA toward the A-site[167].

4.4.5.2 Partial Elucidated Bactobolin Biosynthesis and their Structural Diversity

The biosynthetic locus was partially elucidated via a series of knock-out studies in *B. thailandensis* E264 and was found to be a NRPS-PKS hybrid assembly line as shown in Figure 4-58.

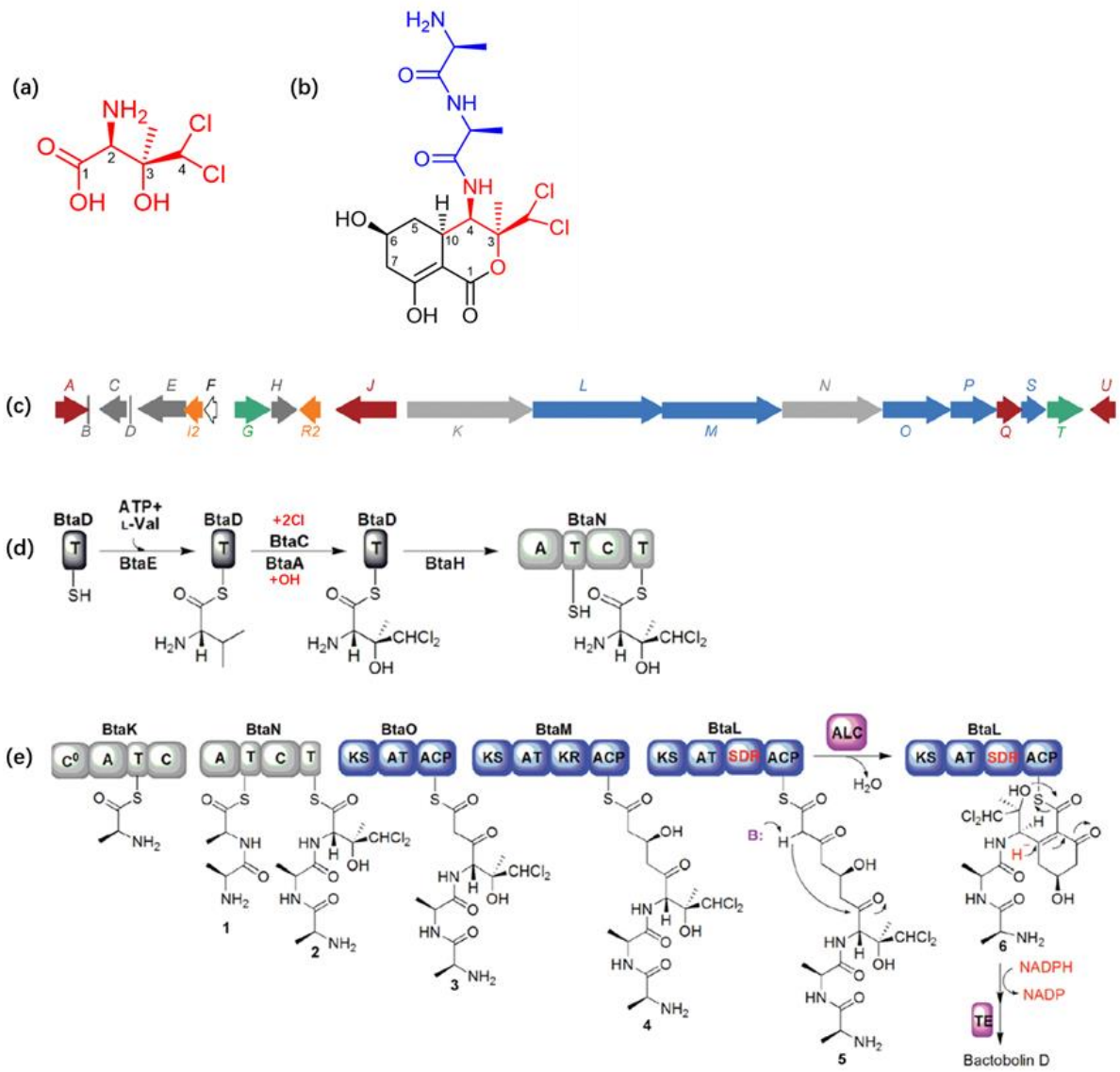

Figure 4-58 The structures of OH-Cl_2-Val and bactobolin D as well as the biosynthetic pathway of bactobolin D. (a) The structure of OH-Cl_2-Val. (b) The structure of bactobolin D. (c) Biosynthesis of OH-Cl_2-Val (grey), Ala-Ala (light grey), polyketide (blue), genes of regulation (orange), product transporters (green), tailoring reactions (brown), and genes of unknown function (white). (d) The biosynthetic pathway of OH-Cl_2-Val. (e) The proposed biosynthetic pathway of Ala-Ala and C6 polyketide[162].

To have a brief look at the bactobolin biosynthetic pathyway as an example, bactobolin D was selected to give more insights. For the biosynthesis of OH-Cl_2-Val, the genes *btaD/E/C/A/H* play important roles as shown in Figure 4-58. Valine as starter unit is first to be activated by BtaE and is then chlorinated and hydroxylated by BtaC and BtaA, respectively. Under the

function of BtaH, the assembled OH-Cl_2-Val is transferred from BtaD to the T domain of BtaN which is part of the NRPS assembly line. The BtaK and BtaN are NRPSs, while the genes *btaO/M/L* coding for PKSs. After these NRPS and PKS modules, the generation of the lactone ring could be catalyzed by BtaS, a predicted type II thioesterase, or BtaP, a predicted β-lactamase[168]. The gene *btaQ*, a predicted acetyltransferase, was thought to be involved in the biosynthesis of N-acetyl bactobolins, which can be cleaved by BtaJ, a predicted oligopeptidase. The hydroxy group at C-5 may be catalyzed by BtaU. According to the predictions above, the biosynthetic pathways of bactobolins A-C could be explained. As a result, they may be generated from bactobolin D by *btaU*, *btaQ* and *btaJ*. The genes *btaG* and *btaT* are transport-related and may play a role in self-protection. BtaB lacks the typical GXDS(L/I) sequence motif and may be inactive. The function of *baF* is still unknown[162].

For the biosynthesis of the unnatural amino acid (OH-Cl_2-Val), two core catalytical steps, chlorination and hydroxylation, were catalyzed by BtaC and BtaA, respectively. However, the order of these two steps is still unclear. In addition, the mechanism involved in the biosynthesis of monochlorinated and dichlorinated substrates is also not fully understood. Moreover, the lack of gene *A* in *B. glumae* ICMP 3729 (Figure 4-42) does not affect the hydroxylation of the unnatural amino acid, while this hydroxylation was thought to play an important role during formation of the bicyclic system of bactobolins. Based on the fact that no monochlorinated bactobolins or acybolins bearing a hydroxy group at C5 position were reported so far, this suggests that the hydroxylase BtaU (Table 4-14) may be specific for a dichlorinated substrate[163]. Additionally, in terms of antibacterial activity, bactobolins A and B that possess the hydroxyl group at C5, were proven to be more potent than bactobolins C and D[162].

Furthermore, the structural diversity of the peptide portion illustrated that BtaK and BtaN must act iteratively (Figure 4-58). However, due to their non-collinear behaviour, the resultant peptide sequences could not be predicted. The unfixed number and order of involved alanyl and glycyl residues in the peptide chains were only elucidated through a chemical approach. The curtailment of the peptide linkers is still not fully explicable either. For example, bactobolin E has three alanyl residues, while bactobolin B bears only two alanyl moieties. Seyedsayamdost *et al*. have predicted that BtaQ (acetyltransferase) could firstly catalyze N-acetylation of bactobolins and subsequently, BtaJ (oligopeptidase) may cleave N-acetyl-bactobolins. Indeed, acetylated bactobolin A has been previously reported. However, the lack of gene Q in *B. glumae* ICMP 3729 does not affect the biosynthesis of bactobolin derivatives, which should be further

investigated. Besides, the question of whether BtaS (thioesterase) or BtaP (ß-lactamase) are involved in the biosynthesis of the lactone ring of bactobolins and acybolins, requires more gene deletion studies.

In the case of acybolins, an additional lipid chain (3-hydroxy-decanoic acid) was connected via an amide bond on the N-terminus of the peptide chain. This kind of lipoinitiation commonly appeared in lipopeptides, but this procedure is not fully understood here, yet. A plausible explanation is that the C domain of BtaK bears the function of a C_0 ($C_{starter}$) as well as a $^{L}C_{L}$ domain. However, only the C domain of the first reused BtaK, being responsible for the insertion of the glycyl residue at the terminus, acts like a C_0 domain. Given that the terminal end of all identified peptide linkers from acybolins is a glycyl residue, which is connected to the lipid chain directly, the remaining C domains of BtaK possibly act as a $^{L}C_{L}$ domain.

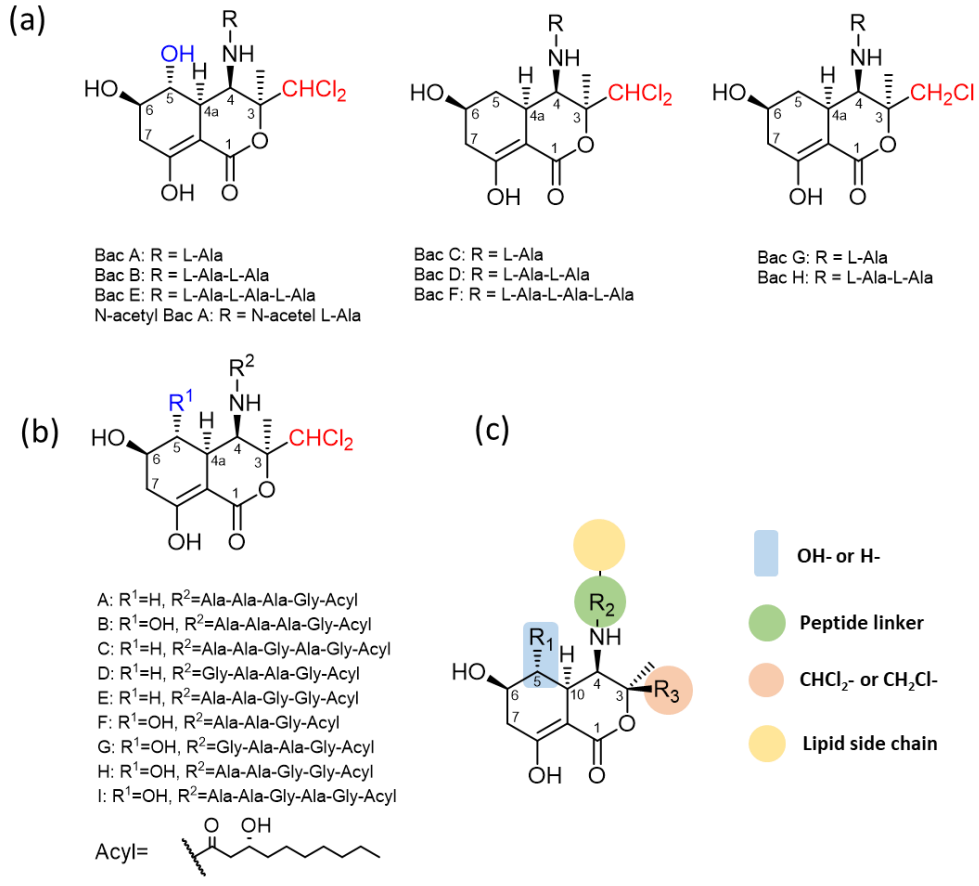

Figure 4-59 All known derivatives from the bactobolin compound family. (a) Bactobolin subgroup 1-3. (b) Acybolins. (c) Variations of the bactobolin-related compounds, different colors represent variation from different positions.

Figure 4-59 summarized all the known bactobolins. The variations stemmed mainly from four parts which are indicated in different colors as described before. In this study, we confirmed

that the plant pathogenic strain *Burkholderia glumae* ICMP 3729, is capable to produce a wide range of bactobolin-related compounds. A new acybolin congener that bears one chlorine, was isolated and elucidated. This new congener acybolin J enriched the diversity of acybolins, as we report the monochloride acybolin for the first time, although bactobolin G and bactobolin H bear only one chlorine as well. The production of bactobolins were reported to be regulated under the quorum-sensing system (BtaR2-BtaI2)[169]. In comparison to bactobolins, all the known acybolins are reported to be void of both antibiotic and antitumoral activity. Hence, they may play some other ecological roles, since acybolins carry a lipid warhead rather than bactobolins. This lipopeptide-like properties may reflect their interaction with other targets.

The biological activity of acybolin J is currently under investigation by collaborators; more details may increasing understanding of the production of this new compound. Given that a relatively low amount of acybolin J, in comparison to acybolin A, was produced during fermentation using minimal media, acybolin J may represent an intermediate from the biosynthetic assembly line. However, considering the medium recipe, showed that numerous chlorine-sources, such as sodium chloride, calcium chloride and ammonium chloride, were present in a sufficient amount. Therefore, the shortage of a chlorine source in the cultivation medium, which could led to the monochlorinated acybolin J, is excluded. This is also in agreement with the isolation of monochlorinated bactobolins G and H, which were isolated as real natural products, and even their bioactivity did not dramatically drop with the loss of one chlorine[163]. All these discussions now point to their biosynthetic origin. The key enzyme, encoded by the gene *C* in the BGC 1.2, catalyzing the chlorination shares a similarity of 87.62% with that of BtaC. Based on the reported experimental results[163], it appears that only the dichlorinated amino acid (Cl_2-Val) could be hydroxylated via BtaU, and that the chlorination must occur before the hydroxylation. Why BtaC is able to generate mono- and dichlorinated bactobolin-related compounds at the same time is still remaining an intriguing question. As acybolin J was presumed to be a real natural product secreted by the strain *B. glumae* ICMP 3729, it could also become a particular indicator for other undiscovered monochlorinated acybolin or bactobolin derivatives, which may lead to the full picture of this compound class.

References

1 Dias, D. A., Urban, S. & Roessner, U. A historical overview of natural products in drug discovery. *Metabolites* **2**, 303-336, doi:10.3390/metabo2020303 (2012).

2 Newman, D. J. & Cragg, G. M. Natural Products as Sources of New Drugs over the Nearly Four Decades from 01/1981 to 09/2019. *Journal of Natural Products* **83**, 770-803, doi:10.1021/acs.jnatprod.9b01285 (2020).

3 Kauffman, G. B. The discovery of penicillin: Twentieth century wonder drug. *Journal of Chemical Education* **56**, 454, doi:10.1021/ed056p454 (1979).

4 Atanasov, A. G., Zotchev, S. B., Dirsch, V. M., International Natural Product Sciences, T. & Supuran, C. T. Natural products in drug discovery: advances and opportunities. *Nat Rev Drug Discov*, doi:10.1038/s41573-020-00114-z (2021).

5 Hutchings, M. I., Truman, A. W. & Wilkinson, B. Antibiotics: past, present and future. *Curr Opin Microbiol* **51**, 72-80, doi:10.1016/j.mib.2019.10.008 (2019).

6 Abdel-Razek, A. S., El-Naggar, M. E., Allam, A., Morsy, O. M. & Othman, S. I. Microbial Natural Products in Drug Discovery. *Processes* **8**, doi:doi.org/10.3390/pr8040470 (2020).

7 Masschelein, J., Jenner, M. & Challis, G. L. Antibiotics from Gram-negative bacteria: a comprehensive overview and selected biosynthetic highlights. *Natural Product Reports* **34**, 712-783, doi:10.1039/c7np00010c (2017).

8 Berdy, J. Bioactive microbial metabolites. *J Antibiot (Tokyo)* **58**, 1-26, doi:10.1038/ja.2005.1 (2005).

9 Fuller, A. T. *et al.* Pseudomonic Acid - Antibiotic Produced by *Pseudomonas-Fluorescens*. *Nature* **234**, 416-&, doi:DOI 10.1038/234416a0 (1971).

10 Sokol, P. A. Production and utilization of pyochelin by clinical isolates of *Pseudomonas cepacia*. *J Clin Microbiol* **23**, 560-562, doi:10.1128/JCM.23.3.560-562.1986 (1986).

11 Rohm, B., Scherlach, K. & Hertweck, C. Biosynthesis of the mitochondrial adenine nucleotide translocase (ATPase) inhibitor bongkrekic acid in *Burkholderia gladioli*. *Org Biomol Chem* **8**, 1520-1522, doi:10.1039/b925483h (2010).

12 Oliver, R. A., Li, R. & Townsend, C. A. Monobactam formation in sulfazecin by a nonribosomal peptide synthetase thioesterase. *Nat Chem Biol* **14**, 5-7, doi:10.1038/nchembio.2526 (2018).

13 Li, R., Oliver, R. A. & Townsend, C. A. Identification and Characterization of the Sulfazecin Monobactam Biosynthetic Gene Cluster. *Cell Chem Biol* **24**, 24-34, doi:10.1016/j.chembiol.2016.11.010 (2017).

14 Barelmann, I., Meyer, J. M., Taraz, K. & Budzikiewicz, H. Cepaciachelin, a new catecholate siderophore from *Burkholderia* (*Pseudomonas*) *cepacia*. *Z Naturforsch C* **51**, 627-630 (1996).

15 Choi, J. E. *et al.* Isolation and characterization of a novel metagenomic enzyme capable of degrading bacterial phytotoxin toxoflavin. *Plos One* **13**, doi:10.1371/journal.pone.0183893 (2018).

16 Tawfik, K. A. *et al.* Burkholdines 1097 and 1229, Potent Antifungal Peptides from *Burkholderia ambifaria* 2.2N. *Organic Letters* **12**, 664-666, doi:10.1021/ol9029269 (2010).

17 Lin, Z. J. *et al.* Burkholdines from *Burkholderia ambifaria*: Antifungal Agents and Possible Virulence Factors. *Journal of Natural Products* **75**, 1518-1523, doi:10.1021/np300108u (2012).

18 Biggins, J. B., Ternei, M. A. & Brady, S. F. Malleilactone, a Polyketide Synthase-Derived Virulence Factor Encoded by the Cryptic Secondary Metabolome of *Burkholderia pseudomallei* Group Pathogens. *Journal of the American Chemical Society* **134**, 13192-13195, doi:10.1021/ja3052156 (2012).

19 Klaus, J. R. *et al.* Malleilactone Is a *Burkholderia pseudomallei* Virulence Factor Regulated by Antibiotics and Quorum Sensing. *Journal of Bacteriology* **200**, doi:10.1128/JB.00008-18 (2018).

20 Nakajima, H. *et al.* New antitumor substances, FR901463, FR901464 and FR901465. II. Activities against experimental tumors in mice and mechanism of action. *J Antibiot (Tokyo)* **49**, 1204-1211, doi:10.7164/antibiotics.49.1204 (1996).

21 Nakajima, H. *et al.* New antitumor substances, FR901463, FR901464 and FR901465. I. Taxonomy, fermentation, isolation, physico-chemical properties and biological activities. *J Antibiot (Tokyo)* **49**, 1196-1203, doi:10.7164/antibiotics.49.1196 (1996).

22 Nakajima, H., Takase, S., Terano, H. & Tanaka, H. New antitumor substances, FR901463, FR901464 and FR901465. III. Structures of FR901463, FR901464 and FR901465. *J Antibiot (Tokyo)* **50**, 96-99, doi:10.7164/antibiotics.50.96 (1997).

23 Cimermancic, P. *et al.* Insights into Secondary Metabolism from a Global Analysis of Prokaryotic Biosynthetic Gene Clusters. *Cell* **158**, 412-421, doi:10.1016/j.cell.2014.06.034 (2014).

24 Nazir, R., Hansen, M. A., Sorensen, S. & van Elsas, J. D. Draft Genome Sequence of the Soil Bacterium *Burkholderia terrae* Strain BS001, Which Interacts with Fungal Surface Structures. *Journal of Bacteriology* **194**, 4480-4481, doi:10.1128/Jb.00725-12 (2012).

25 Pinto-Carbo, M. *et al.* Evidence of horizontal gene transfer between obligate leaf nodule symbionts. *Isme J* **10**, 2092-2105, doi:10.1038/ismej.2016.27 (2016).

26 Ussery, D. W. *et al.* The genus *burkholderia*: analysis of 56 genomic sequences. *Genome Dyn* **6**, 140-157, doi:10.1159/000235768 (2009).

27 Lessie, T. G., Hendrickson, W., Manning, B. D. & Devereux, R. Genomic complexity and plasticity of *Burkholderia cepacia*. *Fems Microbiology Letters* **144**, 117-128, doi:DOI 10.1111/j.1574-6968.1996.tb08517.x (1996).

28 Coenye, T. & Vandamme, P. Diversity and significance of *Burkholderia* species occupying diverse ecological niches. *Environmental Microbiology* **5**, 719-729, doi:10.1046/j.1462-2920.2003.00471.x (2003).

29 Crusemann, M. *et al.* Heterologous Expression, Biosynthetic Studies, and Ecological Function of the Selective Gq-Signaling Inhibitor FR900359. *Angew Chem Int Ed Engl* **57**, 836-840, doi:10.1002/anie.201707996 (2018).

30 Chain, P. S. *et al. Burkholderia xenovorans* LB400 harbors a multi-replicon, 9.73-Mbp genome shaped for versatility. *Proc Natl Acad Sci U S A* **103**, 15280-15287, doi:10.1073/pnas.0606924103 (2006).

31 Yabuuchi, E. *et al.* Proposal of *Burkholderia* gen. nov. and transfer of seven species of the genus *Pseudomonas* homology group II to the new genus, with the type species *Burkholderia cepacia* (Palleroni and Holmes 1981) comb. nov. *Microbiol Immunol* **36**, 1251-1275, doi:10.1111/j.1348-0421.1992.tb02129.x (1992).

32 Validation of the Publication of New Names and New Combinations Previously Effectively Published Outside the IJSB. **43**, 398-399, doi:10.1099/00207713-43-2-398 (1993).

33 Titball, R. W., Burtnick, M. N., Bancroft, G. J. & Brett, P. *Burkholderia pseudomallei* and *Burkholderia mallei* vaccines: Are we close to clinical trials? *Vaccine* **35**, 5981-5989, doi:10.1016/j.vaccine.2017.03.022 (2017).

34 Mahenthiralingam, E., Urban, T. A. & Goldberg, J. B. The multifarious, multireplicon *Burkholderia cepacia* complex. *Nat Rev Microbiol* **3**, 144-156, doi:10.1038/nrmicro1085 (2005).

35 Gillis, M. *et al.* Polyphasic Taxonomy in the Genus *Burkholderia* Leading to an Emended Description of the Genus and Proposition of *Burkholderia-Vietnamiensis* Sp-Nov for N-2-Fixing Isolates from Rice in Vietnam. *Int J Syst Bacteriol* **45**, 274-289, doi:Doi 10.1099/00207713-45-2-274 (1995).

36 Yabuuchi, E., Kosako, Y., Yano, I., Hotta, H. & Nishiuchi, Y. Transfer of two *Burkholderia* and an *Alcaligenes* species to Ralstonia gen. Nov.: Proposal of *Ralstonia pickettii* (Ralston, Palleroni and Doudoroff 1973) comb. Nov., *Ralstonia solanacearum* (Smith 1896) comb. Nov. and *Ralstonia eutropha* (Davis 1969) comb. Nov. *Microbiol Immunol* **39**, 897-904, doi:10.1111/j.1348-0421.1995.tb03275.x (1995).

37 Coenye, T. *et al. Burkholderia ambifaria* sp. nov., a novel member of the *Burkholderia cepacia* complex including biocontrol and cystic fibrosis-related isolates. *Int J Syst Evol Microbiol* **51**, 1481-1490, doi:10.1099/00207713-51-4-1481 (2001).

38 Vandamme, P. *et al. Burkholderia anthina* sp nov and *Burkholderia pyrrocinia*, two additional *Burkholderia cepacia* complex bacteria, may confound results of new molecular diagnostic tools. *Fems Immunol Med Mic* **33**, 143-149, doi:10.1111/j.1574-695X.2002.tb00584.x (2002).

39 Vanlaere, E. *et al. Burkholderia latens* sp nov., *Burkholderia diffusa* sp nov., *Burkholderia arboris* sp nov., *Burkholderia seminalis* sp nov and *Burkholderia metallica* sp nov., novel species within the *Burkholderia cepacia* complex. *Int J Syst Evol Micr* **58**, 1580-1590, doi:10.1099/ijs.0.65634-0 (2008).

40 Vandamme, P. *et al. Burkholderia cenocepacia* sp nov - a new twist to an old story. *Res Microbiol* **154**, 91-96, doi:10.1016/S0923-2508(03)00026-3 (2003).

41 Vandamme, P. *et al.* Occurrence of multiple genomovars of *Burkholderia cepacia* in cystic fibrosis patients and proposal of *Burkholderia multivorans* sp. nov. *Int J Syst Bacteriol* **47**, 1188-1200, doi: 10.1099/00207713-47-4-1188 (1997).

42 Vanlaere, E. *et al.* Taxon K, a complex within the *Burkholderia cepacia* complex, comprises at least two novel species, *Burkholderia contaminans* sp nov and *Burkholderia lata* sp nov. *Int J Syst Evol Micr* **59**, 102-111, doi:10.1099/ijs.0.001123-0 (2009).

43 Vermis, K. *et al.* Proposal to accommodate *Burkholderia cepacia* genomovar VI as *Burkholderia dolosa* sp nov. *Int J Syst Evol Micr* **54**, 689-691, doi:10.1099/ijs.0.02888-0 (2004).

44 Storms, V. *et al.* Polyphasic characterisation of *Burkholderia cepacia*-like isolates leading to the emended description of *Burkholderia pyrrocinia*. *Syst Appl Microbiol* **27**, 517-526, doi:10.1078/0723202041748190 (2004).

45 Vandamme, P. *et al.* Identification and population structure of B*urkholderia stabilis* sp nov (formerly *Burkholderia cepacia* genomovar IV). *Journal of Clinical Microbiology* **38**, 1042-1047, doi: 10.1128/Jcm.38.3.1042-1047.2000 (2000).

46 Yabuuchi, E. *et al. Burkholderia* uboniae sp. nov., L-arabinose-assimilating but different from *Burkholderia thailandensis* and *Burkholderia vietnamiensis*. *Microbiology and Immunology* **44**, 307-317, doi:10.1111/j.1348-0421.2000.tb02500.x (2000).

47 Glass, M. B., Steigerwalt, A. G., Jordan, J. G., Wilkins, P. P. & Gee, J. E. *Burkholderia oklahomensis* sp nov., a *Burkholderia pseudomallei*-like species formerly known as the Oklahoma strain of *Pseudomonas pseudomallei*. *Int J Syst Evol Micr* **56**, 2171-2176, doi:10.1099/ijs.0.63991-0 (2006).

48 Peeters, C. *et al.* Phylogenomic Study of *Burkholderia glathei*-like Organisms, Proposal of 13 Novel *Burkholderia* Species and Emended Descriptions of *Burkholderia sordidicola*, *Burkholderia zhejiangensis*, and *Burkholderia grimmiae*. *Frontiers in Microbiology* **7**, doi:10.3389/fmicb.2016.00877 (2016).

49 Payne, G. W. *et al.* Development of a recA gene-based identification approach for the the entire *Burkholderia* genus. *Appl Environ Microb* **71**, 3917-3927, doi:10.1128/Aem.71.7.3917-3927.2005 (2005).

50 Gyaneshwar, P. *et al.* Legume-nodulating betaproteobacteria: diversity, host range, and future prospects. *Mol Plant Microbe Interact* **24**, 1276-1288, doi:10.1094/MPMI-06-11-0172 (2011).

51 Sawana, A., Adeolu, M. & Gupta, R. S. Molecular signatures and phylogenomic analysis of the genus *Burkholderia*: proposal for division of this genus into the emended genus *Burkholderia* containing pathogenic organisms and a new genus *Paraburkholderia* gen. nov. harboring environmental species. *Front Genet* **5**, 429, doi:10.3389/fgene.2014.00429 (2014).

52 Dobritsa, A. P. & Samadpour, M. Transfer of eleven species of the genus *Burkholderia* to the genus *Paraburkholderia* and proposal of *Caballeronia* gen. nov. to accommodate twelve species of the genera *Burkholderia* and *Paraburkholderia*. *Int J Syst Evol Microbiol* **66**, 2836-2846, doi:10.1099/ijsem.0.001065 (2016).

53 Lopes-Santos, L. *et al.* Reassessment of the taxonomic position of *Burkholderia andropogonis* and description of *Robbsia andropogonis* gen. nov., comb. nov. *Antonie Van Leeuwenhoek* **110**, 727-736, doi:10.1007/s10482-017-0842-6 (2017).

54 Beukes, C. W. *et al.* Genome Data Provides High Support for Generic Boundaries in *Burkholderia* Sensu Lato. *Front Microbiol* **8**, 1154, doi:10.3389/fmicb.2017.01154 (2017).

55 Estrada-de los Santos, P. *et al.* Whole Genome Analyses Suggests that *Burkholderia* sensu lato Contains Two Additional Novel Genera (Mycetohabitans gen. nov., and Trinickia gen. nov.): Implications for the Evolution of Diazotrophy and Nodulation in the Burkholderiaceae. *Genes (Basel)* **9**, doi:10.3390/genes9080389 (2018).

56 Mannaa, M., Park, I. & Seo, Y. S. Genomic Features and Insights into the Taxonomy, Virulence, and Benevolence of Plant-Associated *Burkholderia* Species. *International Journal of Molecular Sciences* **20**, doi:10.3390/ijms20010121 (2019).

57 Liu, X. & Cheng, Y. Q. Genome-guided discovery of diverse natural products from *Burkholderia* sp. *J Ind Microbiol Biotechnol* **41**, 275-284, doi:10.1007/s10295-013-1376-1 (2014).

58 Esmaeel, Q. *et al. Burkholderia* genome mining for nonribosomal peptide synthetases reveals a great potential for novel siderophores and lipopeptides synthesis. *Microbiologyopen* **5**, 512-526, doi:10.1002/mbo3.347 (2016).

59 Esmaeel, Q., Pupin, M., Jacques, P. & Leclere, V. Nonribosomal peptides and polyketides of *Burkholderia*: new compounds potentially implicated in biocontrol and pharmaceuticals. *Environ Sci Pollut Res Int* **25**, 29794-29807, doi:10.1007/s11356-017-9166-3 (2018).

60 Pidot, S. J., Coyne, S., Kloss, F. & Hertweck, C. Antibiotics from neglected bacterial sources. *Int J Med Microbiol* **304**, 14-22, doi:10.1016/j.ijmm.2013.08.011 (2014).

61 Kunakom, S. & Eustaquio, A. S. *Burkholderia* as a Source of Natural Products. *Journal of Natural Products* **82**, 2018-2037, doi:10.1021/acs.jnatprod.8b01068 (2019).

62 Jenul, C. *et al.* Biosynthesis of fragin is controlled by a novel quorum sensing signal. *Nature Communications* **9**, doi:10.1038/s41467-018-03690-2 (2018).

63 Dose, B. *et al.* Unexpected Bacterial Origin of the Antibiotic Icosalide: Two-Tailed Depsipeptide Assembly in Multifarious *Burkholderia* Symbionts. *Acs Chem Biol* **13**, 2414-2420, doi:10.1021/acschembio.8b00600 (2018).

64 Thongkongkaew, T. *et al.* Two Types of Threonine-Tagged Lipopeptides Synergize in Host Colonization by Pathogenic *Burkholderia* Species. *Acs Chem Biol* **13**, 1370-1379, doi:10.1021/acschembio.8b00221 (2018).

65 Hermenau, R. *et al.* Gramibactin is a bacterial siderophore with a diazeniumdiolate ligand system. *Nature Chemical Biology* **14**, 841-+, doi:10.1038/s41589-018-0101-9 (2018).

66 Hermenau, R. *et al.* Genomics-Driven Discovery of NO-Donating Diazeniumdiolate Siderophores in Diverse Plant-Associated Bacteria. *Angew Chem Int Edit* **58**, 13024-13029, doi:10.1002/anie.201906326 (2019).

67 Park, J. D. *et al.* Thailandenes, Cryptic Polyene Natural Products Isolated from *Burkholderia thailandensis* Using Phenotype-Guided Transposon Mutagenesis. *Acs Chem Biol* **15**, 1195-1203, doi:10.1021/acschembio.9b00883 (2020).

68 Niehs, S. P. *et al.* Insect-Associated Bacteria Assemble the Antifungal Butenolide Gladiofungin by Non-Canonical Polyketide Chain Termination. *Angew Chem Int Edit* **59**, 23122-23126, doi:10.1002/anie.202005711 (2020).

69 Niehs, S. P. *et al.* Mining Symbionts of a Spider-Transmitted Fungus Illuminates Uncharted Biosynthetic Pathways to Cytotoxic Benzolactones. *Angew Chem Int Edit* **59**, 7766-7771, doi:10.1002/anie.201916007 (2020).

70 Jenner, M. *et al.* An unusual *Burkholderia* gladioli double chain-initiating nonribosomal peptide synthetase assembles "fungal' icosalide antibiotics. *Chem Sci* **10**, 5489-5494, doi:10.1039/c8sc04897e (2019).

71 Dashti, Y. *et al.* Discovery and Biosynthesis of Bolagladins: Unusual Lipodepsipeptides from *Burkholderia gladioli* Clinical Isolates*. *Angew Chem Int Ed Engl* **59**, 21553-21561, doi:10.1002/anie.202009110 (2020).

72 Dose, B. *et al.* Food-Poisoning Bacteria Employ a Citrate Synthase and a Type II NRPS To Synthesize Bolaamphiphilic Lipopeptide Antibiotics*. *Angew Chem Int Ed Engl* **59**, 21535-21540, doi:10.1002/anie.202009107 (2020).

73 Blin, K. *et al.* antiSMASH 5.0: updates to the secondary metabolite genome mining pipeline. *Nucleic Acids Res* **47**, W81-W87, doi:10.1093/nar/gkz310 (2019).

74 Ziemert, N. *et al.* The natural product domain seeker NaPDoS: a phylogeny based bioinformatic tool to classify secondary metabolite gene diversity. *PLoS One* **7**, e34064, doi:10.1371/journal.pone.0034064 (2012).

75 Rottig, M. *et al.* NRPSpredictor2-a web server for predicting NRPS adenylation domain specificity. *Nucleic Acids Research* **39**, W362-W367, doi:10.1093/nar/gkr323 (2011).

76 Bentley, S. D. *et al.* Complete genome sequence of the model actinomycete *Streptomyces coelicolor* A3(2). *Nature* **417**, 141-147, doi:DOI 10.1038/417141a (2002).

77 Ikeda, H. *et al.* Complete genome sequence and comparative analysis of the industrial microorganism *Streptomyces avermitilis*. *Nat Biotechnol* **21**, 526-531, doi:10.1038/nbt820 (2003).

78 Baltz, R. H. Natural product drug discovery in the genomic era: realities, conjectures, misconceptions, and opportunities. *J Ind Microbiol Biotechnol* **46**, 281-299, doi:10.1007/s10295-018-2115-4 (2019).

79 Paterson, J. *et al.* The contribution of genome mining strategies to the understanding of active principles of PGPR strains. *Fems Microbiol Ecol* **93**, doi:10.1093/femsec/fiw249 (2017).

80 Caboche, S. *et al.* NORINE: a database of nonribosomal peptides. *Nucleic Acids Research* **36**, D326-D331, doi:10.1093/nar/gkm792 (2008).

81 Strieker, M., Tanovic, A. & Marahiel, M. A. Nonribosomal peptide synthetases: structures and dynamics. *Curr Opin Struc Biol* **20**, 234-240, doi:10.1016/j.sbi.2010.01.009 (2010).

82 Wang, X. *et al.* Discovery of recombinases enables genome mining of cryptic biosynthetic gene clusters in Burkholderiales species. *Proc Natl Acad Sci U S A* **115**, E4255-E4263, doi:10.1073/pnas.1720941115 (2018).

83 Partida-Martinez, L. P. & Hertweck, C. A gene cluster encoding rhizoxin biosynthesis in "*Burkholderia rhizoxina*", the bacterial endosymbiont of the fungus *Rhizopus microsporus*. *Chembiochem* **8**, 41-45, doi:10.1002/cbic.200600393 (2007).

84 Challis, G. L. & Naismith, J. H. Structural aspects of non-ribosomal peptide biosynthesis. *Curr Opin Struct Biol* **14**, 748-756, doi:10.1016/j.sbi.2004.10.005 (2004).

85 Sundlov, J. A., Shi, C., Wilson, D. J., Aldrich, C. C. & Gulick, A. M. Structural and Functional Investigation of the Intermolecular Interaction between NRPS Adenylation and Carrier Protein Domains. *Chem Biol* **19**, 188-198, doi:10.1016/j.chembiol.2011.11.013 (2012).

86 Rausch, C., Weber, T., Kohlbacher, O., Wohlleben, W. & Huson, D. H. Specificity prediction of adenylation domains in nonribosomal peptide synthetases (NRPS) using transductive support vector machines (TSVMs). *Nucleic Acids Research* **33**, 5799-5808, doi:10.1093/nar/gki885 (2005).

87 Marahiel, M. A. A structural model for multimodular NRPS assembly lines. *Natural Product Reports* **33**, 136-140, doi:10.1039/c5np00082c (2016).

88 Gulick, A. M. Conformational Dynamics in the Acyl-CoA Synthetases, Adenylation Domains of Non-ribosomal Peptide Synthetases, and Firefly Luciferase. *Acs Chem Biol* **4**, 811-827, doi:10.1021/cb900156h (2009).

89 Konz, D., Doekel, S. & Marahiel, M. A. Molecular and biochemical characterization of the protein template controlling biosynthesis of the lipopeptide lichenysin. *Journal of Bacteriology* **181**, 133-140, doi:Doi 10.1128/Jb.181.1.133-140.1999 (1999).

90 Sussmuth, R. D. & Mainz, A. Nonribosomal Peptide Synthesis-Principles and Prospects. *Angew Chem Int Edit* **56**, 3770-3821, doi:10.1002/anie.201609079 (2017).

91 Fischbach, M. A. & Walsh, C. T. Assembly-line enzymology for polyketide and nonribosomal Peptide antibiotics: logic, machinery, and mechanisms. *Chem Rev* **106**, 3468-3496, doi:10.1021/cr0503097 (2006).

92 Carroll, C. S. & Moore, M. M. Ironing out siderophore biosynthesis: a review of non-ribosomal peptide synthetase (NRPS)-independent siderophore synthetases. *Crit Rev Biochem Mol Biol* **53**, 356-381, doi:10.1080/10409238.2018.1476449 (2018).

93 Bozhuyuk, K. A. J. *et al.* De novo design and engineering of non-ribosomal peptide synthetases. *Nat Chem* **10**, 275-281, doi:10.1038/nchem.2890 (2018).

94 Bozhuyuk, K. A. J. *et al.* Modification and de novo design of non-ribosomal peptide synthetases using specific assembly points within condensation domains. *Nat Chem* **11**, 653-661, doi:10.1038/s41557-019-0276-z (2019).

95 Florez, L. V. *et al.* Antibiotic-producing symbionts dynamically transition between plant pathogenicity and insect-defensive mutualism. *Nat Commun* **8**, 15172, doi:10.1038/ncomms15172 (2017).

96 Song, L. *et al.* Discovery and Biosynthesis of Gladiolin: A *Burkholderia gladioli* Antibiotic with Promising Activity against *Mycobacterium tuberculosis*. *J Am Chem Soc* **139**, 7974-7981, doi:10.1021/jacs.7b03382 (2017).

97 Moebius, N. *et al.* Biosynthesis of the respiratory toxin bongkrekic acid in the pathogenic bacterium *Burkholderia gladioli*. *Chem Biol* **19**, 1164-1174, doi:10.1016/j.chembiol.2012.07.022 (2012).

98 Shen, B. Polyketide biosynthesis beyond the type I, II and III polyketide synthase paradigms. *Curr Opin Chem Biol* **7**, 285-295, doi:10.1016/S1367-5931(03)00020-6 (2003).

99 Staunton, J. & Weissman, K. J. Polyketide biosynthesis: a millennium review. *Nat Prod Rep* **18**, 380-416, doi:10.1039/a909079g (2001).

100 Piel, J. Biosynthesis of polyketides by trans-AT polyketide synthases. *Natural Product Reports* **27**, 996-1047, doi:10.1039/b816430b (2010).

101 Nivina, A., Yuet, K. P., Hsu, J. & Khosla, C. Evolution and Diversity of Assembly-Line Polyketide Synthases. *Chemical Reviews* **119**, 12524-12547, doi:10.1021/acs.chemrev.9b00525 (2019).

102 Du, L. H., Sanchez, C. & Shen, B. Hybrid peptide-polyketide natural products: Biosynthesis and prospects toward engineering novel molecules. *Metab Eng* **3**, 78-95, doi:10.1006/mben.2000.0171 (2001).

103 Du, L., Sanchez, C., Chen, M., Edwards, D. J. & Shen, B. The biosynthetic gene cluster for the antitumor drug bleomycin from *Streptomyces verticillus* ATCC15003 supporting functional interactions between nonribosomal peptide synthetases and a polyketide synthase. *Chem Biol* **7**, 623-642, doi:10.1016/s1074-5521(00)00011-9 (2000).

104 Liu, X. *et al.* Genomics-guided discovery of thailanstatins A, B, and C As pre-mRNA splicing inhibitors and antiproliferative agents from *Burkholderia thailandensis* MSMB43. *J Nat Prod* **76**, 685-693, doi:10.1021/np300913h (2013).

105 Ghosh, A. K. *et al.* Enantioselective Synthesis of Thailanstatin A Methyl Ester and Evaluation of in Vitro Splicing Inhibition. *J Org Chem* **83**, 5187-5198, doi:10.1021/acs.joc.8b00593 (2018).

106 Mahenthiralingam, E. *et al.* Enacyloxins are products of an unusual hybrid modular polyketide synthase encoded by a cryptic *Burkholderia ambifaria* Genomic Island. *Chem Biol* **18**, 665-677, doi:10.1016/j.chembiol.2011.01.020 (2011).

107 Wu, Y. & Seyedsayamdost, M. R. The Polyene Natural Product Thailandamide A Inhibits Fatty Acid Biosynthesis in Gram-Positive and Gram-Negative Bacteria. *Biochemistry* **57**, 4247-4251, doi:10.1021/acs.biochem.8b00678 (2018).

108 Schwyn, B. & Neilands, J. B. Universal chemical assay for the detection and determination of siderophores. *Anal Biochem* **160**, 47-56, doi:10.1016/0003-2697(87)90612-9 (1987).

109 Karongo, R., Jiao, J., Gross, H. & Lammerhofer, M. Direct enantioselective gradient reversed-phase ultra-high performance liquid chromatography - tandem mass spectrometry method for 3-hydroxy alkanoic acids in lipopeptides on immobilized 1.6 mum amylose-based chiral stationary phase. *J Sep Sci*, doi:10.1002/jssc.202100104 (2021).

110 Blin, K. *et al.* antiSMASH 4.0-improvements in chemistry prediction and gene cluster boundary identification. *Nucleic Acids Res* **45**, W36-W41, doi:10.1093/nar/gkx319 (2017).

111 Tatusova, T. *et al.* NCBI prokaryotic genome annotation pipeline. *Nucleic Acids Res* **44**, 6614-6624, doi:10.1093/nar/gkw569 (2016).

112 Lepe, J. A., Dominguez-Herrera, J., Pachon, J. & Aznar, J. Determining accurate vancomycin MIC values for methicillin-resistant Staphylococcus aureus by the microdilution method. *J Antimicrob Chemother* **69**, 136-138, doi:10.1093/jac/dkt308 (2014).

113 Bode, H. B., Bethe, B., Hofs, R. & Zeeck, A. Big effects from small changes: possible ways to explore nature's chemical diversity. *Chembiochem* **3**, 619-627, doi:10.1002/1439-7633(20020703)3:7<619::AID-CBIC619>3.0.CO;2-9 (2002).

114 Wäspi, U., Blanc, D., Winkler, T., Rüedi, P. & Dudler, R. Syringolin, a Novel Peptide Elicitor from *Pseudomonas syringae* pv. *syringae* that Induces Resistance to *Pyricularia oryzae* in Rice. **11**, 727-733, doi:10.1094/mpmi.1998.11.8.727 (1998).

115 Tupe, S. G. *et al.* Possible mechanism of antifungal phenazine-1-carboxamide from *Pseudomonas* sp. against dimorphic fungi *Benjaminiella poitrasii* and human pathogen *Candida albicans*. *J Appl Microbiol* **118**, 39-48, doi:10.1111/jam.12675 (2015).

116 Butt, A. T. & Thomas, M. S. Iron Acquisition Mechanisms and Their Role in the Virulence of *Burkholderia* Species. *Front Cell Infect Mi* **7**, doi:10.3389/fcimb.2017.00460 (2017).

117 Seyedsayamdost, M. R. High-throughput platform for the discovery of elicitors of silent bacterial gene clusters. *P Natl Acad Sci USA* **111**, 7266-7271, doi:10.1073/pnas.1400019111 (2014).

118 Okada, B. K., Wu, Y., Mao, D., Bushin, L. B. & Seyedsayamdost, M. R. Mapping the Trimethoprim-Induced Secondary Metabolome of *Burkholderia thailandensis*. *Acs Chem Biol* **11**, 2124-2130, doi:10.1021/acschembio.6b00447 (2016).

119 Gross, H. Strategies to unravel the function of orphan biosynthesis pathways: recent examples and future prospects. *Appl Microbiol Biotechnol* **75**, 267-277, doi:10.1007/s00253-007-0900-5 (2007).

120 Zhong, L. *et al.* Engineering and elucidation of the lipoinitiation process in nonribosomal peptide biosynthesis. *Nat Commun* **12**, 296, doi:10.1038/s41467-020-20548-8 (2021).

121 Drake, E. J. & Gulick, A. M. Structural characterization and high-throughput screening of inhibitors of PvdQ, an NTN hydrolase involved in pyoverdine synthesis. *Acs Chem Biol* **6**, 1277-1286, doi:10.1021/cb2002973 (2011).

122 Barbeau, K., Rue, E. L., Trick, C. G., Bruland, K. W. & Butler, A. Photochemical reactivity of siderophores produced by marine heterotrophic bacteria and cyanobacteria based on characteristic Fe(III) binding groups. **48**, 1069-1078, doi:10.4319/lo.2003.48.3.1069 (2003).

123 Emery, T. Exchange of iron by gallium in siderophores. *Biochemistry* **25**, 4629-4633, doi:10.1021/bi00364a026 (1986).

124 Skinnider, M. A., Merwin, N. J., Johnston, C. W. & Magarvey, N. A. PRISM 3: expanded prediction of natural product chemical structures from microbial genomes. *Nucleic Acids Res* **45**, W49-W54, doi:10.1093/nar/gkx320 (2017).

125 Mnif, I. & Ghribi, D. Review lipopeptides biosurfactants: Mean classes and new insights for industrial, biomedical, and environmental applications. *Biopolymers* **104**, 129-147, doi:10.1002/bip.22630 (2015).

126 Gross, H. & Loper, J. E. Genomics of secondary metabolite production by *Pseudomonas* spp. *Natural Product Reports* **26**, 1408-1446, doi:10.1039/B817075B (2009).

127 Singh, P. & Cameotra, S. S. Potential applications of microbial surfactants in biomedical sciences. *Trends Biotechnol* **22**, 142-146, doi:10.1016/j.tibtech.2004.01.010 (2004).

128 Stephan, H. *et al.* Ornibactins--a new family of siderophores from *Pseudomonas*. *Biometals* **6**, 93-100, doi:10.1007/BF00140109 (1993).

129 Risse, D., Beiderbeck, H., Taraz, K., Budzikiewicz, H. & Gustine, D. Bacterial constituents part LXXVII. Corrugatin, a lipopeptide siderophore from *Pseudomonas corrugata*. *Z Naturforsch C* **53**, 295-304 (1998).

130 Rosconi, F., Trovero, M. F., de Souza, E. M. & Fabiano, E. Serobactins-mediated iron acquisition systems optimize competitive fitness of *Herbaspirillum seropedicae* inside rice plants. *Environmental Microbiology* **18**, 2523-2533, doi:10.1111/1462-2920.13202 (2016).

131 Kurth, C., Schieferdecker, S., Athanasopoulou, K., Seccareccia, I. & Nett, M. Variochelins, Lipopeptide Siderophores from Variovorax boronicumulans Discovered by Genome Mining. *Journal of Natural Products* **79**, 865-872, doi:10.1021/acs.jnatprod.5b00932 (2016).

132 Kurth, C., Kage, H. & Nett, M. Siderophores as molecular tools in medical and environmental applications. *Organic & Biomolecular Chemistry* **14**, 8212-8227, doi:10.1039/c6ob01400c (2016).

133 Saha, M. *et al.* Microbial siderophores and their potential applications: a review. *Environ Sci Pollut R* **23**, 3984-3999, doi:10.1007/s11356-015-4294-0 (2016).

134 Agnoli, K., Lowe, C. A., Farmer, K. L., Husnain, S. I. & Thomas, M. S. The ornibactin biosynthesis and transport genes of *Burkholderia cenocepacia* are regulated by an extracytoplasmic function sigma factor which is a part of the Fur regulon. *J Bacteriol* **188**, 3631-3644, doi:10.1128/JB.188.10.3631-3644.2006 (2006).

135 Schmelz, S. *et al.* AcsD catalyzes enantioselective citrate desymmetrization in siderophore biosynthesis. *Nature Chemical Biology* **5**, 174-182, doi:10.1038/nchembio.145 (2009).

136 Franke, J., Ishida, K. & Hertweck, C. Plasticity of the Malleobactin Pathway and Its Impact on Siderophore Action in Human Pathogenic Bacteria. *Chem-Eur J* **21**, 8010-8014, doi:10.1002/chem.201500757 (2015).

137 Huang, Y. Z. *et al.* Curb challenges of the "Trojan Horse" approach: Smart strategies in achieving effective yet safe cell-penetrating peptide-based drug delivery. *Adv Drug Deliver Rev* **65**, 1299-1315, doi:10.1016/j.addr.2012.11.007 (2013).

138 Eisendle, M., Oberegger, H., Zadra, I. & Haas, H. The siderophore system is essential for viability of Aspergillus nidulans: functional analysis of two genes encoding L-ornithine N-5-monooxygenase (sidA) and a non-ribosomal peptide synthetase (sidC). *Mol Microbiol* **49**, 359-375, doi:10.1046/j.1365-2958.2003.03586.x (2003).

139 Noinaj, N., Guillier, M., Barnard, T. J. & Buchanan, S. K. TonB-Dependent Transporters: Regulation, Structure, and Function. *Annu Rev Microbiol* **64**, 43-60, doi:10.1146/annurev.micro.112408.134247 (2010).

140 Gama, S. *et al.* Iron Coordination Properties of Gramibactin as Model for the New Class of Diazeniumdiolate Based Siderophores. *Chem-Eur J*, doi:10.1002/chem.202003842 (2021).

141 Schneider, Y. *et al.* Bioactivity of Serratiochelin A, a Siderophore Isolated from a Co-Culture of Serratia sp. and Shewanella sp. *Microorganisms* **8**, doi:10.3390/microorganisms8071042 (2020).

142 Traxler, M. F., Watrous, J. D., Alexandrov, T., Dorrestein, P. C. & Kolter, R. Interspecies interactions stimulate diversification of the *Streptomyces coelicolor* secreted metabolome. *mBio* **4**, doi:10.1128/mBio.00459-13 (2013).

143 Amatuni, A. & Renata, H. Identification of a lysine 4-hydroxylase from the glidobactin biosynthesis and evaluation of its biocatalytic potential. *Org Biomol Chem* **17**, 1736-1739, doi:10.1039/c8ob02054j (2019).

144 Rausch, C., Hoof, I., Weber, T., Wohlleben, W. & Huson, D. H. Phylogenetic analysis of condensation domains in NRPS sheds light on their functional evolution. *BMC Evol Biol* **7**, 78, doi:10.1186/1471-2148-7-78 (2007).

145 Krahn, D., Ottmann, C. & Kaiser, M. The chemistry and biology of syringolins, glidobactins and cepafungins (syrbactins). *Nat Prod Rep* **28**, 1854-1867, doi:10.1039/C1NP00048A (2011).

146 Bian, X., Plaza, A., Zhang, Y. & Muller, R. Luminmycins A-C, cryptic natural products from *Photorhabdus luminescens* identified by heterologous expression in Escherichia coli. *J Nat Prod* **75**, 1652-1655, doi:10.1021/np300444e (2012).

147 Groll, M. *et al.* A plant pathogen virulence factor inhibits the eukaryotic proteasome by a novel mechanism. *Nature* **452**, 755-758, doi:10.1038/nature06782 (2008).

148 Clerc, J. *et al.* Synthetic and structural studies on syringolin A and B reveal critical determinants of selectivity and potency of proteasome inhibition. *Proc Natl Acad Sci U S A* **106**, 6507-6512, doi:10.1073/pnas.0901982106 (2009).

149 Archer, C. R. *et al.* Activity enhancement of the synthetic syrbactin proteasome inhibitor hybrid and biological evaluation in tumor cells. *Biochemistry* **51**, 6880-6888, doi:10.1021/bi300841r (2012).

150 Schellenberg, B., Bigler, L. & Dudler, R. Identification of genes involved in the biosynthesis of the cytotoxic compound glidobactin from a soil bacterium. *Environ Microbiol* **9**, 1640-1650, doi:10.1111/j.1462-2920.2007.01278.x (2007).

151 Ramel, C. *et al.* Biosynthesis of the proteasome inhibitor syringolin A: the ureido group joining two amino acids originates from bicarbonate. *Bmc Biochem* **10**, doi:10.1186/1471-2091-10-26 (2009).

152 Zhao, L. *et al.* Activation, Structure, Biosynthesis and Bioactivity of Glidobactin-like Proteasome Inhibitors from *Photorhabdus laumondii*. *Chembiochem*, doi:10.1002/cbic.202100014 (2021).

153 Shoji, J. *et al.* Isolation of cepafungins I, II and III from *Pseudomonas* species. *J Antibiot (Tokyo)* **43**, 783-787, doi:10.7164/antibiotics.43.783 (1990).

154 Christiansen, G., Philmus, B., Hemscheidt, T. & Kurmayer, R. Genetic variation of adenylation domains of the anabaenopeptin synthesis operon and evolution of substrate promiscuity. *J Bacteriol* **193**, 3822-3831, doi:10.1128/JB.00360-11 (2011).

155 Hoffmann, D., Hevel, J. M., Moore, R. E. & Moore, B. S. Sequence analysis and biochemical characterization of the nostopeptolide A biosynthetic gene cluster from Nostoc sp. GSV224. *Gene* **311**, 171-180, doi:10.1016/s0378-1119(03)00587-0 (2003).

156 Baltz, R. H., Miao, V. & Wrigley, S. K. Natural products to drugs: daptomycin and related lipopeptide antibiotics. *Nat Prod Rep* **22**, 717-741, doi:10.1039/b416648p (2005).

157 Meng, L. *et al.* Epoxomicin, a potent and selective proteasome inhibitor, exhibits in vivo antiinflammatory activity. *Proc Natl Acad Sci U S A* **96**, 10403-10408, doi:10.1073/pnas.96.18.10403 (1999).

158 Theodore, C. M., King, J. B., You, J. & Cichewicz, R. H. Production of cytotoxic glidobactins/luminmycins by *Photorhabdus asymbiotica* in liquid media and live crickets. *J Nat Prod* **75**, 2007-2011, doi:10.1021/np300623x (2012).

159 Slot, J. C. & Rokas, A. Horizontal transfer of a large and highly toxic secondary metabolic gene cluster between fungi. *Curr Biol* **21**, 134-139, doi:10.1016/j.cub.2010.12.020 (2011).

160 Costa, R., van Aarle, I. M., Mendes, R. & van Elsas, J. D. Genomics of pyrrolnitrin biosynthetic loci: evidence for conservation and whole-operon mobility within gram-negative bacteria. *Environ Microbiol* **11**, 159-175, doi:10.1111/j.1462-2920.2008.01750.x (2009).

161 Lopez, J. V. Naturally mosaic operons for secondary metabolite biosynthesis: variability and putative horizontal transfer of discrete catalytic domains of the epothilone polyketide synthase locus. *Mol Genet Genomics* **270**, 420-431, doi:10.1007/s00438-003-0937-9 (2003).

162 Seyedsayamdost, M. R. *et al.* Quorum-sensing-regulated bactobolin production by *Burkholderia thailandensis* E264. *Org Lett* **12**, 716-719, doi:10.1021/ol902751x (2010).

163 Carr, G., Seyedsayamdost, M. R., Chandler, J. R., Greenberg, E. P. & Clardy, J. Sources of diversity in bactobolin biosynthesis by *Burkholderia thailandensis* E264. *Org Lett* **13**, 3048-3051, doi:10.1021/ol200922s (2011).

164 Meusel, M. *et al.* Predicting the Presence of Uncommon Elements in Unknown Biomolecules from Isotope Patterns. *Analytical Chemistry* **88**, 7556-7566, doi:10.1021/acs.analchem.6b01015 (2016).

165 Kondo, S., Horiuchi, Y., Hamada, M., Takeuchi, T. & Umezawa, H. New Anti-Tumor Antibiotic, Bactobolin Produced by *Pseudomonas*. *J Antibiot* **32**, 1069-1071, doi:10.7164/antibiotics.32.1069 (1979).

166 Chandler, J. R. *et al.* Bactobolin resistance is conferred by mutations in the L2 ribosomal protein. *mBio* **3**, doi:10.1128/mBio.00499-12 (2012).

167 Amunts, A. *et al.* Bactobolin A binds to a site on the 70S ribosome distinct from previously seen antibiotics. *J Mol Biol* **427**, 753-755, doi:10.1016/j.jmb.2014.12.018 (2015).

168 Awakawa, T. *et al.* Physically discrete beta-lactamase-type thioesterase catalyzes product release in atrochrysone synthesis by iterative type I polyketide synthase. *Chem Biol* **16**, 613-623, doi:10.1016/j.chembiol.2009.04.004 (2009).

169 Duerkop, B. A. *et al.* Quorum-sensing control of antibiotic synthesis in *Burkholderia thailandensis*. *J Bacteriol* **191**, 3909-3918, doi:10.1128/JB.00200-09 (2009).

Appendix

Appendix A: Trinickia caryophylli DSM 50341

Appendix A-1: FT-IR spectrum of trinickiabactin.

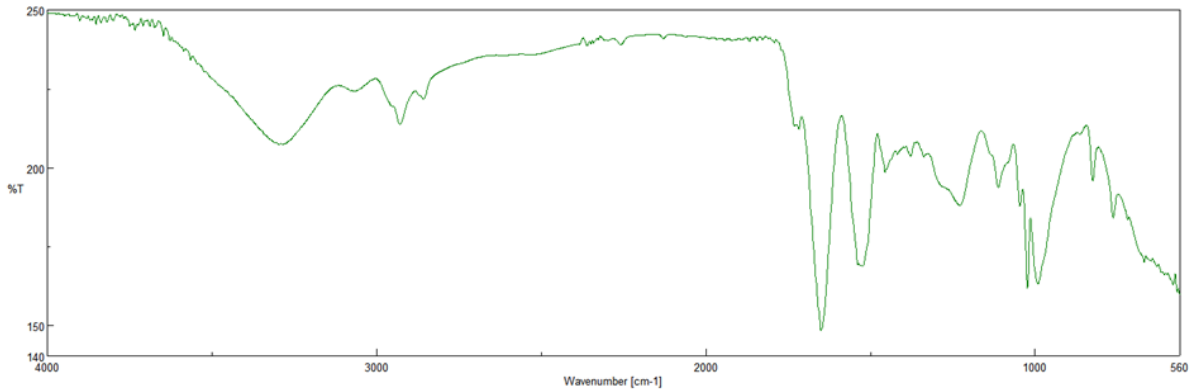

Appendix A-2: UV spectrum of trinickiabatin in MeOH (showing only end-absorption).

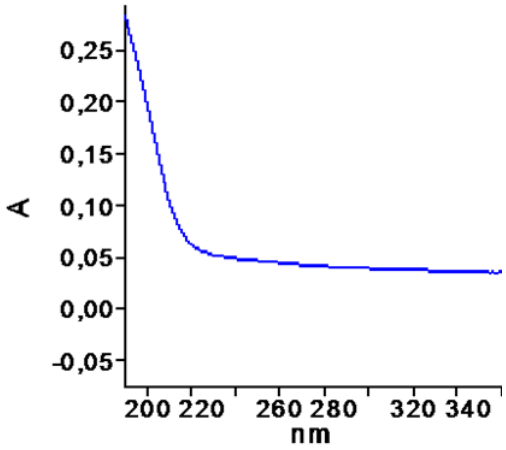

Appendix A-3: Production of gramibactin and trinickiabactin from different media.

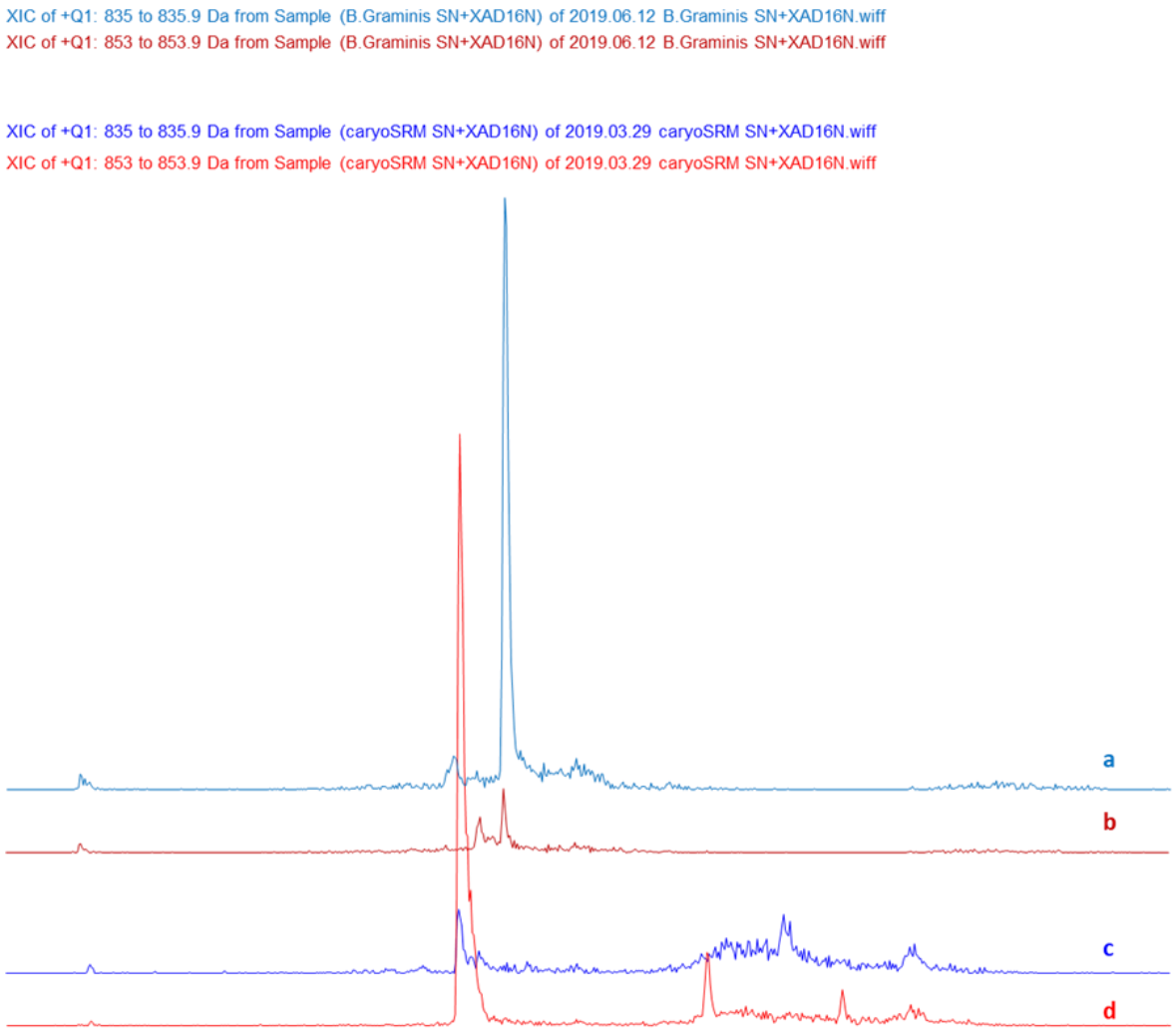

a: ion extraction for the mass range of gramibactin produced from *Burkholderia graminis* in modified M9 medium; **b**: ion extraction for the mass range of trinickiabactin produced from *Burkholderia graminis* in modified M9 medium; **c**: ion extraction of the mass range for gramibactin produced from *Trinickia caryophylli* in in SRM_{HG} medium. **d**: ion extraction of the mass range for trinickiabactin produced from *Trinickia caryophylli* in in SRM_{HG} medium.

Appendix B: *Burkholderia oklahomensis* DSM21774

Appendix B-1: FT-IR spectrum of Hybridobactin A.

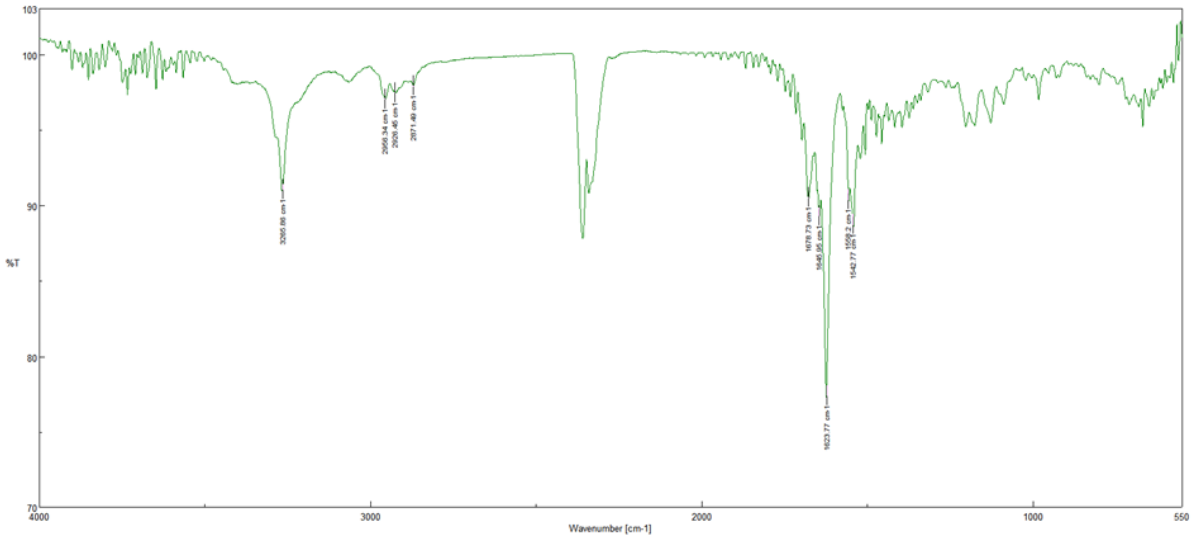

Appendix B-2: UV spectrum of Hybridobactin A.

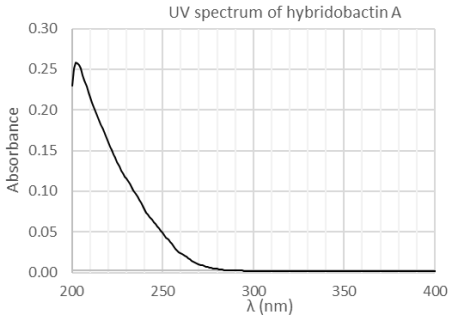

Hybridobactin A in MeOH: λ_{max}(logε): 202(6.7).

Appendix B-3: MS/MS spectrum of Hybridobactin A in positive mode.

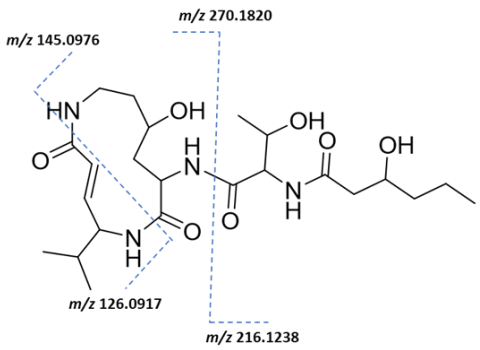

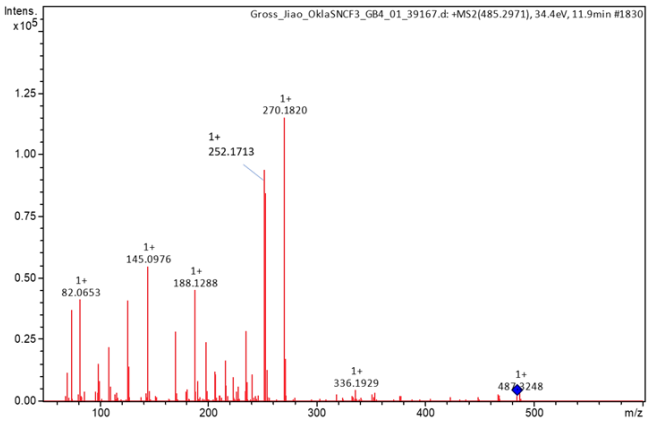

Appendix B-4: FT-IR spectrum of Hybridobactin B.

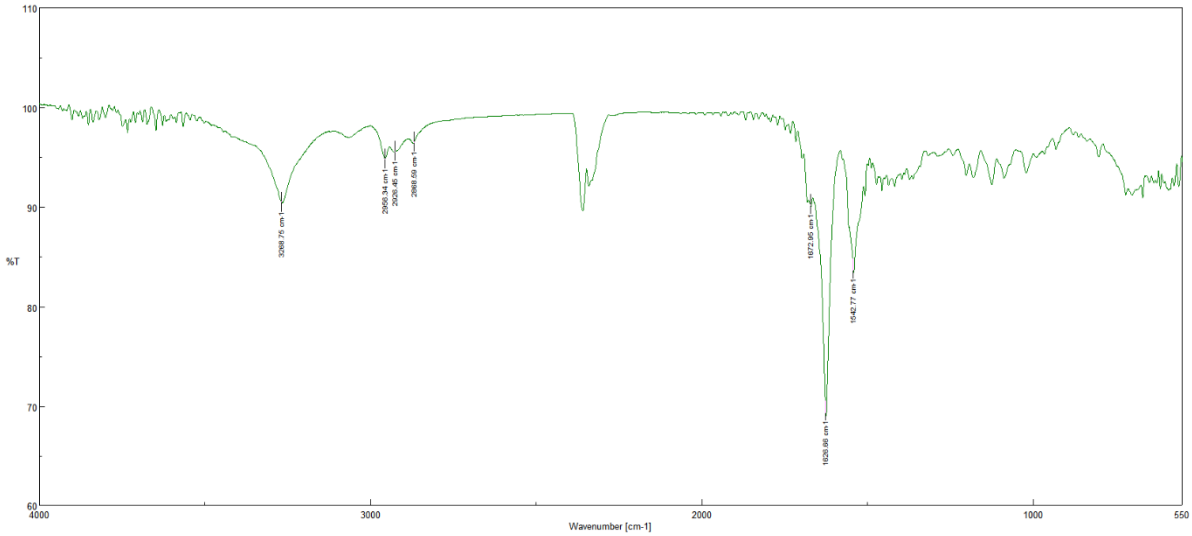

Appendix B-5: UV spectrum of Hybridobactin B.

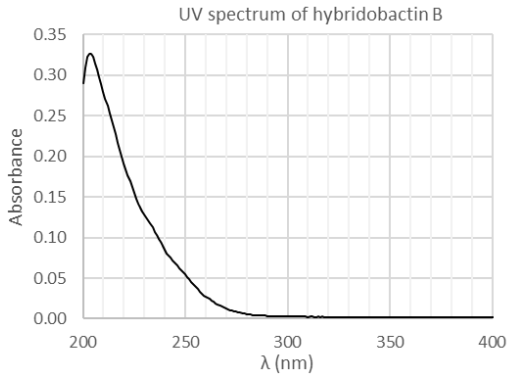

Hybridobactin B in MeOH: λ_{max}(logε): 202(6.5).

Appendix B-6: MS/MS spectrum of Hybridobactin B in positive mode.

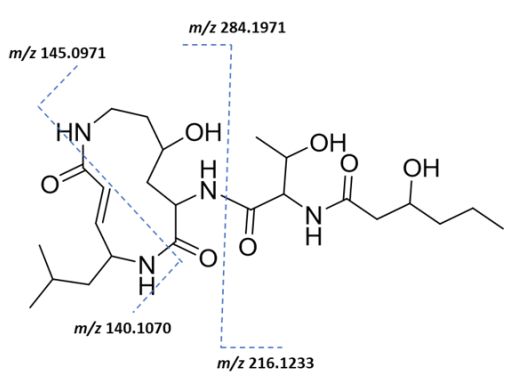

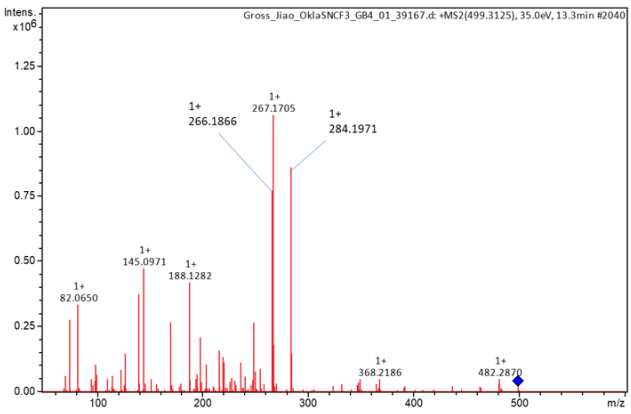

Appendix B-7: 1D and 2D NMR spectra of hybridobactin B (DMSO-d_6).

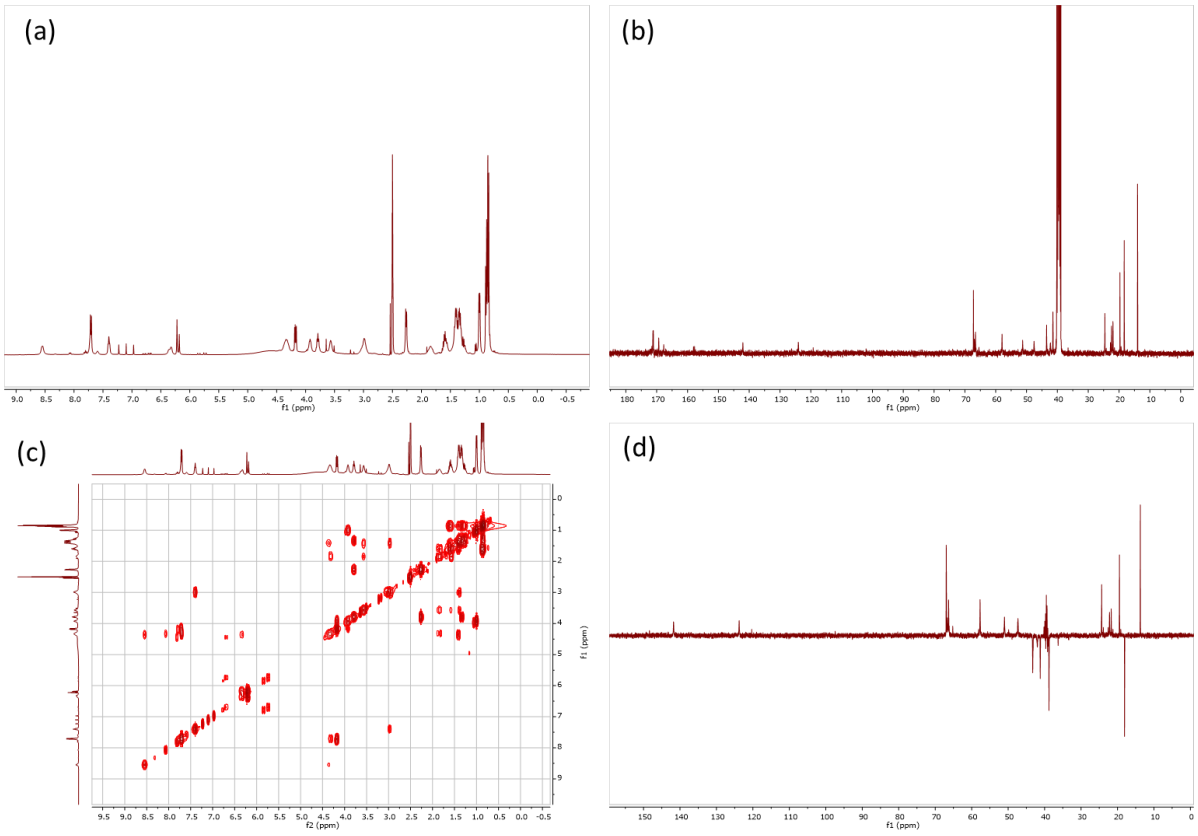

(a) ^{1}H NMR spectrum of hybridobactin B (400 MHz). (b) ^{13}C NMR spectrum of hybridobactin B (100 MHz). (c) ^{1}H-^{1}H COSY spectrum of hybridobactin B (400 MHz). (d) DEPT135 spectrum of hybridobactin B (400 MHz).

Appendix B-8: 2D NMR spectra of hybridobactin B (400 MHz, DMSO-d_6).

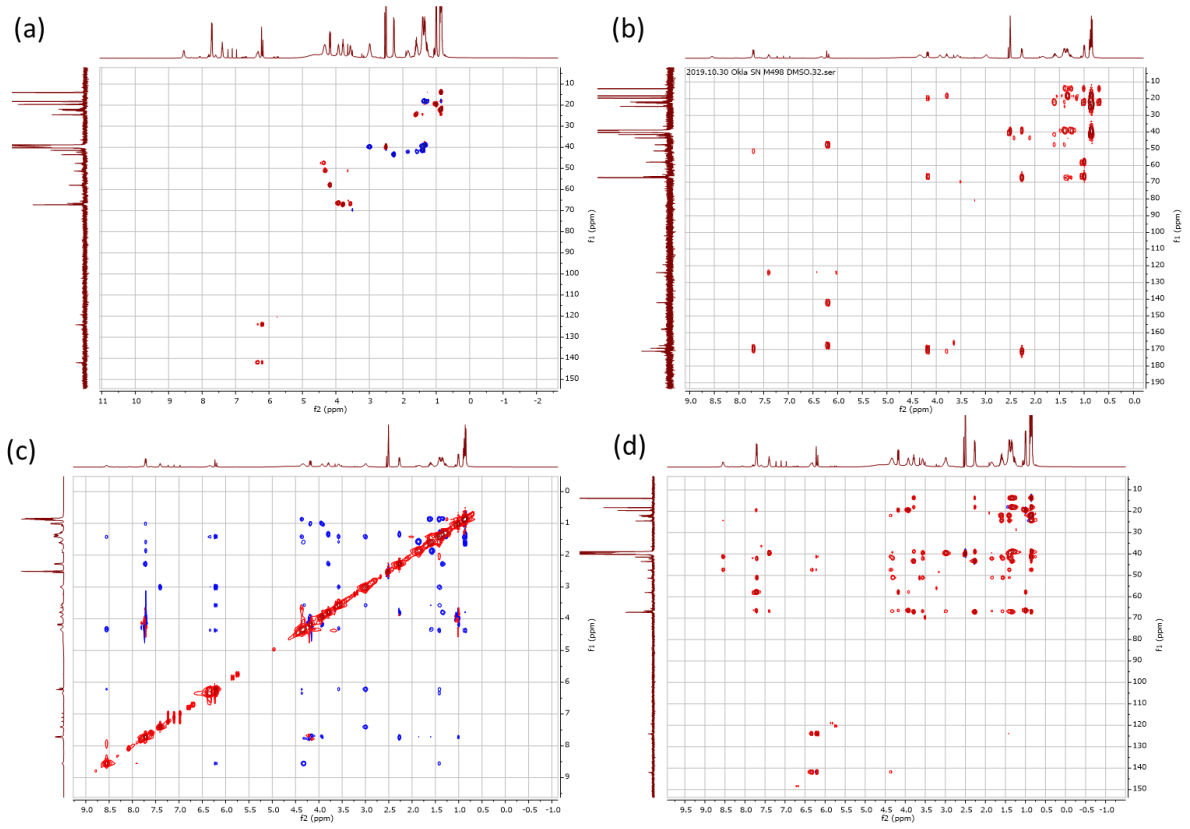

(a) ^{1}H-^{13}C HSQC NMR spectrum of hybridobactin B. (b) ^{1}H-^{13}C HMBC NMR spectrum of hybridobactin B. (c) ^{1}H-^{1}H NOESY spectrum of hybridobactin B. (d) ^{1}H-^{13}C HSQC-TOCSY spectrum of hybridobactin B.

Appendix B-9: FT-IR spectrum of Hybridobactin C.

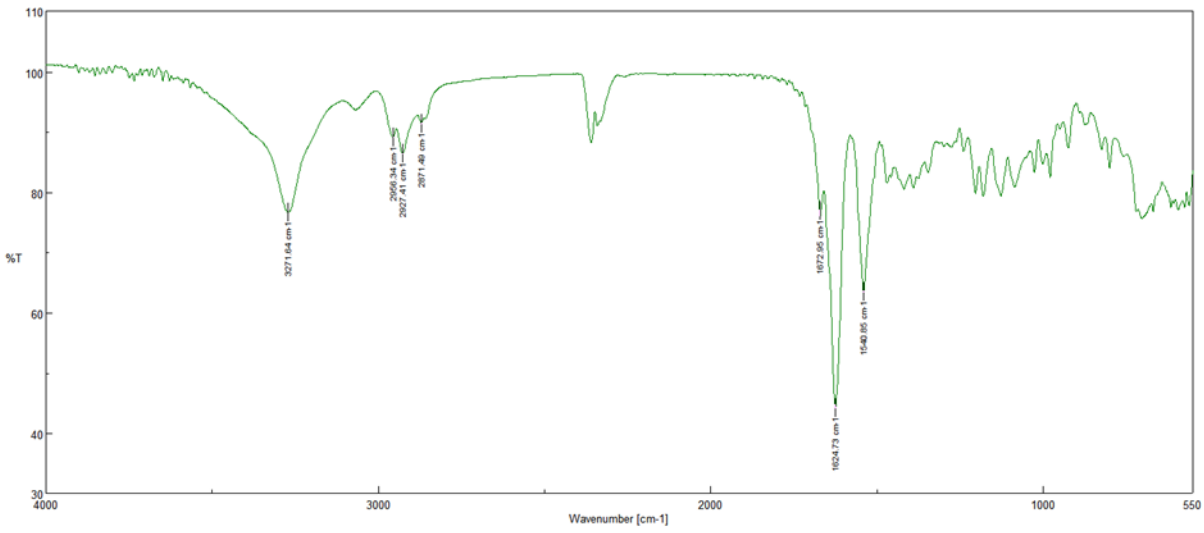

Appendix B-10: UV spectrum of Hybridobactin C.

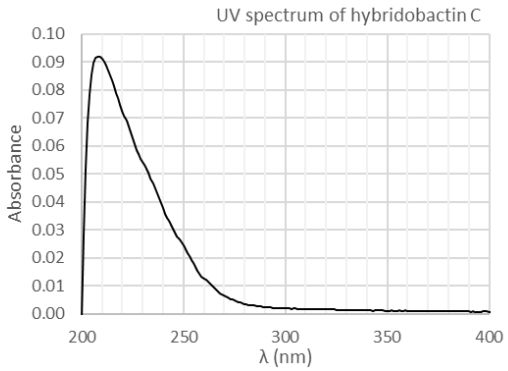

Hybridobactin C in MeOH: λ_{max}(logε): 202(6.4).

Appendix B-11: MS/MS spectrum of Hybridobactin C in positive mode.

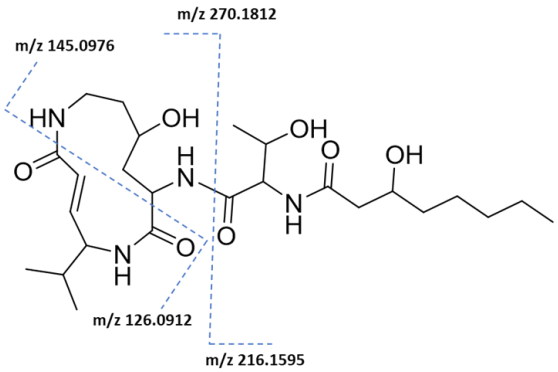

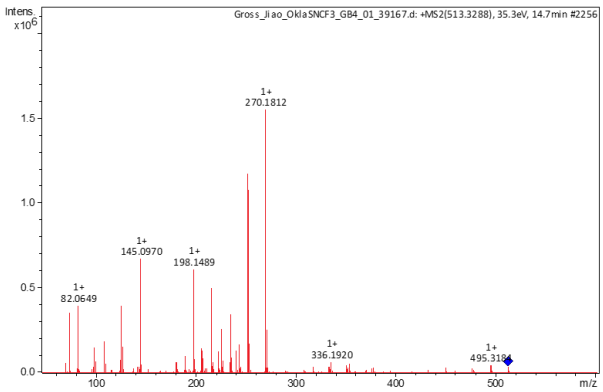

Appendix B-12: NMR spectroscopic data (DMSO-d_6) for hybridobactin C.

unit	position	δC/N, mult.	δH, (mult., J in Hz)
3-hydroxyl-octanoic acid (HOA)	1	171.1, qC	-
	2	43.5, CH2	2.26, 2H (d, 6.6)
	3	67.5, CH	3.77, 1H (m)
	4	36.8, CH2	1.36*, 2H (m)
	5	24.8, CH2	1.24*, 1,36*, 2H (m)
	6	31.3, CH2	1.24*, 2H (m)
	7	22.2, CH2	1.24*, 2H (m)
	8	13.9, CH3	0.86, 3H (t, 7.1)
Thr1	C=O	169.3, qC	-
	α	57.9, CH	4.18, 1H (dd, 8.6, 4.3)
	β	66.6, CH	3.93, 1H (m)
	γ	19.7, CH3	1.00, 3H (d, 6.0)
	NH	121.2	7.71, 1H (d, 7.5)
4-OH Lys2	C=O	171.4, qC	-
	α	51.2, CH	4.36, 1H (t, 8.7)
	β	42.2, CH2	1.85, 1.56, 2H (m)
	γ	66.7, CH	3.57, 1H (Broad s)
	δ	39.2	1.39, 2H (m)
	ε	39.6	2.99, 2H (Broad s)
	α-NH	118.1	7.71, 1H (d, 7.5)
	NH	118.1	7.41, 1H (Broad s)
5-Mah3	C=O	167.8, qC	-
	α	124.8, CH	6.20, 1H (d, 16.2)
	β	140.8, CH	6.32, 1H (dd, 16.4, 6.7)
	γ	55.7, CH	4.05, 1H (q, 7.6)
	δ	30.5, CH	1.75, 1H (m)
	ε	19.1, CH3	0.92, 3H (d, 7.1)
	ζ	19.6, CH3	0.89, 3H (d, 7.0)
	NH	132.6	8.45, 1H (d, 8.1)

*Overlapped signals.

Appendix B-13: 1D and 2D NMR spectra of hybridobactin C (DMSO-*d*$_6$).

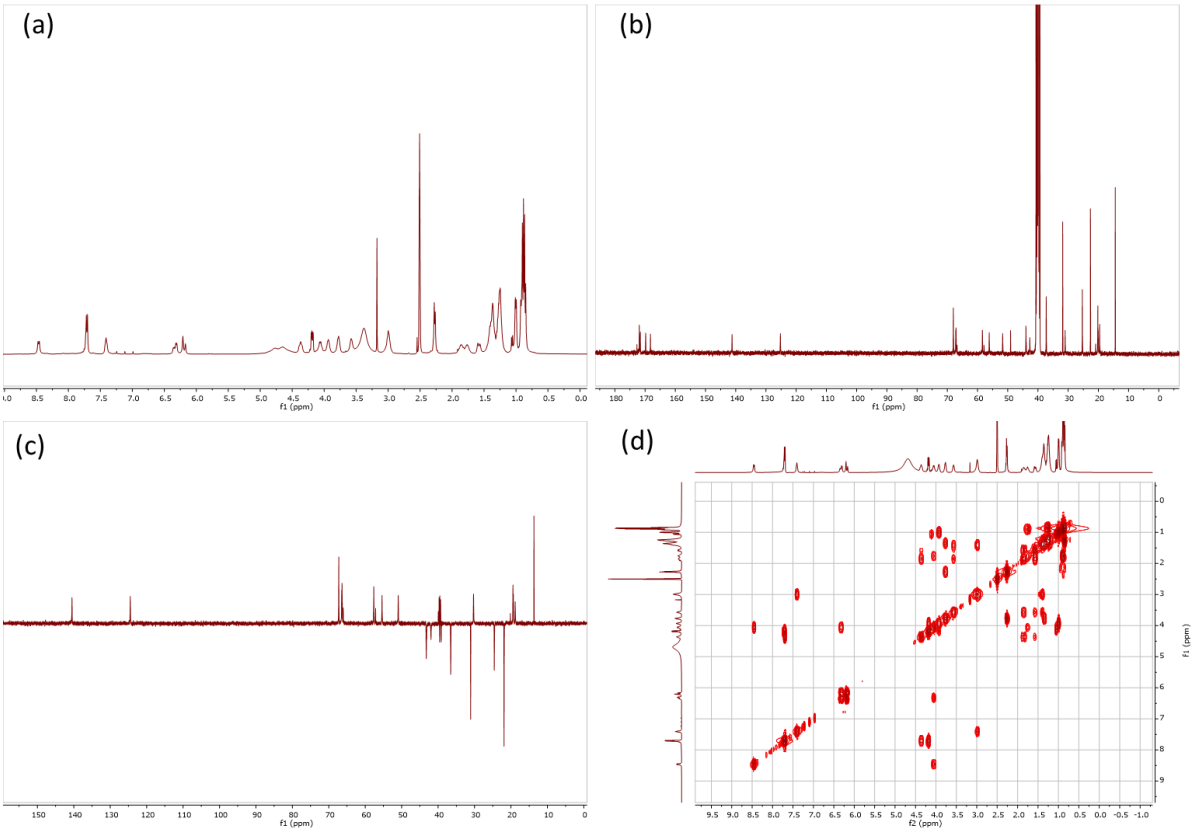

(a) ^{1}H NMR spectrum of hybridobactin C (400 MHz). (b) ^{13}C NMR spectrum of hybridobactin C (100 MHz). (c) ^{1}H-^{1}H COSY spectrum of hybridobactin C (400 MHz). (d) DEPT135 spectrum of hybridobactin C (400 MHz).

Appendix B-14: 2D NMR spectra of hybridobactin C (400 MHz, DMSO-d_6).

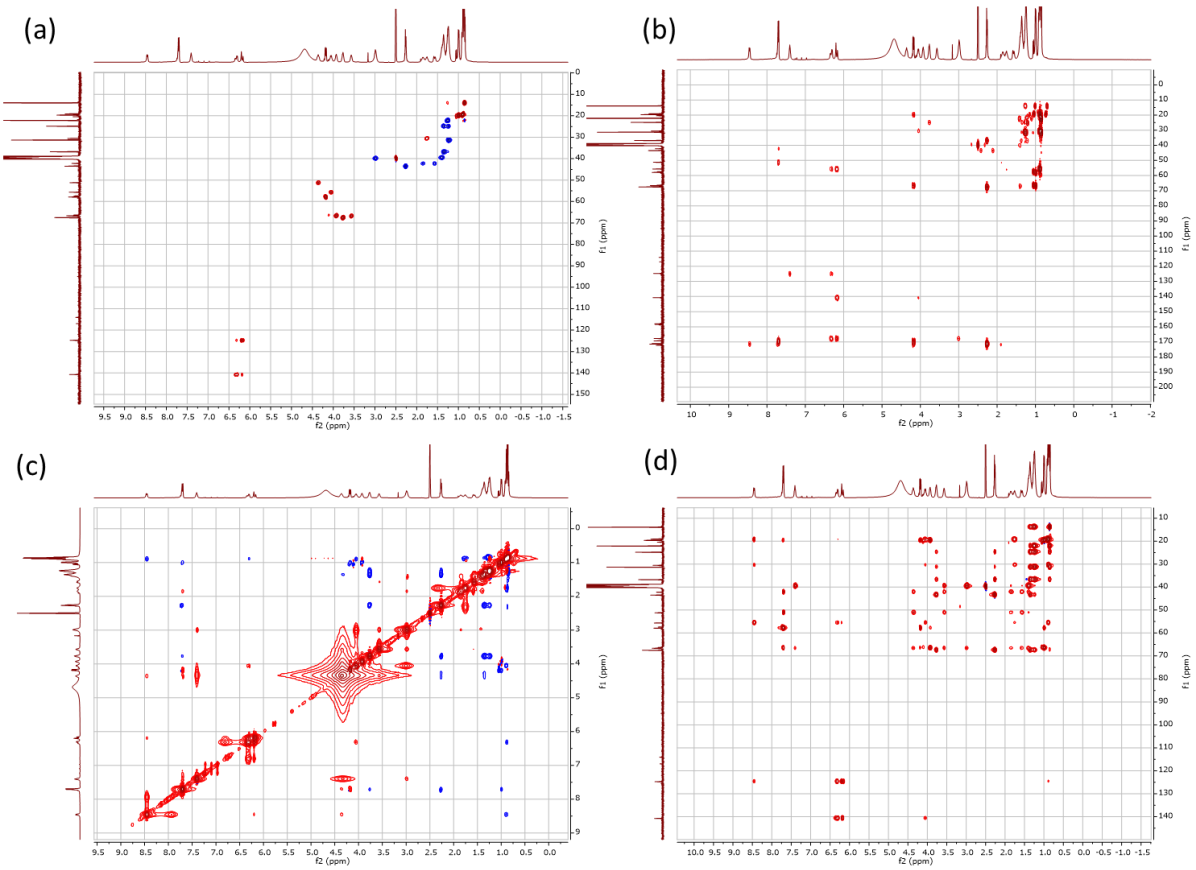

(a) ^{1}H-^{13}C HSQC NMR spectrum of hybridobactin C. (b) ^{1}H-^{13}C HMBC NMR spectrum of hybridobactin C. (c) ^{1}H-^{1}H NOESY spectrum of hybridobactin C. (d) ^{1}H-^{13}C HSQC-TOCSY spectrum of hybridobactin C.

Appendix B-15: FT-IR spectrum of Hybridobactin D.

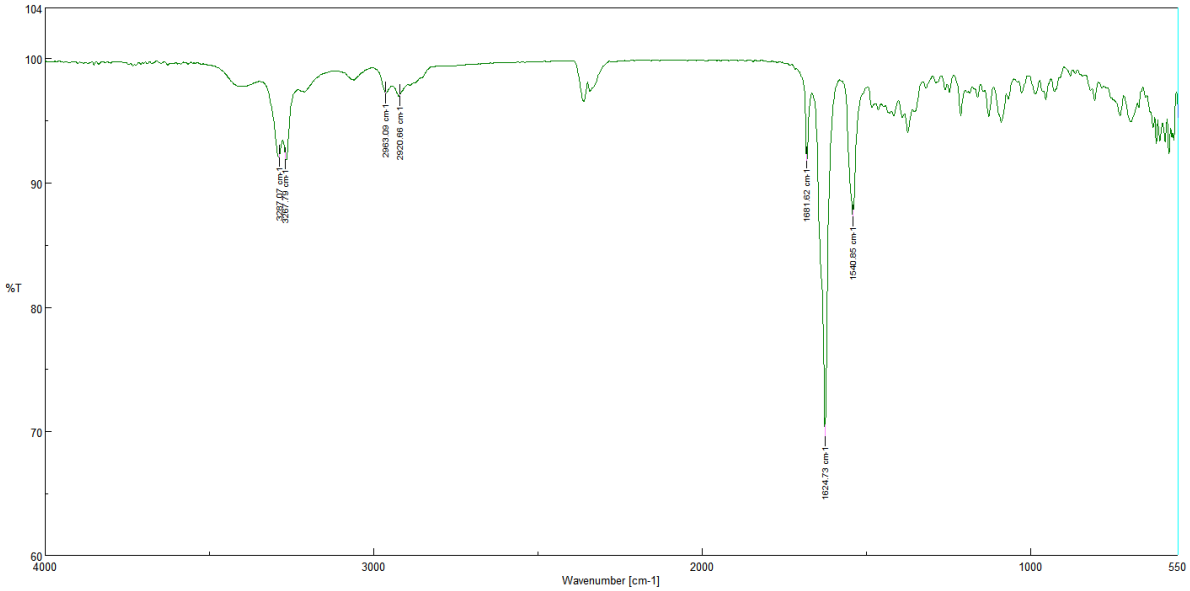

Appendix B-16: UV spectrum of Hybridobactin D.

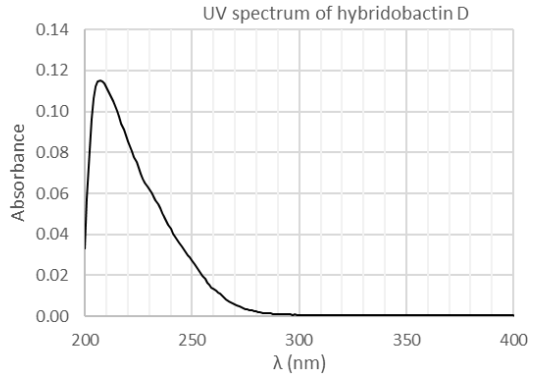

Hybridobactin D in MeOH: λ_{max}(logε): 202(6.3).

Appendix B-17: MS/MS spectrum of Hybridobactin D in positive mode.

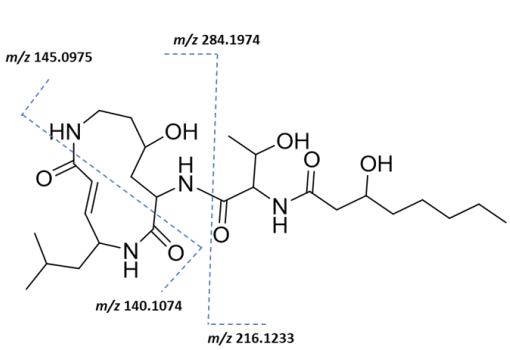

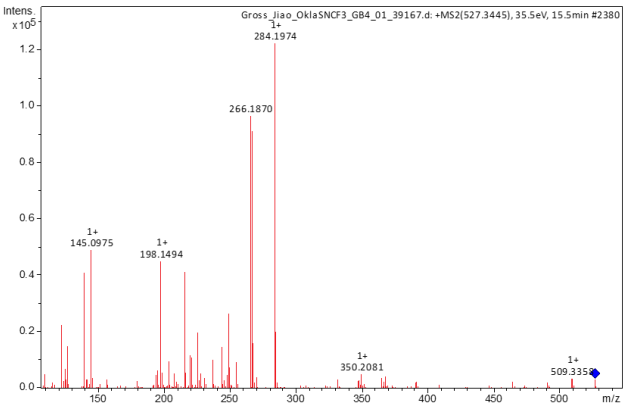

Appendix B-18: NMR spectroscopic data (DMSO-d_6) for hybridobactin D.

unit	position	$\delta_{C/N}$, mult.	δ_H, (mult., *J* in Hz)
3-OH hydroxyl-octanoic acid (HOA)	1	171.6, qC	-
	2	43.5, CH_2	2.25, 2H (d, 6.5)
	3	68.0, CH	3.79, 1H (m)
	4	37.3, CH_2	1.36*, 2H (m)
	5	25.3, CH_2	1.26*, 1.37*, 2H (m)
	6	31.8, CH_2	1.24*, 3H (m)
	7	22.6, CH_2	1.27*, 2H (m)
	8	14.4, CH_3	0.86, 3H (t, 7.5)
Thr1	C=O	169.8, qC	-
	α	58.4, CH	4.18, 1H (dd, 8.8, 4.2)
	β	67.1, CH	3.93, 1H (m)
	γ	20.1, CH_3	1.00, 3H (d, 6.0)
4-OH Lys2	C=O	171.7, qC	-
	α	51.7, CH	4.37, 1H (t, 8.7)
	β	42.2, CH_2	1.84, 1.57, 2H (m)
	γ	67.4, CH	3.57, 1H (Broad s)
	δ	39.8, CH_2	1.42a*, 2H (m)
	ε	40.3, CH_2	2.98, 2H (Broad s)
6Mah3	C=O	168.2, qC	-
	α	124.5, CH	6.22, 1H (d, 16.0)
	β	140.5, CH	6.32, 1H (dd, 16.4, 6.0)
	γ	43.1, CH	4.31, 1H (m)
	δ	41.9, CH_2	1.42b*, 2H (m)
	ε	25.1, CH	1.61, 2H (m)
	ζ	21.9, CH_3	0.84, 3H (d, 7.3)
	η	22.4, CH_3	0.90, 3H (d, 7.0)

*Overlapped signals.

Appendix B-19: 1D and 2D NMR spectra of hybridobactin D (DMSO-*d*$_6$).

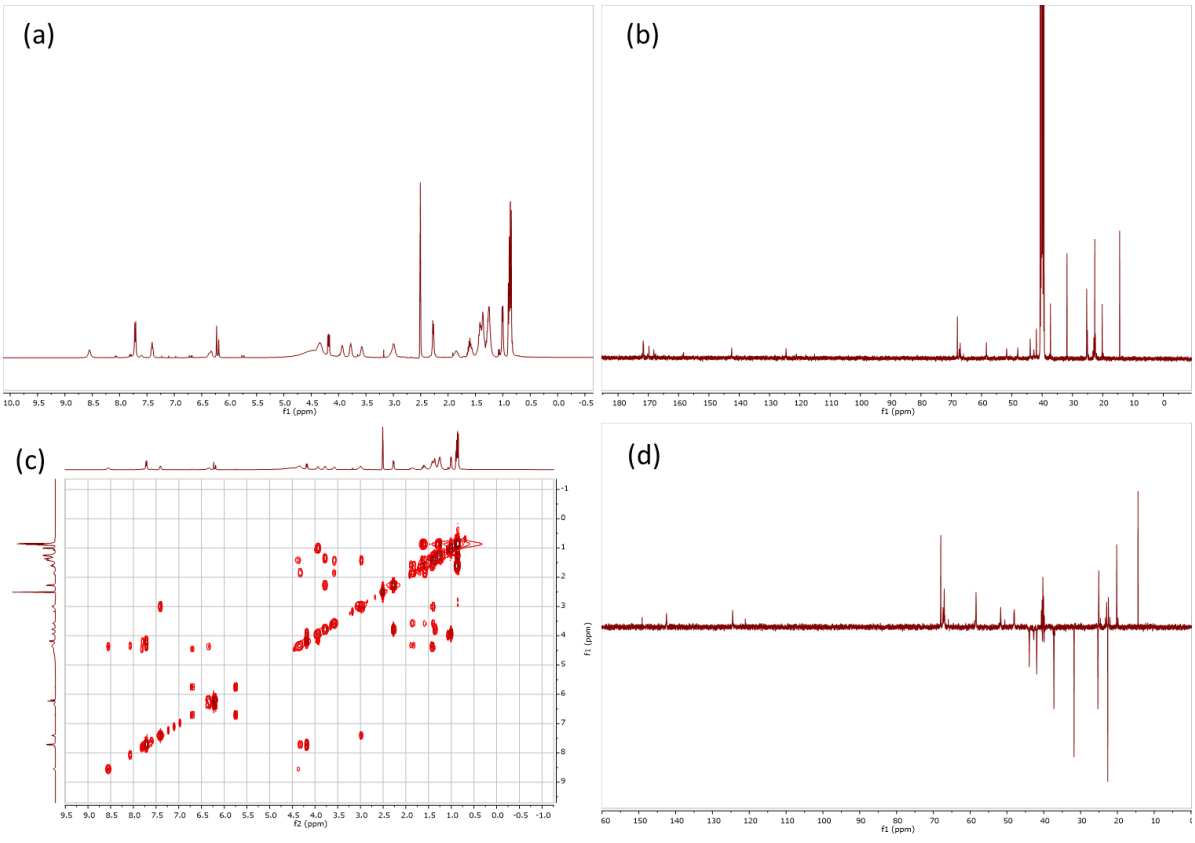

(a) ^{1}H NMR spectrum of hybridobactin D (400 MHz). (b) ^{13}C NMR spectrum of hybridobactin D (100 MHz). (c) ^{1}H-^{1}H COSY spectrum of hybridobactin D (400 MHz). (d) DEPT135 spectrum of hybridobactin D (400 MHz).

Appendix B-20: 2D NMR spectra of hybridobactin D (400 MHz, DMSO-d_6).

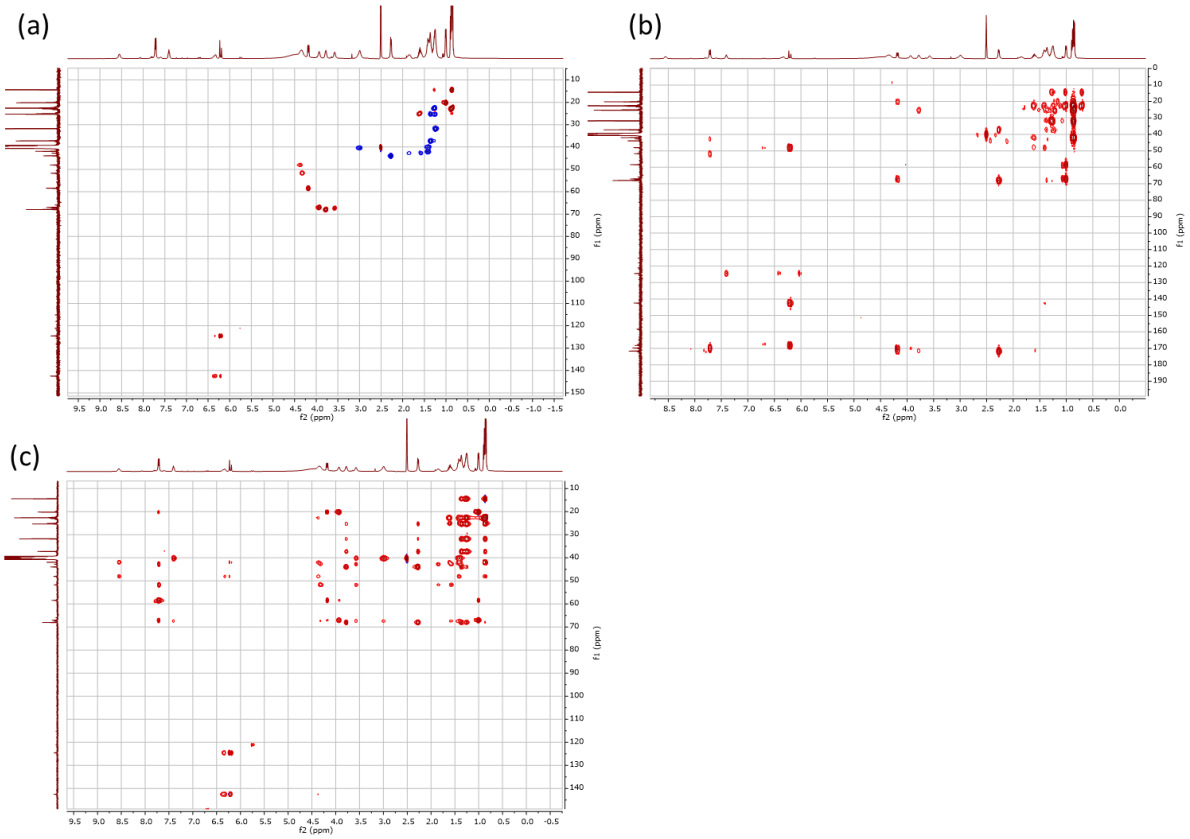

(a) ^{1}H-^{13}C HSQC NMR spectrum of hybridobactin D. (b) ^{1}H-^{13}C HMBC NMR spectrum of hybridobactin D. (c) ^{1}H-^{13}C HSQC-TOCSY spectrum of hybridobactin D.

Appendix C: *Burkholderia glumae* ICMP 3729

Appendix C-1: UV spectrum of acybolin J.

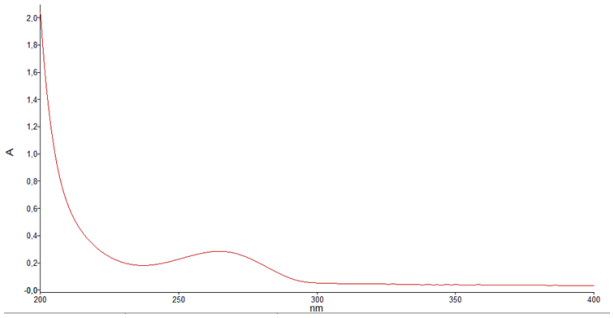

Acybolin J in MeOH: λ_{max} (log ε): 266 (3.6) nm.

Appendix C-2: 1D and 2D NMR spectra of acybolin A (DMF-d_7).

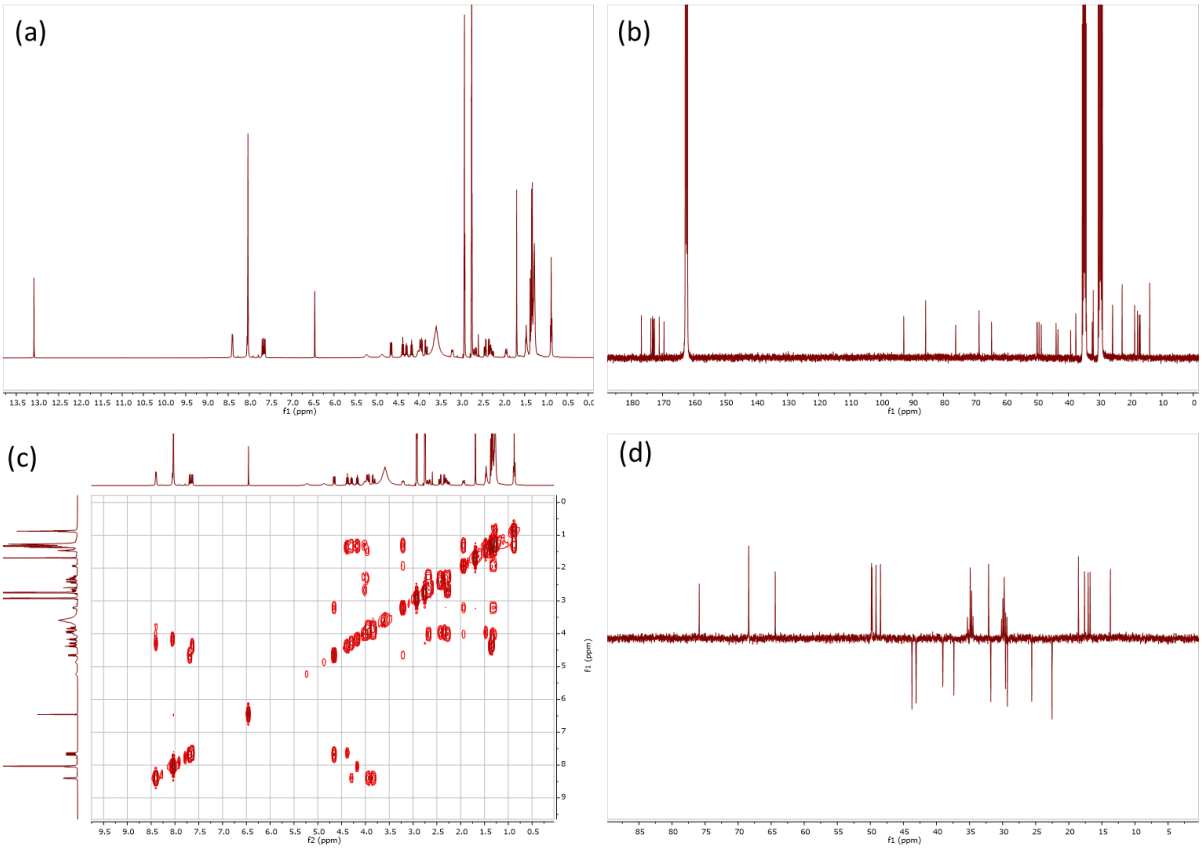

(a) ^{1}H NMR spectrum of acybolin A (400 MHz). (b) ^{13}C NMR spectrum of acybolin A (100 MHz). (c) ^{1}H-^{1}H COSY spectrum of acybolin A (400 MHz). (d) DEPT135 spectrum of acybolin A (400 MHz).

Appendix C-3: 2D NMR spectra of acybolin A (400 MHz, DMF-d_7).

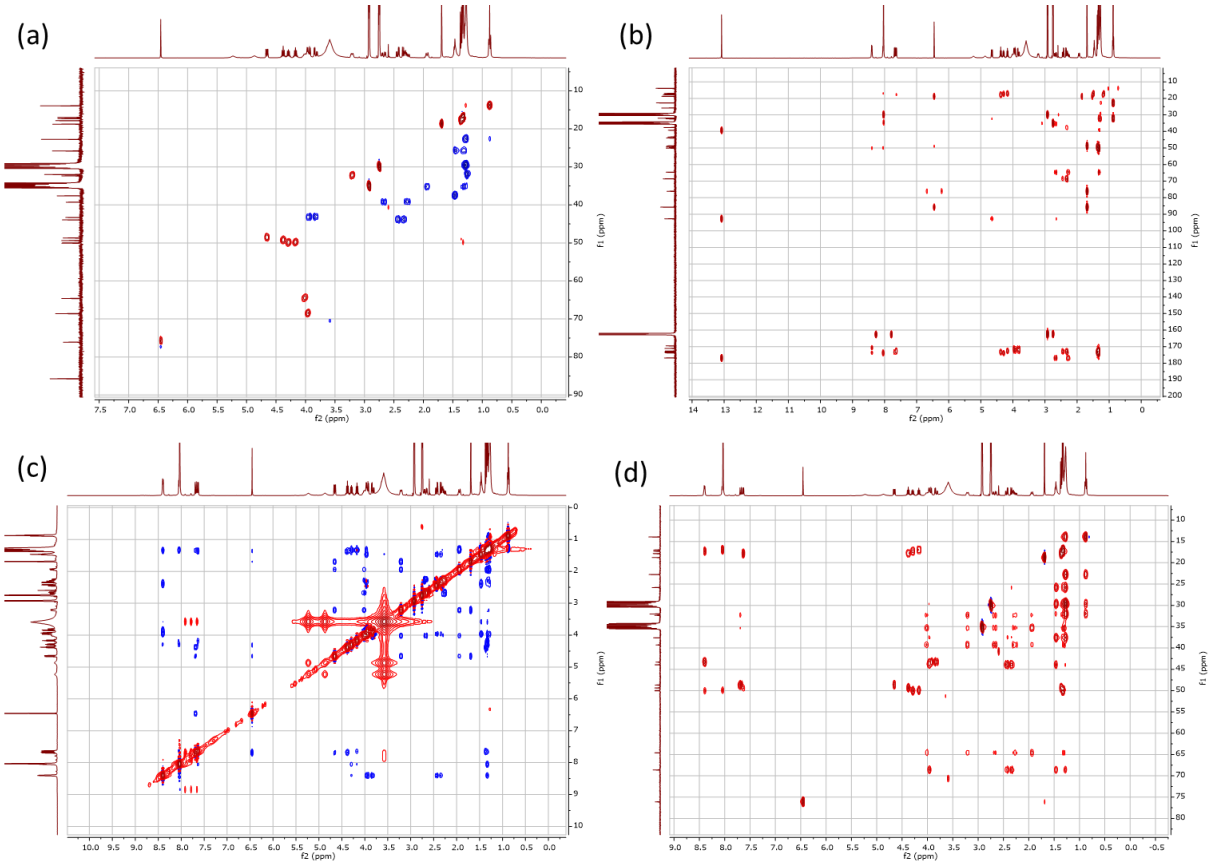

(a) ^{1}H-^{13}C HSQC NMR spectrum of acybolin A. (b) ^{1}H-^{13}C HMBC NMR spectrum of acybolin A. (c) ^{1}H-^{1}H NOESY spectrum of acybolin A. (d) ^{1}H-^{13}C HSQC-TOCSY spectrum of acybolin A.

Appendix C-4: 2D NMR spectra of acybolin A (400 MHz, DMF-d_7).

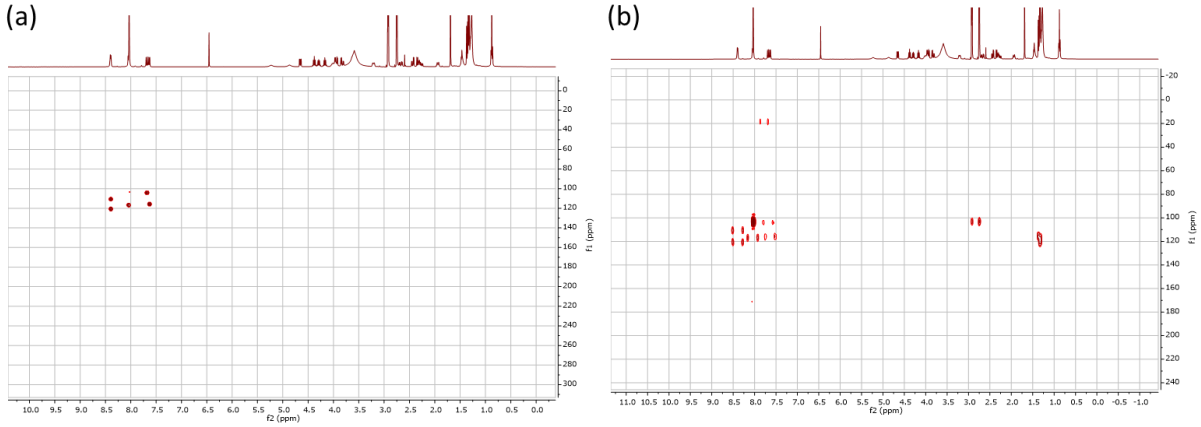

(a) ^{1}H-^{15}N HSQC NMR spectrum of acybolin A. (b) ^{1}H-^{15}N HMBC NMR spectrum of acybolin A.

Appendix C-5: FT-IR spectrum of Acybolin A.

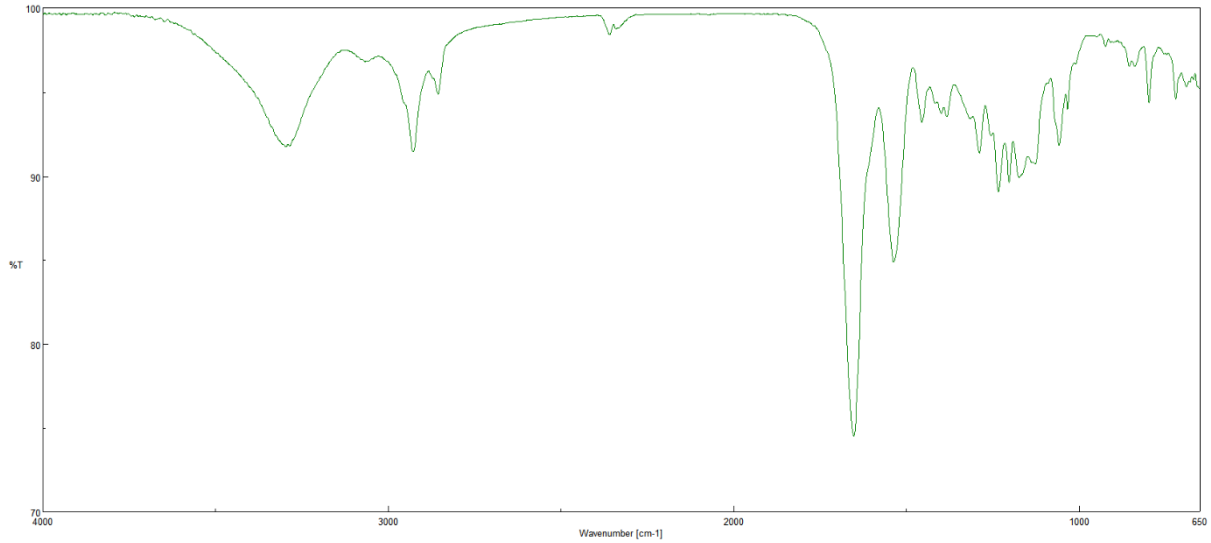

Appendix C-6: UV spectrum of acybolin A.

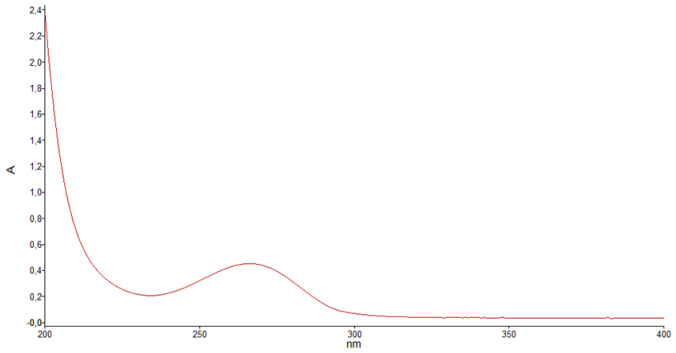

Acybolin A in MeOH: λ_{max} (log ε): 263 (3.1) nm.

Acknowledgements

First and foremost, I would like to express my deepest appreciation to Prof. Dr. Harald Groß, for giving me the opportunity and guiding me through the whole process of my Ph.D. Without his valuable ideas, I would not have smoothly received the CSC fellowship. His unique research style impressed deeply upon me, and his good advice always provided me with inspiration for my research. I thank him for helping me to overcome practical problems during some projects and initiating some collaboration work to push the project forward. Many thanks to his unbelievable patience and kindness as well. However, due to the Corona situation, we weren´t able to hear his intersting and vivid stories during lunch time in the Mensa, which I missed a lot! But I think it will become a good memory and I will appreaciate it forever!

Furthermore, I would like to thank PD. Dr. Gust for being my second examiner and for the useful discussion about the projects. His calm and wise approach impressed me a lot. I'd like to extend thanks to Prof. Dr. Leonard Kaysser and Prof. Dr. Michael Lämmerhofer for their willingness to complement my supervisors as members of my oral examination committee.

I sincerely thank Jiayi and Lei for trusting me to supervise their Master's theses. Also, I would like to thank my colleagues in the microbiology and natural product chemistry labs for supporting me where necessary. I would also like to express my gratitude to Dr. Julia Chen, for giving some sincere opinions about science and life and also for sharing quite some experiences with *Burkholderia* strains. Thanks to Aziz Saefuddin, who taught me a great deal about bacteria, and Hamada Saad, who willingly shared a lot of experience in chemical analysis. Many thanks to Niraj Aryal, as a good friend who always gave useful life advices. I would like to thank Patricia Arlt for ordering chemicals and materials, Irina for NMR measurements and Thomas for sharing a lot of opinions and experiences about life from the perspective of a German. Thanks to Keshab, who is always helpful to other people, and to Fred, who brought a lot of laughs to this lab. I would like to express my thanks to Lina for CAS agar preparation and some lab help, and to Carolina for teamwork of multiple cleaning tasks and sometimes for sharing some molecular biology-related knowledge. Many thanks to our new technical assistants Wolfgang and Manuella for some interesting conversations.

I am also grateful for the considerable efforts of other members past and present of the Pharmaceutical Biology and Biology departments.

This work was in part performed in cooperation with other research groups. For this work, my appreciation goes to:

Dr. D. Wistuba and her team, Mass Spectrometry Dept., Institute for Organic Chemistry, University of Tübingen for HR-MS measurements.

Prof. Dr. Michael Lämmerhofer and his group members, especially Ryan Karongo from the Department of Pharmaceutical Analysis and Bioanalysis, University of Tübingen, for their contribution in analytical experiments.

Dr. Thomas Böttcher, Department of Chemistry, University of Konstanz, for providing the isolated glidobactins.

Dr. Andri Frediansyah and Dr. Nicole Staudt, Pharmaceutical Biology, University of Tübingen, for performing antibacterial assays and for conducting the proteasome inhibition and cell proliferation assays, respectively.

I gratefully acknowledge the funding sources that made my Ph.D. work possible. This work was supported by a fellowship from the China Scholarship Council (CSC).

Finally, I sincerely thank my family and friends for supporting me all the way through life to this point. And most of all, my sincere gratitude goes to my wife Huanlei, I really appreciate her faithful support. Without her love I would not have come this far.